UNIVERSITÀ DEGLI STUDI DI MILANO

Dottorato di Ricerca in Scienze della Terra

Ciclo XXIX

The dark side of the ice:
Glaciological and biological aspects of supraglacial debris

Ph.D. Thesis

Roberto Sergio Azzoni
Matricola R10479

Tutor
Prof.ssa Guglielmina Diolaiuti

Academic Year
2015/2016

Coordinator
Prof. ssa Elisabetta Erba

Co- Tutor
Dott. Andrea Zerboni
Dott. Roberto Ambrosini
Dott. Andrea Franzetti

Foreword

Glaciers are considered, in everyone's mind, inhospitable, white, and cold deserts, where life forms are excluded. Conversely, ice bodies present a dark side teeming with life. In this thesis, we focus to this aspect of glaciers and propose a multidisciplinary analysis of the supraglacial debris. In the first part of the thesis, we analyzed and quantified the physical effects of the debris mantle and its evolution through time and space. In the second part, we focused on the organisms that live in the supraglacial debris, and on the ecological processes acting in it, which are strictly linked to the evolution of ice bodies.

PART I

SUPRAGLACIAL DEBRIS: GLACIOLOGICAL ASPECTS

Introduction

The fate of glaciers and ice sheets have wide-reaching impacts, and can profoundly affect natural ecosystems and human communities (Benn and Evans, 2010). Ice bodies strongly affect the energy balance of the whole planet, due to their high values of albedo (IPCC, 2013) and their surface change is crucial for the equilibrium of some environments. Glacier have also leaved a clear footprint of their passage, shaping the landscapes of huge areas of the Earth's surface (Benn and Evans, 2010). Moreover, ice bodies are an important water resource, in particular for arid and semi-arid regions (Kaser et al., 2010; Immerzeel et al., 2010) and their melting is the main cause of the sea-level change (Benn and Evans, 2010).

Glaciers are sensitive barometers of climate change, constantly and quickly growing and shrinking in response to changes in air temperature, snowfall and other factors (Benn and Evans, 2010). The mass of glacier ice on Earth is constantly changing, on timescales from less than one day to millions of years. Currently, glaciers and ice sheets cover approximately 10% of the Earth's surface (IPCC, 2013).

As a consequence of global warming, glacier resources are considered at risk in many regions, particularly those on mountains at lower latitude (IPCC, 2013). The ongoing climate warming, which since the end of the Little Ice Age (ca. 1850 AD) has been particularly significant in the Alps, dramatically accelerated in the end of the 20th Century (Brunetti et al., 2009; IPCC, 2013). Indeed, many mountain groups in the Alps have lost a significant portion of their glacierized areas over the past 150 years (Maisch, 2000; Rabatel et al., 2005; Gerbaux et al., 2005; Lambrecht and Kuhn, 2007; Smiraglia et al., 2015; Diolaiuti et al., 2011; D'Agata et al. 2014), and a fast acceleration of glacier retreat has been registered in the last two decades (e.g., Paul & et al., 2004; Zemp et al., 2008; 2015 Diolaiuti et al., 2012a; 2012b). In addition, the Italian glaciers are experiencing a large area reduction over the last decades, which is comparable in magnitude and rate to that of other glacierized Alpine sectors (Maragno et al., 2009; D'Agata et al., 2014; Smiraglia et al., 2015; Paul et al., 2004; 2011). In

details, a comparison between the New Italian Glacier Inventory (Smiraglia et al., 2015) and the previous one inventory highlighted a reduction of about 30% of the Italian glacierized surface (from 526.88 km^2 to 369.90 km^2) in the last 50 years (Smiraglia et al., 2015).

Importance of supraglacial debris in glacier system

Besides the large areal variation, the glacier surface undergoes important physical changes: the areal expansion of supraglacial debris cover over the last decades is reported in major mountain ranges (Oerlemans et al., 2009).

The presence of supraglacial debris strongly influences ice melt (Østrem, 1959; Nakawo and Young, 1981). Empirical relationships between supraglacial debris thickness and ice-melt rates were first established by Østrem (1959), who showed that under thin debris (~<2 cm), buried ice melt rates are higher than for clean ice at the same elevation and the ablation rates progressively decline under thicker debris layer. This pattern has been confirmed in numerous subsequent studies (e.g. Loomis, 1970; Mattson and Gardner, 1989; Kayastha et al., 2000; Mihalcea et al., 2006). However, the threshold of the debris thickness determining whether melt rate is enhanced or inhibited varies under the influence of local climate and debris grain size and lithology (Nakawo and Rana, 1999; Conway and Rasmussen, 2000).

The ice bodies where the largest part of the ablation zone (i.e. about 50 %,) has a continuous cover of rock debris are named as debris-covered glaciers (Kirkbride, 2011). Supraglacial debris covers form where debris supply is high and ice flow is relative slow: in this case, a glacier is unable to evacuate rock debris efficiently and a continuous debris cover develops starting from the lower parts of the ablation zone (Kirkbride, 2011). Debris-covered glaciers are widely distributed in the world and are common in the Himalaya (Racoviteanu et al., 2008a), Karakoram (Owen and Derbyshire, 1993; Diolaiuti et al., 2003a; Minora et al., 2015), Caucasus (Stokes et al., 2007), Alaska, New Zealand (Kirkbride, 1993), and parts of the Andes (Racoviteanu et al., 2008b). Debris-covered glaciers are

present also in the Alps and the well-studied ice bodies, Miage and Belvedere, are located in Italy (Diolaiuti et al., 2003b; Mihalcea et al., 2006; Diolaiuti et al., 2009).

The study of debris-covered glaciers has gained particular relevance in recent years because a widening of the supraglacial debris is observed in many glaciers worldwide (Oerlemans et al., 2009). Many studies dealing with the modeling of ablation under the layer of debris where performed, among the others, in Karakoram (Mihalcea et al., 2008b; Minora et al., 2015; Soncini et al., 2015), Alps (Mihalcea et al., 2006; Brock et al., 2010; Reid and Brock, 2010; Fyffe et al., 2014; Bocchiola et al., 2016), and Himalaya (Scherler et al., 2011; Soncini et al., 2016).

Another important issue in the analyses of debris-covered glaciers is the spatial quantification of the debris and its thickness assessments, which were performed by some authors based on remote-sensing data (Kirkbride, 2011). Among the others, Paul et al. (2004) estimated the debris cover of Oberaletsch Glacier (Switzerland) combining multispectral image classification from Landsat TM, ASTER, and SPOT satellite; moreover, Mihalcea et al. (2008a; 2008b) investigate the debris thickness and occurrence at the Miage (Alps) and the Baltoro (Pakistan) glaciers through ASTER kinetic temperature. Minora et al., (2015) analyzed Landsat TM thermal band to derive debris depth on the whole CKNP (Central Karakoram National Park) area (Pakistan).

Debris-covered glaciers have recently become the focus also for ecological and biological researches. Indeed, supraglacial debris is characterized by a wide presence of organisms with well-developed communities (Cook et al., 2016). Vegetation (Caccianiga et al., 2011; Vezzola et al., 2016), arthropods (Gobbi et al, 2011), yeasts (Turchetti et al., 2008), and bacteria (Franzetti et al., 2013) inhabited this environment and largely affect biogeochemical cycles of these environments.

Importance of thin, sparse debris and dust in glacier system

Supraglacial debris plays a strong influence on ice melt and evolution not only if it covers the ice homogeneously, but also being fine and sparse. The dust found at the glacier surface can have many

origins and sources. A significant part consists in humic molecules, being the residue of bacterial decomposition of organic matter (Takeuchi et al., 2001; Takeuchi, 2002; Fujita, 2007), whereas the mineral fraction, can derive from different sources (Gabbi et al., 2015). In particular, it can derive from the areas surrounding the glaciers. For instance, when a glacier has been retreating for some time, the exposed side moraines and the pro-glacial plain become a large source of mineral dust and the dry and unconsolidated material is easily taken up by wind gusts and deposited on the glacier (Oerlemans, 2009). Furthermore, dust can be transported also from far areas, like deserts or arid areas. For instance, the deposition of Sahara dust on glaciers in the Alps is a well-known phenomenon (e.g., Sodemann et al., 2006). Finally, also human activities can have a non-negligible impact on the supraglacial fine debris (Painter et al., 2013). In particular, black carbon (the component of the particulate matter with a diameter ≤ 2.5 μm that consists of pure carbon see Bond et al., 2013), which is formed through the incomplete combustion of fossil fuels, biofuel, and biomass (Ramanathan and Carmicheal, 2008), can reach easily mountain areas and, consequently, glaciers (Painter et al., 2013).

Deposition of mineral dust and black carbon have a fundamental impact on the energy balance of glaciers and snow-covered areas by increasing the absorption of solar radiation (Gabbi et al., 2015). The presence of mineral dust causes an albedo reduction up to 40% (Kaspari et al., 2014) and determine up to 26% of the total annual surface melting (Ginot et al., 2014). Moreover, the radiative forcing of mineral dust deposition can shorten the duration of snow cover by several weeks (Skiles et al., 2012) and can affect also the timing and magnitude of runoff (Painter et al., 2010). Several studies investigated the local impact of black carbon on Himalaya glaciers (Ming et al., 2008; 2009; Menon et al., 2010; Yasunari et al., 2010; Kaspari et al., 2011; Kopacz et al., 2011; Xu et al., 2012). In contrast, on the Alps, studies conducted so far were limited to the analyses of black carbon in ice cores (Thevenon et al., 2009) and no investigations were performed on the glacier surface.

The correct spatial quantification and distribution along the glacier surface of this fine and sparse supraglacial debris is, up to now, an open question (Takeuchi and Li, 2008). The methods applied in

the analyses of continuous and thick supraglacial debris, generally based on remote-sensing data, are ineffective in the investigation of the supraglacial dust, due to their low resolution (Takeuchi and Li, 2008). Field studies conducted on few glaciers are limited to the quantification of small portion of ice (Takeuchi and Li, 2008; Irvine-Fynn et al. 2010; Irvine-Fynn et al. 2011; Takeuchi et al., 2014). Moreover, a clear influence of black carbon on the albedo is not well documented (Painter et al., 2013).

Aim of this study

For a better comprehension of the dynamic, evolution and impact of the dark side of glaciers, in this work we investigated the occurrence of continuous supraglacial debris cover on one of the most important glacierized areas of the Italian Alps. In fact, we analyzed debris occurrence, distribution, and its evolution in the Ortles-Cevedale Group (Southern Alps) in the period 2003-2012 from high-resolution remote sensing data. This study allowed assessing the extent of the ongoing darkening phenomena on a glacierized area of the Southern Alps (Chapter 1). Moreover, we investigated at a finer scale the surface conditions (debris occurrence and distribution, both thin and sparse debris and continuous supraglacial debris) of the melting tongue of the widest ice body in the Ortles Cevedale Group, the Forni Glacier, through the analysis of high-resolution orthophotos obtained by a Unmanned Aerial Vehicle (UAV) flights (Chapter 2). Finally, we focused on the fine and sparse debris of the ablation tongue of Forni Glacier and provided its physical, chemical and sedimentological characterization, a quantification of its influence on ice albedo and its spatial and temporal evolution on Forni ablation tongue (Chapter 3).

References

Benn D. and Evans D. J. (2014): Glaciers and glaciation. Routledge Eds. 802 pp.

Bocchiola D., Senese A., Mihalcea C., Mosconi B., D'Agata C., Smiraglia C. and Diolaiuti G. A. (2016): An ablation model for debris-covered ice: the case study of Venerocolo Glacier (Italian Alps). *Geografia Fisica Dinamica Quaternaria*, 38 (2), 113-128.

Bond T.C., Doherty S.J., Fahey D.W., Forster P.M., Berntsen T., DeAngelo B. J. and Kinne S. (2013): Bounding the role of black carbon in the climate system: A scientific assessment. *Journal of Geophysical Research – Atmosphere*, 118, 5380–5552.

Brock B., Mihalcea C., Kirkbride M., Diolaiuti G., Cutler M.E.J. and Smiraglia C. (2010): Meteorology and surface energy fluxes in the 2005–2007 ablation seasons at Miage debris-covered Glacier, Mont Blanc Massif, Italian Alps. *Journal of Geophysical Research*, 115, D09106.

Brunetti M., Lentini G., Maugeri M., Nanni T., Simolo C. and Spinoni J. (2009): 1961–1990 high-resolution Northern and Central Italy monthly precipitation climatologies. *Advances in Science and Research*, 3(1), 73-78.

Caccianiga M., Andreis C., Diolaiuti G., D'Agata C., Mihalcea C. and Smiraglia C. (2011): Alpine debris-covered glaciers as a habitat for plant life. *The Holocene*, 21(6), 1011-1020.

Conway H. and Rasmussen L.A. (2000): Summer temperature profiles within supraglacial debris on Khumbu Glacier, Nepal, in: Debris-covered glaciers. Proceedings of an International Workshop held at the University of Washington in Seattle, Washington USA, 13–15 September 2000, *IAHS Publication* 264, p. 289.

Cook J., Edwards A., Takeuchi N., Irvine-Fynn T. (2016): Cryoconite: The dark biological secret of the cryosphere. *Progress in Physical Geography*, 40(1), 66-111.

D'Agata C., Bocchiola D., Maragno D., Smiraglia C. and Diolaiuti G. (2014): Glacier shrinkage driven by climate change during half a century (1954–2007) in the Ortles-Cevedale group (Stelvio National Park, Lombardy, Italian Alps). *Theoretical and Applied Climatology,* 116 (1-2), 169-190.

Diolaiuti G., Pecci M. and Smiraglia C. (2003a): Liligo Glacier (Karakoram): reconstruction of the recent history of a surge-type glacier. *Annals of Glaciology*, 36, 168-172.

Diolaiuti G., D'agata C. and Smiraglia C. (2003b): Belvedere Glacier, Monte Rosa, Italian Alps: Tongue Thickness and Volume Variations in the Second Half of the 20th Century. *Arctic Antarctic and Alpine Research*, 35 (2), 155-168.

Diolaiuti G., D'Agata C., Meazza A., Zanutta A. and Smiraglia C. (2009): Recent (1975–2003) changes in the Miage debris-covered glacier tongue (Mont Blanc, Italy) from analysis of aerial photos and maps. *Geografia Fisica Dinamica Quaternaria*, 32, 117–127.

Diolaiuti G., Maragno D., D'Agata C., Smiraglia C. and Bocchiola D. (2011): Glacier Retreat and Climate Change: documenting the last fifty years of Alpine glacier history from area and geometry changes of Dosdè Piazzi glaciers (Lombardy-Alps, Italy). *Progress in Physical Geography*, 35(2), 161-182.

Diolaiuti G., Bocchiola D., D'Agata C. and Smiraglia C. (2012a): Evidence of climate change impact upon glaciers' recession within the Italian Alps: the case of Lombardy glaciers. *Theoretical and Applied Climatology*, 109(3-4): 429-445.

Diolaiuti G., Bocchiola D., Vagliasindi M., D'Agata C. and Smiraglia C. (2012b): The 1975-2005 glacier changes in Aosta Valley (Italy) and the relations with climate evolution. *Progress in Physical Geography*, 36(6), 764-785.

Franzetti A., Tatangelo V., Gandolfi I., Bertolini V., Bestetti G., Diolaiuti G., D'Agata C., Mihalcea C., Smiraglia C. and Ambrosini R. (2013): Bacterial community structure on two alpine debris-covered glaciers and biogeography of *Polaromonas* phylotypes. *The ISME Journal*, 7, 1483-1492.

Fujita K. (2007): Effect of dust event timing on glacier runoff; sensitivity analysis for a Tibetan glacier. *Hydrological Processes*, 21, 2892–2896.

Fyffe C.L., Reid T.D., Brock B.W., Kirkbride M.P., Diolaiuti G., Smiraglia C. and Diotri F. (2014): A distributed energy-balance melt model of an alpine debris-covered glacier. *Journal of Glaciology*, 60(221), 587-602.

Gabbi J., Huss M., Bauder A., Cao F. and Schwikowski M. (2015): The impact of Saharan dust and black carbon on albedo and long-term mass balance of an Alpine glacier. *The Cryosphere*, 9, 1385-1400.

Gerbaux M., Genthon C., Etchevers P., Vincent, C. and Dedieu J.P. (2005): Surface mass balance of glaciers in the French Alps: distributed modeling and sensitivity to climate change. *Journal of Glaciology*, 51(175), 561-572.

Ginot P., Dumont M., Lim S., Patris N., Taupin J.D., Wagnon P., Gilbert A., Arnaud Y., Marinoni A., Bonasoni P. and Laj P. (2014): A 10 year record of black carbon and dust from a Mera Peak ice core (Nepal): variability and potential impact on melting of Himalayan glaciers. *The Cryosphere*, 8, 1479–1496.

Gobbi M., Isaia M. and De Bernardi F. (2011): Arthropod colonization of a debris-covered glacier. *Holocene*, 21, 343–349.

Immerzeel W.W., Van Beek L., Bierkens P.H. and Marc F.P. (2010): Climate change will affect the Asian water towers. *Science*, 328 (5984), 1382-1385.

IPCC (2013): Climate Change 2013 - The Physical Science Basis. Contribution of Working Group I to the Fifth Assessment Report of IPCC the Intergovernmental Panel on Climate Change.

Kayasha R., Takeuchi Y., Nakawo M. and Ageta Y. (2000): Practical prediction of ice melting beneath various thicknesses of debris cover on Kumbu Glacier, Nepal, using a positive degree-day factor, in: Debris-covered Glaciers: Proceedings of an International Workshop Held at the University of Washington in Seattle, Washington, USA, 13–15 September 2000, IAHS Publication 264,p. 289.

Kaser G., Großhauser M. and Marzeion B. (2010): Contribution potential of glaciers to water availability in different climate regimes. *Proceedings of the National Academy of Sciences*, 107, 20223-20227.

Kaspari S., Painter T.H., Gysel M., Skiles S.M. and Schwikowski M. (2014): Seasonal and elevational variations of black carbon and dust in snow and ice in the Solu-Khumbu, Nepal and estimated radiative forcings. *Atmospheric Chemistry and Physics,* 14, 8089–8103.

Kirkbride MP (1993): The temporal significance of transitions from melting to calving termini at glaciers in the central Southern Alps of New Zealand. *The Holocene*, 3(3), 232–240.

Kirkbride M.P. (2011): Debris-Covered Glaciers. In Singh P.; Singh V.P. & Haritashya U. K. (editors) *Encyclopedia of Snow, Ice and Glaciers*. Encyclopedia of Earth Sciences Series, Springer, 190-192.

Kopacz M., Mauzerall D.L., Wang J., Leibensperger E.M., Henze D.K. and Singh K. (2011): Origin and radiative forcing of black carbon transported to the Himalayas and Tibetan Plateau. *Atmospheric Chemistry and Physics*, 11(6), 2837-2852.

Irvine-Fynn T.D., Bridge J.W. and Hodson A.J. (2010): Rapid quantification of cryoconite: granule geometry and in situ supraglacial extents, using examples from Svalbard and Greenland. *Journal of Glaciology*, 56(196), 297-308.

Irvine-Fynn T.D., Bridge J.W. and Hodson A.J. (2011): In situ quantification of supraglacial cryoconite morphodynamics using time-lapse imaging: an example from Svalbard. *Journal of Glaciology*, 57(204), 651-657.

Lambrecht A. and Kuhn M. (2007): Glacier changes in the Austrian Alps during the last three decades, derived from the new Austrian glacier inventory. *Annals of Glaciology*, 46, 177-184.

Loomis S.R (1970): Morphology and ablation processes on glacier ice. Part 1, Morphology and structure of an ice-cored medial moraine, Kaskawulsh Glacier, Yukon, Arctic Institute of North America, Research Paper, 1–65, 1970.

Maisch M. (2000): The longterm signal of climate change in the Swiss Alps: glacier retreat since the end of the Little Ice Age and future ice decay scenarios. *Geografia Fisica Dinamica Quaternaria*, 23, 139-151.

Maragno D., Diolaiuti G., D'Agata C., Mihalcea C., Bocchiola D., Bianchi Janetti E., Riccardi A. and Smiraglia C (2009): New evidence from Italy (Adamello Group, Lombardy) for analysing the ongoing decline of Alpine glaciers. *Geografia Fisica Dinamica Quaternaria*, 32, 31-39.

Mattson L.E. and Gardner J.S. (1989): Energy exchange and ablation rates on the debris-covered Rakhiot Glacier, Pakistan. *Zeitschrift Für Gletscherkunde und Glazialgeologie,* 25(1), 17–32.

Menon S., Koch D., Beig G., Sahu S., Fasullo J. and Orlikowski, D. (2010): Black carbon aerosols and the third polar ice cap. *Atmospheric Chemistry and Physics*, 10(10), 4559-4571.

Mihalcea C., Mayer C., Diolaiuti G., Lambrecht A., Smiraglia C. and Tartari G. (2006): Ice ablation and meteorological conditions on the debris covered area of Baltoro Glacier, Karakoram (Pakistan). *Annals of Glaciology*, 43, 292–300.

Mihalcea C., Brock B., Diolaiuti G., D'Agata C., Citterio M., Kirkbride M.P., Cutlerb M.E.J. and Smiraglia C. (2008a): Using aster satellite and ground- based surface temperature measurements to derive supraglacial debris cover and thickness patterns on Miage Glacier (Mont Blanc Massif, Italy). *Cold Regions Science and Technology,* 52, 341–354.

Mihalcea C., Mayer C., Diolaiuti G., Lambrecht A., Smiraglia C. and Tartari G. (2008b): Ice ablation and meteorological conditions on the debris-covered area of Baltoro glacier, Karakoram, Pakistan. *Annals of Glaciology*, 43, 292-300.

Ming J., Cachier H., Xiao C., Qin D., Kang S., Hou S. and Xu J. (2008): Black carbon record based on a shallow Himalayan ice core and its climatic implications. *Atmospheric Chemistry and Physics*, 8(5), 1343-1352.

Ming J., Xiao C., Cachier H., Qin D., Qin X., Li Z. and Pu J. (2009): Black Carbon (BC) in the snow of glaciers in west China and its potential effects on albedos. *Atmospheric Research*, 92(1), 114-123.

Minora U.F., Senese A., Bocchiola D., Soncini A., D'Agata C., Ambrosini R., Mayer C., Lambrecht A., Vuillermoz A., Smiraglia C. and Diolaiuti G. (2015): A simple model to evaluate ice melt over the ablation area of glaciers in the Central Karakoram National Park, Pakistan. *Annals of Glaciology*, 56 (70), 202-216.

Nakawo M. and Young G.J. (1981): Field experiments to determinate the effect of a debris layer on ablation of glacier ice. *Annals of Glaciology*, 2, 85–91.

Oerlemans J., Giesen R.H. and Van Der Broeke M.R. (2009): Retreating alpine glaciers: increased melt rates due to accumulation of dust (Vadret da Morteratsch, Switzerland). *Journal of Glaciology*, 55(192), 729-736.

Østrem G. (1959): Ice melting under a thin layer of moraine and the existence of ice in moraine ridges. *Geografiska Annaler*, 41, 228–230.

Owen L.A. and Derbyshire E. (1993): Quaternary and Holocene intermontane basin sedimentation in Karakoram Mountains. In Shroder J.F eds. Himalaya to the Sea. Routledge, London.

Painter T., Deems J., Belnap J., Hamlet A., Landry C. and Udall B. (2010): Response of Colorado River runoff to dust radiative forcing in snow. *Proceedings of the National Academy of Sciences*, 10, 6603–6615.

Painter T.H., Flanner M.G., Kaser G., Marzeion B., Van Curen R.A. and Abdalati W. (2013): End of the Little Ice Age in the Alps forced by industrial black carbon. *Proceedings of the National Academy of Sciences*, 110 (38), 15216-15221.

Paul F., Kääb A., Maisch M., Kellenberger T.W. and Haeberli W. (2004): Rapid disintegration of Alpine glaciers observed with satellite data. *Geophysical Research Letters*, 31, L21402.

Paul F., Frey H. and Le Bris R. (2011): A new glacier inventory for the European Alps from Landsat TM scenes of 2003: challenges and results. *Annals of Glaciology*, 52(59), 144-152.

Rabatel A., Dedieu J. P. and Vincent C. (2005): Using remote-sensing data to determine equilibrium-line altitude and mass-balance time series: validation on three French glaciers, 1994–2002. *Journal of Glaciology,* 51(175), 539-546.

Racoviteanu A.E., Williams M.W. and Barry R.G. (2008a): Optical remote sensing of glacier characteristics: A review with focus on the Himalaya. *Sensors*, 8(5), 3355-3383.

Racoviteanu A.E., Arnaud Y., Williams M.W. and Ordonez J. (2008b): Decadal changes in glacier parameters in the Cordillera Blanca, Peru, derived from remote sensing. *Journal of Glaciology*, 54(186), 499-510.

Ramanathan V. and Carmichael G. (2008): Global and regional climate changes due to black carbon. *Nature Geoscience*, 1, 221-227.

Reid T.D., Carenzo M., Pellicciotti F. and Brock B.W. (2012): Including debris cover effects in a distributed model of glacier ablation. *Journal of Geophysical Resources*, 117, D18.

Scherler D., Bookhagen B. and Strecker M.R. (2011): Spatially variable response of Himalayan glaciers to climate change affected by debris cover. *Nature Geosciences*, 4, 156-159.

Skiles S., Painter T., Deems J., Bryant A.C. and Landry C. (2012): Dust radiative forcing in snow of the Upper Colorado River Basin: 2. Interannual variability in radiative forcing and snowmelt rates. *Water Resources Research*, 48, W07522.

Smiraglia C., Azzoni R.S., D'Agata C., Maragno D., Fugazza D. and Diolaiuti G.A. (2015): The evolution of the Italian glaciers from the previous database to the New Italian Inventory. Preliminary considerations and results. *Geografia Fisica Dinamica Quaternaria*, 38(1), 79-87.

Sodemann H., Palmer A.R., Schwierz C., Schwikowski M. and Vernli H. (2006): The transport history of two Saharan dust events archived in an Alpine ice core. *Atmospheric Chemistry and Physics*, 6, 667-688.

Soncini A., Bocchiola D., Confortola G., Bianchi A., Rosso R., Mayer C., Lambrecht A., Palazzi E., Smiraglia C. and Diolaiuti G. (2015): Future hydrological regimes in the upper Indus basin: a case study from a high altitude glacierized catchment. *Journal of Hydrometeorology*, 16, 306-325.

Soncini A., Bocchiola D., Salerno F., Viviano G., Minora U., Senese A., Smiraglia C. and Diolaiuti G. (2016): Future hydrological regimes and glacier cover in the Everest region: the case study of the Dudh Koshi basin. *Science of the Total Environment*, 565, 1084-1101.

Stokes C.R., Popovnin V., Aleynikov A., Gurney S.D. and Shahgedanova M. (2007): Recent glacier retreat in the Caucasus Mountains, Russia, and associated increase in supraglacial debris cover and supra-/proglacial lake development. *Annals of Glaciology*, 46,195–203.

Takeuchi N., Kohshima S. and Seko K. (2001): Structure, formation, darkening process of albedo reducing material (cryoconite) on a Himalayan glacier: a granular algal mat growing on the glacier. *Arctic, Antarctic, and Alpine Research*, 33, 115-122.

Takeuchi N. and Li Z. (2008): Characteristics of Surface Dust on Urumqi Glacier No. 1 in the Tien Shan Mountains, China. *Arctic, Antarctic and Alpine Research*, 40(4), 744-750.

Takeuchi N., Nagatsuka N., Uetake J. and Shimada R. (2014): Spatial variations in impurities (cryoconite) on glaciers in northwest Greenland. *Bulletin of Glaciological Research*, 32, 85-94.

Takeuchi N. (2002): Optical characteristics of cryoconite (surface dust) on glaciers: the relationship between light absorbency and the property of organic matter contained in the cryoconite. *Annals of Glaciology*, 34, 409-414.

Thevenon F., Anselmetti F.S., Bernasconi S.M. and Schwikowski M. (2009): Mineral dust and elemental black carbon records from an Alpine ice core (Colle Gnifetti glacier) over the last millennium. *Journal of Geophysical Research: Atmospheres*, 114,(D17).

Turchetti B., Goretti M., Branda E., Diolaiuti G., D'Agata C., Smiraglia C., Onofri A. and Buzzini P. (2013): Influence of abiotic parameters on culturable yeast diversity in two distinct Alpine glaciers. *FEMS Microbiology Ecology*, 86(2), 327-340.

Vezzola L.C., Diolaiuti G.A., D'Agata C., Smiraglia C. and Pelfini M. (2016): Assessing glacier features supporting supraglacial trees: A case study of the Miage debris-covered Glacier (Italian Alps). *The Holocene*, 26(7), 1138-1148.

Yasunari T.J., Bonasoni P., Laj P., Fujita K., Vuillermoz E., Marinoni A., Cristofanelli P., Duchi R., Tartari G. and Lau K.M. (2010): Estimated impact of black carbon deposition during pre-monsoon season from Nepal Climate Observatory–Pyramid data and snow albedo changes over Himalayan glaciers. *Atmospheric Chemistry and Physics,* 10(14), 6603-6615.

Xu B., Cao J., Joswiak D.R., Liu X., Zhao H. and He J. (2012): Post-depositional enrichment of black soot in snow-pack and accelerated melting of Tibetan glaciers. *Environmental Research Letters*, 7(1), 014022.

Zemp M., Paul F., Hoelzle M. and Haeberli W. (2008): Glacier fluctuations in the European Alps 1850–2000: an overview and spatio-temporal analysis of available data. In: Orlove, B., Wiegandt, E. and B. Luckman (eds.): The darkening peaks: Glacial retreat in scientific and social context. University of California Press: p. 152–167.

Zemp M., Frey H., Gärtner-Roer I., Nussbaumer S.U., Hoelzle M., Paul F., Haeberli W., Denzinger F., Ahlstroem A.P., Anderson B., Bajracharya S., Baroni C., Braun L.N., Caceres B.E., Casassa G., Cobos G., Davila L.R., Delgado Granados H., Demuth M.N., Espizua L., Fischer A., Fujita K., Gadek B., Ghazanfar A., Hagen J.O., Holmlund P., Karimi N., Li Z., Pelto M., Pitte P., Popovnin V.V., Portocarrero C.A., Prinz R., Sangewar C.V., Severskiy I., Sigurdsson O., Soruco A., Usubaliev R. and Vincent C. (2015): Historically unprecedented global glacier decline in the early 21st century. *Journal of Glaciology*, 61(228), 745-762.

Chapter 1
The evolution of debris mantling glaciers in the Stelvio Park (Italian Alps) over the time window 2003-2012 from high-resolution remote-sensing data

Chapter submitted to Progress in Physical Geography

Azzoni R.S., Fugazza D., Zerboni A., Senese A., D'Agata C., Maragno D., Carzaniga A., Cernuschi M. and Diolaiuti G.A. – The evolution of debris mantling glaciers in the Stelvio Park (Italian Alps) over the time window 2003-2012 from high-resolution remote-sensing data.

Abstract

Over the last decades, the expansion of supraglacial debris on worldwide mountain glaciers has been reported. Nevertheless, works dealing with the detection and mapping of quite continuous supraglacial debris and deep analyses aimed at identifying the temporal and spatial trends affecting glacier debris cover are still limited. In this study, we present a high-resolution detection and mapping of quite continuous debris mantling glaciers in the Ortles-Cevedale Group (Stelvio Park, Italy), one of the most representative glacierized sectors of the European Alps. These analyses are based on a maximum likelihood classification applied to high-resolution (pixel size 0.5 m x 0.5 m), aerial color orthophotos acquired during the summer season in the years 2003, 2007, and 2012. We performed tests to evaluate the feasibility of our method and they found our approach able to detect and map debris with an error minor than ± 5%. Our findings suggest that over the period 2003–2012, supraglacial debris cover increased from 16.71% to 30.10% of the total glacierized area. Differences in the covering rates of glaciers were found, mainly driven by the different lithologies featured by the glacial basins; in fact, each lithotype has different susceptibility to physical weathering. In addition, we focused on the largest ice body of this mountain group, the Forni Glacier, analyzing the evolution of the ablation tongue in the period 2003–2015 from aerial and UAV orthophotos. This deeper analysis permitted to confirm that quite continuous debris is enlarging at the glacier melting surface. Finally, we also analysed Landsat ETM+ imagery acquired in 2003, 2007, and 2011 to check their suitability for mapping debris on small glaciers as the ones in the Italian Alps. The results we obtained show no meaningful changes in the debris coverage, thus suggesting that the resolution (pixel size: 30 m x 30 m) of these data is too low to permit to detect debris cover area changes at this scale.

1.1. Introduction

One of the most evident effects of the ongoing climate change, and in particular of the global air temperature warming, is the intense area decrease of glaciers observed worldwide (Dyurgerov and Meier, 2000; IPCC, 2013). Over the last 50 years, for instance, Italian glaciers experienced a dramatic shrinkage (Diolaiuti et al., 2011; 2012a; 2012b; Smiraglia et al., 2015), which is comparable in magnitude and rates with observations of glaciers evolution in other Alpine regions and most of the glacierized mountain groups of the Planet (Zemp et al., 2008; Paul et al., 2011; Maurer et al., 2016). Moreover, the glacier surface undergoes important physical changes: several authors have reported the areal expansion of supraglacial debris cover over the last decades in major mountain ranges, including the Alps (Kellerer-Pirklbauer, 2008), Caucasus (Popovnin and Rozova, 2002; Stokes et al., 2007), Himalaya (Bolch et al., 2008; Shukla et al., 2009), Karakoram (Gibson et al., 2016), and Southern Alps of New Zealand (Kirkbride, 1993).

Glacier darkening is favored by the increased availability of debris in the area surrounding glaciers (Reid et al., 2012). This large presence of debris is related to the ongoing intensification of rock-degradation and macrogelivation (O'Connor and Costa, 1993; Evans and Clague, 1994; Haeberli, 1996; Haeberli et al., 1997; Barla et al., 2000; Deline, 2001; Huggel et al., 2005; Chiarle et al., 2007; Gruber and Haeberli, 2007; Ravanel and Deline, 2008; Diolaiuti et al., 2009). Rock falls and rock avalanches, which have been playing a crucial role in supplying and enlarging the rock-debris layer at the surface of Alpine glaciers, are mainly due to de-buttressing of adjacent rock walls by ice-surface lowering and permafrost degradation, both these processes are driven by climate warming. Moreover, the ongoing reduction in glacier surface also contributes to the progressive debris covering of glaciers (Pelfini et al., 2012).

The high-resolution mapping and analysis of the spatial and temporal evolution of supraglacial debris are complicated, but the knowledge of continuous supraglacial debris for the glacier mass and energy

budgets, and evolution is relevant (østrem, 1959; Nakawo and Young, 1981; D'Agata and Zanutta, 2007; Diolaiuti et al., 2009. Yet, also fine and sparse debris impacts on glacier albedo and ice melt rate in a no negligible way (Azzoni et al., 2016). In fact, debris is one of the main forcing factors of supraglacial albedo and may reduce ice melt rate in relation to its thickness, lithological, and physical properties (Mattson and Gardner, 1989; Mihalcea et al., 2006, Fugazza et al., 2016). Moreover, debris is one of the principal components of biological and geochemical cycles in glacierized areas, hosting vegetation (Caccianiga et al., 2011; Pelfini et al., 2012, Vezzola et al., 2016), arthropods (Gobbi et al., 2011), yeasts (Turchetti et al., 2013), active microbial communities (Franzetti et al., 2016a; 2016b), and meiofauna (Azzoni et al., 2015) that may play an important role in the modification and evolution of debris cover.

Several semi-automatic approaches based on medium-resolution remote sensing data were developed to assess the occurrence and distribution of continuous supraglacial debris covers; these methods applied a combination of radiometric (e.g. visible or infrared channel) and morphometric (e.g. DEM; Shukla et al., 2010) data. Among the others, Paul et al. (2004) estimated the debris cover of a Swiss glacier combining multispectral image classification from Landsat TM, ASTER, and SPOT satellite with data from a high-resolution digital elevation models (DEM). Mihalcea et al. (2008a; 2008b) described supraglacial debris occurrence and thickness on the Miage (Italian Alps) and the Baltoro (Central Karakoram, Pakistan) glaciers analyzing ASTER kinetic temperatures data. Veetil (2012) mapped the supraglacial debris cover of the Baltoro Glacier (Karakoram, Pakistan) using Landsat TM and ETM+, and a digital elevation model (SRTM) with different semi-automatic methods. More recently, Minora et al. (2015) applied the same approach using 2011 Landsat TM thermal data and deriving the supraglacial debris thickness distribution on a wide and representative glacierized area encompassing the whole Central Karakoram National Park (Pakistan). Furthermore, the same authors applied the image classification to the 2011 Landsat TM panchromatic data to describe the occurrence and pattern of supraglacial debris (Minora et al., 2016). Sasaki et al. (2016) compiled a global map of

debris on glaciers derived from multi-temporal ASTER images. Finally, Maurer et al. (2016) used Landsat ETM+ and declassified spy images from the Hexagon program for quantifying the debris occurrence in the Eastern Himalaya.

However, the accuracy of methods based on medium resolution satellite images decreases analyzing small ice bodies such as Alpine glaciers (Paul et al., 2013). Fugazza et al., 2015 proposed the use of unmanned aerial vehicles (UAVs), which allow high-resolution and low-cost investigations of supraglacial conditions. However, these studies mapped only on small portions of few glaciers and the issue of detailed debris cover quantification is still open. In this paper, we propose a method to map and describe the almost continuous supraglacial debris cover on glaciers in a representative sector of the Alps (Ortles-Cevedale Group, Stelvio Park) through multi-temporal and high-resolution remote sensing data (aerial color orthophotos). These methods permitted us to analyze the evolution of supraglacial debris over the last decade.

1.1.1. Study Area

The focus of this research is the Lombardy Sector of the Stelvio Park, whose glaciers belong to the Ortles-Cevedale Group: 51 glaciers are located in this mountain region, covering ca. 29.27 km^2 (2007 data, see: D'Agata et al., 2014; Smiraglia et al., 2015). These glaciers have significantly retreated over the past decades, losing about the 40 % of their surface between 1954 and 2007 (D'Agata et al., 2014). The widest ice body of the area is the Forni Glacier, which covers ca. 11.34 km^2, thus representing the second widest glacier of the Italian Alps and one of the most studied Italian ice bodies (Senese et al., 2012a; 2012b; 2014). On this glacier, high-resolution analyses of fine and sparse supraglacial debris were conducted by Azzoni et al. (2016).

The Ortles-Cevedale area is geologically heterogeneous, with a close contact between sedimentary and metamorphic rocks (see the geological map by Montrasio et al., 2008). In particular, the Zebrù Tectonic Line separates Pre-Permian micaschist and paragneiss, in the Southern area, from the Rhaetian dolomite and limestone, outcropping in the Northern part of the region (Montrasio et al.,

2008). The local bedrock and the debris originating from it exhibit different colors, which has different effects on the albedo (Hall et al., 2005); metamorphic rocks are mostly dark grey, brown, or reddish brown, whereas sedimentary rocks feature a light gray to whitish color.

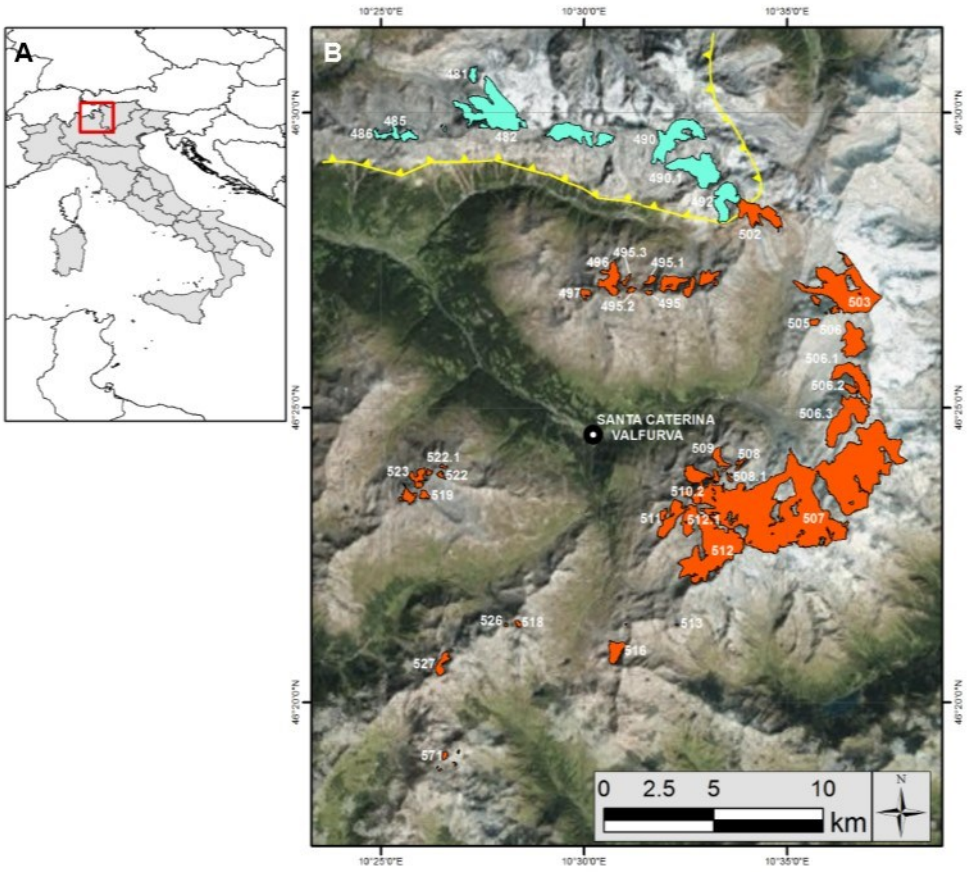

Fig. 1: (A) Location map of the studied glaciers (Stelvio Park, Ortles-Cevedale Group, Lombardy Sector, Italian Alps). (B) Google Earth™ imagery indicating glaciers considered in this study (with 2012 glacier limits); glaciers lying on metamorphic bedrock are in orange, whereas those lying on sedimentary bedrock are in light blue. The yellow line indicates the Zebrù Tectonic Line that divides sedimentary bedrocks in the North from metamorphic bedrocks in the South. The numbers refer to glaciers reported in Tab.7.

1.2. Material and methods

1.2.1. Remotely-sensed data and glacier outlines

We analyzed aerial color orthophotos acquired in the years 2003, 2007, and 2012. Orthophotos are purchasable products (BLOM-CGR SPA - flight code IT2000) and feature a pixel resolution of 0.5 m

x 0.5 m. The flights were performed during the summer season (when the snow coverage is at its minimum) in days featuring an almost negligible cloud cover.

In addition, we analyzed Landsat ETM+ imagery (30 m x 30 m pixel resolution) acquired on 16 September 2003, 26 August 2007, and 21 August 2011. In the 2012 summer season, no cloud-free images of the Ortles-Cevedale Group are available; therefore, we analyzed a Landsat scene from the previous year.

In this study, we focused on the largest ice body of the study area, the Forni Glacier; for a detailed investigation of its ablation tongue we used, in addition to aerial orthophotos, two orthophotos from UAV flights performed in 2014 and 2015 featuring a spatial resolution of 0.15 m x 0.15 m (for further details see: Fugazza et al., 2015).

Among glaciers belonging to the Ortles-Cevedale Group, we considered 63 ice bodies covering 31.58 km^2 in 2003, 51 glaciers covering 29.27 km^2 in 2007 and 60 glaciers covering 27.08 km^2 in 2012. The different number of glaciers considered in the three years is due to the extinction of the smallest ice bodies and the fragmentation of glaciers in two (or three) smaller ice bodies. Glacier outlines were available from previous works (Diolaiuti et al., 2012a; D'Agata et al., 2014; Smiraglia et al., 2015).

In the timeframe of our analysis, the ice bodies of the Lombardy sector of Stelvio Park retreated by 11.94% (which rises up to 14% considering only the glaciers common to the three years of analyses).

1.2.2. Supervised classification of orthophotos and accuracy

The evaluation of supraglacial debris cover based on the orthophotos was performed by means of a supervised classification through ArcMap software. In particular, we used the maximum likelihood classification to discriminate four different classes and form a signature file: debris, ice, snow, and shadow. The reason behind adopting a specific class for shadow is to remove these areas from the subsequent analysis; in fact, it is not possible to investigate efficiently their surface conditions.

The chromatic difference between the two main lithotypes outcropping in the area could be problematic for the maximum likelihood classification, due to the different colors of supraglacial debris: to avoid this problem, we used a different classification scheme in relation to the two different lithologies. Moreover, to avoid some classification problems due to the different illumination conditions of the orthophotos in distinct years, we created a different signature file for each orthophoto. The training areas were chosen on glaciers where field activities have been performed over the last years and whose surface conditions are well known.

To assess the accuracy of the supervised classification, we defined separate sets of random points in the adopted software: 120 random points in 2003, 106 in 2007, and 79 in 2012. We manually checked the conformity between the predicted values from the supervised classification (i.e. debris, ice, snow, and shadow) and the observed ones in the orthophotos. In this way, we were able to assess the overall precision of the method and the one of every single class according to Fitzgerald and Lees, 1994:

(1) $$overall\ accuracy = \frac{number\ of\ correct\ predictions}{total\ number\ of\ point}$$

Moreover, to better assess the potential error affecting the mapping of glacier boundaries and classified areas, we applied the method developed by Vögtle & Schilling (1999) and adopted, among the others, on Alpine (Diolaiuti et al., 2012a; 2012b; Smiraglia et al., 2015) and Karakoram glaciers (Minora et al., 2016). The area precision for each glacier and for each surface was evaluated by buffering the surface perimeter, considering the area uncertainty (half the resolution of the image pixel, in our case 0.5 m). The final precision of the whole outlines was determined by taking the root of the squared sum of all the buffer areas.

Finally, we performed the debris cover quantification on Landsat TM and ETM+ imagery. To investigate the surface characteristics, we calculated a TM4/TM5 band ratio and used a threshold of two to discriminate ice from supraglacial debris (see for details: Paul et al., 2004). We assess the potential error of the classified areas applying the Vögtle & Schilling (1999) method.

1.3. Results

1.3.1. Definition of surface properties over the whole region

We classified the different types of glacier surfaces (debris, ice, snow, and shadow) in 2003, 2007, and 2012 based on the high-resolution orthophotos.

The analysis of the 2003 orthophotos (Tab. 1) highlights that debris covered 16.71% (5.28 km^2 ± 0.01% of the total glacierized area (31.58 km^2 ± 0.01%)); bare ice covered 48.12% (15.20 km^2 ± 0.01%) of the whole area, and snow 16.89% (5.33 km^2 ± 0.01%) of the total. These orthophotos showed a non-negligible occurrence of shadows (18.28%, 5.77 km^2 of the area), because the images were acquired in late summer, when the solar zenithal angle is wide. However, shadows did not affect the debris quantification significantly, because they are mostly located at high elevation relative to glaciers (in the accumulation basins), where the presence of debris is scarce or completely lacking. The debris cover is not homogenously distributed; most of the debris-covered areas (64.24% of the total; Tab. 1) are located in regions featuring a dominant metamorphic lithology. However, this is simply due to metamorphic rocks being the most common lithology of the area, covering about 400 km^2 against ca. 100 km^2 covered by sedimentary bedrock.

If we discern the debris cover of the two lithologies (Tab. 1), we find that on glaciers resting on metamorphic rocks, the debris cover is ca. 13.47% of the total (3.39 km^2). Conversely, on glaciers belonging to the sedimentary domain, debris is more common, covering ca. 29.44% (1.89 km^2) of the total area of these ice bodies.

	GLACIERS located on SEDIMENTARY BEDROCK (km^2)	**GLACIERS located on METAMORPHIC BEDROCK** (km^2)	**TOTAL** (km^2)	**TOTAL** (%)
TOTAL AREA	6.41	25.17	31.58	100.00
DEBRIS- COVERED	1.89	3.39	5.28	16.71

AREA				
BARE ICE AREA	2.98	12.22	15.20	48.12
SNOW-COVERED AREA	1.03	4.31	5.33	16.89
SHADOW AREA	0.52	5.25	5.77	18.28

Tab. 1: ***Surface properties of the considered glaciers in 2003; data derived from the maximum likelihood classification applied to color orthophotos***

In 2007, the condition of the glaciers surface was the following (Tab. 2): debris covered 22.54% (6.59 $km^2 \pm 0.01\%$) of the total glacierized area (29.25 $km^2 \pm 0.01\%$), bare ice covered 35.04% (10.25 $km^2 \pm$ 0.01%) of the total area, and the snow mantle was 37.01% of the area (10.82 $km^2 \pm 0.01\%$). However, snow is located mainly in the accumulation areas, where the debris cover is negligible or absent, thus not affecting the results of our analysis. Shadows covered only 5.41% of the total area. The debris mantle is largely due to glaciers surrounded by metamorphic rocks (65.32% of the total debris cover); nevertheless, considering only the glacierized area on metamorphic rocks, the percentage of debris over the total is equal to 18.40%. Conversely, debris is more common in areas with sedimentary rocks, where it amounts to 39.14% of the total area.

	GLACIERS located on SEDIMENTARY BEDROCK (km^2)	**GLACIERS located on METAMORPHIC BEDROCK** (km^2)	**TOTAL** (km^2)	**TOTAL** (%)
TOTAL AREA	5.84	23.43	29.25	100.00
DEBRIS- COVERED AREA	2.29	4.31	6.59	22.54
BARE ICE AREA	2.16	8.09	10.25	35.04
SNOW-COVERED AREA	1.17	9.66	10.82	37.01
SHADOW AREA	0.23	1.35	1.58	5.41

Tab. 2: Surface properties of the considered glaciers in 2007; data derived from the maximum likelihood classification applied to color orthophotos.

In 2012 (Tab. 3), debris covered 30.08% (8.15 km^2 ± 0.01%) of the total glacierized area (27.08 km^2 ± 0.01%). Bare ice covered 48.15% (13.04 km^2 ± 0.01%) of the whole area and snow mantled 18.28% (4.95 km^2 ± 0.01%) of the total area. In this year, the presence of shadows is limited (3.49 %). The debris cover is 27.57% of the total area of glaciers laying on a metamorphic bedrock, whereas it covers 40.11 % of the total area of the glaciers on the sedimentary bedrock.

	GLACIERS located on SEDIMENTARY BEDROCK (km^2)	**GLACIERS located on METAMORPHIC BEDROCK** (km^2)	**TOTAL** (km^2)	**TOTAL** (%)
TOTAL AREA	5.41	21.68	27.08	100.00
DEBRIS- COVERED AREA	2.17	5.97	8.15	30.08
BARE ICE AREA	1.97	11.07	13.04	48.15
SNOW-COVERED AREA	1.00	3.95	4.95	18.28
SHADOW AREA	0.27	0.68	0.95	3.49

Tab. 3: Surface properties of considered glaciers in 2012; data derived from the maximum likelihood classification applied to color orthophotos.

The analyses performed on the Landsat TM and ETM+ imagery, and in particular the TM4/TM5 band ratio we applied using a threshold of 2 (following Paul et al. 2004), permitted to map ice and supraglacial debris. This method shows a debris cover of 17.11% in 2003 (5.42 km^2 ± 0.01%), 15.49% in 2007 (4.55 km^2 ± 0.01%), and 17.62% in 2011 (4.81 km^2 ± 0.01%) (Tab.4). Despite of the different resolution of orthophotos and Landsat images (0.5 x 0.5 m and 30 x 30 m, respectively), the results are rather similar for the year 2003 (16.71% from orthophotos and 17.11% from Landsat image). However, regarding 2007 and 2011 data, the debris-covered area is lower if based on Landsat image compared to orthophotos (15.49% and 22.54%, respectively for the 2007; 17.62% and 30.08% in 2011).

DATE OF ACQUISITION	BARE ICE AREA (km^2)	DEBRIS (km^2)	TOTAL AREA (km^2)	DEBRIS COVER (% with respect to the total glacierized area)
16/09/2003	26.25	5.42	31.67	17.11%
26/08/2007	24.85	4.55	29.40	15.49%
06/09/2011	22.47	4.81	27.28	17.62%

Tab. 4: Debris cover of Ortles-Cevedale glaciers; data derived from Landsat TM4/TM5 band ratio.

1.3.2. The Forni Glacier tongue

On Forni Glacier ablation tongue, where we extent our analysis also to 2014 and 2015, the measured debris cover was ca. 27% in 2003, 32% in 2007, 51% in 2012, 48% in 2014, and 47% in 2015 (Tab.5). No shadows were evident in 2014 and 2015 and snow did not cover the glacier tongue in 2012 and 2014.

	DEBRIS-COVERED AREA (km^2)	BARE ICE AREA (km^2)	SNOW-COVERED AREA (km^2)	SHADOW AREA (km^2)	TOTAL ABLATION TONGUE AREA (km^2)	DEBRIS COVER (% with respect to the total tongue area)
2003	0.31	0.65	0.13	0.07	1.16	26.72
2007	0.34	0.55	0.15	0.01	1.05	32.38
2012	0.47	0.45	-	0.01	0.92	51.09
2014	0.39	0.42	-	-	0.81	48.15
2015	0.33	0.35	0.02	-	0.70	47.14

Tab. 5: Surface features of the Forni Glacier tongue in the time window 2003–2015; data derived from the maximum likelihood classification applied to color orthophotos. Note that 2014 and 2015 orthophotos were derived from UAV flights and thus feature a higher resolution.

1.3.3. Error assessment

To assess the error affecting results from the maximum likelihood classification, we manually checked the correct classification of the surface on the orthophotos (according to approach applied by Fitzgerald and Lees, 1994), comparing it to the supervised classification for a random set of points

generated via ArcMap (305 points in total). This type of error assessment is made possible by the high resolution of the images and the many studies available for the area (see: Senese et al., 2012a; 2012b; 2014; 2016; Fugazza et al., 2015; 2016; Azzoni et al., 2016). The overall precision of this supervised classification resulted in 0.87 (see the error matrix in Tab. 6), but the precision of debris classification (i.e., the ability of the classification to detect the differences between debris and the other surfaces) is higher, up to 0.95.

The high precision of this method is mainly due to the application of two different classifications for the different lithologies, which prevents some misclassification between ice and sedimentary debris characterized by a comparable color. Moreover, the creation of proper training areas and a proper signature file for each year of analysis can prevent the misclassification of the surface typology introduced by the different optical characteristics of orthophotos (different cameras, brightness, contrast, and acquisition time). In addition, the precision in the classification of ice and shadows is high (0.91 and 0.97, respectively). The lowest precision of this method was noticed in the classification of snow; this is due to the similar spectral characteristics of snow, ice, and firn. However, the distinction between ice and snow is not critical for this study and does not affect the debris cover quantification. Snow, in fact, mainly covers the accumulation basins, where the occurrence of debris is negligible.

Moreover, we performed the error assessment following Vögtle & Schilling (1999). In spite of the high fragmentation of the classified surfaces but thanks to the very high quality and resolution of the orthophotos, the error in the classification of the area of each class (snow, debris, ice and shadow) is lower than ± 0.03%. Furthermore, also the error of the glacier limit is negligible (± 0.03%).

	PREDICTED BY SUPERVISED CLASSIFICATION ON ORTHOPHOTOS	MANUAL CLASSIFICATION			
		DEBRIS COVER	BARE ICE	SNOW COVER	SHADOW
DEBRIS COVER	98	94	3	0	1
BARE ICE	119	5	90	24	0
SNOW COVER	52	0	6	46	0
SHADOW	36	0	0	0	36
TOTAL	305	99	99	70	37

Tab. 6: Error matrix for the maximum likelihood classification applied in this study: on the left the number of points for each type of glacier surface predicted by the classification on the orthophotos 2003, 2007 and 2012, and on the right the surface conditions obtained by a manual classification (with the respective number of points). The control points were chosen randomly via ArcMap.

1.4. Discussion

1.4.1. The evolution of debris cover

Our analysis suggests that glacier area in the Lombardy sector of the Stelvio Park over the period 2003–2012 decreased by 11.94%, at a rate of 0.50 km^2 per year. The area decrease rises up to 14%, if we examine the subset of glaciers reported in all the three years considered, which excluded the disappeared glacial bodies (for a detailed discussion see D'Agata et al., 2014).

Over the same period, if we consider all the glaciers located in the Ortles-Cevedale Group, we notice a clear increase in debris cover (Tab. 7, Fig. 2 and 3). In particular, the area covered by rock debris was 16.72% of the total in 2003, 22.54% in 2007, and 30.10% in 2012. The area went from 5.28 km^2 in 2003, to 6.59 km^2 in 2007, to 8.15 km^2 in 2012, displaying a rate of increase of 0.32 km^2 per year. These values are consistent with the mean debris-covered area reconstructed in the Alps (26.1%) by means of ASTER images over the period 2009–2013 (Sasaki et al., 2016).

	2003	2007	2012
TOTAL DEBRIS- COVERED AREA (km^2)	5.28	6.59	8.15
SEDIMENTARY DEBRIS-COVERED AREA (km^2)	1.89	2.29	2.17
METAMORPHIC DEBRIS-COVERED AREA (km^2)	3.39	4.31	5.97
AREA OF GLACIERS located on SEDIMENTARY BEDROCK (km^2)	6.41	5.84	5.41
AREA OF GLACIERS located on METAMORPHIC BEDROCK (km^2)	25.17	23.43	21.67
AREA OF ALL GLACIERS (km^2)	31.58	29.24	27.08
DEBRIS COVER (%)	16.72	22.54	30.10

Tab. 7: Surface features of all the glaciers located in the Ortles-Cevedale Group in the time frame 2003-2012 derived from the maximum likelihood classification applied to the color orthophotos.

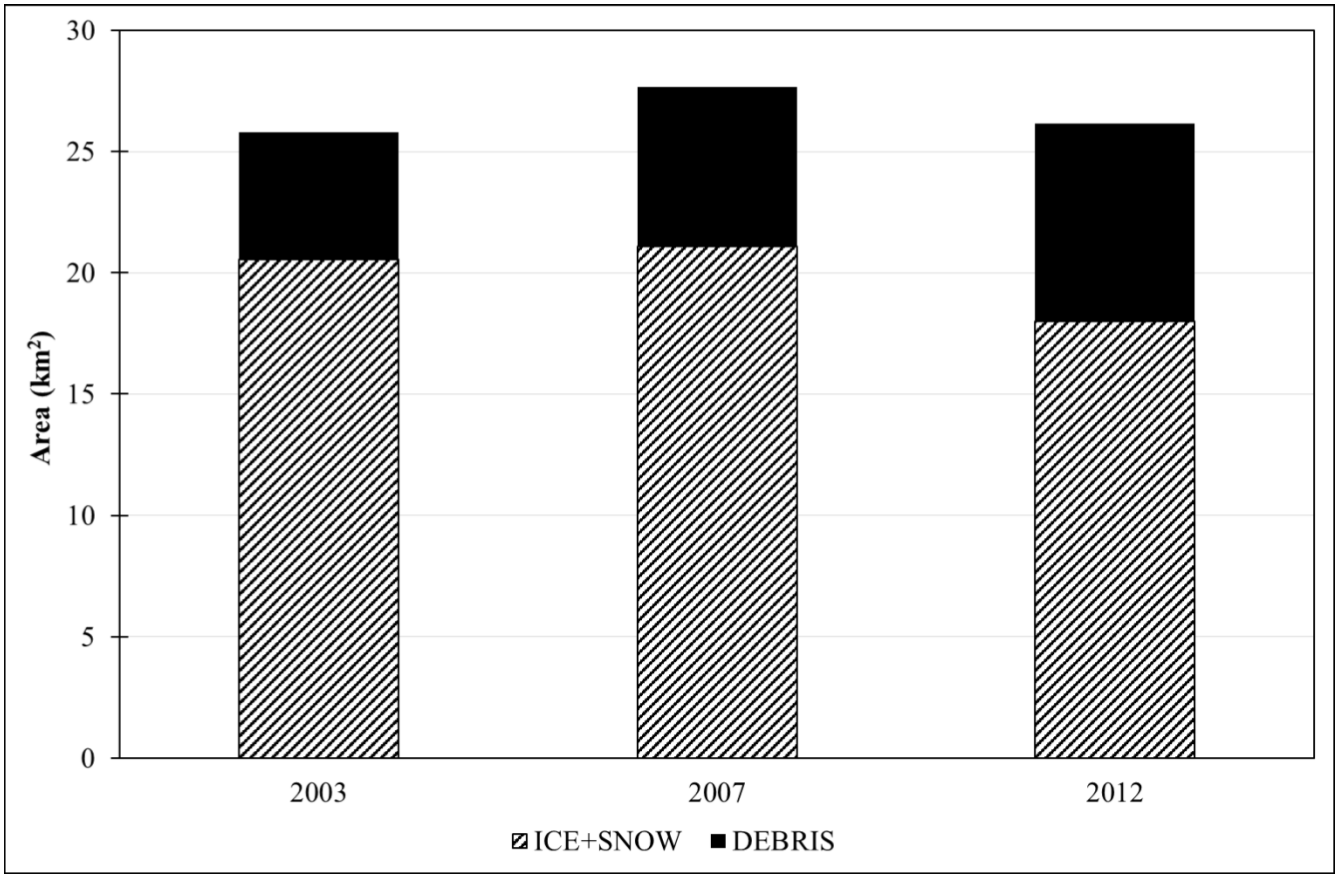

Fig. 2: Evolution of supraglacial debris cover on glaciers in the Ortles-Cevedale Group

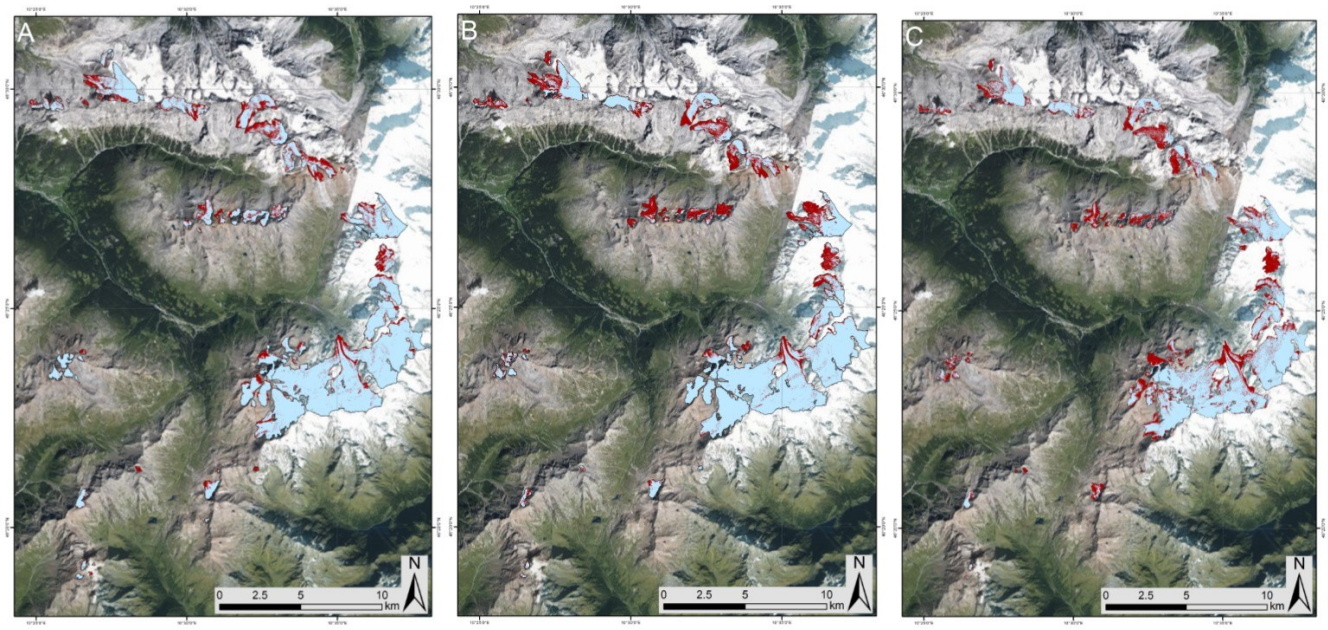

Fig. 3: Evolution of debris on the glaciers of the Ortles-Cevedale Group in 2003 (A), 2007 (B), and 2012 (C). The glaciers area is represented in light blue, the debris cover in red.

In addition, we considered only glaciers reported both in the 2003 and 2012 database and not subjected to fragmentations, which could have modified the trend in the evolution of debris cover (Tab. 8). We therefore took into account 38 glaciers, covering 28.41 km ^{2} in 2003 and 24.85 km ^{2} in 2012 (with a reduction of about 13%). On most of the ice bodies, debris cover is clearly increased, reaching in 2012 a mean value of 30.2%. Only one glacier, Gran Zebrù I, shows a reduction of the debris cover from 53.2% (0.46 km^2) in 2003, to 30.4% (0.19 km^2) in 2012. This is probably due to the complete melting of a wide debris-covered area.

	GLACIER CODE	NAME	2003 AREA COVERED BY DEBRIS (%)	2012 AREA COVERED BY DEBRIS (%)
SEDIMENTARY BEDROCK	481	Platigliole	16.4%	71.9%
	482	Vitelli	22.9%	27.6%
	485	Cristallo Centrale	22.5%	34.4%
	486	Cristallo Ovest	41.5%	69.3%
	490	Zebrù I	35.4%	36.2%
	490.1	Zebrù II	40.7%	60.9%
	492	Miniera	22.7%	59.2%

METAMORPHIC BEDROCK	495	Montagna Vecchia I	5.3%	68.8%
	495.1	Montagna Vecchia II	21.0%	72.1%
	495.2	Montagna Vecchia III	32.3%	68.5%
	495.3	Montagna Vecchia IV	80.6%	92.1%
	496	Forà	32.0%	71.7%
	497	Confinale Ovest	28.2%	87.4%
	502	Gran Zebrù I	53.2%	30.1%
	503	Cedèc	15.3%	19.8%
	505	Pasquale Sud	23.7%	86.7%
	506	Rosole	52.5%	84.1%
	506.1	Col de la Mare I	11.4%	35.7%
	506.2	Col de la Mare II	15.4%	44.4%
	506.3	Palon de la Mare	8.5%	25.0%
	507	Forni	6.6%	16.3%
	508	San Giacomo Est	33.6%	89.6%
	508.1	San Giacomo Sud	37.2%	80.8%
	509	San Giacomo Ovest	6.5%	48.2%
	510.2	Pizzo Tresero Nord	4.2%	40.1%
	511	Tresero	16.2%	52.7%
	512	Dosegù	6.4%	17.3%
	512.1	Punta Pedranzini I	12.2%	37.4%
	513	Passo di Dosegù I	88.7%	99.8%
	516	Sforzellina	22.4%	66.8%
	518	Gavia	95.2%	98.3%
	519	Alpe Sud I	3.9%	46.2%
	522	Sobretta Nord Est Superiore	12.0%	73.0%
	522.1	Sobretta Nord Est Inferiore	73.7%	80.3%
	523	Sobretta Nord Ovest	4.7%	59.6%
	526	Monte Gavia Nord Ovest	16.8%	94.2%
	527	Savoretta	11.1%	23.9%
	571	Pietre Rosse Nord	17.1%	27.2%

Tab. 8: Debris cover evolution in 2003–2012 for a subset of 38 glaciers. Percentages refer to the fraction of debris-covered area compared to the whole glacier surface.

Debris does not homogeneously cover the glacier surfaces: in fact, some sectors of glaciers are totally covered (the medial or lateral moraine ridges) and it is more common on small glaciers, compared to the large ones. In Figure 4, the glaciers of Ortles-Cevedale Group are sorted in 7 size classes according to Paul et al. (2009), and the fraction of debris-covered ice is reported for each class (based on the 2012 classification). Over the whole glacierized area, it is evident that the largest debris cover values

are found to occur the smallest glaciers. In particular, on glaciers with a surface smaller than 0.1 km^2, the debris cover is about 70% (excluding shadows from the analysis); conversely, the largest ones exhibit a debris cover of about 17% of their whole surface. This trend is evident both for glaciers on sedimentary and metamorphic bedrocks: only the smallest size class of glaciers lying on a sedimentary bedrock shows a lower debris cover, but in this case the total analyzed area is only 0.76 km^2, thus not completely representative.

We can explain the larger debris cover on the smallest ice bodies considering their geomorphological settings; in fact, these glaciers are predominantly located in small cirques or in narrow valleys, often at the foot of steep rock walls where the debris availability is large. Moreover, their dynamics are limited and the rate of debris transport along the glacier is very low. Conversely, the larger valley or mountain glaciers are characterized by wide accumulation basins, where the presence of debris is scarce and the dynamics of the ice allows carrying debris towards the glacier snout.

The results of the debris cover quantification through Landsat ETM+ imagery are in contrast with the ones obtained from the analysis of orthophotos: the debris cover is comparable in 2003, but is clearly underestimated in 2007 (-7.05%) and in 2011 (-12.10%), and no trends are observed. This highlights the importance of high-resolution data for the analysis of supraglacial features of small ice bodies: the improved resolution of the orthophotos (the pixel of the orthophotos covers an area of 0.25 m^2, whereas the pixel of Landsat ETM+ covers an area of 900 m^2, 3600 times the former) allows an accurate description of the supraglacial features of Alpine glaciers.

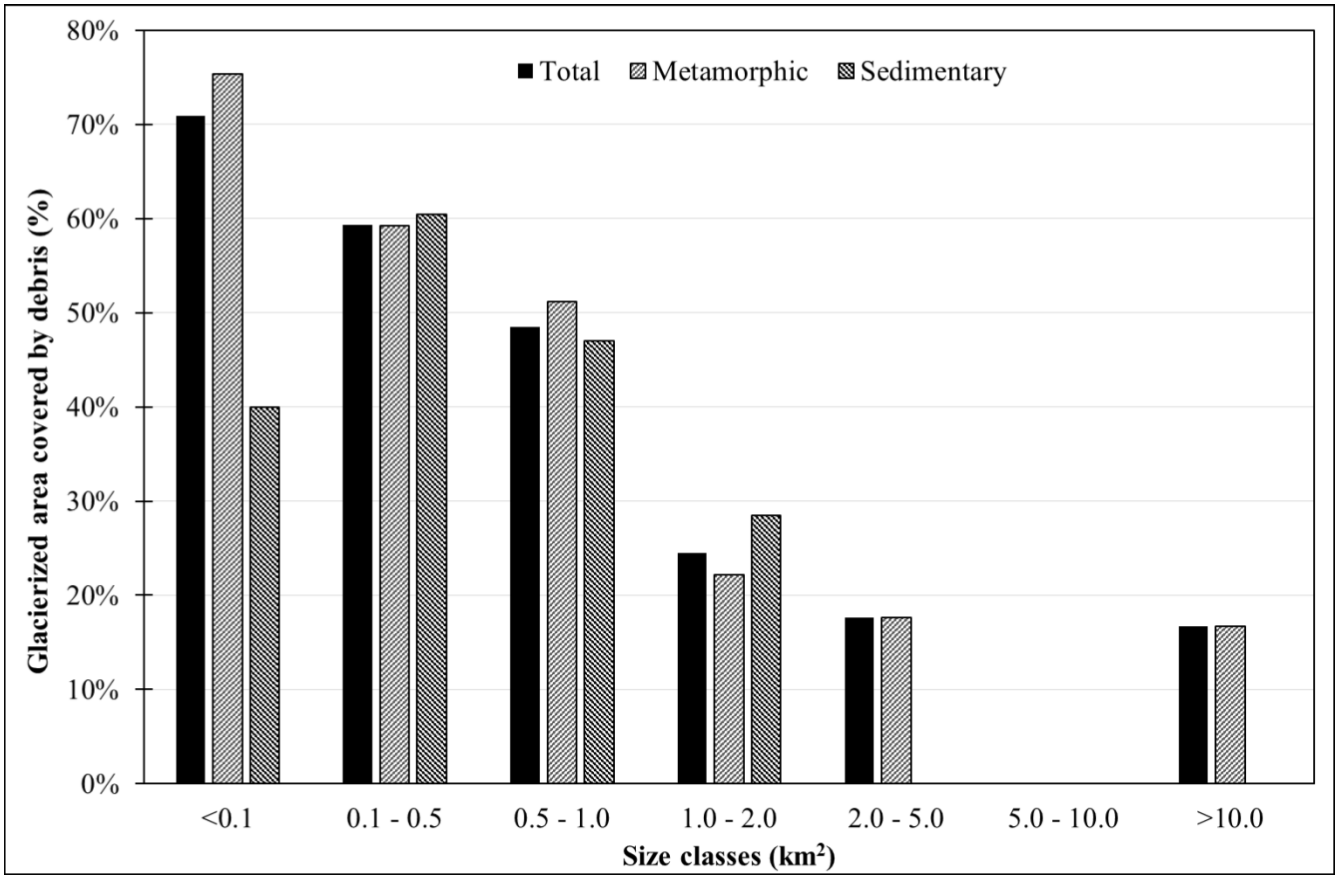

Fig. 4: Fraction of debris-covered area of glaciers in 2012. Black bars indicate the total glacierized area of the Ortles-Cevedale Group (Lombardy Sector); the light grey bars indicate glaciers resting on metamorphic bedrock; the dark grey bars indicate glaciers resting on sedimentary bedrock.

The detailed analyses of the evolution of debris cover on the ablation tongue of the Forni Glacier (Fig.5) underline that this ice body shrank by about 8% between 2003 and 2012 (from 11.71 km^2 to 10.83 km^2). The area decrease is more significant considering only the ablation sector, which lost ca. 20% of its area in the time frame 2003–2012. Extending the analysis up to 2015, the loss in the ablation area is about 40%. Over the same period, the debris cover increased from 26.72% in 2003 to 51.09% in 2012 (from 0.31 km^2 ± 0.03% to 0.47 km^2 ± 0.03%), which means a rate of 0.018 km^2 per year.

Conversely, considering the analysis of the 2014 and 2015 UAV-derived orthophotos, we observe a slight decrease of supraglacial debris cover: it varies from 0.39 km^2 ± 0.03% in 2014 to 0.33 km^2 ± 0.03% in 2015. The acceleration in glacier shrinkage evident over the same period (area loss between 2012 and 2015 is 23.91%, with a rate of retreat of 0.073 km^2 per year) may explain the apparent

decrease in debris-covered surface. In fact, over the period 2012–2015 the rate of retreat was 4 times that of 2003–2012: 0.073 and 0.018 km^2/year, respectively. The area decrease over the past three years is mainly due to the lower sector of the tongue, which is where a wider debris cover is generally found.

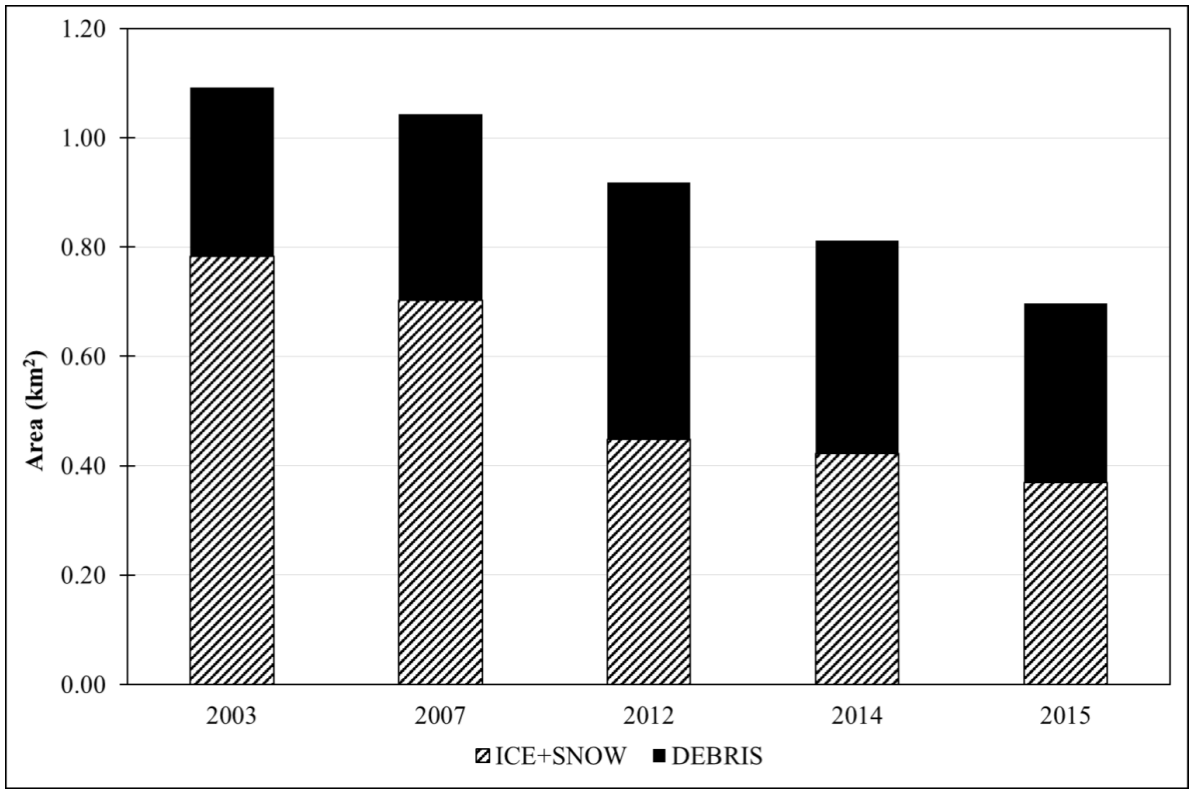

Fig. 5: Evolution of supraglacial debris cover on the Forni Glacier ablation tongue in the timeframe 2003–2015.

The detailed analysis of this paradigmatic glacier of the Italian Alps can provide some information about the spatial evolution and sources of debris cover (Figs. 6 and 7).

In 2003 (Fig. 6A and Fig. 7), the debris cover is mainly located at the glacier snout and along a narrow band, coinciding with the medial moraine (about 90 m large in the frontal area and 50 m large in the highest part of the ablation tongue). The lateral moraines are small and limited mainly to the frontal area. In 2007 (Fig. 6B), we noticed the development of a further moraine ridge that divides the central part of the tongue from the western one. In addition, lateral moraines are more developed and the central moraine is wider than in 2003 (120 m large in the frontal area and 50 m large in the highest part). In 2012 (Fig. 6C and Fig. 7), the increase of debris cover is significant: the western tongue and the glacier snout are almost completely debris-covered. Moreover, the area located at the base of the

eastern icefall undergoes a wide increase in debris. The medial moraine is wider (130 m large in the frontal area and 75 m large in the highest part) and exhibits a bifurcation in the upper part of the ablation tongue (about 30 m wide). We also observed the formation of a debris cone (about 30 m wide) in the lower part of the central tongue. In 2014 (Fig. 6D), the total debris-covered area shows a reduction (Tab. 4), but this is related to the complete melting of the western tongue and the snout of the glacier. Moreover, the medial moraine is wider than in the previous years and its bifurcation is well defined; the debris cone is still present and is more evident. Finally, in 2015 (Fig. 6E), we observed a strong surface reduction of the ablation tongue and the widening of the central moraine ridge (150 m large in the frontal area and 80 m large in the higher part, +20 m and +5 m compared to 2012, respectively). In Fig. 6E, the formation of a new moraine in the central part of the main tongue is also evident.

This detailed analysis allows assessing the evolution of debris on a glacier surface and in particular we observed: i) a general widening of the medial moraine ridges due to the increased availability of debris from the rock outcrops, which also experienced a massive widening; ii) an increase in the rate of debris cover in the frontal area of the glacier, caused by diffuse collapse of the medial and lateral moraine systems; iii) the emergence of new rock outcrops due to enhanced ice melting promoting the formation of new medial moraine ridges; iv) formation of new lateral moraine ridges (or widening of the already existing ones) due to the higher availability of debris from surrounding steep rock walls; v) the formation of a new debris cone owing to the emergence of englacial debris.

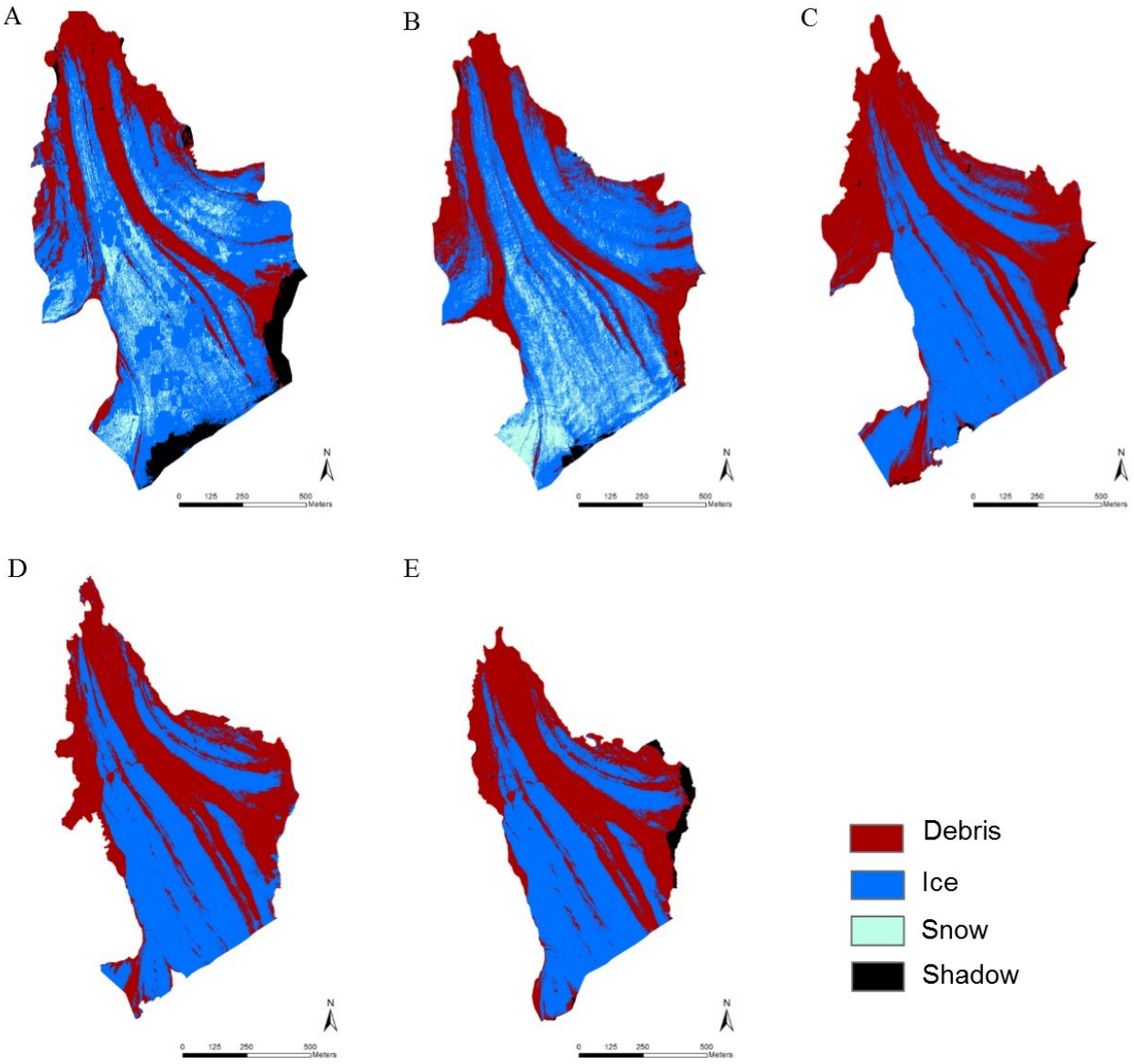

Fig. 6: Evolution of the debris cover on the ablation tongue of Forni Glacier in 2003 (A), 2007 (B), 2012 (C), 2014 (D), and 2015 (E). Debris-covered areas are in red, bare ice is in blue, snow in light blue, and shadows in black.

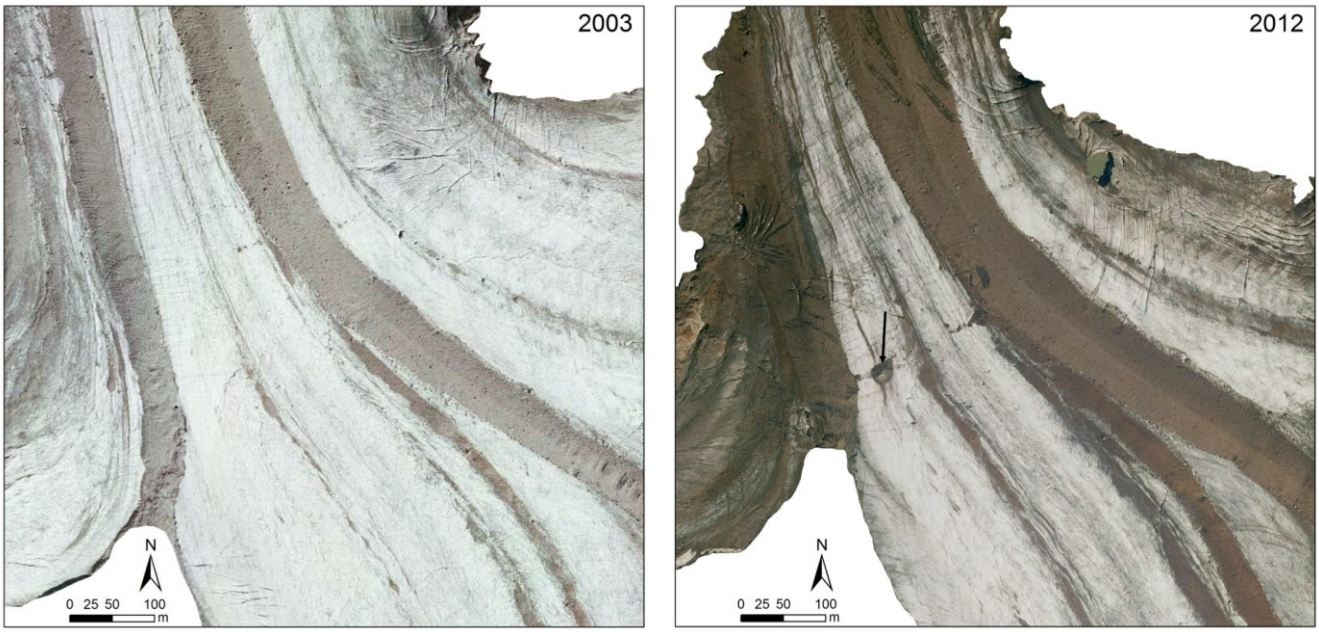

Fig. 7: A detail of the 2003 (left) and 2012 (right) orthophotos of the ablation tongue of the Forni Glacier: a general widening of the medial moraine is observed. Moreover, the formation of a debris cone is evident on the central tongue (indicated by a black arrow).

1.4.2. Lithology of glacial basins and its role in controlling magnitude and rates of debris production

Some attention has to be spent analyzing the role played by the different lithologies in controlling debris cover production and then in influencing glacier reduction rates and debris cover magnitude. On the basis of our data, over the period 2003–2012 glaciers lying on sedimentary bedrock experienced a decrease of 1 km^2 (15.60%), whereas glaciers lying on metamorphic bedrock retreated by 3.5 km^2 (13.91%).

The slight difference in the rate of glacier shrinkage (1.69%) is partially due to the different dominant aspect of glaciers lying on metamorphic bedrock with respect to those resting on sedimentary rocks. In fact, the glaciers belonging to the first group feature a dominant northward orientation (328°), and those included in the second group are generally oriented westward (281°). This different aspect implies a non-negligible difference in the incoming solar input and then in the magnitude and rates of

ice melt. In fact, the amount of solar radiation received by a given surface is controlled, on the global scale, by the geometry of the Earth, atmospheric transmittance, and the relative location of the sun. On a local scale, radiation is additionally controlled by surface slope, aspect and elevation (Allen et al., 2006). In a previous study focused on the whole surface of the Forni Glacier (Senese et al., 2016), the largest cumulative annual value of exo-atmospheric radiation (about 12000 MJ/m^2) was found to be reached on a south-facing surface with a slope of 22.7°, while the smallest one (about 1350 MJ/m^2, corresponding to 11% of the maximum value) was observed on a north-facing surface with a slope of 62.8°. In addition, auto-shading conditions (i.e. null solar input during daytime) can occur for northerly facing slopes higher than 23.3° and whenever the slope exceeds 70°, auto-shading is permanent. As the absorbed solar radiation is the parameter that most affects snow/ice losses (Senese et al., 2012a), a different solar input can explain the different glacier melt magnitude and rate found for the two groups of investigated glaciers.

If we consider the condition of supraglacial debris, we observe that the debris cover is larger for glaciers located in sedimentary rock basins (ca. 40%) than for those on metamorphic rock basins (ca. 28%). However, in the timeframe investigated, the increase in debris cover is higher for glaciers on metamorphic bedrock (+52.00%) than for those on sedimentary rocks (+15.07%). We may interpret the higher increase in debris experienced by glaciers in the metamorphic domain as related to a higher susceptibility to physical (mechanical and thermal) weathering of schist compared to sedimentary rocks (Gerrard, 2012). In fact, it is well known that rocks composed of different minerals exhibit a different susceptibility to weathering (Amiotte Suchet et al., 2003). Moreover, bedding planes, joints, and fractures provide pathways for the entry of water. A rock with lots of these features (such as the metamorphic schists in the Ortles-Cevedale Group) disaggregates more rapidly than a massive rock with no or few bedding planes, joints, or fractures. In the region, schist, being more prone to disaggregation, permits a larger and faster debris production, as confirmed by our interpretation. Summarizing, a lower solar input due to glaciers orientation coupled with a larger availability of debris

in the metamorphic domain have slightly reduced glacier melt and retreat, thus causing a lower retreat rate in this glacier sector of the Ortles-Cevedale Group.

1.5. Conclusion

The analysis of high resolution remote sensing data permitted to detect an appreciable increase in debris-covering glaciers in the Ortles-Cevedale Group in the time frame 2003–2012. In fact, in this period the glacier area covered by rock debris passed from 16.72% of the total in 2003, to 22.54% in 2007, to 30.10% in 2012.

Our values are consistent with the mean debris-covered area reconstructed in the Alps (26.1%) by means of ASTER images over the period 2009–2013 (Sasaki et al., 2016).

Debris resulted not homogeneously covering the glacier surfaces: in fact, some sectors of glaciers were totally covered (the medial or lateral moraine ridges) and it was found more common on small glaciers, compared to the large ones. Moreover, considering the lithology of supraglacial debris, we observed that the debris cover was larger for glaciers nested by sedimentary rock basins (ca. 40%) than for those on metamorphic rock basins (ca. 28%). However, in the timeframe investigated, the increase in debris cover was higher for glaciers on metamorphic bedrock (+52.00%) than for those on sedimentary rocks (+15.07%). We interpreted the higher increase in debris experienced by glaciers in the metamorphic domain as related to a higher susceptibility to physical (mechanical and thermal) weathering of schist compared to sedimentary rocks (Gerrard, 2012).

In addition, this work highlighted the main problems of a high-resolution analysis of supraglacial features based on supervised classification of optical data: the characterization of the debris lithology is fundamental to train the supervised classification based on a different debris coloration. In addition, the creation of different signature files for different orthophotos allows minimizing some errors in the classification due to the different optical properties of the images. These expedients are fundamental

for this kind of analysis on Alpine glaciers because the widely adopted investigation based on medium-resolution data (i.e. Landsat) cannot provide an accurate representation of supraglacial features. Moreover, after this preliminary assessment of the quality of the methodology and of the rapidly changing situation of debris cover, this analysis can be extended to all the Italian glaciers providing useful information about the characteristics of glacier surfaces. In fact, the mapping of debris covered ice, linked with field activities and a desirable improvement in the resolution of satellite thermal data, now limited to 100 m with Landsat 8, can greatly contribute to glacier modeling, and in particular to the assessment of the glacier energy balance.

1.6. Acknowledgements

The data analyses were supported by DARAS (Department of Regional Affairs, Autonomies and Sport) of the Presidency of the Council of Ministers of the Italian government through the GlacioVAR project (PI G. Diolaiuti) and by the Central Scientific Committee of the Italian Alpine Club. The work was also supported by Sanpellegrino Levissima Spa.

1.7. References

Allen R.G., Trezza R. and Tasumi M. (2006): Analytical integrated functions for daily solar radiation on slopes. *Agricultural and Forest Meteorology*, 139, 55-73.

Amiotte Suchet P., Probst J.L. and Ludwig W. (2003): Worldwide distribution of continental rock lithology: Implications for the atmospheric/soil CO2 uptake by continental weathering and alkalinity river transport to the oceans. *Global Biogeochemical Cycles*, 17(2), 1-14.

Azzoni R.S., Franzetti A., Fontaneto D., Zullini A. and Ambrosini R. (2015): Nematodes and rotifers on two Alpine debris-covered glaciers. *Italian Journal of Zoology*, 82(4), 1-8.

Azzoni R.S, Senese A., Zerboni A., Maugeri M., Smiraglia C. and Diolaiuti G.A. (2016): Estimating ice albedo from fine debris cover quantified by a semi-automatic method: The case study of Forni Glacier, Italian Alps. *The Cryosphere*, 10, 665-679.

Barla G., Dutto F. and Mortara G. (2000): Brenva glacier rock avalanche of 18 January 1997 on the Mount Blanc range, northwest Italy. *Landslide News*, 13, 2–5.

Bolch T., Buchroithner T.M., Pieczonka T. and Kunert A. (2008): Planimetric and volumetric glacier changes in the Khumbu Himal, Nepal, since 1962 using Corona, Landsat TM and ASTER data. *Journal of Glaciology*, 54(187), 592–600.

Brock B., Mihalcea C., Kirkbride M. and Smiraglia C. (2010): Meteorology and surface energy fluxes in the 2005–2007 ablation seasons at Miage debris-covered Glacier, Mont Blanc Massif, Italian Alps. *Journal of Geophysical Research*, 115, D09106.

Brock B.W., Willis I.C., and Sharp M.J. (2000): Measurement and parameterization of albedo variations at Haut Glacier d'Arolla, Switzerland. *Journal of Glaciology*, 46 (155), 675-688.

Caccianiga M., Andreis C., Diolaiuti G., D'Agata C., Mihalcea C. and Smiraglia C. (2011): Alpine debris-covered glaciers as a habitat for plant life. *The Holocene*, 21, 1011–1020.

Chiarle M., Iannotti S., Mortara G. and Deline P. (2007): Recent debris flow occurrences associated with glaciers in the Alps. *Global and Planetary Change*, 56, 123–136.

D'Agata C. and Zanutta A. (2007): Reconstruction of the recent changes of a debris-covered glacier (Brenva Glacier, Mont Blanc Massif, Italy) using indirect sources: Methods, result and validation. *Global and Planetary Change*, 56, 57–68.

D'Agata C., Bocchiola D., Maragno D., Smiraglia C. and Diolaiuti G. (2014): Glacier shrinkage driven by climate change during half a century (1954–2007) in the Ortles-Cevedale group (Stelvio National Park, Lombardy, Italian Alps). *Theoretical and Applied Climatology*, 116: 169. doi:10.1007/s00704-013-0938-5.

Deline P. (2001): Recent Brenva rock avalanches (Valley of Aosta): New chapter in an old story? *Geografia Fisica e Dinamica Quaternaria*, 5, 55–63.

Deline P. (2002): Etude géomorphologique des interactions entre écroulements rocheux et glaciers dans la haute montagne alpine: Le versant sud-est du massif du Mont Blanc (Vallee d'Aoste, Italie). PhD Thesis, Université de Savoie.

Deline P. (2005): Change in surface debris cover on Mont Blanc massif glaciers after the 'Little Ice Age' termination. *The Holocene*, 15(2), 302–309.

Deline P. (2009): Interactions between rock avalanches and glaciers in the Mont Blanc massif during the late Holocene. *Quaternary Science Reviews*, 28, 1070–1083.

Diolaiuti G., Maragno D., D'Agata C., Smiraglia C. and Bocchiola D. (2011): Glacier Retreat and Climate Change: documenting the last fifty years of Alpine glacier history from area and geometry changes of Dosdè Piazzi glaciers (Lombardy- Alps, Italy). *Progress in Physical Geography*, 35(2), 161-182.

Diolaiuti G., D'Agata C., Meazza A., Zanutta A. and Smiraglia C. (2009): Recent (1975–2003) changes in the Miage debris-covered glacier tongue (Mont Blanc, Italy) from analysis of aerial photos and maps. *Geografia Fisica e Dinamica Quaternaria*, 32, 117–127.

Diolaiuti G., Bocchiola D., D'Agata C. and Smiraglia C. (2012a): Evidence of climate change impact upon glaciers' recession within the Italian Alps: the case of Lombardy glaciers. *Theoretical and Applied Climatology*, 109(3-4), 429-445.

Diolaiuti G., Bocchiola D., Vagliasindi M., D'Agata C. and Smiraglia C. (2012b): The 1975-2005 glacier changes in Aosta Valley (Italy) and the relations with climate evolution. *Progress in Physical Geography*, 36(6), 764-785.

Dyurgerov M.B. and Meier M.F. (2000): Twentieth century climate change: evidence from small glaciers. *Proceeding of the National Academy of Science,* 97(4),1406–1411.

Evans S.G. and Clague J.J. (1994): Recent climatic change and catastrophic geomorphic processes in mountain environments. *Geomorphology*, 10, 107–128.

Fitzgerald R.W. and Lees B.G. (1994): Assessing the classification accuracy of multisource remote sensing data. *Remote Sensing of Environment,* 47(3), 362-368.

Franzetti A., Tagliaferri I., Gandolfi I., Bestetti G., Minora U., Mayer C., Azzoni R.S., Diolaiuti G., Smiraglia C. and Ambrosini R. (2016a): Light-dependent microbial metabolisms drive carbon fluxes on glacier surfaces. *The ISME Journal*, 1-5.

Franzetti A., Navarra F., Tagliaferri I., Gandolfi I., Bestetti G., Minora U., Azzoni R.S., Diolaiuti G.A., Smiraglia C. and Ambrosini R. (2016b): Temporal variability of bacterial communities in cryoconite on an Alpine glacier: Temporal variation of cryoconite bacteria. *Environmental Microbiology Reports*

Fugazza D., Senese A., Azzoni R.S., Smiraglia C., Cernuschi M., Severi D., and Diolaiuti G.A. (2015): High resolution mapping of glacier surface features. The UAV survey of the Forni Glacier (Stelvio National Park, Italy). *Geografia Fisica e Dinamica Quaternaria*, 38(1), 25-33.

Fugazza D., Senese A., Azzoni R.S., Maugeri M., Diolaiuti G.A. (2016): Spatial distribution of surface albedo at the Forni Glacier (Stelvio National Park, Central Italian Alps). *Cold Regions Science and Technology*, 125, 128-137.

Gerrard J. (2012): Rocks and landforms. Springer Science & Business Media, 320 p.

Gibson M.J., Glasser N.F., Quincey D.J., Rowan A.V. and Irvine-Fynn T.D. (2016): Changes in glacier surface cover on Baltoro glacier, Karakoram, north Pakistan, 2001–2012. *Journal of Maps*, 13(2), 100-108.

Gobbi M., Isaia M. and De Bernardi F. (2011): Arthropod colonisation of a debris-covered glacier. *The Holocene*, 21, 343–349.

Gruber S. and Haeberli W. (2007): Permafrost in steep bedrock slopes and its temperature-related destabilization following climate change. *Journal of Geophysics Resources*, 112, F02S18

Hall K., Lindgren B.S. and Jackson P. (2005): Rock albedo and monitoring of thermal conditions in respect of weathering: some expected and some unexpected results. *Earth Surface Processes and Landforms*, 30(7), 801-812.

Haeberli W. (1996): On the morphodynamics of ice/debris-transport systems in cold mountain areas. *Norsk Geografisk Tidsskrift*, 50, 3–9.

Haeberli W., Wegmann M. and Vonder Muhll D. (1997): Slope stability problems related to glacier shrinkage and permafrost degradation in the Alps. *Eclogae Geologicae Helvetiae*, 90, 407–414.

Huggel C., Zgraggen-Oswals S. and Haeberli W. (2005): The 2002 rock/ ice avalanche at Kolka/Karmadon, Russian Caucasus: Assessment of extraordinary avalanche formation and mobility, and application of QuickBird satellite imagery. *Natural Hazards and Earth System Sciences*, 5, 173–187.

IPCC (2013). Climate Change 2013: The Physical Science Basis. Contribution of Working Group I to the Fifth Assessment Report of the Intergovernmental Panel on Climate Change. Stocker, T.F., D. Qin, G.K. Plattner, M. Tignor, S.K. Allen, J. Boschung, A. Nauels, Y. Xia, V. Bex and P.M. Midgley (eds.). Cambridge University Press, Cambridge, United Kingdom and New York, NY, USA, 1535 pp, doi:10.1017/CBO9781107415324.

Kellerer-Pirklbauer A. (2008): The supraglacial debris system at the Pasterze glacier, Austria: Spatial distribution, characteristics and transport of debris. Z. *Geomorphology Supplement*, 52(1), 3–25.

Kirkbride M.P. (1993): The temporal significance of transitions from melting to calving termini at glaciers in the central Southern Alps of New Zealand. *The Holocene*, 3(3), 232–240.

Mattson L.E. and Gardner J.S. (1989): Energy exchange and ablation rates on the debris-covered Rakhiot Glacier, Pakistan. *Zeitschrift Für Gletscherkunde und Glazialgeologie,* 25(1), 17–32.

Maurer J.M., Rupper S.B. and Schaefer J.M. (2016): Quantifying ice loss in the eastern Himalayas since 1974 using declassified spy satellite imagery. *The Cryosphere*, 10, 2203-2215.

Mihalcea C., Mayer C., Diolaiuti G., Lambrecht A., Smiraglia C. and Tartari G. (2006): Ice ablation and meteorological conditions on the debris covered area of Baltoro Glacier, Karakoram (Pakistan). *Annals of Glaciology*, 43, 292–300.

Mihalcea C., Brock B., Diolaiuti G., D'Agata C., Citterio M., Kirkbride M.P., Cutlerb M.E.J. and Smiraglia C. (2008a): Using aster satellite and ground- based surface temperature measurements to derive supraglacial debris cover and thickness patterns on Miage Glacier (Mont Blanc Massif, Italy). *Cold Regions Science and Technology*, 52, 341–354.

Mihalcea C., Mayer C., Diolaiuti G., Lambrecht A., Smiraglia C. and Tartari G. (2008b): Ice ablation and meteorological conditions on the debris-covered area of Baltoro glacier, Karakoram, Pakistan. *Annals of Glaciology*, 43, 292-300.

Minora U.F., Senese A., Bocchiola D., Soncini A., D'Agata C., Ambrosini R., Mayer C., Lambrecht A., Vuillermoz A., Smiraglia C. and Diolaiuti G.A. (2015): A simple model to evaluate ice melt over the ablation area of glaciers in the Central Karakoram National Park, Pakistan. *Annals of Glaciology*, 56 (70), 202-216.

Minora U.F., Bocchiola D., D'Agata C., Maragno D., Mayer C., Lambrecht A., Vuillermoz E., Senese A., Compostella C., Smiraglia C. and Diolaiuti G.A. (2016): Glacier area stability in the Central Karakoram National Park (Pakistan) in 2001–2010: the ''Karakoram Anomaly'' in the spotlight. *Progress in Physical Geography*, 40(5), 629-660.

Montrasio A., Berra F., Cariboni M., Ceriani M., Deichmann N., Ferliga C., Gregnanin A., Guerra S., Guglielmin M., Jadoul F., Longhin M., Mair V., Mazzoccola D., Sciesa E. and Zappone A. (2008): Note illustrative della Carta Geologica d'Italia: foglio 024, Bormio, ISPRA, Servizio Geologico d'Italia, Roma.

Nakawo M. and Young G.J. (1981): Field experiments to determinate the effect of a debris layer on ablation of glacier ice. *Annals of Glaciology*, 2, 85–91.

O'Connor J.E. and Costa J.E. (1993): Geologic and hydrologic hazards in glacierized basins in North America resulting from 19th and 20th century global warming. *Natural Hazards*, 8, 121–140

Oerlemans J., Giesen R.H. and Van Der Broeke M.R. (2009): Retreating alpine glaciers: increased melt rates due to accumulation of dust (Vadret da Morteratsch, Switzerland). *Journal of Glaciology*, 55(192), 729-736.

Østrem G. (1959): Ice melting under a thin layer of moraine and the existence of ice in moraine ridges. *Geografiska Annaler*, 41, 228–230.

Paul F., Huggel C. and Kaab A. (2004): Combining satellite multispectral image data and a digital elevation model for mapping debris-covered glaciers. *Remote Sensing of Environment*, 89, 510–518.

Paul F., Barry R.G., Cogley J.G., Frey H., Haeberli W., Ohmura A., Ommanney C.S.L., Raup B., Rivera A. and Zemp M. (2009): Recommendations for the compilation of glacier inventory data from digital sources. *Annals of Glaciology*, 50(53), 119–126.

Paul F., Frey H. and Le Bris R. (2011): A new glacier inventory for the European Alps from Landsat TM scenes of 2003: challenges and results. *Annals of Glaciology*, 52(59), 144-152.

Paul F., Barrand N., Berthier E., Bolch T., Casey K., Frey H., Joshi S.P., Konovalov V.P., Le Bris R., Mölg N., Nosenko G., Nuth C., Pope A., Racoviteanu A., Rastner A., Raup B., Scharrer K., Steffen S. and Winsvold S. (2013): On the accuracy of glacier outlines derived from remote sensing data. *Annals of Glaciology*, 54(63), 171-182.

Pelfini M., Diolaiuti G., Leonelli G., Bozzoni M., Bressan N., Brioschi D. and Riccardi A. (2012): The influence of glacier surface processes on the short-term evolution of supraglacial tree vegetation: the case study of the Miage Glacier, Italian Alps. *The Holocene*, 22, 847-856.

Popovnin V.V. and Rozova A.V. (2002): Influence of sub-debris thawing on ablation and runoff of the Djankuat glacier in the Caucasus. *Nord Hydrology,* 33(1), 75–94.

Ravanel L. and Deline P. (2008): La face ouest de Drus (Massif du Mont Blanc): évolution de l'instabilité d'une paroi rocheuse dans la haute montagne alpine depuis la fin du Petit Age Glaciaire. *Géomorphologie*, 4, 261–272.

Reid T.D, Carenzo M., Pellicciotti F., Brock B.W. (2012): Including debris cover effects in a distributed model of glacier ablation. *Journal of Geophysical Resources*, 117, D18105.

Sasaki O., Noguchi O., Zhang Y., Hirabayashi Y. and Kanae S. (2016): A global high-resolution map of debris on glaciers derived from multitemporal ASTER images. *The Cryosphere discussion*, doi:10.5194/tc-2016-222.

Senese A., Diolaiuti G., Mihalcea C. and Smiraglia C. (2012a): Energy and mass balance of Forni Glacier (Stelvio National Park, Italian Alps) from a 4-year meteorological data record. *Arctic Antarctic and Alpine Resources*, 44, 122–134.

Senese A., Diolaiuti G., Verza G.P. and Smiraglia C. (2012b): Surface energy budget and melt amount for the years 2009 and 2010 at the Forni Glacier (Italian Alps, Lombardy). *Geografia Fisica e Dinamica Quaternaria*, 35, 69-77.

Senese A., Maugeri M., Vuillermoz E., Smiraglia C. and Diolaiuti G. (2014): Using daily air temperature thresholds to evaluate snow melting occurrence and amount on Alpine glaciers by T-index models: the case study of the Forni Glacier (Italy). *The Cryosphere*, 8, 1921-1933.

Senese A., Maugeri M., Ferrari S., Confortola G., Soncini A., Bocchiola D. and Diolaiuti G. (2016): Modelling shortwave and longwave downward radiation and air temperature driving ablation at the Forni Glacier (Stelvio National Park, Italy). *Geografia Fisica e Dinamica Quaternaria*, 39(1), 89-100.

Shukla A., Gupta R.P. and Arora M.K. (2009): Estimation of debris cover and its temporal variation using optical satellite sensor data: A case study in Chenab basin, Himalaya. *Journal of Glaciology*, 55(191), 444–452.

Smiraglia C., Azzoni R.S., D'Agata C., Maragno D., Fugazza D. and Diolaiuti G.A. (2015): The evolution of the Italian glaciers from the previous database to the New Italian Inventory. Preliminary considerations and results. *Geografia Fisica e Dinamica Quaternaria*, 38(1), 79-87.

Stokes C.R., Popovnin V., Aleynikov A., Gurney S.D. and Shahgedanova M. (2007): Recent glacier retreat in the Caucasus Mountains, Russia, and associated increase in supraglacial debris cover and supra-/proglacial lake development. *Annals of Glaciology*, 46, 195–203.

Turchetti B., Goretti M., Branda E., Diolaiuti G., D'Agata C., Smiraglia C., Onofri A. and Buzzini P. (2013): Influence of abiotic parameters on culturable yeast diversity in two distinct Alpine glaciers. *FEMS Microbiology Ecology*, 86(2), 327-340.

Veetil B.K. (2012): A Remote sensing approach for monitoring debris-covered glaciers in the high altitude Karakoram Himalayas. *International Journal of Geomatics and Geosciences*, 2(3), 833-841.

Vezzola L.C., Diolaiuti G.A., D'agata C., Smiraglia C. and Pelfini M. (2016): Assessing glacier features supporting supraglacial trees: A case study of the Miage debris-covered Glacier (Italian Alps). *The Holocene*, 26(7), 1138-1148.

Vogtle T. and Schilling K. (1999): Digitizing Maps. In: Bähr H.P. & Vögtle T. (Eds.), "GIS for Environmental Monitoring", Schweizerbart, Stuttgart, 201–216.

Zemp M., Paul F., Hoelzle M. and Haeberli W. (2008): Glacier fluctuations in the European Alps, 1850–2000: an overview and a spatiotemporal analysis of available data. In: Orlove B., Wiegandt E. & Luckman B.H. (Eds). "Darkening peaks: Glacier retreat, science, and society". Berkeley, CA, University of California Press, 152–167.

Chapter 2
High-resolution mapping of glacier surface features. The UAV survey of the Forni Glacier (Stelvio Park, Italy)

Chapter published on Geografia Fisica e Dinamica Quaternaria

Fugazza D., Senese A., Azzoni R.S., Smiraglia C., Cernuschi M., Severi D. and Diolaiuti G.A. (2015) - High resolution mapping of glacier surface features. The UAV survey of the Forni Glacier (Stelvio National Park, Italy). *Geografia Fisica e Dinamica Quaternaria*, 38(1), 25-33.

Abstract

Fast, reliable and accurate methods for glacier mapping are necessary for understanding glacier dynamics and evolution and assessing their response to climate change. Conventional semi-automatic approaches are based on medium-resolution satellite images, but their use can cause significant loss of accuracy when analyzing small glaciers, which are predominant in the Alps. In this paper, we present a semi-automatic segmentation approach based on very high-resolution visible RGB images acquired from a UAV (Unmanned Aerial Vehicle) survey of the Forni Glacier, in the Italian Alps, using an off-the-shelf digital camera. The method has the ability to map large-scale morphological features, i.e. bare ice and medial moraines, with better accuracy than methods relying on medium-resolution satellite imagery, with only slight misclassification at the margins. By using segmentation, we also mapped small-scale morphologies not discernible on satellite images, including epiglacial lakes and snow patches, in a semi-automatic way. On a small portion of the eastern ablation tongue, featuring homogeneous illumination conditions, we also investigated in finer detail the occurrence of fine and sparse debris and tested a texture filter technique for mapping crevasses, which showed promising results. Our analyses confirm that the glacier is undergoing intense dynamic processes, including darkening of the ablation tongue and increased surface instability, and show the potential of UAVs to revolutionize glaciological studies. We suggest that by using a combination of different payloads, mapping of glacier features via UAVs could reach high levels of accuracy and speed, making them useful tools for glacier inventories and geomorphological maps.

2.1. Introduction

Retreat of glaciers worldwide since the Little Ice Age is one of the clearest clues of climate change. In the Alps, glacier shrinkage has been particularly severe since the 1980s and if the trend continues, many Alpine glaciers could disappear during the 21st century, with a serious impact on the energy and water supply (EEA, 2012). During its active phase, glacier recession is also followed by geomorphological changes such as an increase in supraglacial debris cover and formation of epiglacial lakes (Diolaiuti & Smiraglia, 2010). Debris cover affects ice albedo and plays an important role in the glacier energy balance (Oerlemans et al., 2009), while ice-contact lakes can increase ice ablation via calving processes (Benn et al., 2012).

Fast and reliable methods for glacier mapping are necessary to study the evolution of glaciers and assess their response to climate change. For this purpose, several semi-automatic approaches employing medium-resolution satellite imagery such as ASTER and Landsat (15-30 m of pixel resolution) have been developed, using a combination of optical, thermal and/or morphometric data (for a review see Shukla et al., 2010). Accuracy of medium-resolution methods, however, decreases when analyzing changes in smaller glaciers (Paul et al., 2013). This precludes mapping of small-scale geomorphological features, including crevasses, snow patches and small epiglacial lakes, and of fine and sparse debris, which is widespread on most glaciers and likewise has an impact on the albedo (Azzoni et al., 2014).

In theory, images with higher resolution could provide a more detailed discrimination of supraglacial features. High-resolution satellite imagery however is available at a high cost to the end users, and so far it has mainly been employed as a means of validating lower resolution methods, substituting fieldwork. In glacier inventories, orthomosaics from aerial surveys are also employed for mapping glacier boundaries via manual delineation, as in the recently developed Swiss Glacier inventory (Fischer et al., 2014). However, this process is slow and further information is usually needed to

identify glacier margins on highly debris-covered glaciers. A semi-automatic approach, developed by Knoll & Kerschner (2009) for the Tyrol Inventory, was based on Airborne Laser Scanning (ALS) surveys, but whenever it was applied over debris-covered glaciers manual correction was required. ALS surveys are also expensive, and this limits their application on a global scale.

More recently, unmanned aerial vehicles (UAV) have been introduced to the field of glacier studies. These enable low cost on-demand inspection of relatively wide areas of interest, with the ability to carry different types of payload (e.g. a digital camera, near-infrared or thermal sensor) and to survey an area with a better resolution than commercial satellites. UAV-derived orthomosaics have been used to analyze specific features such as cryoconite holes and granules, in combination with ground photography (Hodson et al., 2007), supraglacial lakes (Immerzeel et al., 2014), and crevasses, mapped by Ryan et al. (2015) via manual delineation. In this paper, we assess the feasibility of mapping several glacier features (i.e. snow, buried- and bare-ice, epiglacial lakes, and crevasses) of the Forni Glacier from a UAV high-resolution orthomosaic produced using an off-the-shelf digital camera with a semi-automatic approach. In addition, we investigate in more detail these glacier features analyzing a smaller area along the Forni Glacier ablation tongue featuring homogeneous illumination conditions. Finally, to evaluate the advantages provided by this methodology we compare it to classification based on medium-resolution data acquired by Landsat 8.

2.1.1. Study Area

The Forni Glacier is part of the Ortles-Cevedale group, Lombardy Alps, and of the Stelvio National Park (Fig. 1). It is the widest Italian valley glacier (ca. 11.36 km^2; D'Agata et al., 2014), with a northerly aspect and an elevation range between 3670 and 2600 m. It is a composite glacier, formed by three ice streams joining into a tongue that extends for ca. 2 km. Two medial moraines are located on the tongue, originating from rock outcrops located below the snow line and nourished by supra-glacial debris derived from valley rocks (Smiraglia, 1989). The ablation tongue is mostly debris-free, although a recent increase in fine and sparse debris deposition due to the ongoing glacier shrinkage has been

reported (Diolaiuti & Smiraglia, 2010; Senese et al., 2012a). Other considerable morphological changes have lately taken place, including the appearance of debris cones, epiglacial ponds and the formation of neo-moraines. Owing to this diverse range of glacial features, together with the ease of access and the long series of volume, area and length dataset, the Forni Glacier is an ideal ground for evaluating our methodology.

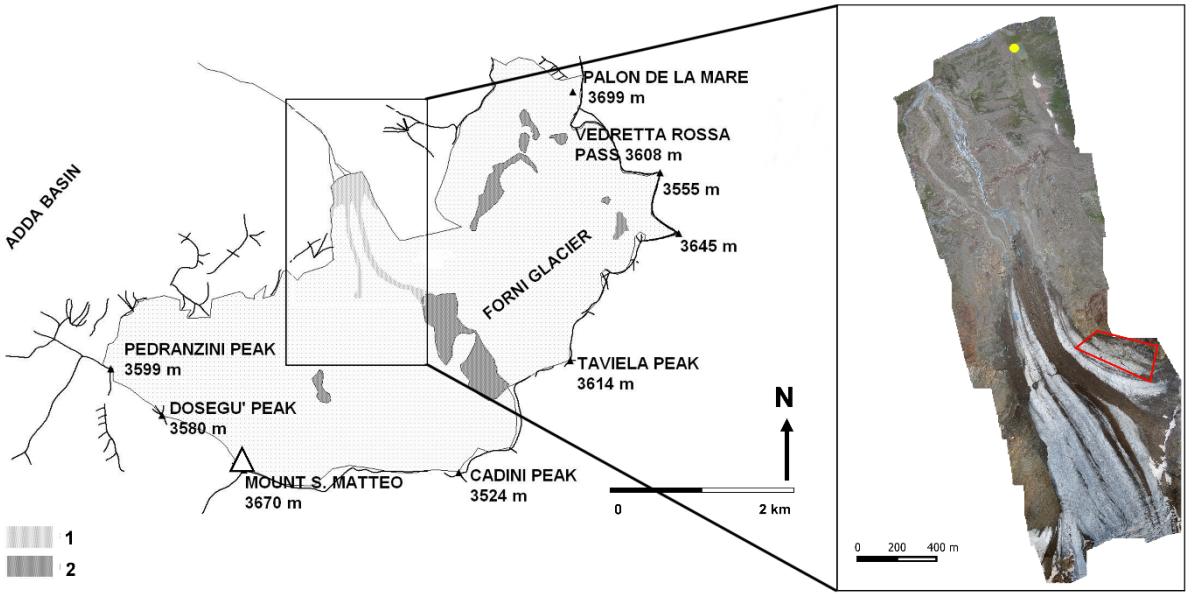

Fig. 1: Map of the Forni Glacier from aerial orthophoto acquired in 2003: medial moraines and supraglacial debris are indicated in light-grey (1), and nunataks are highlighted in dark-grey (2). (B) Area imaged by the UAV in August 2014: the yellow dot displays the UAV launch and landing location, while the area investigated in higher detail is shown as the red box

2.2. Material and methods

The methodology proposed in this study aims at classifying both large-scale and small-scale features on the surface of the Forni Glacier ablation tongue. We consider as large-scale features the main glacier body and the medial moraines. These are much larger than a Landsat pixel, and thus clearly identifiable on both Landsat and UAV images. It follows that small-scale features are those smaller than a Landsat pixel, and we considered among them debris-rich ice, snow-patches, epiglacial lakes and crevasses.

2.2.1. Remotely-sensed data and glacier outlines

The UAV used in this study was SwingletCAM, built by SenseFly. SwingletCAM is a fixed-wing UAV, with a weight of only 0.5 kg including GPS receiver, altimeter, wind speed sensor and a Canon IXUS 125 HS digital camera, automatically triggered for picture acquisition. The camera has a 16 megapixel CMOS sensor, capable of 4608 by 3456 pixels resolution with a 4:3 aspect ratio, and captures JPEG format images in the visible light range. The device operates in full-auto mode, including self-adjustment of aperture, ISO and shutter speed for the given light condition. In our survey, this resulted in ISO values in the range 100–500 and shutter speeds of 1/125–1/640 s with an aperture of f/2.7.

The survey took place on 28 August 2014, at approximately 8:20 AM. This time was chosen i) to avoid direct illumination of the glacier surface and thus a higher solar reflection which could saturate the pictures, and ii) to minimize wind speed that can cause staggering of the UAV and consequently produce blurred pictures (katabatic winds can occur along the Forni ablation tongue, see Senese et al., 2012b). Launch and landing location was set beside Rosole Lake at 2493 m a.s.l. (the yellow dot in Fig. 1b), close to Branca refuge and on the way to the glacier, and the maximum flight height was 250 m. The UAV was flown on the central and eastern parts of the tongue (see Fig. 1b), for a total flight time of less than 30 minutes. The upper basins were not investigated due to UAV flight limitations, including battery life and line-of-sight operation and considering that reaching higher elevation in a short time could have entailed significant radial distortion in the acquired pictures. Images were processed via bundle block adjustment, including geometric correction to compensate for radial distortion in Menci APS software, to produce an orthomosaic with a ground resolution of 0.15 m x 0.15 m and a DEM with slightly lower resolution of 0.60 m x 0.60 m, to avoid gaps and artefacts generated by the stereo-matching process. In the absence of ground control points (GCPs), we estimated positional accuracy of the orthophoto and DEM to be about 3 m in the x and y coordinates, following Küng et al. (2011).

To compare this high-resolution image with a medium-resolution one, we obtained from USGS a Landsat 8 OLI/TIRS image acquired on 14/9/2014. This was the closest date of a Landsat overpass where the ablation tongue was free from cloud cover and shadows. We converted DN values (i.e. quantized and calibrated scaled Digital Numbers) to units of reflectance and brightness temperature using the coefficients found in the scene metadata (USGS, 2013). Geometric accuracy of the Landsat 8 OLI/TIRS sensors is estimated to be approximately 12 m (Storey et al., 2014).

2.2.2. Extraction of glacier large-scale features based on the UAV orthomosaic

Concerning separability in the spectral domain, the medial moraines clearly stand out due to overall low values in all RGB channels of the orthomosaic, an effect that is also visible to a lesser degree on the Landsat image, caused by absorption of light at visible wavelengths by meltwater. Other features however are less distinct. In particular, the proglacial stream (i.e. Frodolfo stream) has similar spectral features as the glacier itself, with colors varying from a clear blue to almost saturation of the sensor, depending on water turbidity. Fine and sparse debris located on the tongue and on snow patches is also spectrally similar to proglacial debris.

In order to isolate large-scale features from the rest of the scene, we adopted a segmentation approach, identifying connected segments where pixels show similar spectral characteristics. This is in fact the recommended approach when dealing with high-resolution imagery, where objects to be identified are much larger than pixel size (Blaschke, 2010). We adopted different strategies to discriminate between features: the blue channel is ideal for identifying the glacier surface and the red channel for identifying the medial moraines.

2.2.3. Extraction of glacier large-scale features based on Landsat imagery

To classify large-scale features of the Forni Glacier ablation tongue based on the Landsat OLI/TIRS image acquired on 14 September 2014, we employed optical and thermal information. First, we performed a supervised classification of the whole glacier surface using a stack of Landsat 8 bands,

excluding band 1 (used for coastal aerosol detection), 8 (panchromatic) and 9 (cirrus detection), and including both thermal bands (i.e. 10 and 11). In particular, we defined training areas for the classification process by using the UAV image as a reference. Finally, by means of the shapefile created from the UAV orthomosaic, we selected the glacier ablation tongue on the Landsat image. This allowed a direct comparison between the two different approaches for identifying large-scale features: segmentation based on the UAV orthomosaic and supervised classification based on the Landsat OLI/TIRS image.

2.2.4. Classification of the glacier small-scale features based on the UAV orthomosaic

Once the glacier area was identified via segmentation, we attempted to further classify the different glacier surfaces by

i) segmentation (i.e. snow, exposed ice, debris-rich ice, moraines, and water pond)

ii) partitioning into different classes based on RGB values (i.e. debris free or debris covered ice)

iii) Gabor filters (i.e. crevasses).

Concerning segmentation, given the differences in water color, no single spectral threshold could be used to extract all of the lakes, so they were identified separately. The largest lakes exhibit a greenish hue, likely due to a combination of suspended sediments and populations of algae that have colonized them (see also Boggero et al., 2014). One example is the epiglacial pond on the eastern tongue, extracted based on the condition green > red > blue, whereas smaller ponds were identified via the blue channel. Snow patches featured different RGB values depending on clean and dirty snow, thus requiring two separate segmentation steps to identify them.

Concerning the second approach, an underlying assumption was made that over a glacier surface lower RGB values represent an increasing amount of fine debris deposition (in case of snow or ice), a wet surface (whenever water ponds occur) or shadows. In fact, localized shadow effects produced by surface topography at the time of image acquisition made it difficult to apply a single classification

approach over the whole glacier surface. Over large areas, two pixels can feature a similar RGB value even if characterized by different surface conditions, e.g. one can be shadowed and the other one can feature a debris-covered surface. We therefore generated a hillshading map using the DEM extracted from the UAV survey (see section on Data Sources) and solar zenith and azimuth angles (Dozier & Frew, 1990) in order to identify an area with relatively uniform shadowing. We found that a limited part of the eastern tongue revealed these characteristics (red box in Fig. 1b). Finally, we performed a decision-tree classification based on spectral properties in the RGB domain. This approach was chosen over supervised classification given the difficulty inherent in selecting homogeneous training areas.

Concerning crevasses, previous work on automatic delineation by Johannesson et al. (2011) was based on the local curvature of the ice surface obtained from a LiDAR digital elevation model (DEM). The photogrammetric DEM obtained from the UAV survey however was of insufficient resolution to test this method. In fact, most crevasses on the surface of the Forni Glacier that can be located on the orthomosaic are less than 0.50 m wide, whereas the resolution of the DEM was slightly coarser (0.60 x 0.60 m). Besides, photogrammetric DEM generation is known to be prone to errors in crevassed areas (Barrand et al., 2009; Noh & Howat, 2015). The orthomosaic was therefore chosen to perform the detection. Our approach was based on Gabor filters, an image analysis technique for texture extraction that emphasizes linear features in an image, with tunable parameters of orientation, wavelength and frequency. In a glaciological context, Gabor filters have been used by Brenning et al. (2012) to map rock glacier flow patterns. Here we used a bank of filters with 8 different orientations and wavelengths between 5 and 10 m. The analysis was performed using OpenCV implementation of Gabor filters, written in the Python programming language.

2.3. Results and discussion

2.3.1. Identification of large-scale features

Firstly, we identified the two large-scale features: the glacier area and the debris-ice transition zones (i.e. moraines). Based on the UAV orthomosaic, the glacier is easily separated from the rest of the

scene (Fig. 2) and when compared against visual assessment the approach identifies the terminus correctly, although misclassification occurs at the margins of the medial moraines. On the western part of the glacier tongue, a transition zone from glacier ice to medial moraine to lateral moraine is well visible (see also Fig. 2) and the glacier margin is quite difficult to delimit correctly here. Slight overestimation of the glacier boundaries also occurs at the right margin of the eastern ice stream, because of fine debris located below a rock spur outside the glacier. Inclusion of morphometric parameters (such as slope and curvature) from the DEM in the classification process does not significantly improve the results. In fact, a DEM obtained via stereo-matching needs several images from different view angles and this does not occur at the margins. Therefore, the DEM quality decreases significantly along these areas (Küng et al., 2011).

The segmentation process produces gaps in the final glacier and moraine segments due to very different RGB values compared to the neighboring pixels. On the upper parts of the moraines, these are mostly caused by isolated larger dry clasts not affected by meltwater, and thus possessing higher reflectance. Conversely on the actual glacier surface and on the terminal part of the eastern moraine, gaps appear as crevasses or at the debris/ice interface. If the final purpose is to produce a glacier map for inventories, it is recommended that these gaps should be removed via vector analysis. In this study however, they were included in the classification process. Isolated clasts can be considered as part of the medial moraine, and we included them in this category by performing neighborhood analysis, applying a 5x5 pixels neighborhood smoothing filter on unclassified data surrounded by medial moraine pixels. Conversely, gaps surrounded by glacier ice pixels were automatically assigned to the class debris-rich ice. This can leave clasts misclassified if larger than the filter size, and this issue could be solved using another segmentation step or individual correction to refine the overall classification.

To evaluate the advantages provided by the UAV orthoimage, we compared it to the classification based on medium-resolution data acquired by Landsat 8 (Fig. 2 and Tab. 1). Figure 2 shows the

comparison between segmentation applied on UAV orthoimage (dark blue, yellow colours) and supervised classification using a combination of optical and thermal bands applied on Landsat 8 OLI/TIRS image (cyan, red colours). The higher resolution semi-automatic approach (based on the UAV orthoimage), even if using optical data alone, identifies the glacier surface better than the lower resolution method (based on the Landsat 8 image). In fact, through visual assessment we found that the latter misses the debris-covered sections of the glacier terminus and the terminal part of the western medial moraine. Another means of validating the accuracy of these approaches could consist in sampling reference points on the ground. However, this appears not necessary since the resolution of the UAV image is 0.15 m, much finer than the size of the large-scale features.

To better discriminate the medial moraines on the Landsat image, thermal bands could be excluded, because of their coarseness compared to optical bands. This way, however, relatively clean parts of the glacier would be classified as debris-covered.

Table 1 reports the areas of glacier features calculated from the final high- and medium-resolution classification maps: the total area of medial moraine pixels is very similar. Conversely, the medium-resolution-based approach underestimates the exposed ice area, as can be seen by looking at the eastern ice stream on Figure 2 and by considering the glacier ice area (Tab. 1). As a result, the total area occupied by the glacier in the Landsat based classification is also slightly lower. To evaluate the area estimation accuracy, we followed the methodology suggested by Vögtle & Shilling (1997) and applied among others by D'Agata et al. (2014), buffering the glacier perimeter to account for the sharpness of glacier limits, using a value of half the pixel size as the linear resolution error (O'Gorman, 1996). The uncertainty in the total area estimation from pixel resolution alone associated with a medium-resolution based classification is significantly larger (12 % compared to 0.002%), giving the limited size of the Forni glacier. Over short time scales, estimation of areal changes using medium-resolution tools like Landsat would thus be subject to an important noise component.

A direct comparison between the two approaches is only possible when considering large-scale features, since the small-scale ones, i.e. snow patches, epiglacial lakes and crevasses are smaller than a single pixel on the Landsat scene. Although fine debris is also not visible on the Landsat images, a shift towards lower reflectance values for ice is observable downglacier, especially closer to the terminus.

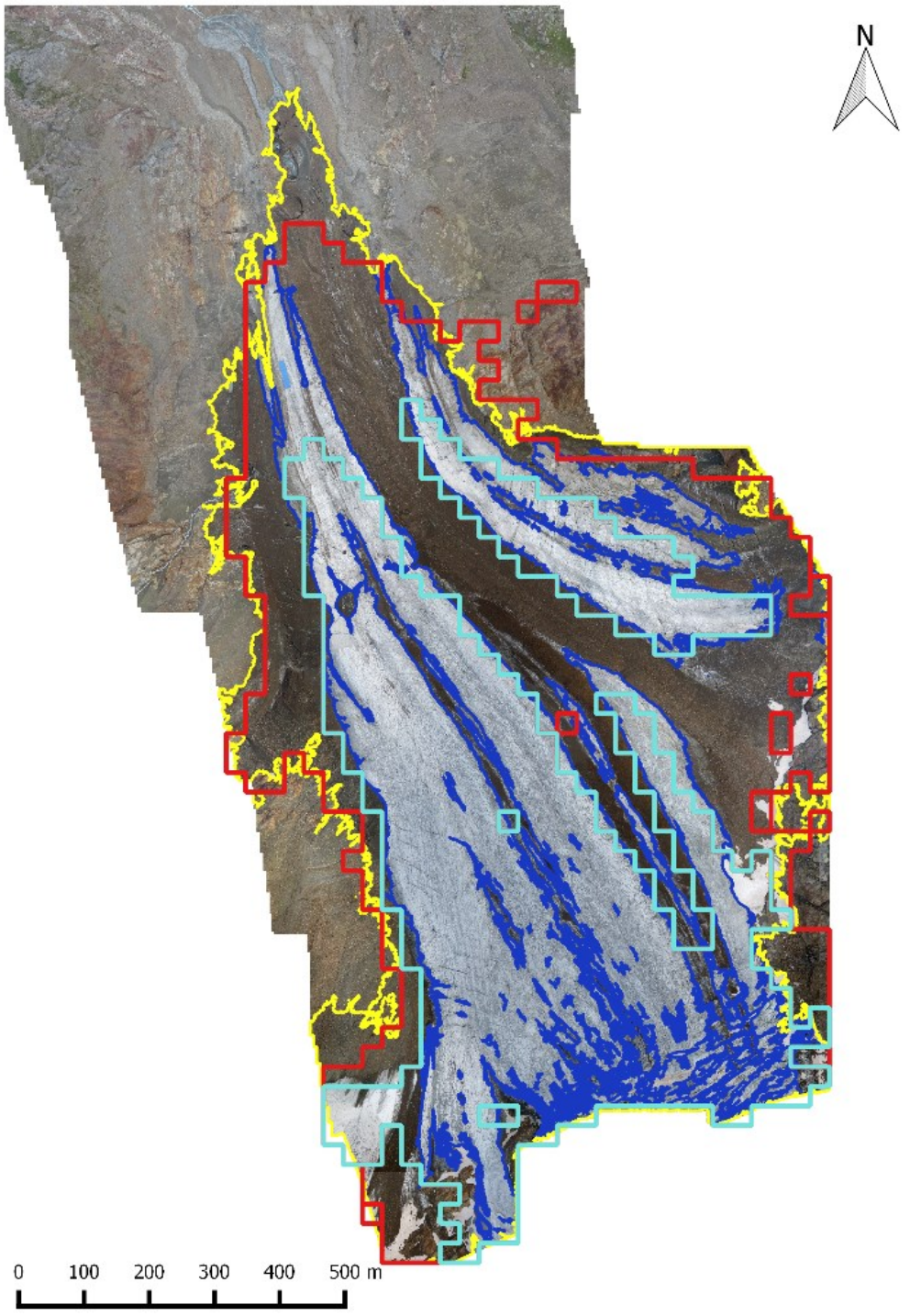

Fig. 2: Comparison between areas of bare ice and glacier perimeter derived from UAV-based (dark blue and yellow, respectively) and Landsat 8-based (light blue and red, respectively) classification. The base layer is the UAV image

Category	UAV-based classification		Landsat 8 -based classification		Δ area (Landsat 8 - UAV)
	Area (m^2)	Area (%)	Area (m^2)	Area (%)	Area (m^2 and %)
Glacier ice	512870 ± 0.006%	53.93	496568 ± 24%	52.48	-16302 or - 3.2%
Moraines	448036 ± 0.006%	46.07	449571 ± 24%	47.52	+1535 or + 0.34%
Total	960906 ± 0.002%	100.00	946139 ± 12%	100.00	-14767 or – 1.5%

Tab. 1: Comparison *between areas resulting from high- and medium-resolution classification of the Forni Glacier ablation tongue.*

2.3.2. Identification of small-scale features based on the UAV orthomosaic

Visual inspection of the entire UAV orthomosaic reveals many features not discernible on lower resolution images, namely: i) snow patches prominent on the upper parts (relative to the study area) of the eastern and central ice streams; ii) fine and sparse debris patches and debris bands located on the glacier surface; iii) the debris cone on the central part of the tongue; iv) the supraglacial pond located on the eastern part of the tongue and the small lake at the take-off site (Rosole Lake), as well as smaller scattered proglacial and epiglacial ponds; and v) longitudinal and transverse crevasses widespread on the glacier surface, especially the eastern ice stream.

The final map produced by the segmentation approach is shown in Figure 3. Slight misclassification errors occurred for dirty snow, as some patches were missed by the segmentation approach because of insufficient contrast with the surrounding terrain. For this reason, snow patches are displayed in purple in Figure 3, not distinguishing between clean and dirty ones, and they cover 25132 m^2 (Tab. 3). Unlike snow, the ice surfaces were well detected, and labelled differently whether partially or completely debris-covered (yellow and brown pixels, respectively) or debris-free (cyan pixels). As expected along the ablation tongue in August, the glacier ice (cyan pixels) covers a wider area compared to snow (45.66% and 2.58%, respectively, Tab. 2). Like the medial moraines, the small neo-moraines are correctly identified by the segmentation approach. In addition, the terminal part of the eastern medial moraine results correctly characterized by a mix of supraglacial debris (brown pixels), debris-rich ice

(yellow pixels) and epiglacial lakes (blue pixels). In fact, recently the glacier has undergone very intense dynamic processes, compromising surface stability and causing enlargement of crevasses especially along the eastern tongue, and collapse of other areas. An example of the latter is indeed found on the terminal part of the eastern medial moraine (visible as cyan pixels in Fig. 3). As an evidence of the darkening phenomena reported by previous studies (Diolaiuti & Smiraglia, 2010; D'Agata et al., 2014), the supraglacial debris covers a similar area with respect to the glacier ice (i.e. ca. 46%, Tab. 2). Moreover, the large pond located at the margin of the eastern ice stream is correctly identified compared to visual assessment, with an area of 309.23 m^2, and the two smaller ponds at the frontal glacier margin are properly recognized as well. The total area of epiglacial lakes covers 841 m^2 (blue pixels in Fig. 3, see also Tab. 2).

Finally, we applied the Gabor filter over the whole UAV orthoimage (not shown). The largest number of crevasses is recognized when using a low wavelength value of 5 m, consistent with the spacing of crevasses on the glacier surface. However, a significant number of false positives is also produced, mostly due to shadows projected by larger clasts that appear as linear features. Overall, the approach showed promising results. As suggested by Brenning et al. (2012), further research aimed at improving the classification should combine different methodologies, including other texture measures or terrain parameters (i.e. local curvature) to filter out unwanted shadow effects.

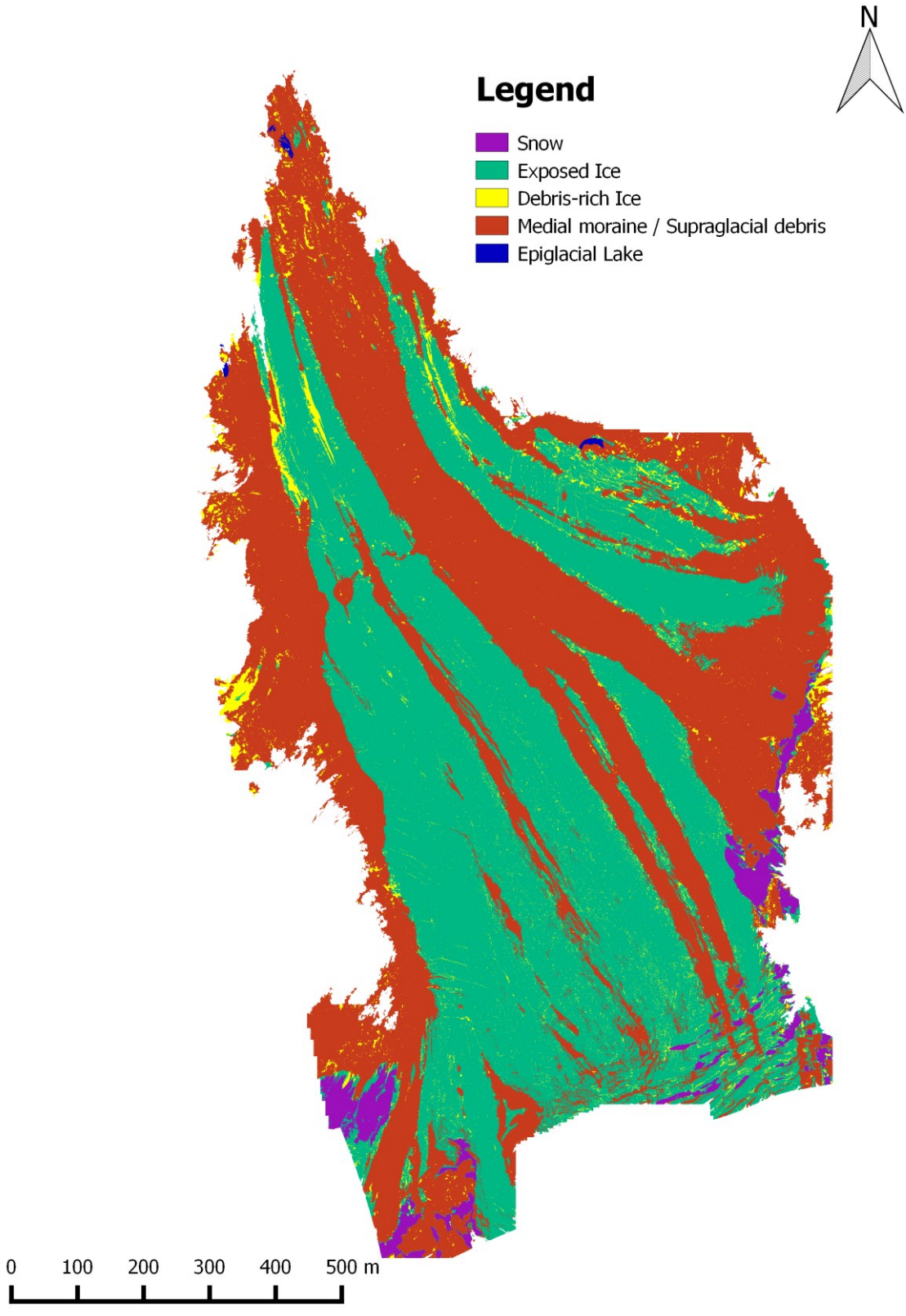

Fig. 3: Segmentation-based classification of UAV orthoimage of the ablation tongue of the Forni Glacier.

Category	UAV-based classification	
	Area (m^2)	**Area (%)**
Snow	25132	2.58
Debris-Free Ice	453841	46.66
Debris-Rich Ice	33058	3.40
Moraines	448036	46.07
Lakes	841	0.09
Total	960906	100.00

Tab. 2: Area values covered by small-scale features resulting from high-resolution classification of the Forni Glacier ablation tongue.

A more detailed analysis was performed over an area with relatively uniform shadowing along the eastern ablation tongue (47544 m^2, Fig. 4). There, in addition to the delineation of water ponds and crevasses, fine debris cover is more deeply analyzed. In this area, debris supply comes mostly from macrogelivation and rock degradation processes (Azzoni et al., 2014) and a transition from supraglacial debris (i.e. buried-ice) to exposed ice (i.e. bare-ice) is well discerned away from the margin towards the center (lower part of both the images in Fig. 4). Here, the darkening phenomena are even more evident compared to the picture showing the entire tongue (Fig. 3): the bare-ice pixels are 7.49% of the total excluding water pond and crevasses. The area is also heavily crevassed and here application of the Gabor filter is particularly successful (black pixels in Fig. 4). This is a consequence of uniform illumination restricting the range of RGB values, although some sections are still missed because of lack of contrast. As expected the water pond is also well identified. The analysis shown in Figure 4 is a further proof of the intensity of the recent glacier dynamics. In fact, in spite of crevasses covering only 2.79% of the total investigated area, the surface appears very fragmented due to their wide spatial distribution. In addition, the water pond was likely created by a significant collapse.

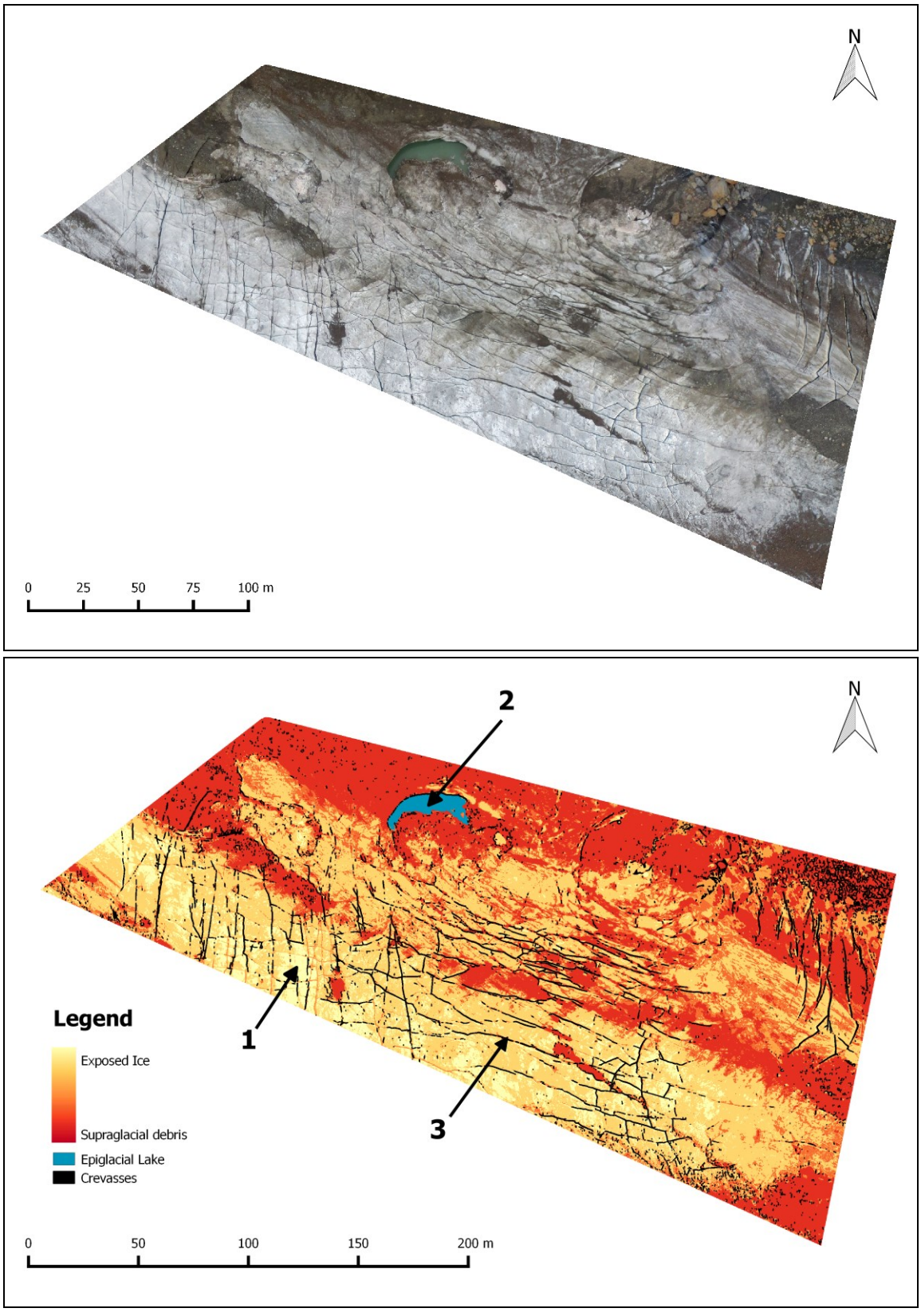

Fig. 4: (A) Original UAV orthoimage and (B) classified test area for fine debris occurrence, from exposed ice to supraglacial debris (red color scale). Crevasses are also shown in black and the large epiglacial lake in blue. With the numbers 1 to 3 are displayed examples of exposed ice, epiglacial lake and crevasses, respectively.

2.4. Conclusions

The methodology presented here shows that it is possible to provide high-resolution mapping of a glacier using a semi-automatic approach based on uncalibrated RGB data, obtained with a low cost on-demand UAV survey, with an accuracy comparable or higher than when using medium-resolution satellite data. Large-scale features (i.e. exposed glacier surface and medial moraines) could be easily identified using this approach, with only slight misclassification at the margins of the medial moraines. This suggests that for the purpose of generating glacier inventories a segmentation step based on high-resolution orthoimagery (from UAV or conventional aerial surveys) could speed up delineation of glacier boundaries especially on debris free glaciers. Another significant advantage of a high-resolution approach is the decrease in uncertainty related to pixel size, potentially enabling estimation of areal changes over short periods. Classification of debris-covered glaciers with different lithology and morphology of debris cover remains to be tested, although the capability of UAVs to carry different payloads means that different data sets, including near infrared, thermal and morphometric data could be used to improve accuracy of the results. The inclusion of these data sets could also lead to faster algorithms. In fact, compared with coarser resolution approaches, the methodology we proposed requires considerable user input for threshold selection and manual checking of the segments.

An important improvement over medium-resolution based classification is the ability to map smaller geomorphological features, including snow coverage, epiglacial lakes and crevasses. For the latter, a new approach was presented here based on Gabor filters, which showed promising results. Continuous mapping of these features can inform the local communities, as these features can represent a hazard, and give important clues as to the evolution of the glacier and the magnitude of the stresses acting upon the surface.

Our findings represent a further proof of the general darkening phenomena occurring at the Alpine debris-free glaciers (Oerlemans et al., 2009; Diolaiuti & Smiraglia, 2010) and in particular at the Forni

Glacier tongue (D'Agata et al., 2014). Indeed, we found that the bare-ice surfaces cover a similar area compared to the buried-ice ones. In addition, the intensity of recent glacier dynamics and the resulting surface instability is evident in the mapped morphologies such as crevasses (2.79% of the total area investigated in detail) and water ponds.

UAV-based remote sensing is still explorative, and at present there is a lack of standard procedures for correct calibration of the data, when they are used to estimate physical quantities (e.g. reflectance) rather than for qualitative assessment such as mapping. As an example, in our research we found the shadowing effect of local topography and geometry of the illumination to be important factors in driving the final RGB values of the orthomosaic. This prevented further classification of fine debris glacier-wide, and although these issues have been tackled for spaceborne sensors, the algorithms will have to be adapted for the platform shift.

Another critical issue of UAV-based remote sensing, also noted by Whitehead et al. (2013), is that limitations imposed by battery life and line-of-sight operation currently restrict flight time, so that for instance an entire survey of the Forni Glacier would have required multiple flights. However, this is the largest valley glacier in the Italian Alps, where instead smaller glaciers are predominant. Since small glaciers are more likely to be inaccurately classified when using lower resolution data and have been shown to react strongly to climate change (e.g. D'Agata et al., 2014; Diolaiuti et al., 2012), the introduction and improvement of low-cost mapping methods can make an important contribution to Alpine glaciological and geomorphological studies.

2.5. Acknowledgments

The research was performed under the umbrella of an agreement between the Università degli Studi di Milano and Sanpellegrino SpA brand Levissima. Moreover the Agricola 2000 S.c.p.A supported this study taking part with their UAV to the field investigations and also participating to the Lab analysis. The authors kindly acknowledge the Stelvio National Park managers and staff for their help and

support. This work was also performed in the framework of the PRIN project 2010/2011 (2010AYKTAB_006), local leader C. Smiraglia. The results of this research also represent a contribution to the development of the updated guidelines of the New Italian Geomorphological Map under the umbrella of the AIGEO working group.

2.6. References

Azzoni R.S., Senese A., Zerboni A., Maugeri M., Smiraglia C. and Diolaiuti G. (2014): A novel integrated method to describe dust and fine supraglacial debris and their effects on ice albedo: the case study of Forni Glacier, Italian Alps. *The Cryosphere Discussion*, 8, 3171-3206.

Barrand N.E., Murray T., James T.D., Barr S.L. and Mills J.P. (2009): Optimizing photogrammetric DEMs for glacier volume change assessment using laser-scanning derived ground-control points. *Journal of Glaciology*, 55, 106-116.

Benn D.I., Bolch T., Hands K., Gulley J., Luckman A., Nicholson L.I., Quincey D., Thompson S., Toumi R. and Wiseman S. (2012): Response of debris-covered glaciers in the Mount Everest region to recent warming, and implications for outburst flood hazards. *Earth Science Reviews*, 114, 156-174.

Blaschke T. (2010): Object-based image analysis for remote sensing. *ISPRS Journal of Photogrammetry and Remote Sensing*, 65, 2-16.

Boggero A., Rogora M., Musazzi S., Zaupa S., Lami A., Salerno F., Guzzella L., Gambelli S., Guyennon N., Viviano G., Thakuri S. and Tartari G. (2013): Un Mondo D'acqua In Alta Quota. Le acque del Parco Nazionale dello Stelvio, un laboratorio a cielo aperto per lo studio dei cambiamenti climatici. Ed. Associazione Comitato Ev-K2-CNR, 91 pp.

Brenning A., Long S. and Fieguth P. (2012): Detecting rock glacier flow structures using Gabor filters and IKONOS imagery. *Remote Sensing of Environment*, 125, 227-237.

D'Agata C., Bocchiola D., Maragno D., Smiraglia C. and Diolaiuti G. (2014): Glacier shrinkage driven by climate change during half a century (1954–2007) in the Ortles-Cevedale group (Stelvio National Park, Lombardy, Italian Alps). *Theoretical and Applied Climatology*, 116, 169-190.

Diolaiuti G., Bocchiola D., D'Agata C. and Smiraglia C. (2012): Evidence of climate change impact upon glaciers' recession within the Italian alps: the case of Lombardy glaciers. *Theoretical and Applied Climatology*, 109, 429-445.

Diolaiuti G. and Smiraglia C. (2010): Changing glaciers in a changing climate: how vanishing geomorphosites have been driving deep changes in mountain landscapes and environments. *Géomorphologie: relief, processus, environnement*, 2, 131-152.

Dozier J. and Frew J. (1990): Rapid calculation of terrain parameters for radiation modeling from Digital Elevation Data. *IEEE Transactions on Geoscience and Remote Sensing*, 28, 963-969.

EEA (European Environment Agency) (2012): Climate change, impacts and vulnerability in Europe 2012. http://www.eea.europa.eu/publications/climate-impacts-and-vulnerability-2012/at_download/file.

Fischer M., Huss M., Barboux C. and Hoelzle M. (2014): The new Swiss Glacier Inventory SGI2010: relevance of using high-resolution source data in areas dominated by very small glaciers. *Arctic, Antarctic, and Alpine Research*, 46, 933–945.

Hodson A., Anesio A.M., Ng F., Watson R., Quirk J., Irvine-Fynn T., Dye A., Clark C., Mccloy P., Kohler J. and Sattler B. (2007): A glacier respires: Quantifying the distribution and respiration CO2 flux of cryoconite across an entire Arctic supraglacial ecosystem. *Journal of Geophysical Research*, 112, 1-9.

Immerzeel W.W., Kraaijenbrink P.D.A., Shea M.J., Shrestha A.B., Pellicciotti F., Bierkens M.F.P. and De Jong, S.M. (2014): High-resolution monitoring of Himalayan glacier dynamics using unmanned aerial vehicles. *Remote Sensing*, 150, 93-103.

Johannesson T., Bjornsson H., Palsson F., Sigurdsson O. and Thorsteinsson T. (2011): LiDAR mapping of the Snæfellsjökull ice cap, western Iceland. *Jokull*, 61, 19-32.

Knoll C. and Kerschner H. (2009): A glacier inventory for South Tyrol, Italy, based on airborne laser-scanner data. *Annals of Glaciology*, 50, 46-52.

Küng O., Strecha C., Beyeler A., Zufferey J.C., Floreano D., Fua P. and Gervaix, F. (2011): The Accuracy Of Automatic Photogrammetric Techniques On Ultra-Light Uav Imagery. 38, International Archives of the Photogrammetry, Remote Sensing and Spatial Information Sciences, Conference on Unmanned Aerial Vehicle in Geomatics, Zurich, Switzerland.

Noh M.J. and Howat I.M. (2015): Automated stereo-photogrammetric DEM generation at high latitudes: Surface Extraction from TIN-Based Search Minimization (SETSM) validation and demonstration over glaciated regions. *GIScience and Remote Sensing*, 52, 198-217.

Oerlemans J., Giesen R.H. and Van Den Broeke M.R. (2009): Retreating alpine glaciers: increased melt rates due to accumulation of dust (Vadret da Morteratsch, Switzerland). *Journal of Glaciology*, 55, 729-736.

O'Gorman L. (1996): Subpixel precision of straight-edged shapes for registration and measurement. *IEEE Transactions on Pattern Analysis and Machine Intelligence,* 18, 746-751.

Paul F., Barrand N.E., Baumann S., Berthier E., Bolch T., Casey K., Frey H., Joshi S.P., Konovalov V., Le Bris N., Molg N., Nosenko G., Nuth C., Pope A., Racoviteanu A., Rastner P., Raup B., Scharrer K., Steffen S. and Winsvold S. (2013): On the accuracy of glacier outlines derived from remote-sensing data. *Annals of Glaciology*, 54, 171-182.

Ryan J.C., Hubbard A.L., Box J.E., Todd J., Christoffersen P., Carr J.R., Holt T.O. and Snooke N. (2015): UAV photogrammetry and structure from motion to assess calving dynamics at Store Glacier, a large outlet draining the Greenland ice sheet. *The Cryosphere*, 9, 1-11.

Senese A., Diolaiuti G., Mihalcea C. and Smiraglia C. (2012a): Energy and mass balance of Forni Glacier (Stelvio National Park, Italian Alps) from a 4-year meteorological data record. *Arctic, Antarctic, and Alpine Research*, 44, 122-134.

Senese A., Diolaiuti G., Verza G.P. and Smiraglia C. (2012b): Surface energy budget and melt amount for the years 2009 and 2010 at the Forni Glacier (Italian Alps, Lombardy). *Geografia Fisica e Dinamica Quaternaria*, 35, 69-77.

Shukla A., Arora M.K. and Gupta R.P. (2010): Synergistic approach for mapping debris-covered glaciers using optical–thermal remote sensing data with inputs from geomorphometric parameters. *Remote Sensing of Environment,* 114, 1378-1387.

Smiraglia C. (1989): The Medial moraines of Ghiacciaio dei Forni, Valtellina, Italy: morphology and sedimentology. *Journal of Glaciology*, 35, 81-84.

Storey J., Choate M. and Lee K. (2014): Landsat 8 Operational Land Imager On-Orbit Geometric Calibration and Performance. *Remote Sensing*, 6, 11127-11152.

USGS (United States Geological Survey) (2013): Using the USGS Landsat 8 Product. Available at: http://landsat.usgs.gov/Landsat8_Using_Product.php, Last Accessed 17/5/2013.

Vögtle T. and Schilling K.J. (1999): Digitizing Maps. In: BÄHR H.-P. & VÖGTLE T. (eds.), «GIS for Environmental Monitoring», Stuttgart, Germany, Schweizerbart, 201-216.

Whitehead K., Moorman B.J. and Hugenholtz C.H. (2013): Brief Communication: Low-cost, on-demand aerial photogrammetry for glaciological measurement. *The Cryosphere*, 7, 1879-1884.

Chapter 3
Estimating ice albedo from fine debris cover quantified by a semi-automatic method: the case study of Forni Glacier, Italian Alps

Chapter published on The Cryosphere

Azzoni R.S., Senese A., Zerboni A., Maugeri M., Smiraglia C. and Diolaiuti G.A. (2016) - Estimating ice albedo from fine debris cover quantified by a semi-automatic method: The case study of Forni Glacier, Italian Alps. *The Cryosphere*, 10(10), 665-679.

Abstract

In spite of the quite abundant literature focusing on fine debris deposition over glacier accumulation areas, less attention was paid to the glacier melting surface. Accordingly, we proposed a novel method based on semi-automatic image analysis to estimate ice albedo from fine debris coverage (*d*). Our procedure was tested on the surface of a wide Alpine valley glacier (the Forni Glacier, Italy), in summer 2011, 2012 and 2013 acquiring parallel datasets of in-situ measurements of ice albedo and high-resolution surface images. Analysis of 51 images yielded *d* values ranging from 0.01 to 0.63 and albedo was found varying from 0.06 to 0.32. The estimated *d* values are in a linear relation with the natural logarithm of measured ice albedo (R = -0.84). The robustness of our approach in evaluating *d* was analyzed through five sensitivity tests, and we found that it is largely replicable. On the Forni Glacier, we also quantified a mean debris coverage rate (C_r) equal to 6 g/m^2 per day during ablation season 2013, thus supporting previous studies that describe ongoing darkening phenomena at Alpine debris-free glaciers surface. In addition to debris coverage, we also considered the impact of water (both from melt and rainfall) as a factor tuning albedo: meltwater occurs during the central hours of the day, decreasing the albedo due to its lower reflectivity, instead rainfall causes a subsequent mean daily albedo increase slightly higher than 20%, although short lasting (from 1 to 4 days).

3.1. Introduction

3.1.1. Research motivation and study aims

An understanding of how albedo varies in response to changes in the state of the surface is a crucial component in modeling ice melt and in describing the climate of the ice-covered regions and the climate in general (see Grenfell, 2011). Moreover, in the recent climate modeling studies, attention is paid to the "ice-albedo feedback" and to its action in modulating the changes in the total energy balance of the analyzed area (Grenfell, 2011). One of the most important factors driving albedo changes is the occurrence of debris at the glacier surface, as it influences the features and evolution of glaciers and glacierized areas in numerous ways (Bolch, 2011). Recently, dust and black carbon deposition on glacier accumulation areas (i.e. at the surface of snow and firn) are of increasing interest to the scientific community due to accelerated snow melting rates affecting glaciers in the high elevation glacierized areas of Asia (Flanner et al., 2009; Yasunari et al., 2010). In addition, Dumont et al. (2014) found that the Greenland springtime darkening since 2009 stems from a widespread increase in the amount of light-absorbing impurities in snow, as well as in the atmosphere. Clarke and Noone (1985) found that the black carbon deposition caused an Arctic snow albedo reduction of 1–3% in fresh snow and by an additional factor of 3 as the snow ages. Hansen and Nazarenko (2004) modeled this decreased albedo in Arctic snow and sea ice and found this resulted in a hemispheric radiative forcing of +0.3 W m^{-2}, which may have substantially impacted the Northern Hemisphere climate in recent decades.

In spite of this abundant literature, the effects of fine (mainly dust) debris cover at the melting surface of debris-free (mountain) glaciers are still poorly debated and sometimes underestimated.

In this contribution, we quantified fine debris coverage at the melting surface of an Alpine debris-free glacier in order to evaluate its seasonal variability and its influence on ice albedo. In particular, to permit comparisons between different glacier zones and among different glaciers, we developed a

protocol to standardize field and laboratory analyses. Moreover, we assessed the influence of water (originating from ice melt and liquid precipitation) on the ice albedo variability. Finally, we analyzed the short-term evolution of fine debris occurring at the glacier surface by describing its sedimentological properties and the debris coverage rate during the ice melting season.

3.1.2. Previous studies and recent literature on fine debris occurring at glacier surface

One of the most important factors driving glacier albedo (apart from, for instance, the meteorological conditions and light scattering by bubbles and cracks) is light absorption by fine debris and dust (Brock et al., 2000, Brock, 2004; Klok et al., 2003).

Fine debris and dust vary across the glacier surface both in space and in time, and consist of mineral and organic fractions with a mean diameter lower than 2 mm. Both components may be autochthonous or allochthonous from both englacial origin and wind transport. The organic elements can originate from bacterial decomposition of organic matter (in situ or outside the glacier), or they can consist of black carbon (so they derive from fossil combustion and fires), as well as living organisms, pollens and other vegetal and organic residuals remain in the aerosols (Fujita, 2007; Takeuchi et al., 2001; Takeuchi, 2002). The mineral fraction can be locally derived from the weathering of rock outcrops and nunataks or from lateral moraines and debris slopes. In fact, during the summer, when warmer climatic conditions occur, the dry and unconsolidated materials constituting moraines are easily transported by wind gusts and deposited tens to hundreds of meters away and even higher, depending on wind speed and the roughness of the area surrounding the glacier (Oerlemans et al., 2009). In the case of englacial origin, the fine debris can also originate from mechanical disintegration of the bedrock below the glacier or the deformation and weathering processes of the rocks embedded in the ice. Dust and fine debris can also be transported for long distances by atmospheric circulation from non-glaciated areas (Ming et al., 2009; Ramanathan, 2007). For instance, the deposition of Saharan dust (Sodermann et al., 2006) or volcanic ash (Conway et al., 1996) on glaciers is a well-known phenomenon that darkens mountain debris-free glaciers (e.g.: Paul and Kääb, 2005; Paul et al., 2007; Oerlemans et al., 2009;

Diolaiuti and Smiraglia, 2010; Casey, 2012; Painter et al., 2013) thus changing their albedo and affecting melt magnitude and rates.

The occurrence of fine debris at the surface of debris-free glaciers and the role it plays in ice melting rates make correctly determining ice albedo important. The albedo parameterizations used in energy and mass balance models are, however, often inadequate to represent spatial and temporal changes in the surface albedo and are consequently regarded as a major source of errors (e.g.: Arnold et al., 1996; Klok and Oerlemans, 2002; Klok et al., 2003). Therefore, studies that combine measurements of fine debris distribution and features with systematic measurements of glacier albedo are needed.

Dust deposition on snowpacks has been well studied (e.g.: Qian et al., 2011; Yasunari et al., 2010). A possible snow albedo reduction due to black carbon contamination was revealed by radiation measurements at the snow surface performed at Barrow, Alaska (Aoki et al., 1998, 2006) and in Japanese urban areas (Motoyoshi et al., 2005). In the case of snow and firn, a field procedure was developed, followed by further standardized lab-analyses to quantify and describe black carbon presence and features (Yasunari et al., 2010).

However, less attention has been paid to fine debris and dust deposition at the glacier melting surface. A first attempt to parameterize not only snow albedo variability but also the ice albedo on a debris-free glacier was performed by Brock et al. (2000). In spite of the good results they obtained analyzing snow covered areas, their evaluation of the impact of debris cover on ice albedo was less accurate. In fact, they assessed the debris cover using only a 0.5 m^2 quadrat and basing their investigation on just two criteria (i.e. cumulative melt and number of days, both calculated following exposure of the ice surface). Recently, Pope and Rees (2014) investigated the spectral responses of different ash/debris cover types on the glaciers of Midtre Lovénbreen (Svalbard) and Langjökull (Iceland). These studies suggested the need for further research to standardize the measurements of fine debris and dust at the glacier ice surface, thus avoiding the use of surrogates unable to fully describe debris coverage and its seasonal variability.

3.1.3. Study Area

Our experiments were carried out on the ablation tongue of the Forni Glacier (Figure 1), the widest Italian valley glacier, featuring a surface area of 11.34 km^2 (2007 data, Garavaglia et al., 2012). It is located in the Ortles-Cevedale Group, Stelvio National Park, Lombardy Alps. It is widely debris-free, even if darkening phenomena are ongoing (D'Agata et al., 2014), and some authors have recently pointed out that fine and sparse debris is becoming abundant due to the ongoing glacier shrinkage (Diolaiuti and Smiraglia, 2010; Diolaiuti et al., 2012; Senese et al., 2012a). For this reason, the Forni Glacier can be considered a good laboratory to evaluate fine and sparse debris distribution and seasonal evolution and its influence on ice albedo. The Forni Glacier is facing toward North, is about 3 km long and its altitude ranges from 2600 m to about 3670 m a.s.l. Metamorphic rocks, mostly micaschist rich in quartz, muscovite, chlorite and sericite, constitute the dominant lithology (Montrasio et al., 2008); these rocks emerge from the glacier surface as nunataks (mainly in the accumulation basins) and as rock outcrops (surrounding the glacier tongue). The latter are increasing in size and becoming very frequent due to the ongoing glacier retreat and thinning (Diolaiuti and Smiraglia, 2010; Diolaiuti et al., 2012).

Studies on short-term changes of the Forni Glacier have been performed through an Automatic Weather Station (named AWS1 Forni) in operation since 2005 at the glacier melting surface. The AWS1 Forni is located on the ablation tongue (c. 2631 m a.s.l.), about 800 m from the glacier terminus, and it is equipped with sensors for measuring air temperature and humidity, wind speed and direction, atmospheric pressure, liquid precipitation and snow depth, and longwave and shortwave radiation, both incoming and outgoing (Citterio et al., 2007; Diolaiuti et al., 2009; Senese et al., 2010, 2012a, 2012b, 2014).

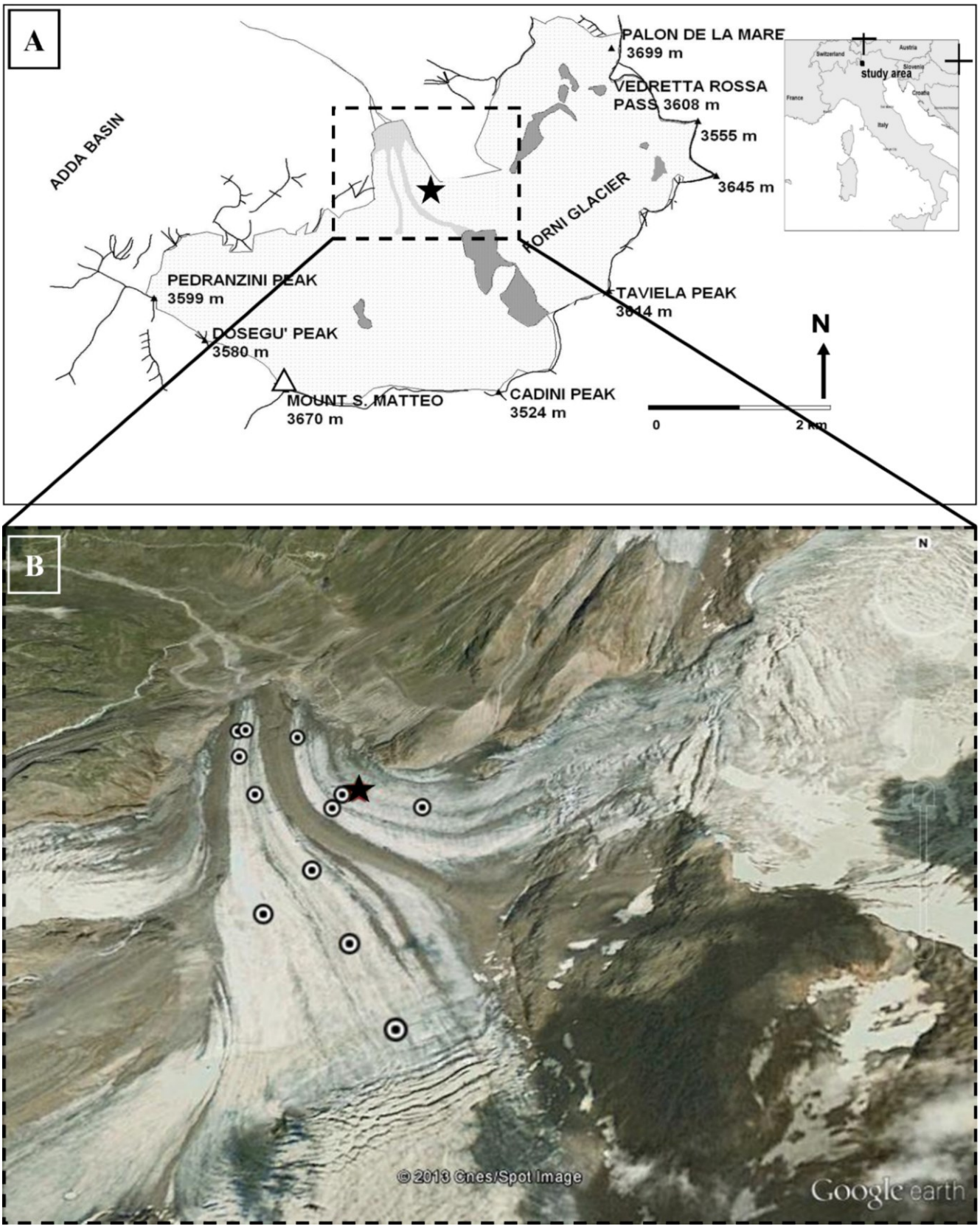

Fig. 1: (A) The position of Forni Glacier in the Italian Alps and of AWS1 Forni (black star, in both panels). (B) Enlarged view of the Forni Glacier (image credit: GoogleEarthTM) showing the location of field measurements (black dots).

3.2. Methods

In the time frame 2011-2013, 51 field measurements in all were obtained on the debris-free ablation tongue of the Forni Glacier (Figure 1b): both fine debris quantification (i.e. spatial coverage) and albedo evaluation (Figure 2). Moreover, we sampled fine debris at the glacier melting surface to assess the debris coverage rate (C_r) and the sedimentological properties (i.e. grain size, humified and total organic carbon and mineralogical properties). The sites for field measurements were chosen considering: i) homogeneity in debris cover, ii) presence or absence of fine sparse debris, iii) diverse debris grain size, and iv) different distances from rock slopes and medial moraines, which are the main debris suppliers, thus assuring that the selected sites are representative of the range of surfaces present at the glacier melting area. At each site, we sampled a 1 m x 1 m parcel with the aim of assuring the effectiveness and the repeatability of the measurements. Larger areas would have required more time for data collection and would have limited the number of sites analyzed, while smaller quadrats would not have captured the spatial heterogeneity of the surface. Each sampling area was selected to be representative of as wide an area as possible. The medial moraines were excluded from this work because we only focused on fine and sparse debris-covered ice and not on actual buried ice (i.e. ice covered by a thick and quite continuous debris layer). Figure 1 shows the study area and the positions of the sites analyzed.

Fig. 2: Series of pictures illustrating: (A) sampling supraglacial debris, (B) measuring albedo and (C) acquiring high-resolution digital images of the glacier surface.

3.2.1. Debris cover quantification

The quantification of sparse and fine debris at the glacier melting surface was performed by acquiring high resolution digital images at each site analyzed (Figure 2c) and processing them with image analysis software *ImageJ* following Irvine-Fynn et al. (2010) (Figure 3). Digital RGB (red-green-blue, in color composite) photographs of the 1 m x 1 m parcel were taken using a digital camera (Nikon D40, 6.1 megapixels). The images affected by shadows, deformations, photographic imperfections (e.g.: poor exposure, incorrect focus) were excluded from the analysis, and for each measurement site (total 51) we selected the image that best captured sharp differences between bare ice and fine debris-covered ice.

The selected images were first cropped delimiting the 1 m x 1 m parcel (Figure 3a). Second, we converted them to 8-bit greyscale in order to highlight the contrast between glacier ice and debris/dust.

Third, as a darker grey pixel denotes the presence of debris or water or shadow (the latter due to surface roughness), we assumed that debris granules could be isolated by thresholding for those pixels with brightness values that fall below a specified GrayScale Threshold level (T_{GS}, Figure 3b), specified by a supervised classification. In particular, the threshold was iteratively adjusted until the isolated image pixels best coincided with the debris/dust (Figure 3c). An 8-bit image is composed of 256 grey tones ranging from 0 (black) to 255 (white) and ice surfaces can be isolated by selecting the pixels with brightness values higher than a specified T_{GS}; for instance, if the T_{GS} value is fixed at 100, pixels with a grey tones from 0 to 100 represent debris and pixels with a grey tone from 101 to 255 represent ice. For each image, the pixels with a value lower than T_{GS} were turned into black color and the other ones into white color (Figure 3d). Finally, the ratio of the surface covered by debris (d) was obtained as:

$$d = \frac{number\ of\ black\ pixels}{total\ number\ of\ pixels} \quad (1)$$

where the total number of pixels is 6.1 x 10^6.

As only the grey-scale threshold choice is manual and the other steps are automatic ones, the proposed method for quantifying the ratio of glacier surface covered by debris (d) can be defined semi-automatic. The reliability of this method was evaluated through five tests. More precisely, we selected 10 images from the 51 photos used in this work and we compared the d values obtained from the chosen T_{GS} data (i.e. applying our semi-automatic procedure) to d values derived from changed T_{GS} or from the application of different methods. These d values are: i) d_{10PI} data derived from point intercept approach (i.e. another largely applied method based on a visual estimation by placing a grid on the investigated area, for a detailed discussion of this approach see Elzinga et al., 2001), ii) d_{10IJ} data derived from the application of our procedure by several non-trained users (thus showing the sensitivity of our method to changes in the user), iii) $d_{+10\%}$ and $d_{-10\%}$ values obtained varying the

selected T_{GS} up to ±10% of its initial value ($T_{GS+10\%}$ and $T_{GS-10\%}$, respectively), iv) d_{MOD} data obtained selecting the modal grey-value as the threshold (T_{GS-MOD}), and v) d_{AVE} data derived averaging all 51 T_{GS} values to obtain an average threshold (T_{GS-AVE}).

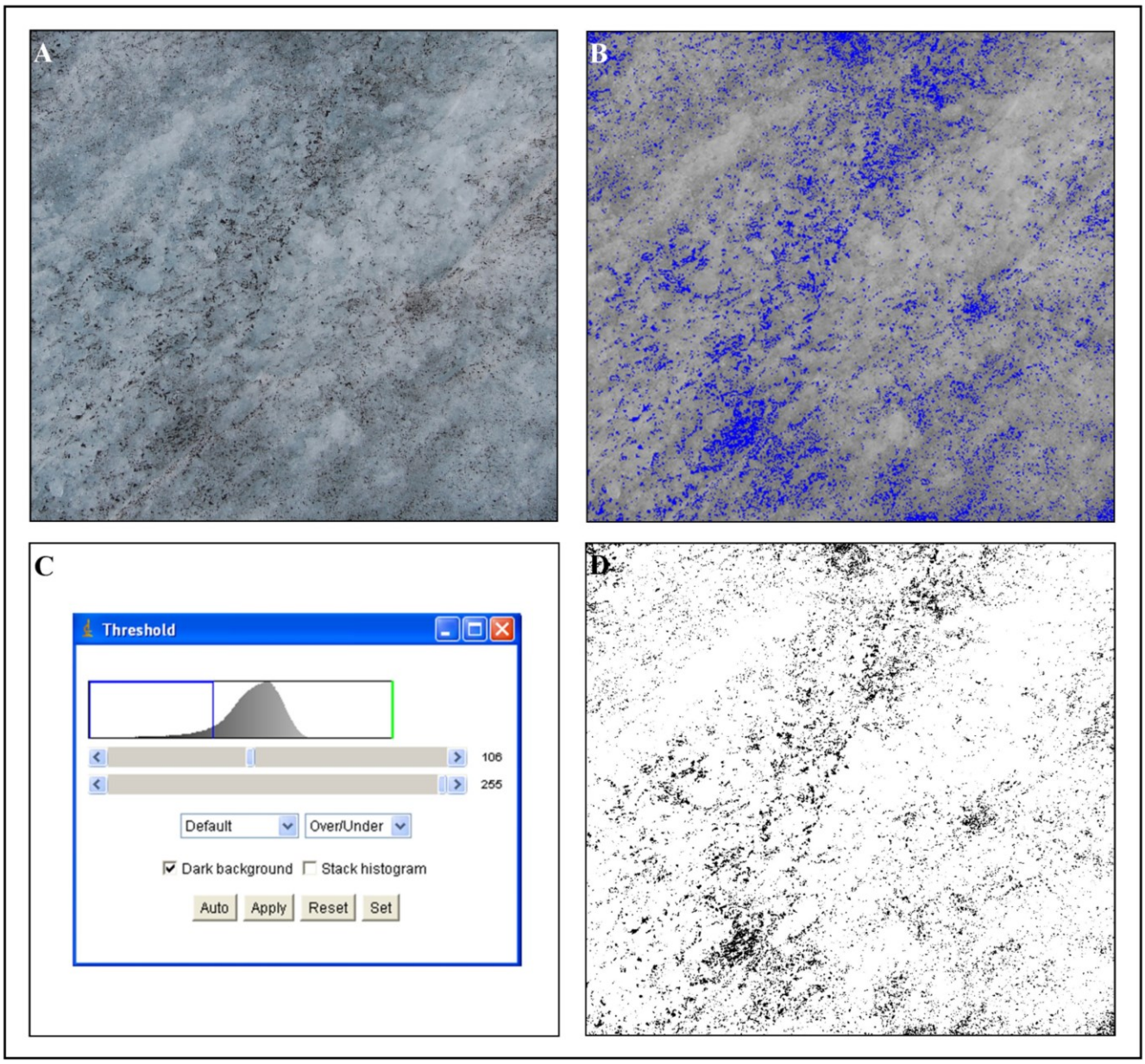

Fig. 3: Example of the procedure followed in image analysis: (A) original cut frame; (B) 8-bit conversion and discrimination between the debris-covered (in blue) and debris-free ice surface; (C) definition of the threshold; (D) calculated debris cover ratio.

3.2.2. Albedo

The bihemispherical reflectance, generally called albedo (α), is defined as the ratio of the radiant flux reflected from a unit surface area into the whole hemisphere to the incident radiant flux of

hemispherical angular extent (Schaepman-Strub et al., 2006) in the approximate spectral range 350-3000 nm (Grenfell, 2011). The albedo is an apparent optical property. This means that it depends on the angular distribution and spectral composition of the ambient radiation field as well as on the inherent optical properties, which depend only on the structural and optical properties of the medium (Grenfell, 2011). Thus, it is important to consider solar elevation, cloudiness, presence of liquid water, crystal structure, ice surface conditions, and the presence or absence of materials at the surface (rock debris, dust, organic matter, etc.). It is estimated as the ratio of measured outgoing shortwave (SW_{out}) to measured incoming shortwave (SW_{in}):

$$\alpha = \frac{SW_{out}}{SW_{in}} \quad (2)$$

For this study, the albedo was calculated from radiation data measured using two pyranometers (the ones installed in the net radiometer CNR1, Kipp&Zonen; see Figure 2). The sensor features an accuracy of ±5%. The net radiometer was equipped with a waterproof box containing a data logger, a 5 Ah battery and a 10 W solar panel on the lateral face. Moreover, a tripod was used to raise the net radiometer for short periods (c. 20-30 min for each measurement) above the ice surface. Tests regarding the influence of the height of the sensor above the surface on albedo values were performed, installing the sensor at various distances from the surface. Since we chose sites featuring homogeneous surfaces, we did not find appreciable differences between albedo values measured at the same site varying the distance between the instrument and the ice surface, thus suggesting a negligible influence of the sensor height.

The CNR1 net radiometer was chosen for its accuracy and resolution in measuring shortwave radiation, and it is also the same type as the one running at the AWS1 Forni (Citterio et al., 2007; Senese et al., 2012a), thus assuring the comparability between the two datasets (accomplishing the recommendation described by Grenfell, 2011). Then the radiation data collected using the portable

instrument were crosschecked and analyzed against the data acquired by the AWS1 Forni. The measurements were carried out following the guidelines of the WMO (2008).

The radiation data were acquired every second, and every minute the minimum, average, maximum and standard deviation values were calculated. Albedo measurements were taken in the central hours of clear-sky days (i.e. from 11:00 am to 3:00 pm, when the solar incidence angles are smaller), thus ensuring the greatest possible accuracy and reliability of the albedo calculations (Brock et al., 2000; Brock, 2004; Oerlemans, 2010). The mean geographic coordinates (WGS84 datum) for each measurement site were recorded by a GPS receiver and the features characterizing the local ice surface were also noted. Fifty-one measurements were carried out from the beginning of the ice ablation period (when snow coverage at the melting tongue disappeared, exposing ice to solar radiation and dust/debris deposition) to the end of the ice melting season (before the occurrence of the first snow fall event covering the glacier ice and preventing dust/debris deposition): 30 June and 25 August 2011, 4 July, 7 August and 9 September 2012, and 31 July and 6 September 2013.

In addition to debris, water plays a significant role in changing ice albedo; water washes out the finer sediments on the glacier (Oerlemans et al., 2009) and makes smooth the ice surface. Thus, the effect of water (derived from both melting processes and rainfall) on glacier albedo variability was assessed during each ice ablation season from 2011 to 2013. The length of the ice ablation period was investigated coupling albedo and melting data (i.e. considering the time window featuring melt and with an albedo lower than 0.40, more details in Senese et al., 2012a). The occurrence of melting was investigated by applying the energy balance model from meteorological data and energy fluxes measured by the AWS1 Forni (for more details regarding the melting model see Senese et al., 2012a; 2012b; 2014). Finally, the temporal length (i.e. number of rainy days) and amount (i.e. mm of rain) of liquid precipitation were measured by an unheated pluviometer installed at the AWS1 Forni (DQA035, LSI-Lastem). The effect of liquid precipitation was quantified by comparing albedo values before, during and after the occurrence of liquid precipitation. Any event featuring an hourly liquid

precipitation higher than 0.2 mm (i.e. the threshold to activate the toggle switch of the rain gauge) was considered to be rainfall.

3.2.3. Sedimentological analyses and debris coverage rate evaluation

Several bulk samples of sediment were collected from the glacier surface (Figure 2a) and divided into sub-samples for physical and chemical analyses. In 2011, eight samples were collected choosing surfaces with diverse debris grain size and different distances from rock slopes and medial moraines, and these samples were used to characterize the spatial variability of debris at the glacier melting surface. Then in 2012 (4 July, 7 August and 9 September), the temporal evolution of debris features was studied by sampling three sites (identified by ablation stakes) with different conditions of debris cover: i) samples 9a, 9b and 9c fine and sparse sediment, ii) samples 10a, 10b and 10c widespread debris cover, and iii) samples 11a, 11b and 11c coarse debris. Finally, in 2013 we assessed the debris coverage rate (C_r, the fine debris amount reaching the surface over a defined time frame). The samples were collected 4 times (samples 12a, 12b, 12c, 12d): 11 July, 31 July, 6 September and 4 October 2013.

Each sample was collected by scraping the glacier surface with a cleaned chisel, completely removing the surface layer (from 2 to 5 cm deep, depending on the surface roughness); the collected material was preserved in appropriate holders. A cold chain (ice boxes) was used to preserve sediment samples at cold temperature conditions (lower than +4°C) during transport to the laboratory, where further analyses were carried out.

For evaluating the debris coverage rate, debris samples were periodically collected from the same sites. First, it was necessary to clean the 1 m x 1 m parcel, completely removing surface debris (i.e. scraping at least 2 cm of surface ice). Second, about one month later, the sampling of the surface sediments was repeated on the same glacier parcel, which was marked on the field. Then in the lab, debris samples were dried and weighed. The ratio between the weight of the debris deposited at the ice surface (in g/m^2) and the time frame (days) permitted evaluation of the debris coverage rate (C_r in g/m^2 per day):

$$C_r = \frac{sample\ weight}{time\ frame} \quad (3)$$

The samples collected in 2011 and 2012 for evaluating the spatial and temporal variability were subjected to the analytical procedures summarized as follows. Grain size analyses (Gale and Hoare, 1991) were performed after removing organics using hydrogen peroxide (130 vol) treatment; sediments were wet sieved (diameter from 1000 to 63 μm), then the finer fraction (63 μm) was determined by aerometer on the basis of Stokes's law. Humified organic carbon was identified by means of the Walkley and Black (1934) method, using chromic acid to measure the oxidizable organic carbon (titration). Total organic carbon (*TOC*) was estimated by loss on ignition (LOI; Heiri et al., 2001), with an uncertainty margin of ±0.1%; samples were air-dried and organic matter was oxidized at 500-550°C to carbon dioxide and ash; the samples were weighed before and after heating to calculate the quantity lost during the reaction.

Additionally, we performed several XRD (X-Ray Diffraction) and SEM (Scanning Electron Microscope) analyses on randomly oriented powder from the bulk debris samples to investigate the mineralogical properties of the fine debris and dust and the occurrence of micro features (e.g.: pollen, spores, micro- and meso-fauna, algae, etc.).

3.3. Results

3.3.1. Debris coverage ratio (d) and ice albedo (α)

Image analysis yielded 51 *d* values ranging from 0.01 to 0.63 (Figure 4). The ice albedo acquired by the portable net radiometer varied from 0.06 to 0.32.

$$ln\,\alpha = (-2.04 \pm 0.19) \cdot d + (-1.50 \pm 0.04) \quad (4)$$

The correlation is -0.84 (the 95% and 99% confidence intervals ranging from -0.91 to -0.74 and from -0.92 to -0.69, respectively); the p value of the correlation coefficient is lower than 10^{-9}. For low values of debris cover ratio, the correlation appears less accurate. This can be due to the occurrence of other influencing parameters that become dominant whenever debris is limited or absent (i.e. $d < 0.10$). Among the most important factors, bubble and other air inclusions modulate the volume scattering and then albedo (see Mullen and Warren, 1988). Moreover, Grenfell (2011) reported ice inhomogeneities (also at a microscale) to be significant in determining albedo. Nevertheless, these other factors become negligible whenever the debris cover ratio is higher than 0.10.

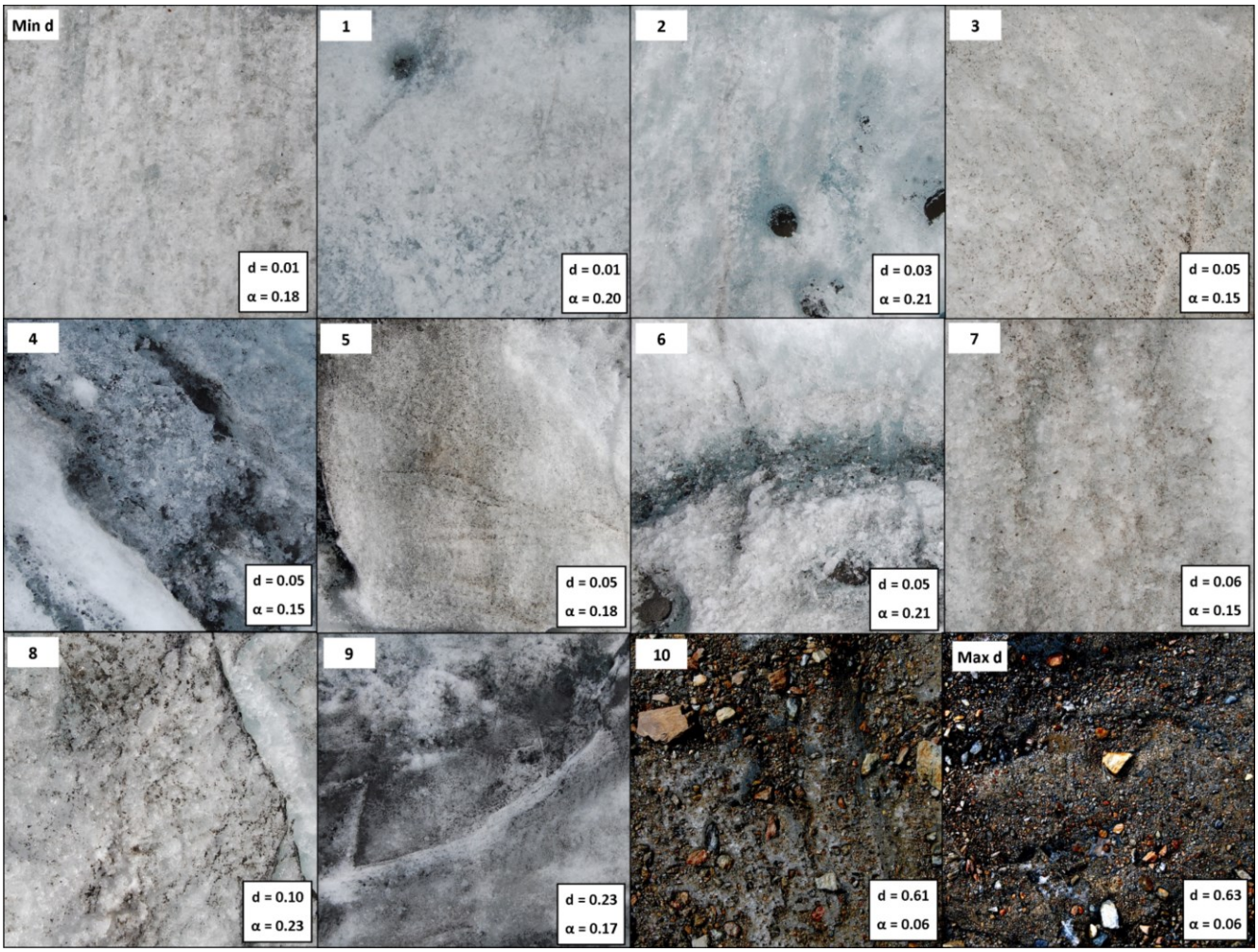

Fig. 4: Examples of Forni Glacier surfaces: debris cover ratio (d) and measured albedo (*α*) values are shown. The first and last images show the minimum and maximum d values. Images 1-10 are used for further sensitivity tests (see Discussion section).

The most frequently occurring *d* value was 0.03 but the wide variability of surface features indicates that a large number of samples is required to describe a *d* pattern and albedo distribution. Points featuring a high debris cover ratio are less numerous than the ones showing low values. In fact, in our study we considered glacier areas featuring fine and sparse debris coverage and not zones characterized by a quite continuous debris coverage (d > 0.60) such as medial moraines or actual buried ice sectors.

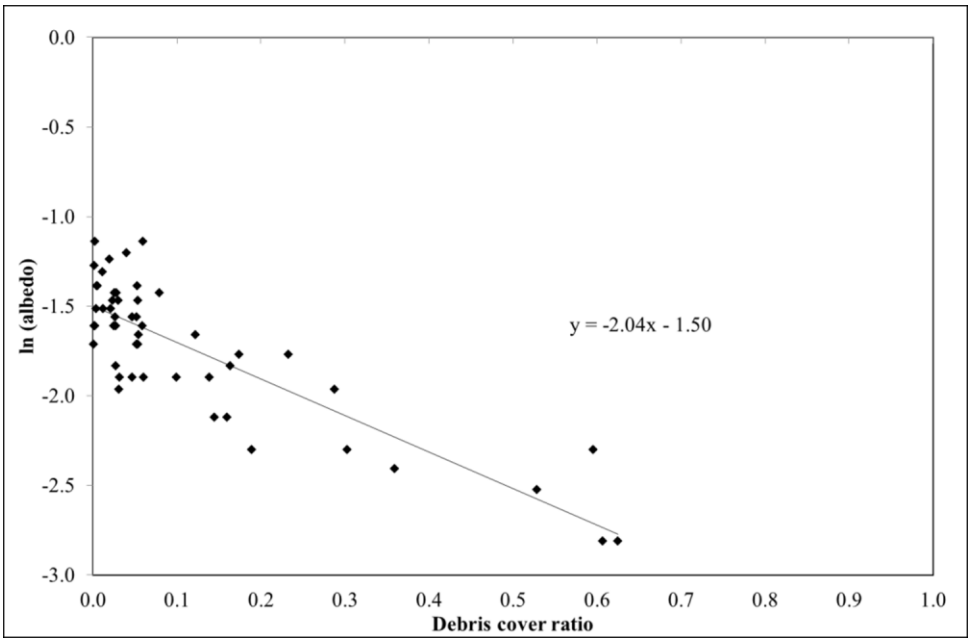

Fig. 5: Debris cover ratio vs albedo natural logarithm values (2011-2013 data)

In addition to debris occurrence, ice albedo depends on water presence. To evaluate the impact of water on albedo we considered both melting processes and rainfall occurrence during each ice ablation season from 2011 to 2013. The beginning and the end of each ice melting period are shown in Table 1. The meteorological data from the 3rd to the 13th of July 2013 are lacking; however, on July the 3rd, the albedo was equal to 0.55, indicating snow cover, while on the 13th of the same month the albedo was 0.18. The latter value is characteristic of bare ice, thus indicating that the ablation season started between these dates.

By coupling melt and albedo data, higher ablation rates were found to correspond to decreases in ice albedo (Figure 6). When melting was less intense, the albedo decrease was smaller (e.g. on 20/06/2012, see Figure 6). In general, we can deduce that meltwater occurs during the central hours of the day (when the solar radiation input is higher, the melting processes are more intense) decreasing the albedo due to its lower reflectivity (i.e. equal to 0.05-0.10, Hartmann, 1994). This lower albedo implies a more intense absorption of incoming solar radiation, which leads to more energy being available for melting. As a consequence, these factors (i.e. solar radiation input, melt and water) have a positive feedback in influencing albedo.

Before a rainy event		During a rainy event				After a rainy event	Albedo increase (%)
Date	**α**	**Date**	**Rain (mm)**	**α**	**Date**	**α**	
Beginning of ice ablation season 2011: 14 Jun 11							
16 Jun 11	0.33	17-18 Jun 11	46.2	0.21	19 Jun 11	0.41	24.2
20 Jun 11	0.31	21-23 Jun 11	33.2	0.21	24 Jun 11	0.31	0.0
24 Jun 11	0.31	25-26 Jun 11	0.6	0.20	27 Jun 11	0.32	3.2
28 Jun 11	0.18	29 Jun 11	15.4	0.18	30 Jun 11	0.20	11.1
3 Jul 11	0.23	4-8 Jul 11	38.6	0.20	9 Jul 11	0.25	8.7
2 Aug 11	0.20	3 Aug 11	10.8	0.19	4 Aug 11	0.24	20.0
31 Aug 11	0.25	1 Sep 11	3.4	0.25	2 Sep 11	0.28	12.0
2 Sep 11	0.28	3-6 Sep 11	63.6	0.24	7 Sep 11	0.29	3.6
7 Sep 11	0.29	8 Sep 11	1.0	0.22	9 Sep 11	0.31	6.9
11 Sep 11	0.22	12 Sep 11	10.8	0.23	13 Sep 11	0.25	13.6
End of ice ablation season 2011: 6 Oct 11							
Beginning of ice ablation season 2012: 16 Jun 12							
19 Jun 12	0.20	20-26 Jun 12	20.0	0.21	27 Jun 12	0.22	10.0
1 Jul 12	0.17	2-7 Jul 12	68.4	0.22	8 Jul 12	0.19	11.8
8 Jul 12	0.19	9-11 Jul 12	28.8	0.19	12 Jul 12	0.23	21.0
12 Jul 12	0.23	13-15 Jul 12	64.6	0.20	16 Jul 12	0.29	26.1
19 Jul 12	0.20	20-22 Jul 12	28.8	0.24	22 Jul12	0.27	35.0
23 Jul 12	0.21	24-25 Jul 12	1.2	0.20	26 Jul 12	0.22	4.8
26 Jul 12	0.22	27-31 Jul 12	27.4	0.20	1 Aug 12	0.23	4.5
2 Aug 12	0.20	3-6 Aug 12	40.0	0.18	7 Aug 12	0.24	20.0
24 Aug 12	0.16	25-26 Aug 12	36.2	0.19	27 Aug 12	0.26	62.5
23 Sep 12	0.22	24-27 Sep 12	93.6	0.23	28 Sep12	0.32	45.4
28 Sep 12	0.32	29 Sep-2 Oct 12	64.4	0.24	3 Oct 12	0.32	0.0
6 Oct 12	0.27	7 Oct 12	1.0	0.23	8 Oct 12	0.30	11.1
End of ice ablation season 2012: 12 Oct 12							
Beginning of ice ablation season 2013: 3-13 Jul 13							
16 Jul 13	0.16	17-24 Jul 13	35.6	0.18	25 Jul 13	0.17	6.3
25 Jul 13	0.17	26 Jul 13	0.2	0.16	27 Jul 13	0.18	5.9
28 Jul 13	0.16	29 Jul 13	4.2	0.15	30 Jul 13	0.23	43.7
30 Jul 13	0.23	31 Jul 13	0.4	019	1 Aug 13	0.25	8.7
6 Aug 13	0.16	7-9 Aug 13	61.2	0.16	10 Aug 13	0.26	62.5
12 Aug 13	0.19	13-15 Aug 13	13.0	0.19	16 Aug 13	0.24	26.3
31 Aug 13	0.18	1 Sep 13	1.0	0.18	2 Sep 13	0.24	33.3
26 Sep 13	0.16	27 Sep 13	1.4	0.15	28 Sep 13	0.24	50.0
End of ice ablation season 2013: 9 Oct 13							

Mean	**0.22**	**0.20**	**0.26**	**21.3**

Tab. 1: Influence of rainfall on ice albedo (α) measured from the AWS1 Forni. In the table are reported the 30 rainy events (and relative rain amount) that occurred during the 2011, 2012 and 2013 ablation seasons and the albedo values before, during and after every rainfall.

This trend is found also analyzing the liquid precipitation. In particular, we report in Table 1 the mean daily albedo values before, during and after rainfall events. First, the days before the rainfall featured a mean daily albedo equal to 0.22. Second, whenever precipitation occurred the mean daily reflectivity was reduced to 0.20, probably due to water albedo being lower than ice. This phenomenon occurred in 18 of 30 events. Of the remaining 12 cases, 6 featured an albedo increase and 6 steady state albedo conditions. This variable trend can be attributed to the rain amount: in fact, a misty rain decreases the surface albedo less than a heavy liquid precipitation. Third, once the rain event has washed out the dust and smoothed the surface, the mean daily albedo resulted 0.26. Almost all rain events (28 over a total number of 30) showed a mean daily albedo increase slightly higher than 20%. On the contrary when albedo before the rainfall was higher than 0.30, the water effect was not so appreciable. In fact, this reflectivity value is typical of bare ice with no fine debris coverage.

The occurrence of the rainfall washing out effect, and the consequent reflectivity increase, was found to be short lasting. The mean time period to restore the previous albedo value results equal to 1.8 days (ranging from 1 to 4 days) occurring over 10 events over a total of 30. The rain effect is less evident and effective whenever the time interval between two rainfalls is very restricted (i.e. 1 day).

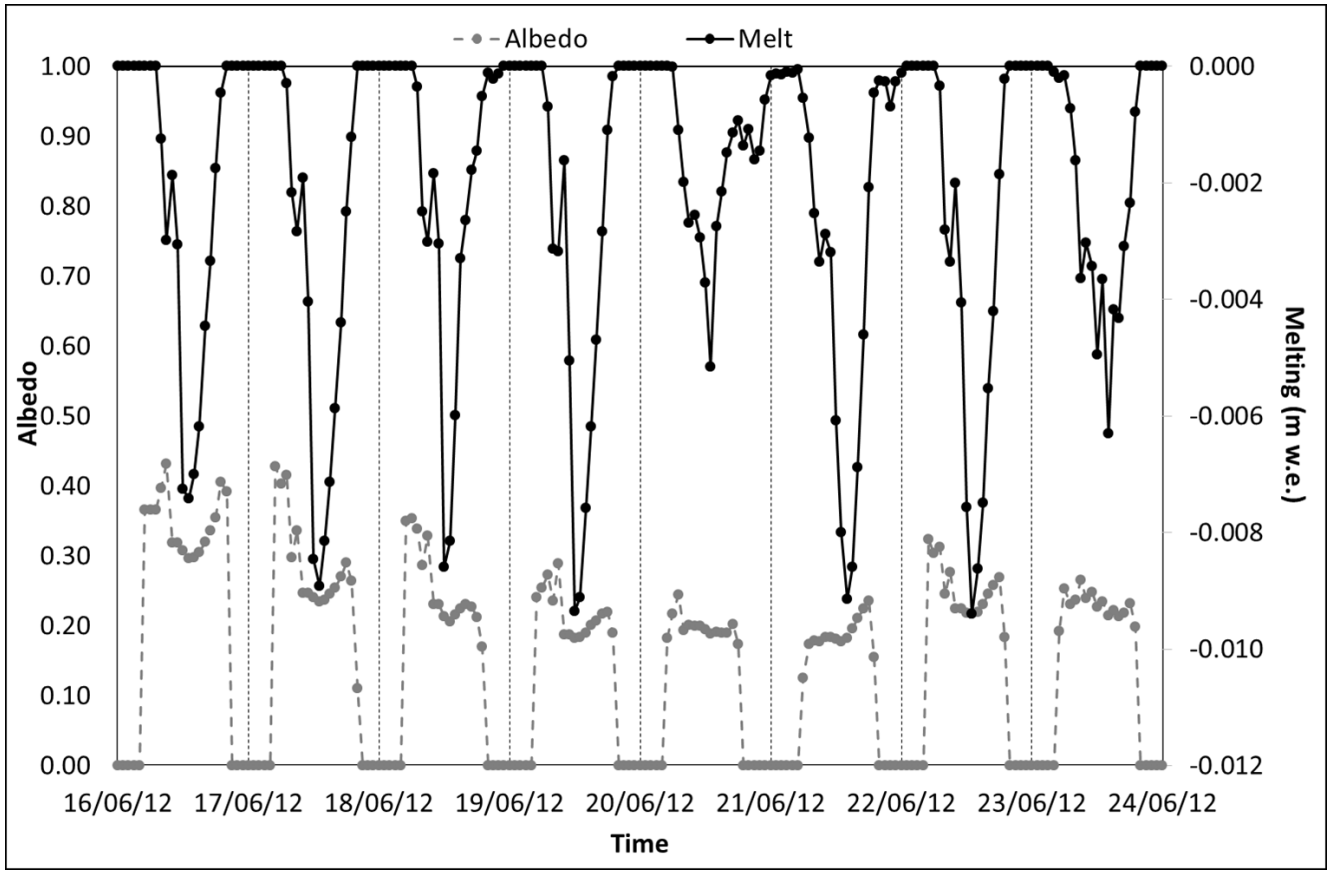

Fig. 6: Comparison between albedo measured by the AWS1 Forni (grey line) and melting amount estimated by the energy balance model (black line).

3.3.2. Debris composition and debris coverage rate (*Cr*)

The spatial variability of fine debris cover is highlighted from 2011 data. The sediment analysis performed in the laboratory indicates significant variability in total organic carbon (*TOC*, from 0.6% to 5.9%, see Table 2). The highest content of organic matter was found in samples 5, 6 and 8; in particular, sample 5 was wholly cryoconite, where generally the development of algae and bacteria communities is extremely favored (Takeuchi et al., 2000, 2005). The lowest value of total organic carbon was found in sample 2, which was collected on a glacier area located close to the flank of the nesting rock walls, a site which receives a high amount of debris originating from rock weathering processes such as the macrogelivation, which in this area has been reported by Guglielmin and Notarpietro (1997). Rock debris deposits in the area are active and unstable; they are continuously

suffering renewal of the surface, therefore poorly colonized by supraglacial organisms. Moreover, the grain-size analysis shows that samples collected at these sites are characterized by coarser sediments, in keeping with their origin, mostly due to mechanical weathering.

Regarding the lithology of the debris, X-Ray Diffraction indicates that the samples are enriched with quartz, muscovite, chlorite, sericite, and albite. This reflects the local geological bedrock, which corresponds to micaschist (Montrasio et al., 2008; Chiesa et al., 2011). According to regional geological maps (Montrasio et al., 2008; Chiesa et al., 2011), we may exclude a contribution in the formation of debris from nearby localities. In fact, outside the Forni Glacier basin at about 8 km northward a lithological and tectonic discontinuity (namely the Zebrù Line) is located, where the carbonate-bearing sedimentary rocks (i.e. dolomite) outcrop. Moreover, at about 18 km southward the intrusive rocks of the Adamello Pluton are present.

Sample	Sampling Date	Description	Gravel (%)	Sand (%)	Silt (%)	Clay (%)	TOC (g/kg)	Weight (g)
1	30 Jun 11	Central tongue	2.1	17.4	58.8	12.3	2.7	/
2	30 Jun 11	Eastern tongue	6.6	69.7	19.6	0.6	0.6	/
3	30 Jun 11	Median moraine (5 cm thick debris)	18.9	50.2	24.3	4.5	1.6	/
4	30 Jun 11	Central tongue, predominantly bare ice	0.4	29.4	30.9	15.8	3.6	/
5	30 Jun 11	Central tongue, cryoconite	5.6	32.9	30.9	15.8	5.1	/
6	30 Jun 11	Eastern tongue.	0.1	14.5	35.3	20.5	5.0	/
7	25 Aug 11	Eastern tongue	6.2	72.4	15.7	3.4	1.9	/
8	25 Aug 11	Eastern tongue.	0.1	21.4	31.7	22.8	5.9	/
9a	4 Jul 12	Central tongue	19.7	66.3	8.9	2.2	1.6	67.7
10a	4 Jul 12	Central tongue	8.6	33.6	25.7	12.3	26.3	1559.4
11a	4 Jul 12	Eastern tongue	0.1	17.7	35.5	19.7	18.3	432.0
9b	7 Aug 12	Central tongue, the same site of sample 9a	13.0	75.0	7.4	2.1	1.3	11.9
10b*	7 Aug 12	Central tongue, the same site of sample 10a	/	/	/	/	40.8	4026.9
9c	9 Sep 12	Central tongue, the same site of samples 9a and 9b	22.5	66.3	7.9	2.3	5.4	49.4
10c	9 Sep 12	Central tongue, the same site of samples 10a and 10b	2.4	23.6	40.9	16.7	38.1	2356.7
11c	9 Sep 12	Eastern tongue, the same	2.6	25.4	35.2	14.9	41.9	462.4

		site of sample 11a						
12a*	11 Jul 13	Central tongue	/	/	/	/	/	29.1
12b*	31 Jul 13	Central tongue, the same site of sample 12a	/	/	/	/	/	159.5
12c*	6 Sep 13	Central tongue, the same site of sample 12a and12b	/	/	/	/	/	308.3
12d*	4 Oct 13	Central tongue, the same site of sample 12a, 12b and 12c	/	/	/	/	/	59.5

Tab. 2: Properties of sites sampled for sedimentological analyses and results. The grain-size classes are referred to Krumbein's scale (Wentworth, 1922). An asterisk indicates a debris sample insufficient for grain-size analysis.

SEM analyses (Figure 7) revealed algae, spores, pollen and mesofauna. Moreover, we also observed spherical structures (Figure 7d) characterized (from EDS analysis) by an abundance of FeO (45.3%) and Al_2O_3 (19.8%). This composition confirms that these structures are cenospheres (i.e. a residual product of carbon combustion, see Kolay and Singh, 2001). These cenospheres may have been brought by wind and are probably derived from diesel fuel combustion or also from siderurgic factories, suggesting allochthonous inputs and human impacts at the glacier surface, even if limited. However, the assessment of the source and origin of fine debris was not of particular interest to this study and therefore remains at least partly open.

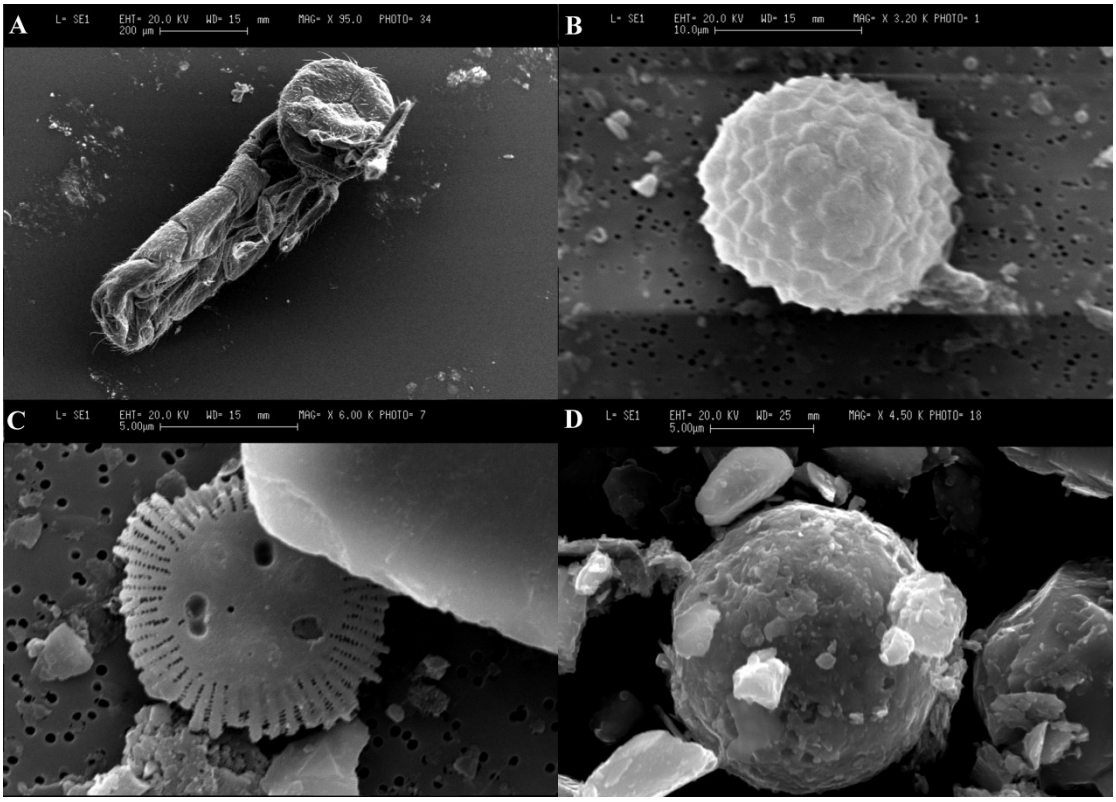

Fig. 7: SEM investigation on bulk samples from Forni Glacier evidenced the presence of (a) organisms of collembolan order, (b) spores, (c) diatoms and (d) cenospheres (a residual product of carbon combustion)

To assess the evolution of the fine debris cover, debris coverage rate (C_r) was evaluated (see equation 3) from 11 July to 4 October 2013 (i.e. sample 12, Table 2) and it was found to be equal to 6 g/m^2 per day. Immediately after each sampling, the cleaned 1 m^2 parcel can be clearly distinguished from the glacier areas nearby (see also the portion of cleaned ice in Figure 2a). However, at the following survey the sampled parcel resulted completely covered by fine debris and it was identified only thanks to the signals we putted on the field. This suggests that the development of debris coverage occurs at a fast rate. This evolution is highlighted also from the sedimentological analyses performed on the 2012 samples. During the ablation season, the grain-size remained almost equivalent with a slight increase of finer sedimentological classes (i.e. silt and clay). However, a rapid increase in total organic carbon (*TOC*) along the season was observed. At the beginning of July the *TOC* ranges from 1.6 g/kg (at sample 9a) to 26.3 g/kg (at sample 10a), at the end of the ablation period the organic carbon increases

up to 41.9 g/kg. The higher values correspond to finer debris (i.e. samples 9a, 9b, 9c, 11a and 11c, enriched in silt and clay); on the contrary, in coarser samples 10a, 10b and 10c the *TOC* is lower.

The debris evolution is also analyzed through SEM observations. At the beginning of the melting time frame, the sediment was characterized by sharp and angular clasts, suggesting a supraglacial mass transport; the samples collected in September 2012 featured more rounded shapes, suggesting an englacial mass transport.

3.3.3. Accuracy assessment of semi-automatic debris cover quantification

We performed several tests to evaluate the robustness of our semi-automatic method to quantify α from the estimation of d. Firstly, we asked a representative sample of users (10 geologists, but non glaciologists) to apply different approaches to 10 images randomly selected from the whole sample (see Figure 4). In particular, they estimated the debris coverage ratio applying both the point intercept method obtaining d_{10PI} (see an example in Figure 8b) and the *ImageJ* procedure we proposed obtaining d_{10IJ} from $T_{GS\text{-}10IJ}$ (see Figure 8c).

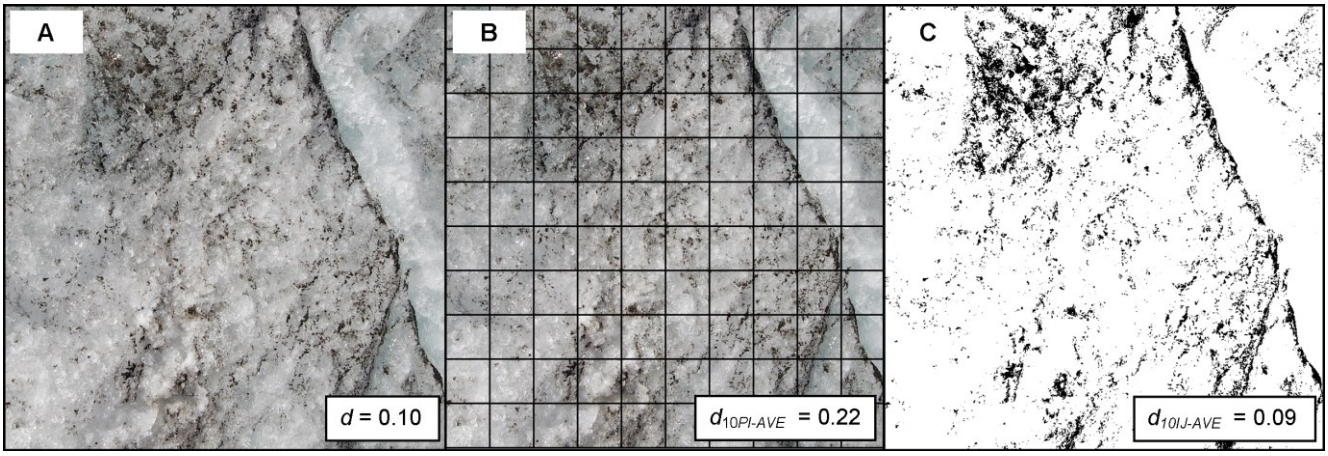

Fig. 8: An example of the application of different approaches to the same image. The original image is shown in A. In B and C, the application of the point intercept method and our approach, respectively.

The average d_{10PI} and d_{10IJ} for each of 51 images ($d_{10PI\text{-}AVE}$ and $d_{10IJ\text{-}AVE}$, light-blue and green circles in Figure 9) were compared with the debris coverage ratio values obtained by the well-trained operator

and used in equation 4 (d, red diamonds in Figure 9). The d_{10PI} values were affected by a very high standard deviation (from ±0.09 to ±0.34, see the light-blue errors bars in Figure 9, displayed only for positive errors), suggesting that this method is suffered from a too high subjectivity. Conversely, the d_{10IJ} values featured a much lower variability, due to homogenous $T_{GS\text{-}10IJ}$ values: the latter fall within ±10% from the corresponding T_{GS} values. Beside a low variability, the $d_{10IJ\text{-}AVE}$ values are also very close to d thus indicating the replicability of the method.

Secondly, as almost all $T_{GS\text{-}10IJ}$ values fell within ±10% from the corresponding T_{GS} values, we selected also the extremes of this interval ($T_{GS\text{-}10\%}$ and $T_{GS+10\%}$, respectively) to investigate the sensitivity of our method to changes in the chosen T_{GS}. For example, whenever the applied T_{GS} value was 100, we recalculated d with 90 ($T_{GS\text{-}10\%}$, obtaining $d_{\text{-}10\%}$, black dashes in Figure 9) and with 110 ($T_{GS+10\%}$, obtaining $d_{+10\%}$, black crosses in Figure 9). We applied this test also to all the measurements taken (51 field data), thus obtaining 51 $d_{\text{-}10\%}$ values and 51 $d_{+10\%}$ values. Subsequently, we evaluated the departures of $d_{\text{-}10\%}$ from d (i.e. d - $d_{\text{-}10\%}$) which resulted up to -0.07 (with a mean value of -0.02). Moreover, we calculated the departures of $d_{+10\%}$ from d (i.e. d - $d_{+10\%}$), which were found to be lower than +0.09 (with a mean value of +0.02). We discovered that whenever d was higher than 0.25 the d - $d_{\text{-}10\%}$ and d - $d_{+10\%}$ values reached their maxima. In fact d - $d_{\text{-}10\%}$ was -0.07 with a d value equal to 0.28 and d - $d_{+10\%}$ was +0.09 with a d value of 0.60. Considering the sample as a whole, slightly more than 70% of d featured d - $d_{\text{-}10\%}$ values of up to -0.02 and d - $d_{+10\%}$ values lower than +0.03.

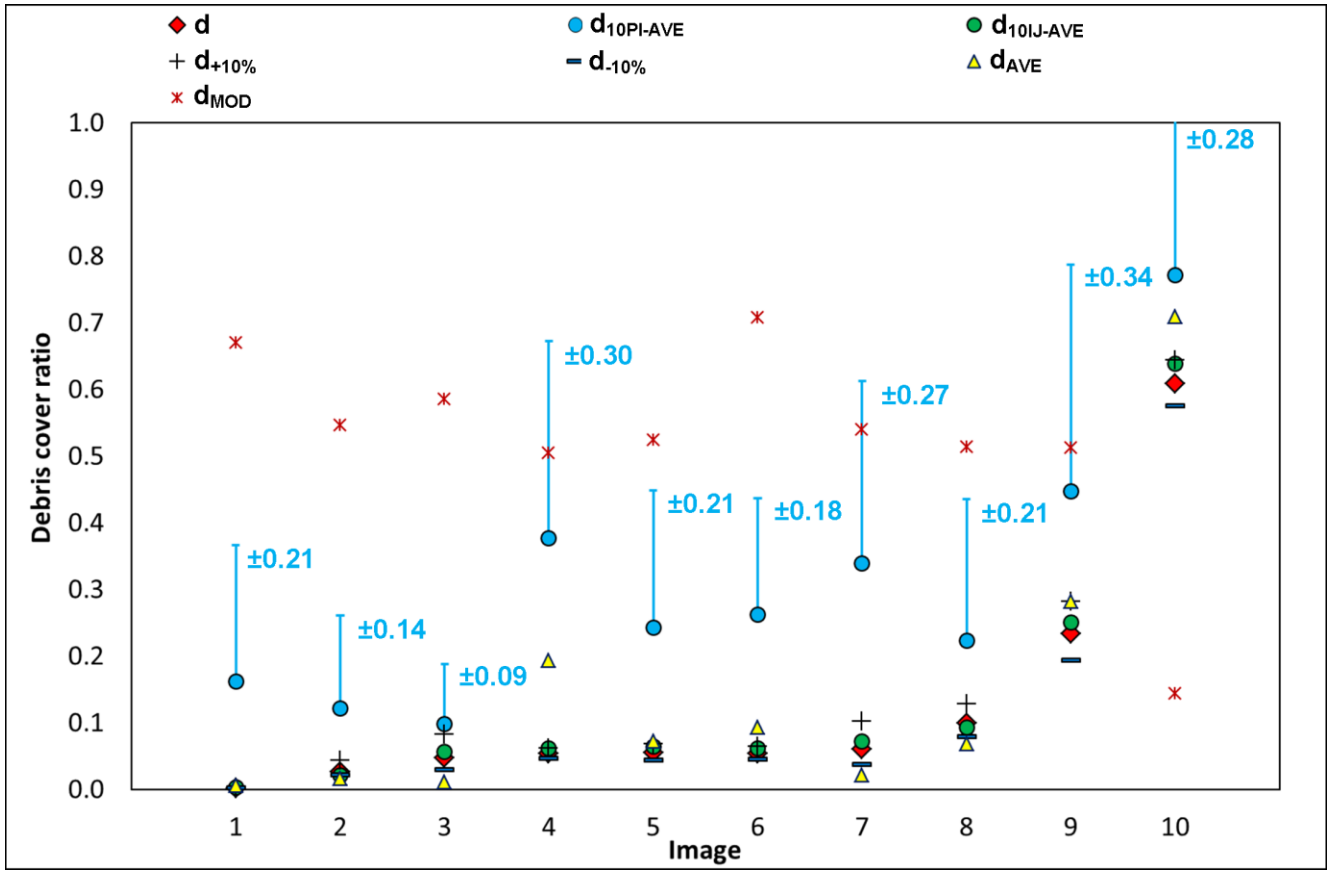

Fig. 9: Values of debris cover ratio from analyzing 10 randomly selected images (shown in Figure 4).

In addition, we used $d_{-10\%}$ and $d_{+10\%}$ values to obtain two more relations with α (reported in Table 3 together with equation 4). Applying these three equations to the d dataset, it was possible to estimate glacier albedo; the albedo values modeled with the three relations were compared to the albedo data obtained from the field radiation measurements and the departures between the modeled and the observed records proved to be very small, with a mean value lower than ±0.01 and a standard deviation of 0.04 (Figure 10). This suggests that, besides giving evidence of a good performance in estimating albedo, our method is also robust to changes in the applied threshold, supporting the replicability of the results.

Relation equation	R	p	Min (α_M - α_C)	Mean (α_M - α_C)	Max (α_M - α_C)
$ln(\alpha) = (-2.20 \pm 0.21) \cdot d_{-10\%} + (-1.52 \pm 0.04)$	-0.833	$<10^{-13}$	-0.06	+0.011	+0.13
$ln(\alpha) = (-2.04 \pm 0.19) \cdot d + (-1.50 \pm 0.04)$	-0.842	$<10^{-9}$	-0.07	+0.005	+0.12
$ln(\alpha) = (-1.89 \pm 0.17) \cdot d_{+10\%} + (-1.48 \pm 0.04)$	-0.837	$<10^{-14}$	-0.07	-0.001	+0.12
$ln(\alpha) = (-1.38 \pm 0.21) \cdot d_{AVE} + (-1.58 \pm 0.05)$	-0.842	$<10^{-6}$	-0.06	+0.010	+0.13

Tab. 3: Depending on the four different ratio datasets (considering d+10%, d, d-10% and dAVE), the differences between measured (αM) and calculated (αC) albedo data are shown.

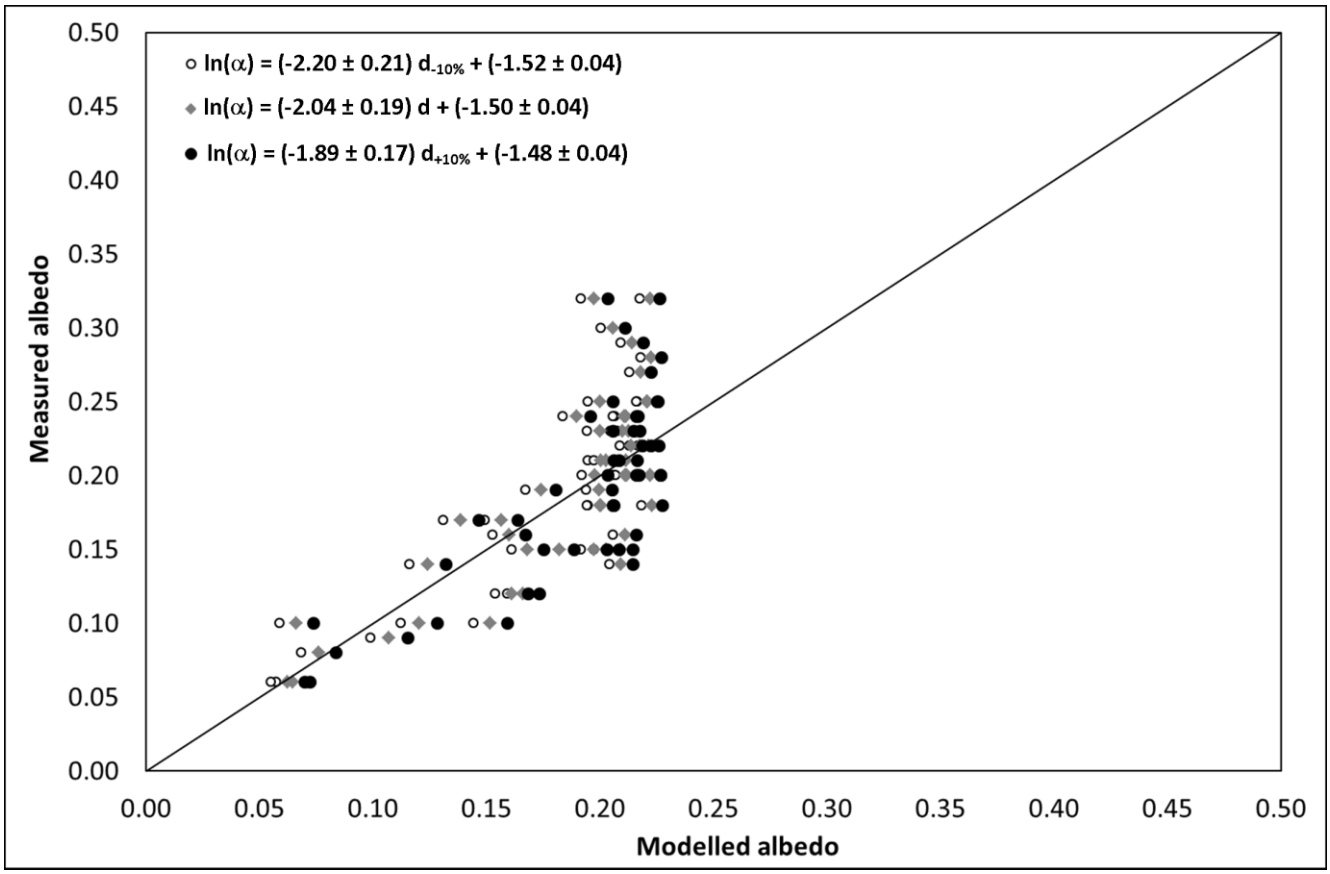

Fig. 10: Comparison between measured and modeled albedo values. The applied equations (Table 3) are shown in the legend

Finally, we tested the utility of a user-defined threshold, thus different for each image. For this experiment, we performed other two sensitivity tests: we considered the most frequent grey tone for each image (the top of the curve in Figure 11c), obtaining 51 $T_{GS\text{-}MOD}$ values, and we used a unique value averaging all the 51 T_{GS} values ($T_{GS\text{-}AVE}$). This latter threshold was found equal to 92.

Applying $T_{GS\text{-}MOD}$ gave an incorrect selection of the pixels; in particular, some pixels with clean ice are selected as debris-covered ones, thus overestimating the *d* value (an example is shown in Figure 11 where d_{MOD} is 0.50 instead of the actual *d* value of 0.10). In fact, the most frequent grey tone could correspond to pixels of ice featuring a thin film of water and not covered by debris. This is also evident from Figure 9 (red stars).

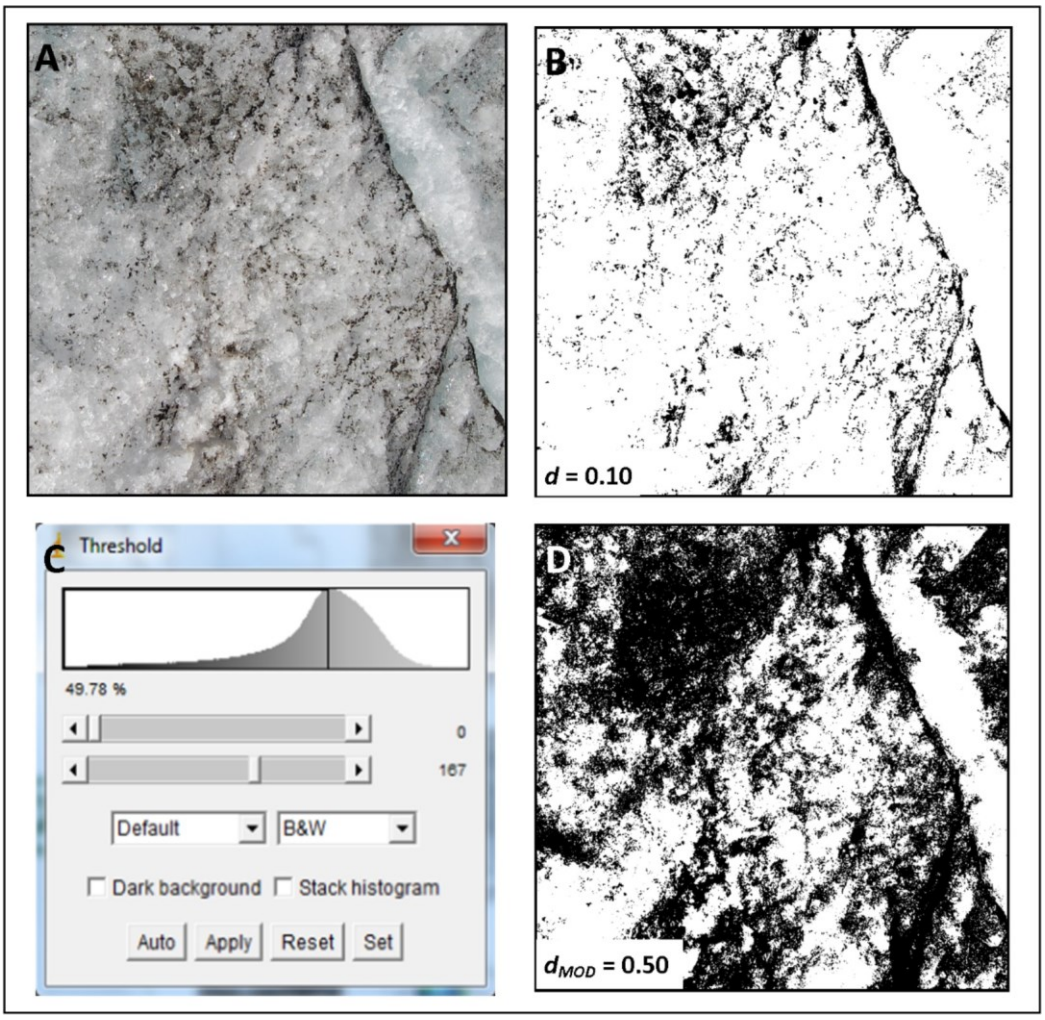

Fig. 11: Comparison between the application of the threshold chosen correctly by the user, TGS (B), and the one corresponding to the most frequent grey tone, TGS-MOD (D) deducted by the frequency distribution curve (C). The relative d and dMOD values are shown (B and D). In Panel A, the analyzed surface is presented.

As far as $T_{GS\text{-}AVE}$ is concerned, Figure 12 shows the comparison between *d* (obtained from T_{GS}) and d_{AVE} (obtained from $T_{GS\text{-}AVE}$) values. The relation between the two datasets was not negligible, thus suggesting that a unique threshold value could be sufficient to describe debris distribution on different

images (see also yellow triangles in Figure 9); then we applied the obtained 51 d_{AVE} values to calculate a new relation with α data:

$$ln\,\alpha = (-1.38 \pm 0.21) \cdot d_{AVE} + (-1.58 \pm 0.05) \quad (5)$$

Equation 5 features a R value of -0.68 (p value < 10^{-6}, Table 3), meaningful but lower than the one given by equation 4, thus suggesting that the different T_{GS} values we found for each image (even if they required spending more time in the image analysis) permit a better and more detailed determination of debris distribution, and consequently a more accurate d evaluation.

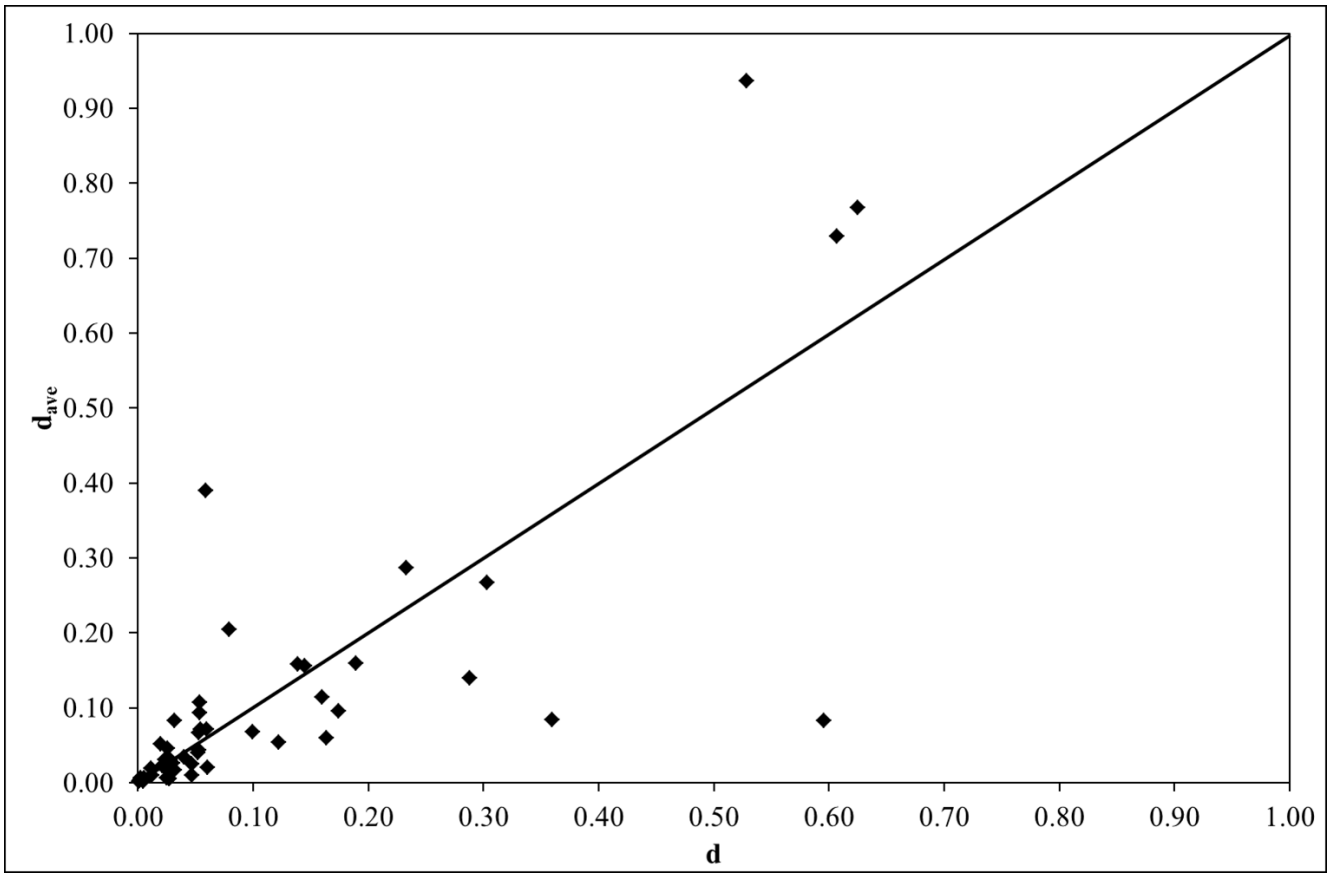

Fig. 8: Scatter plot reporting d (obtained from TGS) vs dAVE (obtained from TGS-AVE) values.

3.4. Discussion

The main task of this study was to evaluate the role of fine debris in modulating ice albedo, thus in driving ice ablation. Accordingly, we measured and analyzed the present debris coverage at the melting surface of a wide and representative Alpine glacier finding an actual relation with measured ice albedo. An advantage of our approach is that a thorough analysis of debris origin (autochthonous or allochthonous) and history (from englacial origin or transported by wind) is not required. Nevertheless, research focused on the human impact, if any, on glacier ice (mainly black carbon deposition) should also consider these issues. In this case, distinguishing between local debris and particles transported by wind, and also considering the paleo-implications of emerging englacial debris would be desirable.

Moreover, our findings support the recent literature describing darkening phenomena occurring at the Alpine debris-free glaciers (Paul and Kääb, 2005; Paul et al., 2007; Oerlemans et al., 2009; Painter et al., 2013; Diolaiuti et al., 2012; Gabbi et al., 2014; Brun et al., 2015; Naegeli et al., 2015) and in particular at the Forni Glacier tongue (Diolaiuti and Smiraglia, 2010; D'Agata et al., 2014). Indeed, we found that the albedo range (i.e. 0.06-0.32) agrees with the values characteristic for debris-rich ice albedo found by Cuffey and Paterson (2010). They reported a range of 0.06-0.30, whereas clean ice is described as varying from 0.30 to 0.46. Moreover, on average from our results the ice albedo decreases along the ablation tongue becoming more absorptive. This can be due to high melt rates and long exposure times (Klok and Oerlemans, 2002). Effectively, debris can be concentrated not only over a single melting season, but cumulated over many years (Cuffey and Paterson, 2010). In addition to spatial variability, we also observed that albedo decreases over time in the melt season (see also Senese et al., 2012). This entails that the period of most effective energy absorption occurs later than the peak of insolation. Maximum of exoatmospheric insolation is at the solstice (except in the tropics), but much of the winter snow still covers glaciers at this time. As the melt season progresses, darkening of the surface increases the absorbed shortwave radiation available for melt by a factor of three to four

(Cuffey and Paterson, 2010). This is one possible reason (in addition to warmer air in mid-summer) to explain why the peak of melt rates occurs on mid-latitude glaciers one to two months after the solstice (Cuffey and Paterson, 2010).

3.5. Conclusion

In spite of the quite abundant literature focusing on fine debris deposition over glacier accumulation areas, less attention was paid to the glacier melting surface. Accordingly, we proposed a novel method based on semi-automatic image analysis to quantify fine debris coverage (d) on glacier ice. We tested this procedure over the widest Italian valley glacier (Forni, Stelvio National Park). Analysis of 51 images yielded d values ranging from 0.01 to 0.63. Together with image acquisition, we also measured ice albedo, which varied from 0.06 to 0.32. The estimated d values were found in a linear relation with the natural logarithm of measured ice albedo (R = -0.84). We performed five sensitivity tests to investigate the robustness of our approach in evaluating d: i) 10 users estimated d_{10PI} using the point-intercept method and their results were affected by a high variability, thus suggesting strong subjectivity; ii) the same 10 users quantified d_{10IJ} using our approach and these values featured a variability lower than 10% thus supporting a wide replicability by non-trained operators; iii) we computed $d_{-10\%}$ and $d_{+10\%}$ varying the selected threshold up to ±10% for each image ($T_{GS-10\%}$ and $T_{GS+10\%}$), we found that more than 70% of departures of $d_{-10\%}$ from d were up to -0.02 and of $d_{+10\%}$ from d were lower than +0.03; iv) we derived d_{MOD} by applying as T_{GS} the most frequent grey-scale value (T_{GS-MOD}), but this in several cases caused an incorrect selection of the debris pixels; and v) we computed d_{AVE} applying a unique averaged threshold (T_{GS-AVE}) which led to a slight loss of accuracy. Summarizing, these tests suggest that the method we propose gives results featuring a lower variability thus suggesting a lower subjectivity than point intercept. Moreover, the sensitivity of our method to changes in the applied threshold is not so high as to affect the reliability of the results also supporting the replicability of the approach. In addition, even if T_{GS} analysis is more time-consuming, the specific

T_{GS} value found for each image permits a better and more detailed determination of debris distribution and therefore a more accurate d evaluation. Then, to look for the most reliable relation between d and α, the best and most suitable solution is to apply a specific T_{GS} value for each image.

On the Forni Glacier, we also evaluated the debris coverage rate (C_r) during ablation season 2013. Our data show a mean C_r equal to 6 g/m^2 per day, thus supporting the recent literature which describes the ongoing darkening phenomena at the Alpine debris-free glaciers (Paul and Kääb, 2005; Paul et al., 2007; Oerlemans et al., 2009; Diolaiuti and Smiraglia, 2010; Painter et al., 2013; D'Agata et al., 2014).

In addition to debris coverage, we considered both melting processes and rainfall occurrence during each ice ablation season from 2011 to 2013. Our analyses indicate that meltwater occurs during the central hours of the day decreasing the albedo due to its lower reflectivity. This lower albedo implies a more intense absorption of incoming solar radiation, which leads to more energy being available for melting. Consequently, these factors (i.e. solar radiation input, melt and water) play a positive feedback in influencing albedo. In addition, we found that almost all rain events caused a mean daily albedo increase slightly higher than 20%, although short lasting (from 1 to 4 days).

In conclusion, the semi-automatic image analysis method we are proposing could potentially be applied to images acquired by an Unmanned Aerial Vehicle (UAV) covering the entire ablation tongue of the Forni Glacier. The UAV could provide an excellent basis for capturing high-resolution images of a much larger expanse glacier surface than would have been possible using ground-based surveillance (Hodson et al., 2007; Fugazza et al., 2015). Once quantified the extension of the surface covered by fine debris, the relation between d and α could be applied, thus deriving an albedo map. The latter will feature a higher resolution (pixel size of few cm) than the ones derived from other approaches such as Landsat images (pixel size of 15 m x 15 m, Fugazza et al., 2016).

3.6. Acknowledgments

This work was conducted within the framework of the SHARE-Stelvio Project, funded by Regione Lombardia and managed by FLA (Fondazione Lombardia per l'Ambiente) and Ev-K2-CNR Association. The AWS1 Forni is already included in the international meteorological network SHARE (Stations at High Altitude for Research on the Environment) managed by EvK2CNR Association. It is also the only Italian site inserted in the SPICE (Solid Precipitation Intercomparison Experiment) and the Cryonet projects managed and promoted by WMO (World Meteorological Organization). The field activities and the data analysis were supported by Sanpellegrino S.P.A. - Brand Levissima through an agreement with UNIMI and by the PRIN project 2010/2011 (2010AYKTAB_006). We are grateful to the Stelvio National Park management Staff, the municipality of Valfurva, the Italian Alpine Club, Eraldo Meraldi and Gian Pietro Verza for their fundamental technical assistance on the field, to Chiara Compostella for assistance during sedimentological analyses, to Agostino Rizzi for assistance during SEM-EDS analyses, and to Carol Rathman for checking and improving the English language of this manuscript.

3.6. References

Aoki T., Aoki T., Fukabori M., Tachibana Y., Zaizen Y., Nishio F. and Oishi T. (1998): Spectral albedo observation on the snow field at Barrow, Alaska. *Polar Meteorology and Glaciology*, 12, 1–9.

Aoki T., Motoyoshi H., Kodama Y., Yasunari T.J., Sugiura K. and Kobayashi H. (2006): Atmospheric aerosol deposition on snow surfaces and its effect on albedo. *Sola*, 2, 13–16.

Arnold N.S., Willis I.C., Sharp M.J., Richards K.S., and Lawson W.J. (1996): A distributed surface energy-balance model for a small valley glacier. Development and testing for Haut Glacier d'Arolla,Valais, Switzerland. *Journal of Glaciology*, 42, 77–89.

Bolch T. (2011): Debris, in: Encyclopedia of Snow, Ice and Glaciers, edited by: Singh, V., Singh, P., and Haritashya, U., Springer Publications, Utrecht, the Netherlands, 186–188.

Brock B.W. (2004): An analysis of short-term albedo variations at Haut Glacier d'Arolla, Switzerland. *Geografiska Annalere series A*, 86, 53–65.

Brock B.W., Willis I.C. and Sharp M.J. (2000): Measurement and parameterization of albedo variations at Haut Glacier d'Arolla, Switzerland. *Journal of Glaciology*, 46, 675–688.

Brun F., Dumont M., Wagnon P., Berthier E., Azam M.F., Shea J.M., Sirguey P., Rabatel A. and Ramanathan, A. (2015): Seasonal changes in surface albedo of Himalayan glaciers from MODIS data and links with the annual mass balance. *The Cryosphere*, 9(1), 341–355.

Casey K.A. (2012): Supraglacial dust and debris: geochemical comparisons from glaciers in Svalbard, southern Norway, Nepal and New Zealand. *Earth System Science Data Discussions*, 5, 107-145.

Chiesa S., Micheli P., Cariboni M., Tognini P., Motta D., Longhin M., Zambotti G., Marcato E., Ferrario A., Ferliga C. and Gregnanin A. (2011): Note illustrative della Carta Geologica d'Italia: foglio 041, Ponte di Legno, ISPRA, Servizio Geologico d'Italia, Roma.

Citterio M., Diolaiuti G., Smiraglia C., Verza G. and Meraldi E. (2007): Initial results from the automatic weather station (AWS) on the ablation tongue of Forni Glacier (Upper Valtellina, Italy). *Geografia Fisica e Dinamica Quaternaria*, 30, 141–151.

Clarke A.D. and Noone J. (1985): Measurements of soot aerosol in Arctic snow. *Atmospheric Environment*, 19, 2045-2054.

Conway J., Gades A. and Raymond C.F. (1996): Albedo of dirty snow during conditions of melt. *Water Resources Research,* 32, 1713–1718.

Cuffey K.M. and Paterson W.S.B. (2010): The physics of glaciers. Academic Press, 704 pp.

D'Agata C., Bocchiola D., Maragno D., Smiraglia C. and Diolaiuti G. (2014): Glacier shrinkage driven by climate change during half a century (1954–2007) in the Ortles-Cevedale Group (Stelvio National Park, Lombardy, Italian Alps). *Theoretical and Applied Climatology*, 116, 169–190.

Diolaiuti G. and Smiraglia C. (2010): Changing glaciers in a changing climate: how vanishing geomorphosites have been driving deep changes in mountain landscapes and environments. *Geomorphologie*, 2, 131–152.

Diolaiuti G., Smiraglia C., Verza G.P., Chillemi R. and Meraldi E. (2009): La rete micrometeorologica glaciale lombarda: un contributo alla conoscenza dei ghiacciai alpini e delle loro variazioni recenti, in: Clima e Ghiacciai, la Crisi delle Risorse Glaciali in Lombardia, Regione Lombardia, edited by: Smiraglia, C., Morandi, G., Diolaiuti, G., Regione Lombardia, Milan, 69–92.

Diolaiuti G., Bocchiola D., D'Agata C. and Smiraglia C. (2012): Evidence of climate change impact upon glaciers recession within the Italian Alps: the case of Lombardy glaciers. *Theoretical and Applied Climatology*, 109, 429–445.

Dumont M., Brun E., Picard G., Michou M., Libois Q., Petit J.R., Geyer M., Morin S. and Josse B. (2014): Contribution of light-absorbing impurities in snow to Greenland's darkening since 2009. *Nature Geoscience*, 7, 509-512.

Elzinga C.L., Salzer D.W., Willoughby J.W. and Gibbs J.P. (2001): Monitoring Plant and Animal Populations, Blackwell Publishing. 368 pp.

Fugazza D. Senese A., Azzoni RS., Smiraglia C., Cernuschi M., Severi D., Diolaiuti GA. (2015): High resolution mapping of glacier surface features. The UAV survey of the Forni Glacier (Stelvio National Park, Italy). *Geografia Fisisca e Dinamica Quaternaria*, 38(1), 25-33.

Fugazza D., Senese A., Azzoni R.S., Maugeri M., Diolaiuti G.A. (2016): Spatial distribution of surface albedo at the Forni Glacier (Stelvio National Park, Central Italian Alps). *Cold Regions Science and Technology*, 125, 128-137.

Flanner M.G., Zender C.S., Hess P.G., Mahowald N.M., Painter T.H., Ramanathan V. and Rasch P.J. (2009): Springtime warming and reduced snow cover from carbonaceous particles. *Atmospheric Chemistry and Physics*, 9, 2481–2497.

Fujita K. (2007): Effect of dust event timing on glacier runoff: sensitivity analysis for a Tibetan glacier. *Hydrological Processes*, 21, 2892–2896.

Gabbi J. Carenzo M. Pellicciotti F. Bauder A. and Funk M. (2015): A comparison of empirical and physically based glacier surface melt models for long-term simulations of glacier response. *Journal of Glaciology*, 60 (224), 1140–1154.

Gale S.J. and Hoare P.G. (1991): Quaternary Sediments, Belhaven Press, New York.

Garavaglia V., Pelfini M., Diolaiuti G., Pasquale V., and Smiraglia C. (2012): Evaluating tourist perception of environmental changes as a contribution to managing natural resources in glacierized areas. A case study of the Forni Glacier (Stelvio National Park, Italian Alps). *Environmental Management*, 50, 1125–1138.

Gardner A.S. and Sharp M.J. (2010): A review of snow and ice albedo and the development of a new physically based broadband albedo parameterization. *Journal of Geophysical Resources*, 115, F01009.

Grenfell T.C. (2011): Albedo, Encyclopedia of Snow, Ice and Glaciers, edited by: Singh, V., Singh, P., and Haritashya, U., Springer Publications, Utrecht, the Netherlands, 186–188.

Guglielmin M. and Notarpietro A. (1997): Il permafrost alpino: concetti, morfologia, metodi di individuazione (con tre indagini esemplificative in alta Valtellina). *Quaderni di Geodinamica Alpina e Quaternaria*, 5, 117.

Hansen J. and Nazarenko L. (2004): Soot climate forcing via snow and ice albedos. *Proceedings of the National Academy of Sciences*, 101, 423-428.

Hartmann D. L. (1994): Global Physical Climatology (International Geophysics), Academic Press, San Diego, 56, 411 pp.

Heiri O., Lotter A.F. and Lemcke G. (2001): Loss on ignition as a method for estimating organic and carbonate content in sediments: reproducibility and comparability of results. *Journal of Paleolimnology*, 25, 101–110.

Hodson A., Anesio A.M., Ng F., Watson R., Quirk J., Irvine-Fynn T., Dye A., Clark C., McCloy P., Kohler J. and Sattler B. (2007): A glacier respires: Quantifying the distribution and respiration CO_2 flux of cryoconite across an entire Arctic supraglacial ecosystem. *Journal of Geophysical Resources*, 112, G04S36.

Irvine-Fynn T., Bridge J. and Hodson A. (2010): Rapid quantification of cryoconite: granule geometry and in situ supraglacial extents, using examples from Svalbard and Greenland. *Journal of Glaciology*, 56, 297–308.

Klok E.J. and Oerlemans J. (2002): Model study of the spatial distribution of the energy and mass balance of Morteratschgletscher, Switzerland. *Journal of Glaciology*, 48, 505–518.

Klok E.J., Greuell J.W. and Oerlemans J. (2003): Temporal and spatial variation of the surface albedo of the Morteratschgletscher, Switzerland, as derived from 12 Landsat images. *Journal of Glaciology*, 49, 491–502.

Kolay P.K. and Singh D.N. (2001): Physical, chemical, mineralogical, and thermal properties of cenospheres from an ash lagoon. *Cement and Concrete Resources*, 31, 539–542.

Ming M., Xiao C., Cachier H., Qin D., Qin X., Li Z. and Pu J. (2009): Black Carbon (BC) in the snow of glaciers in West China and its potential effects on albedos. *Atmospheric Research*, 92, 114–123.

Montrasio A., Berra F., Cariboni M., Ceriani M., Deichmann N., Ferliga C., Gregnanin A., Guerra S., Guglielmin M., Jadoul F., Longhin M., Mair V., Mazzoccola D., Sciesa E. and Zappone A. (2008): Note illustrative della Carta Geologica d'Italia: foglio 024, Bormio, ISPRA, Servizio Geologico d'Italia, Roma.

Motoyoshi H., Aoki T., Hori M., Abe O. and Mochizuki S. (2005): Possible effect of anthropogenic aerosol deposition on snow albedo reduction at Shinjo, Japan. Journal of Meteorological Society of Japan, 83A, 137–148.

Mullen P.C. and Warren S.G. (1988): Theory of the optical properties of lake ice. Journal of Geophysical Resources, 93(D7), 8403-8414.

Naegeli K. Damm A. Huss M. Schaepman M. and Hoelzle M. (2015): Imaging spectroscopy to assess the composition of ice surface materials and their impact on glacier mass balance. *Remote Sensing of Environment*, 168, 388-402.

Oerlemans J. (2010): The microclimate of valley glaciers, Utrecht university Ed., Utrecht.

Oerlemans J., Giesen R.H. and Van Den Broeke M.R. (2009): Retreating alpine glaciers: increased melt rates due to accumulation of dust (Vadret da Morteratsch, Switzerland). *Journal of Glaciology*, 55, 729–736.

Painter T.H., Flanner M.G., Kaser G., Marzeion B., Van Curen R.A. and Abdalati W. (2013): End of the Little Ice Age in the Alps forced by industrial black carbon. *Proceedings of the National Academy of Science*, 110, 15216–15221.

Paul F. and Kääb A. (2005): Perspectives on the production of a glacier inventory from multispectral satellite data in the Canadian Arctic: Cumberland Peninsula, Baffin Island. Annals of Glaciology, 42, 59–66.

Paul F., Kääb A. and Haeberli W. (2007): Recent glacier changes in the Alps observed from satellite: consequences for future monitoring strategies. *Global Planetary Change*, 56, 111–122.

Pope A. and Rees G. (2014): Using in situ spectra to explore Landsat classification of glacier surfaces, *International Journal of Applied Earth Observation and Geoinformation*, 27, 42–52.

Qian Y., Flanner M.G., Leung L R. and Wang W. (2011): Sensitivity studies on the impacts of Tibetan Plateau snowpack pollution on the Asian hydrological cycle and monsoon climate. *Atmospheric Chemistry and Physics*, 11, 1929–1948.

Ramanathan V. (2007): Role of Black Carbon in Global and Regional Climate Change, Testimonial to the House Committee on Oversight and Government Reform, 18 October 2007, available at: http://www-ramanathan.ucsd.edu/files/brt20.pdf.

Schaepman-Strub G., Schaepman M.E., Painter T.H., Dange S. and Martonchik J.V. (2006): Reflectance quantities in optical remote sensing - Definitions and case studies. *Remote Sensing of Environment*, 103(1), 27-42.

Senese A., Diolaiuti G., Mihalcea C. and Smiraglia C. (2010): Meteorological evolution on the ablation zone of Forni Glacier, Ortles-Cevedale Group (Stelvio National Park, Italian Alps) during the period 2006–2008. *Bollettino Società Geografica Italiana*, 3, 845–864.

Senese A., Diolaiuti G., Mihalcea C. and Smiraglia C. (2012a): Energy and mass balance of Forni Glacier (Stelvio National Park, Italian Alps) from a 4-year meteorological data record. *Arctic, Antarctic and Alpine Resources*, 44, 122–134.

Senese A., Diolaiuti G., Verza G.P. and Smiraglia C. (2012b): Surface energy budget and melt amount for the years 2009 and 2010 at the Forni Glacier (Italian Alps, Lombardy). *Geografia Fisica e Dinamica Quaternaria*, 35, 69–77.

Senese A., Maugeri M., Vuillermoz E., Smiraglia C. and Diolaiuti G. (2014): Using daily air temperature thresholds to evaluate snow melting occurrence and amount on Alpine glaciers by T -index models: the case study of the Forni Glacier (Italy). *The Cryosphere*, 8, 1921–1933.

Takeuchi N. (2002): Surface albedo and characteristics of cryoconite on an Alaska glacier (Gulkana Glacier in the Alaska Range). *Bulletin of Glaciological Resources*, 19, 63–70.

Takeuchi N., Kohshima S., Yoshimura Y., Seko K. and Fujita K. (2000): Characteristics of cryoconite holes on a Himalayan glacier, Yala Glacier Central Nepal. *Bulletin of Glaciological Resources*, 17, 51–59.

Takeuchi N., Kohshima S. and Seko K. (2001): Structure, formation, darkening process of albedo reducing material (cryoconite) on a Himalayan glacier: a granular algal mat growing on the glacier. *Arctic, Antarctic and Alpine Resources*, 33, 115–122.

Takeuchi N., Matsuda Y., Sakai A. and Fujita K. (2005): A large amount of biogenic surface dust (cryoconite) on a glacier in the Qilian Mountains, China. *Bulletin of Glaciological Resources*, 22, 1–8.

Walkley A. and Black I.A. (1934): An examination of Degtjareff method for determining soil organic matter and a proposed modification of the chromic acid titration method. *Journal of Soil Sciences*, 37, 29–38.

Wentworth C.K. (1922): A scale of grade and class terms for clastic sediments. *The Journal of Geology*, 377-392.

World Meteorological Organization (2008): Guide to meteorological instruments and method of observation, Seventh edition, Geneve, 2008.

Yasunari T.J., Bonasoni P., Laj P., Fujita K., Vuillermoz E., Marinoni A., Cristofanelli P., Duchi R., Tartari G. and Lau K.M. (2010): Estimated impact of black carbon deposition during pre-monsoon season from Nepal Climate Observatory – Pyramid data and snow albedo changes over Himalayan glaciers. *Atmospheric Chemistry and Physics*, 10, 6603–6615.

PART II

SUPRAGLACIAL DEBRIS: BIOLOGICAL ASPECTS

Introduction

Since the turn of the last millennium, our perception of glaciers and ice sheets has shifted from considering them as a lifeless, abiotic realm to realizing that they constitute a distinct biome with a microbial biomass broadly similar to that of unfrozen freshwaters (Hodson et al., 2008; Laybourn-Parry et al., 2012). This paradigm shift was a long time coming. The very earliest explorers crossing the Greenland Ice Sheet in the 1890s had already highlighted the discoloring of snow and ice surfaces by microorganisms, and investigations of snow micro-biota were conducted during expeditions to Antarctica in the 1900s (Hodson et al., 2015). Meiofauna, algae, protozoa and bacteria of snow, glaciers and ice sheets were then studied from the 1930s onwards. However, the data collected in those studies were qualitative rather than quantitative, and the overall number of studies on these arguments was limited. Only in the last decades, the number of studies dealing with the ecological processes of these extreme environments has largely increased (Anesio and Laybourn-Parry, 2012).

Glaciers and ice sheets are a biome dominated by microorganisms adapted to live under low temperature conditions (Anesio and Laybourn-Parry, 2012). Moreover, also algal communities (Lutz et al., 2016), as well as Tardigrada, Nematoda, Enchytraeidae, Rotifera and Arachnida colonize these areas (Coulson & Midgley 2012). All these organisms have a strong impact both on glacier evolution, forcing the energy balance of ice bodies, and on biogeochemical cycles on the surface of glaciers and throughout the Earth's cryosphere, providing an intense flux of carbon and nitrogen (Hodson et al., 2005). Consequently, the life on glacier is strongly connected with the abiotic dynamics, processes and evolution of glaciers. A better knowledge of the biological processes acting in these environments can therefore allow a deeper understanding of these extreme areas (Lutz et al., 2016). In this work, in particular, we investigated the structure and the functions of the biological components of three cold environments: supraglacial debris in a debris-covered glacier (Chapter 4), snow (Chapter 5) and cryoconites holes (chapters 6, 7 and 8).

Life on debris-covered glaciers

Debris-covered glaciers comprise a significant fraction of glaciers worldwide and are widespread in the mountain chains of Asia, such as Karakoram, Himalaya (Hambrey et al., 2008) and Tien Shan; they are also common in Alaska, New Zealand (Fickert et al., 2007; Kirkbride and Warren, 1999) and in the Andes. These glaciers are rare in the Alps and in the other European mountains, but their number has increased in recent years, as the debris cover on the lower part of the ablation zone of many Alpine glaciers is widening and thickening (Kellerer-Pirklbauer, 2008). The present warming period and the consequent deglaciation cause the increasing occurrence of rock falls from surrounding slopes resulting from micro- and macrogelivation processes, which deliver large volumes of debris to the glacier surface (Kellerer-Pirklbauer, 2008). The debris, once has fallen down on glacier, is then transported down valley for times that, on some glaciers, can be as long as a century (Pelfini et al., 2007). As a result, a continuous debris layer, whose thickness generally increases toward the glacier terminus, covers the glacier surface (Fig. 1). This debris cover has a strong impact on the evolution of glaciers, reducing the rate and magnitude of buried ice ablation (Østrem, 1959), but can also favor the colonization of glaciers by organisms. In fact, in the last years, several studies have investigated the presence of organisms in this environment, but the description of many phyla that colonize the debris is lacking. In particular, animals (for example, arthropods, see Gobbi et al., 2011) and plants (Pelfini et al., 2012, Caccianiga et al., 2011) are widely present on the surfaces of debris-covered glaciers. Moreover, also microbes are described on these glaciers: Franzetti et al., (2013) found well-developed heterotrophic bacterial communities on two of the largest debris-covered glaciers of the Italian Alps, Miage (Aosta Valley) and Belvedere (Piedmont). However, the characterization of organisms that live in supraglacial debris is still incomplete. Meiofauna (i.e. metazoan smaller in size than 2 mm) is an important but still neglected component of the fauna of supraglacial debris, since we are aware of no study that investigated it so far. To contribute to fill this gap of knowledge, in Chapter 4 we analyze the nematode and rotifer communities that inhabit the surface of the two widest Italian debris-covered

glaciers, the Miage and the Belvedere. Nematodes are particularly important because they are the dominant phylum in the soil, while Rotifers were abundant in the Antarctic soils (Fontaneto et al., 2015).

Fig. 1: The Belvedere Glacier (Piedmont) one of the largest debris-covered glaciers of the Alps. In the foreground the glacier tongue covered by a thick and continuous layer of sediment is clearly visible.

Life in snow

Seasonal snow cover extends over one third of the Earth's land surface, covering up to 47 million km^2 (Hinkler et al., 2008). Snow cover influences global energy budget, thereby influencing climate (Hinkler et al., 2008). The influence of seasonal snow cover on soil and permafrost has a considerable impact on carbon exchange between the atmosphere and the ground and on the hydrological cycle in cold regions (Zhang, 2005). Snow cover acts as a radiation shield due to its high radiative properties,

and reflects as much as 80%–90% of the incoming radiation (for fresh snow; Hinkler et al., 2008). This high surface albedo reduces absorbed solar energy and lowers snow surface temperature (Zhang, 2005). Moreover, snow cover can be considered as a dynamic habitat of limited temporal duration (Jones, 1999) that favors an interaction among microorganisms, plants, animals, nutrients, atmosphere and soil (Pomeroy and Brun, 2001).

Many studies focused on characterizing bacteria in ice or permafrost, while little is known about life in snow. The snow cover might support a microbial community composed of snow algae, bacteria, yeasts and snow fungi (Jones, 1999). Snow algae represent an ecologically and physiologically specialized group that can form visible blooms, however their development is dependent on the availability of liquid water and they are only active during spring and summer, when air temperature is above zero (Komarèk et al., 2007). Moreover, these algae have a significant impact in reducing the snow albedo and favoring melting (Lutz et al., 2016). Snow algae have been studied extensively (see among the others Stibal et al., 2007); in contrast, data on bacteria inhabiting seasonal snow cover are sparse (Larose et al., 2013). High levels of diversity in the microbial communities are found in the Arctic (Larose et al., 2010) and large variation in diversity was also reported, maybe related to seasonal changes in the snow environment (i.e., pH, water content and temperature; Larose et al., 2010). Segawa et al. (2005) observed seasonal changes in bacterial biomass in mountain snow, with increases during the melting season (March to October) that were attributed to nutrient enrichment and/or variation on environmental conditions in the snow. These results highlight the links between environmental conditions and changes in community structure. Therefore, the snowpack appears to be a habitat characterized by a high microbial diversity and strongly linked to the environmental conditions where the snowfalls occurs. Moreover, the characteristics of the communities in the snowpack of many areas or the world are completely unknown, in particular in the mid-latitude areas. Information about the microbial communities from these areas is therefore needed. In this work we investigated and described the microbial communities of snow samples collected on four mid-latitude

glacierized areas (Alps, Karakoram, Eastern Anatolia and Himalaya). These results are presented in Chapter 5 in the form of an unpublished manuscript.

Life in cryoconite holes

In the glacier environment some peculiar environments occur, which are considered biodiversity hotspots: cryoconite holes. Cryoconite is a dark microorganism-mineral aggregate that forms through interactions between microorganisms and dust deposited on glacier ice, leading to localized reduction in ice surface albedo and accelerated melting of ice in contact with cryoconite (Takeuchi et al., 2001a;b; Edwards et al., 2014). As the cryoconite absorbs solar radiation and promotes melting of the ice beneath it, cylindrical holes are formed called cryoconite holes (Takeuchi, 2011, see Fig. 2). Complex interactions between cryoconite and hydrology on glacier surface occur (Irvine-Fynn et al., 2011) and influence surface melting rates and hence glacier mass balance (Fountain et al., 2004). Despite having been recognized as important glaciological and biological entities in the nineteenth century, cryoconite and cryoconite holes remain poorly understood, mainly outside the Polar areas (Cook et al., 2016).

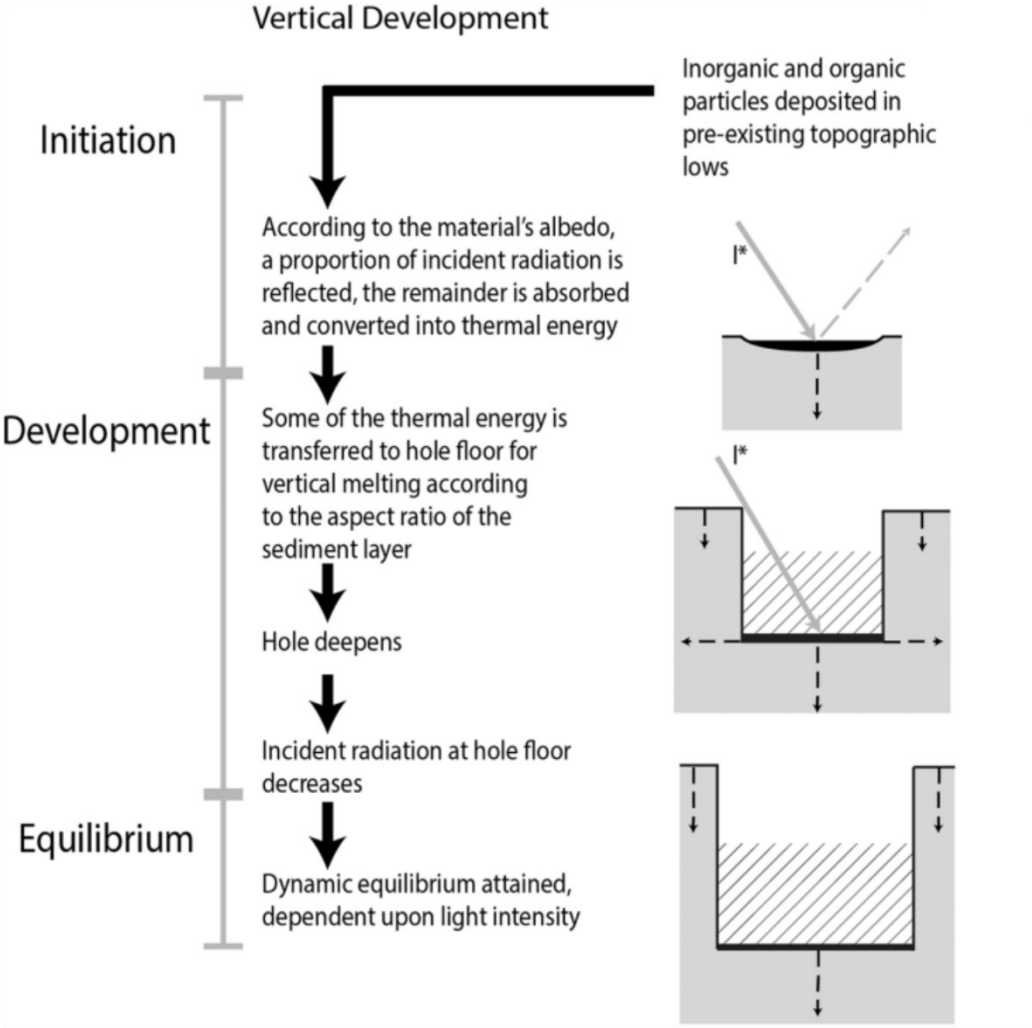

Fig. 2: Process leading to the formation of a cryoconite hole (Cook et al., 2016).

Components of cryoconite

Terrestrial mineral particles are major components of cryoconite. They usually include fine mineral particles (0.1–10 μm in diameter), often dominated by phyllosilicate, tectosilicate and quartz (Stibal et al. 2008) that are supplied from surrounding grounds by wind. Differences in source geology, however, likely cause geographic variation in cryoconite mineralogy (Cook et al., 2016). These particles are also carried from arid regions; for example, the occurrence of Saharan dust is well documented in the Alps (see among the others Meola et al., 2015). Coarser mineral particles (>10 mm in diameter) are derived from rock wall, *nunataks*, and glacier moraines (Takeuchi, 2011). In addition, pollutants deriving from industrial emissions, such as black carbon, are often incorporated into

cryoconite (Aamas et al., 2011). Black carbon, which is a product of incomplete combustion of fossil fuels, has attracted research attention because it is an extremely effective heat absorber, possibly accelerating ice melt (Clarke and Noone, 1985) and its longevity on ice surfaces is probably enhanced by incorporation into cryoconite (Bøggild, 2010). Moreover, also contaminants are found in cryoconite holes (Stibal et al., 2012a).

The other major component of cryoconite is the organic matter that includes living and dead microbes, their exudates, decomposition products and allochthonous biotic and biogenic matter (Cook et al., 2016). Cryoconite is an important microbial habitat and a major component of supraglacial ecosystems (Anesio and Laybourn-Parry, 2012). Already in the 1980s, a complex microbial community in ice, snow and in cryoconite holes was described by Kohshima (1984); nevertheless advances in the microbiology of cryoconite and ice-related ecosystems were performed in the last twenty years. Anesio and Laybourn-Parry (2012) proposed the cryosphere as one of the earth's major biomes. In this biome, cryoconite holes represent important sites of concentrated microbial activity and biodiversity. They represent the most biodiverse supraglacial habitat, which harbors communities with several trophic levels (Cook et al., 2016). Different food webs have been observed up to now in cryoconites. Some authors (among the others Stibal and Tranter, 2007 and Hodson et al., 2010) found that cryoconite are underpinned by photoautotrophy and primary producers use mainly solar energy to fix atmospheric CO_2 into organic matter, providing substrate for heterotrophs (see e.g. Stibal and Tranter, 2007 and Hodson et al., 2010). However, also heterotrophic communities are described (Edwards et al., 2011). In addition to bacteria, other heterotrophs at higher trophic levels also inhabit cryoconite holes, surviving by grazing upon smaller organisms. These include tardigrades, rotifers, copepods, ice worms and midge larvae (e.g. Zawierucha et al. 2013).

In conclusion, despite the Alps are one of the glacierized areas where the impact of the climate change is stronger (Oerlemans, 2001), a few study analysed the microbial communities, their sources and, above all, their evolution in this fast-changing environment.

Carbon fluxes in cryoconite

The microbial communities living on ice surface strongly affect the biogeochemical cycles not only of the cryoconites holes but also of the whole glacier. In particular, cryoconite holes represent very active sites of carbon fixation and release into the atmosphere (Hodson et al., 2010), with rates comparable to warm, nutrient rich environments (Anesio et al., 2010). Carbon transformations may determine glacier albedo through aggregation and darkening of cryoconite (Hodson et al., 2010) and influence the quality and quantity of carbon exported to extra glacial environments (e.g. Hood et al. 2009) and the net ecosystem productivity (Hodson et al., 2007). Autochthonous production of organic matter involves fixation of atmospheric CO_2 into organic molecules predominantly by photo-synthesis. Allochthonous organic carbon (OC) is primarily deposited on glaciers by wind and precipitation and comprises fragments of plants, mineral dust, microbes, black carbon and anthropogenic pollutants from local and distant sources (e.g. Hodson, 2014). Englacial OC can be released by melt out and provides a significant source of ancient bioavailable OC for down-stream ecosystems (Stubbins et al., 2012). OC also likely provides an energy source for cryoconite microbes. Subglacial OC might also be delivered to the supraglacial zone by thrust faulting (Stibal et al., 2012b), supplementing allochthonous OC in cryoconite holes in some locations. The influence of these carbon fluxes in the regional and global carbon cycling models have been estimated by Anesio et al. (2009) who suggest a net C fixation of about 64 Gg a^{-1} to all glacierized areas outside of Antarctica. However, this estimate is based on data from a small number of sites in Svalbard, Greenland and Alps, and further analyses are therefore needed for confirming or updating these estimates, due to the variability of cryoconite features on different glacierized areas worldwide. Indeed, cryoconite on low-latitude mountain glaciers is distinct from cryoconite on polar glaciers and ice sheets (Cook et al., 2016). This difference is primarily due to local glaciological and meteorological conditions. Low-latitude glaciers are generally small, fast flowing and subject to large diurnal fluctuations in energy balance. Solar radiation is more intense during the day at lower latitudes; however dark nights and variable cloud cover can produce complex

melt dynamics. Due to the abundance of deglaciated land in close proximity to most low-latitude glaciers, there is a greater deposition of aeolian dusts and soluble ions from terrestrial and anthropogenic sources than on polar glaciers. Takeuchi and Li (2008) showed that this causes rapid microbial production and high cryoconite coverage. High melt rates on low-latitude glaciers tend to produce shallower cryoconite holes with shorter life spans than those on polar ice (Takeuchi et al., 2000), and more frequent redistribution of cryoconite across ice surfaces might therefore be expected. High microbial production and abundant inorganic impurities encourage diverse microfauna and meiofauna to inhabit the glacier surface. These include glacial midges, copepods, collembolans, tardigrades and rotifers. Identification of operational taxonomic units (OTUs) and metabolite profiles has revealed different microbial community structures and functions in cryoconite from Arctic and Alpine glaciers (Edwards et al., 2014). Cryoconite biogeochemistry on low-latitude glaciers is probably similar to that of ice sheet margins, where fast flowing and rapidly melting ice favors net heterotrophy (Stibal et al., 2012b). Anesio et al. (2010) investigated the carbon fluxes in Arctic, Antarctic and Alpine cryoconite holes finding a low bacterial production (about 2–3% of the respiration of communities from similar habitats), indicating that other types of microbes (e.g. eukaryotic organisms) may also play a role in the C cycle of glaciers. Moreover, they estimated that only up to 7% of the OC in cryoconite is used annually by the heterotrophic bacteria, suggesting that the surface of glaciers can accumulate OC, which may be important for biogeochemical activities downstream.

In short, the knowledge of carbon fluxes on the glacier surface and on cryoconite holes in particular is still scarce and limited to some sites, mainly in polar areas. In addition, these communities on different glaciers and even on the same glacier seem to show a very large spatial and temporal variability. Finally, on the Alps these studies are lacking and limited to very few glaciers.

Aim of this study

In this work we analyzed the life on different ice-related forms. In particular, we described rotifers and nematodes on two large debris-covered glaciers for assessing the characteristics and the structure of these communities (Chapter 4). Moreover, we investigated the life in snow, one of the most diffuse cold environments of the world, by describing the microbial communities inhabiting the snow sampled in four different glacierized areas of the world (Chapter 5). Finally, we investigated the microbial communities of cryoconites holes, the most active supraglacial environment and, in particular, we described the probable sources of these communities (Chapter 6), their seasonal variability (Chapter 7) and we estimated the role of bacteria in the carbon fluxes on glacier surfaces (Chapter 8). Finally, in the Chapter 9, we investigate the close relation between the microbial communities on glacier and the human impact: in particular we analyze the role of the bacteria in the degradation of a pesticide (chlorpyrifos) accumulated in the cryoconite holes.

References

Aamaas B., Bøggild C.E., Stordal F., Berntsen T., Holmen K. and Ström J. (2011): Elemental carbon deposition to Svalbard snow from Norwegian settlements and long-range transport. *Tellus Series B, Chemical and Physical Meteorology*, 63(3), 340–351.

Anesio A.M., Hodson A.J., Fritz A., Psenner R. and Sattler, B. (2009): High microbial activity on glaciers: importance to the global carbon cycle. *Global Change Biology*, 15(4), 955-960.

Anesio A.M., Sattler B., Foreman C., Telling J., Hodson A., Tranter M. and Psenner R. (2010): Carbon fluxes through bacterial communities on glacier surfaces. *Annals of Glaciology*, 51 (56), 32-40.

Anesio A.M. and Laybourn-Parry J. (2012): Glaciers and ice sheets as a biome. *Trends in Ecology and Evolution*, 27(4), 219–225.

Bøggild C.E., Brandt R.E., Brown K.J. and Warren S.G. (2010): The ablation zone in northeast Greenland: ice types, albedos and impurities. *Journal of Glaciology*, 56, 101–113.

Caccianiga M., Andreis C., Diolaiuti G., D'Agata C, Mihalcea C. and Smiraglia C. (2011): Alpine debris-covered glaciers as a habitat for plant life. *The Holocene*, 21, 1011–1020.

Clarke A.D. and Noone K.J. (1985): Soot in the Arctic snowpack: a cause for perturbations in radiative transfer. *Atmospheric Environment*, 19(12), 2045-2053.

Cook J., Edwards A., Takeuchi N. and Irvine-Fynn T. (2016): Cryoconite - The dark biological secret of the cryosphere. *Progress in Physical Geography*, 40(1), 66-111.

Coulson S.J. and Midgley N.G. (2012): The role of glacier mice in the invertebrate colonisation of glacial surfaces: The moss balls of the Falljokull. Iceland. *Polar Biology*, 35, 1651–1658.

Edwards A., Anesio A.M., Edwards Rassner S.M., Sattler B., Hubbard B.P., Perkins W.T., Young M. and Griffith G.W. (2011): Possible interactions between bacterial diversity, microbial activity and supraglacial hydrology of cryoconite holes in Svalbard. *ISME Journal*, 5(1), 150-160.

Edwards A., Mur L., Girdwood S., Anesio A.M., Stibal M., Edwards Rassner S., Hell K., Pachebat J., Post B., Bussell J.S., Cameron S., Griffith G., Hodson A.J. and Sattler B. (2014): Coupled cryoconite ecosystem structure–function relationships are revealed by comparing bacterial communities in alpine and Arctic glaciers. *FEMS Microbiology Ecology*, 89(2), 222-237.

Fountain A.G., Tranter M., Nylen T.H., Lewis K.J. and Mueller D.R. (2004): Evolution of cryoconite holes and their contribution to meltwater runoff from glaciers in the McMurdo Dry Valleys, Antarctica. *Journal of Glaciology*, 50, 35–45.

Fickert T., Friend D., Grüninger F., Molnia B. and Richter M. (2007): Did debris-covered glaciers serve as Pleistocene refugia for plants? A new hypothesis derived from observations of recent plant growth on glacier surfaces. *Arctic, Antarctic and Alpine Research*, 39, 245–257.

Fontaneto D., Iakovenko N. and De Smet W.H. (2015): Diversity gradients of rotifer species richness in Antarctica. *Hydrobiologia,* 761, 235-248.

Franzetti A., Tatangelo V., Gandolfi I., Bertolini V., Bestetti G., Diolaiuti G., D'Agata C., Mihalcea C., Smiraglia C. and Ambrosini R. (2013): Bacterial community structure on two alpine debris-covered glaciers and biogeography of *Polaromonas* phylotypes. *The ISME Journal*, 7, 1483-1492.

Gobbi M., Isaia M. and De Bernardi F. (2011): Arthropod colonisation of a debris-covered glacier. *The Holocene*, 21, 343–349.

Hambrey M.J, Quincey D.J, Glasser N.F, Reynolds J.M, Richardson S.J. and Clemmens S. (2008): Sedimentological, geomorphological and dynamic context of debris-mantled glaciers, Mount Everest (Sagarmatha) region, Nepal. *Quaternary Science Reviews*, 27, 2361-2389.

Hodson A.J., Mumford P.N., Kohler J. and Wynn P.M. (2005): The High Arctic ecosystem: new insights from nutrient budgets. *Biogeochemistry*, 72, 233–256.

Hodson A.J., Anesio A.M., Ng F., Watson R., Quirk J., Irvine-Fynn T., Dye A., Clark C.D., McCloy P., Kohler J. and Sattler B. (2007): A glacier respires: quantifying the distribution and respiration CO_2 flux of cryoconite across an entire Arctic glacial ecosystem. *Journal of Geophysical Research (Biogeosciences)*, 112, G04S36.

Hodson A., Anesio A.M., Tranter M., Fountain A., Osborn M., Priscu J., Laybourn-Parry J. and Sattler B. (2008): Glacial ecosystem. *Ecological Monographs*, 78, 41–67.

Hodson A.J., Bøggild C.E., Hanna E., Huybrechts P., Langford H., Cameron K. and Houldsworth, A. (2010): The cryoconite ecosystem on the Greenland ice sheet. *Annals of Glaciology*, 51(56), 123-129.

Hodson A.J. (2014): Understanding the dynamics of black carbon and associated contaminants in glacial systems. *Wiley Interdisciplinary Reviews: Water,* 1, 141–149.

Hodson A., Brock B., Pearce D., Laybourn-Parry J. and Tranter, M., (2015): Cryospheric ecosystems: a synthesis of snowpack and glacial research. *Environmental Research Letters*, 10(11), 110201.

Hodson A.J., Cameron K.A., Bøggild C.E., Irvine-Fynn T.D., Langford H., Pearce D.A. and Banwart, S.A. (2010): The structure, biological activity and biogeochemistry of cryoconite aggregates upon an Arctic valley glacier: Longyearbreen, Svalbard. *Journal of Glaciology*, 56(196), 349-362.

Hood E., Fellman J., Spencer R.G.M., Hernes P.J., Edwards R., D'Amore D. and Scott D. (2009): Glaciers as a source of ancient and labile organic matter to the marine environment. *Nature*, 462, 1044-1047.

Hinkler J., Hansen B.U., Tamstorf M.P., Sigsgaard C. and Petersen D. (2008): Snow and snow-cover in central northeast Greenland. *Advances in Ecological Research*, 40, 175–195.

Irvine-Fynn T.D.L., Bridge J.W. and Hodson A.J. (2011): In situ quantification of supraglacial cryoconite morpho-dynamics using time-lapse imaging: an example from Svalbard. *Journal of Glaciology*, 57, 651–657.

Jones H.G. (2009): The ecology of snow-covered systems: A brief overview of nutrient cycling and life in the cold. *Hydrological Processes*, 13, 2135–2147.

Kellerer-Pirklbauer A. (2008): The supraglacial debris system at the Pasterze Glacier, Austria: Spatial distribution, characteristics and transport of debris. *Zeitschrift für Geomorphologie*, 52, 3–25.

Kirkbride M.P. and Warren C.R. (1999): Tasman Glacier, New Zealand: 20th-century thinning and predicted calving retreat. *Global and Planetary Change*, 22, 11–28.

Komárek J. and Nedbalová L. (2007): Green cryosestic algae. In Algae and Cyanobacteria in Extreme Environments; Seckbach, J., Ed.; Springer: Amsterdam, Netherlands, 2007; Volume 11, pp. 321–342.

Kohshima S. (1984): A novel cold-tolerant insect found in a Himalayan glacier. *Nature*, 310, 225–227.

Larose C., Berger S., Ferrari C., Navarro E. Dommergue A., Schneider D. and Vogel T.M. (2010): Microbial sequences retrieved from environmental samples from seasonal arctic snow and meltwater from Svalbard, Norway. *Extremophiles*, 14, 205-212.

Larose C., Dommergue A. and Vogel T.M. (2013): The dynamic Arctic snow pack: an unexplored environment for microbial diversity and activity. *Biology*, 2, 317-330.

Laybourn-Parry J., Tranter M. and Hodson A. (2012): The ecology of snow and ice environments. Oxford: Oxford University Press, 192 pp.

Lutz S., Anesio A.M., Raiswell R., Edwards A., Newton R.J., Gill F. and Benning L.G. (2016): The Biogeography of Red Snow Microbiomes and their Role in Melting Arctic Glaciers. *Nature Communications*, 7, 11968.

Meola M., Lazzaro A. and Zeyer J. (2015): Bacterial composition and survival on Sahara dust particles transported to the European Alps. *Frontiers in Microbiology*, 6, 1454.

Oerlemans L. (2001): Glaciers and Climate Change. A.A. Balkema Publishers, 148 pp.

Østrem G. (1959): Ice melting under a thin layer of moraine and the existence of ice cores in moraine ridges. *Geografiska Annaler*, 41, 228–230.

Pelfini M., Santilli M., Leonelli G. and Bozzoni M. (2007): Investigating surface movements of debris-covered Miage Glacier (Western Italian Alps) using dendroglaciological analysis. *Journal of Glaciology,* 53(180), 141–152.

Pelfini M., Diolaiuti G., Leonelli G., Bozzoni M., Bressan. N, Brioschi D. and Riccardi A. (2012): The influence of glacier surface processes on the short-term evolution of supraglacial tree vegetation: a case study of the Miage Glacier, Italian Alps. *The Holocene*, 22, 847–856.

Pomeroy J.W. and Brun E. (2001): Physical properties of snow. In Snow Ecology. An Interdisciplinary Examination of Snow-Covered Ecosystems; Jones, H.G., Pomeroy, J.W., Walker, D.A., Hoham, R.W., Eds.; Cambridge University Press: Cambridge, UK, pp. 45–126.

Segawa T., Miyamoto K., Ushida K., Agata K., Okada N. and Kohshima S. (2003): Seasonal change in bacterial flora and biomass in mountain snow from the Tateyama mountains, Japan, analyzed by 16s rRNA gene sequencing and real-time PCR. *Applied and Environmental Microbial,* 71, 123-130.

Stibal M. and Tranter M. (2007): Laboratory investigation of inorganic carbon uptake by cryoconite debris from Werenskioldbreen, Svalbard. *Journal of Geophysical Research-Biogeosciences*, 112, G04S33.

Stibal M., Elster J., Sabacka M. and Kastovska K. (2007): Seasonal and diel changes in photosynthetic activity of the snow alga C*hlamydomonas nivalis* (chlorophyceae) from Svalbard determined by pulse amplitude modulation fluorometry. *FEMS Microbiology Ecology*, 59, 265-273.

Stibal M., Bælum J., Holben W.E., Sørensen S.R., Jensen A. and Jacobsen C.S. (2012): Microbial degradation of 2, 4-dichlorophenoxyacetic acid on the Greenland ice sheet. *Applied and environmental microbiology*, 78(15), 5070-5076.

Stibal M., Sabacka M. and Zarsky J. (2012b): Biological processes on glacier and ice sheet surfaces. *Nature Geoscience*, 5(11), 771-774.

Stubbins A., Hood E., Raymond P.A., Aiken G.R., Sleighter R.L., Hernes P.J., Butman D., Hatcher P.G., Striegl R.G., Schuster P. and Spencer R.G.M. (2012): Anthropogenic aerosols as a source of ancient dissolved organic matter in glaciers. *Nature Geoscience*, 5(3), 198-201.

Takeuchi N., Kohshima S., Yoshimura Y., Seko K. and Fujita K. (2000): Characteristics of cryoconite holes on a Himalayan glacier, Yala Glacier Central Nepal. *Bulletin of Glaciological Research*, 17, 51-59

Takeuchi N. and Li Z. (2008): Characteristics of surface dust on Ürümqi glacier No. 1 in the Tien Shan mountains, China. *Arctic, Antarctic, and Alpine Research,* 40 (4), 744-750.

Takeuchi N., Kohshima S. and Seko K. (2001a): Structure, formation, and darkening process of albedo-reducing material (cryoconite) on a Himalayan glacier: a granular algal mat growing on the glacier. A*rctic, Antarctic and Alpine Resources*, 33, 115–122.

Takeuchi N., Kohshima S., Goto-Azuma K., and Koerner R. (2001b): Biological characteristics of dark colored material (cryoconite) on Canadian Arctic glaciers (Devon and Penny ice caps). *Polar Research*, 54, 495–505.

Takeuchi, N. (2011): Cryoconite in Singh V.P., Singh P. and Haritashya U.K.: Encyclopedia of Snow, Ice and Glaciers", Springer eds.

Zawierucha K., Coulson S.J., Michalczyk L. and Kaczmar L. (2013): Current knowledge of the Tardigrada of Svalbard with the first records of water bears from Nordaustlandet (High Arctic). *Polar Research*, 32, 20866.

Zhang T. (2005): Influence of the seasonal snow cover on the ground thermal regime: An overview. *Reviews of Geophysics*, 43, RG4002.

Chapter 4
Nematodes and rotifers on two Alpine debris-covered glaciers

Chapter published on the Italian Journal of Zoology

Azzoni R.S., Franzetti A., Fontaneto D., Zullini A. and Ambrosini R. (2015) - Nematodes and rotifers on two Alpine debris-covered glaciers. *Italian Journal of Zoology*, 82(4), 1-8.

Abstract

Debris-covered glaciers (DCGs) are glaciers whose ablation area is mostly covered by a continuous layer of debris and are considered to be among the continental glacierized environments richest in life. DCG colonization by microorganisms, plants and animals, has been investigated in a few studies, while the meiofauna (metazoan smaller than 2 mm) of these environments has been neglected so far. In this study we analyzed nematode and rotifer fauna on the two largest debris-covered glaciers of the Italian Alps: the Miage Glacier and the Belvedere Glacier. In total, we collected 38 debris samples on the glaciers in July and September 2009. All the rotifers we found belonged to the bdelloid *Adineta vaga*. Nematodes belonged to 19 species. Miage Glacier hosted a richer and more diverse nematode fauna than the Belvedere. The dominant genus was *Plectus*, a common genus in habitats at high latitude and altitude. Analysis of the feeding type of nematodes highlighted that bacterivores were dominant on Miage Glacier, while bacterivores and herbivores were more widespread on Belvedere Glacier. Predator nematodes were absent. Analysis of the food-web structure indicated that nematode assemblages on both glaciers were typical of environments with depleted food availability, probably resulting from instability of the glacier surface and the short exposure of sediments preventing the evolution of true soil and enrichment in organic matter of the debris. The scarcity of bacterial primary producers suggests that deposition of allochthonous organic matter is the principal organic carbon source in this environment.

4.1. Introduction

Cryosphere is the part of the world where water is frozen, for either long periods or seasonally (Laybourn-Parry et al. 2012). It includes ice caps and ice sheets, glaciers, lake ice, snow cover and permafrost on the continents, and sea ice on the oceans (Laybourn-Parry et al. 2012). Despite at first glance these extreme environments may seem not to host habitats that can support life, they have been proven to sustain active ecological processes, and are now considered as ecosystems (Hodson et al. 2008). Sea ice is particularly well studied in this respect (see e.g., Gradinger 2001), but recently also glaciers and ice sheets have been proposed as a biome in their own right (Anesio and Laybourn-Parry 2012). The surface of glaciers can be colonized by bacterial and algal communities (Takeuchi et al. 2001; Hodson et al. 2008; Schütte et al. 2010), as well as by communities of multicellular organisms, such as mosses, which, in turn, could be inhabited by species of Tardigrada, Nematoda, Enchytraeidae and Arachnida (Coulson and Midgley 2012). However, many other cryophilic invertebrates, mostly connected with aquatic/semi-aquatic environments, such as Chironomidae (Kohshima 1984), Plecoptera (Kohshima 1985), Collembola (Fjellberg 2010) and Enchytraeidae (Shain et al. 2001), can live directly on the surface of the ice (Zawierucha et al. 2015). Moreover, supraglacial cryoconite holes can be considered biodiversity hotspots for invertebrates such as Copepoda, Annelida, Tardigrada, Nematoda, Rotifera inhabiting glacial ecosystems (Zawierucha et al. 2015).

The debris cover of debris-covered glaciers (DCGs) is probably one of the continental glacierized environments richest in life (Nakawo et al. 2000). DCGs are mountain glaciers whose ablation area is mostly covered by a continuous layer of debris mainly composed of clasts, ranging in size from millimetres to metres, which fall on the glacier surface from surrounding mountains (Hambrey et al. 2008). The debris is then transported down valley by glacier movements for times that, on some glaciers, can be as long as a century (Pelfini et al. 2007). Most of the ablation area of DCGs is therefore covered by a continuous debris layer, whose thickness generally increases toward the glacier

terminus (Hambrey et al. 2008). The thick debris cover of DCGs reduces ice ablation (Nakawo and Rana, 1999), but the debris surface can be heated by solar radiation to temperatures that can exceed +30 °C (Brock et al. 2010). During the long transport on the glacier surface, the debris is weathered and altered, and can be colonized by microorganisms (Franzetti et al. 2013), plants (if the glacier elevation is lower than the treeline) (Pelfini et al. 2007, 2012; Caccianiga et al. 2011) and animals (Gobbi et al. 2011). It is important to notice that not only pioneer organisms can live on the surface of DCGs. For example, trees up to 2 m high grow on the surface of the Miage glacier (Caccianiga et al. 2011), and herbaceous plant can colonize DCG surface above the tree line, suggesting that organisms typical of soil fauna can live in the debris of DCGs.

The fauna of soils is mainly composed by microscopic organisms such as nematodes, rotifers and tardigrades, while larger ones, such as springtails, mites and other arthropods, are less abundant (Coleman et al. 2004; Chesworth 2008). Nematodes, rotifers and tardigrades, forming the so-called "meiofauna" of the soil, have been found in debris and thin soils from extreme habitats connected to ice in different areas of the world, including the polar regions (Sohlenius et al. 1996). Nematodes are the dominant phylum in soil, where they are present at densities ranging from one to several million individuals per square meter. Specific studies of nematodes in glacial environments are lacking. Nkem et al. (2006) found on the Antarctic ice only three nematode species: *Plectus antarcticus*, *Eudorylaimus antarcticus* and *Scottnema lindsayae*. Rotifers are usually less abundant in soils than nematodes, but they were found to be relatively more abundant in areas surrounding glaciers, such as Antarctic soils (Convey and McInnes 2005; Fontaneto et al. 2015).

Since nematodes and rotifers have been found in glacial environments, they may be present also in the debris cover of DCGs, but no study on their occurrence in these environments is known to us. In this study, we present a first report on the nematode and rotifer fauna found in the debris cover of two DCGs of the Italian Alps, the Miage Glacier (Valle d'Aosta, Italy) and the Belvedere Glacier (Piemonte, Italy) and analysed the structure of the nematode assemblages we found.

4.1.1. Study sites and field methods

Miage Glacier (45° 47’ N, 6° 52’ E, Mont Blanc massif) is the widest debris-covered glacier of the Italian Alps, with a total surface area of 10.47 km2 (2009 data, Smiraglia et al. 2015). Its ablation zone is covered by debris from above 2,400 m a.s.l. to the terminus (1,700 m a.s.l.). The debris covers 4 km2 and is mainly composed by gneisses, schistes and granites (Brock et al. 2010), and ranges in thickness between a few centimeters to more than 1 m at the snout of the glacier (Mihalcea et al. 2008).

Belvedere Glacier (45° 57’ N, 7° 55’ E, Monte Rosa massif) has a total surface area of 4.53 km2 (2010 data, Smiraglia et al. 2015) and is debris-covered from about 2,300 m a.s.l. to the glacier snout at 1,750 m a.s.l. Rock debris is mainly composed by gneisses, micaschists and granites with a thickness ranging between a few centimeters to more than 1 m at the terminus (Diolaiuti et al. 2003).

During each of the sampling campaigns, debris samples were collected both on July (the 28th on Miage and the 2nd on Belvedere) and September (the 10th on Miage and the 18th on Belvedere) 2009 at the same location, with the only exception of one site on the Miage Glacier, where in September a crevasse prevented us to reach the same sampling site of July (Fig. 1). Nine debris samples (approximately 500 ml) were collected at the surface of the debris cover of Miage Glacier from 1,749 to 2,169 m a.s.l. and 10 at that of the Belvedere Glacier from 1,803 to 2,085 m a.s.l. At all sampling sites we removed the dry debris (< 1 cm) at the very surface of the debris cover, and collected the first centimeters of the underlying fresh and moist debris. Collecting samples deeper was impractical, due to the presence of large stones or iced debris close to the glacier surface. On both glaciers sampling sites were chosen at approximately constant intervals (elevation and distance) from the glacier terminus (Fig. 1). Overall, we collected 18 debris samples from Miage Glacier and 20 from Belvedere Glacier.

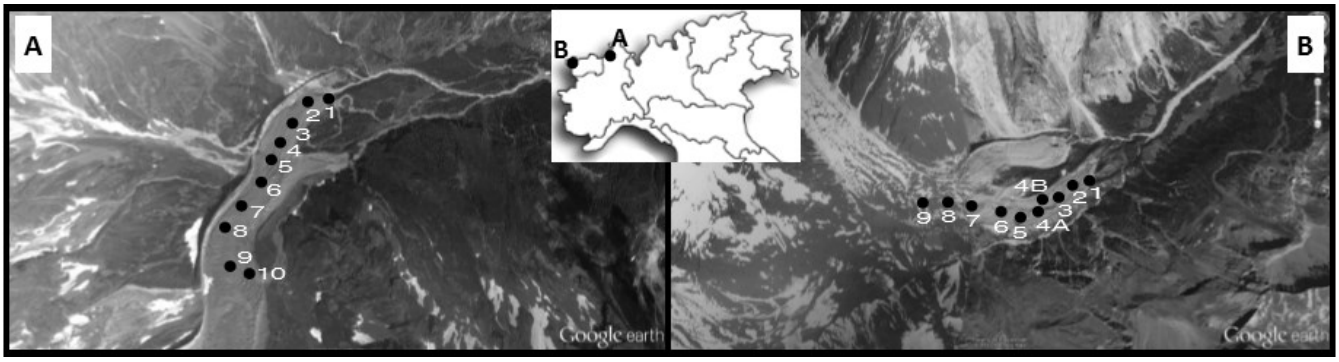

Fig.1: Sampling sites on Belvedere Glacier (on the left) and on Miage Glacier (on the right) from Google Earth ™. Site 4 on Miage Glacier was sampled at different positions in July and September.

This sampling design was chosen because we originally aimed at assessing whether the structure of nematode and rotifer assemblages changed along the glacier and to identify the ecological variables driving such variation. For this aim, we also collected information on several features of the environment at each sampling site (namely elevation, debris thickness, annual surface velocity, organic carbon content, pH) by methods that are fully described in Franzetti et al. (2013). However, number of individual nematodes and rotifers collected at each sample (about 6 nematodes and 1 rotifer per sample on average, see Results) was too low to perform any statistical analysis at site level. We also considered that, even if we had extracted nematodes and rotifers from the whole amount of debris collected at each sample, and not from a sub-sample (see below), the number of individuals extracted would have been too low for performing any analysis at site level. We therefore considered our samples as replicated samples collected at the same glacier, and performed all the analyses with the only aim of describing and comparing nematode and rotifer faunas living in the debris cover of the Miage and Belvedere glaciers. All information on environmental variables was therefore discarded.

4.2. Material and methods

4.2.1. Nematode and rotifer extraction and identification

Each debris sample was mixed, and a 200 ml sub-sample extracted. Nematodes were extracted from the sub-sample by a modified Baermann method (Baermann 1917). Briefly, the debris was folded in tissue paper and placed on a wire mesh that, in turn, was put in a dish filled with water. This method for nematode extraction takes advantage of the natural tendency of nematodes to move toward the water, crossing the debris. After two days of incubation at room temperature, we collected the nematodes in the dish and fixed them in dimethyl sulfoxide solution (Kilpatrick 2002). Transfer and mounting of nematodes on permanent slides followed standard methods (Seinhorst 1959). Taxonomy and nomenclature of nematodes followed Peneva and Bongers (2013).

Rotifers were extracted from the sub-samples using Devetter's (2010) method: briefly, 20 ml of soil sample were spread on a plastic sieve with a very thin layer of cellulose submerged in distilled water in a Petri dish. The Petri dish was situated on a cooled panel and light from the top by fluorescent lamps. The temperature of the base panel was 5 °C, whereas no heating from the top was used, as it is known to reduce extraction efficiency for rotifers (Devetter 2010). In addition, in order to check that no additional slowly-moving rotifers or animals that do not detach from soil particles were present, 20 ml of soil sample was put in Petri dishes with water and directly observed using a microscope, to look for living animals. Taxonomic identification of rotifers followed Donner (1965), whereas the adopted nomenclature was that of the recent List of Available Names for rotifers (Segers et al. 2012).

4.2.2. Data analysis

We investigated nematode diversity at each glacier by calculating Simpson and Shannon (base *e*) diversity indices. We also aimed at estimating the total number of nematode species on each glacier, given the observed species. Several tools are described in the literature for these estimates, both based

on parametric and non-parametric methods, but the application of different tools to the same data set usually provides different estimates (Hill et al. 2003). To mitigate the impact of this (unavoidable) problem we used the CatchAll software (beta 4 version; http://www.northeastern.edu/catchall/). CatchAll fits four parametric models via maximum likelihood and five non-parametric richness estimates to the data. The best model is then chosen as the model that shows the best fit to the data i.e. has both low standard error (SE) of the estimated total number of species in the community and low values of goodness-of-fit (GOF) statistic on the observed data (Hong et al. 2006; see also the CatchAll manual for further details).

We also compared relative abundance of each species (number of individuals of each taxon divided by the total number of individuals collected on each glacier) between the two glaciers by a binomial mixed model where the glacier was entered as a dichotomous fixed factor and species as a random factor. Glacier was also entered as a random slope within species. This model is analogous to a paired sample t-test, but accounts for the non-Gaussian distribution of relative abundances (Zuur et al. 2009).

We analysed the nematode species we found following the Ferris et al. (2001) concepts and criteria. The nematode fauna provides information on the food webs of a soil, particularly on their complexity and connectance (the proportion of possible links between species that are realized; Dunne et al. 2002) and on how resources flow in them (Ferris et al. 2001). Briefly, nematodes can be divided into functional guilds according to their feeding habits (bacterivores, fungivores, herbivores, carnivores and omnivores), and their position along a colonizer-persistent (c-p) gradient (partially reflecting the r-K strategist gradient of the species; Bongers 1990). Abundance of nematode functional guilds can be used to calculate two indices, a Structure Index (SI) indicating whether the food web is simple (low values) or complex (high values), and the Enrichment Index (EI) indicating whether a soil is depleted (low values) or enriched (high values) in organic matter (Ferris et al. 2001). Both indices range from 1 to 100 and depict different and independent pieces of information on soil features (Ferris et al. 2001). They can be used to draw a “functional guilds square”, which is a Cartesian plot with SI as x-axis and

the EI as y-axis. The square can be then divided in quadrants according to values of both indices being larger or smaller than 50. Since the SI and the EI indices are independent, nematode assemblages can stay everywhere in the square (Ferris et al. 2001). Given the small number of specimens found at each sampling site, analyses of nematode presence were run by pulling together all the individuals collected on each glacier from both sampling campaigns. Analyses were made with the Ninja software (Sieriebriennikov et al. 2014; http://spark.rstudio.com/bsierieb/ninja/).

4.3. Results

Nematodes were found in 11 of the 18 samples (61%) collected on Miage Glacier and in 16 of the 20 samples (80%) collected on Belvedere Glacier. Average number of individuals collected at each sample was 5.8 ± 1.5 SE (range 0 – 46, n = 38 samples).

We identified 19 nematode taxa (Table 1). In 14 cases we were able to identify taxa to species level while in 5 cases only to the genus level. Only in the case of *Tylencholaimus sp.* more than one individual was found. However, in this case, specimens were indistinguishable, therefore we consider them as belonging to the same species, albeit we could not precisely assess to which one.

On the Miage Glacier the most abundant species was *Plectus rhizophilus* (20 individuals), while on the Belvedere Glacier it was *Tylenchus davainei* (57 individuals). Considering both glaciers, all Nematodes assemblages were dominated by *Plectus pusteri* and *Tylenchus davainei*. Nematode diversity was larger on the Miage (14 taxa) than on the Belvedere Glacier (9 taxa), but the total number of organisms sampled was higher on Belvedere (137) than on Miage Glacier (83). Both Simpson and Shannon diversity indices were larger on the Miage than on the Belvedere Glacier (Table 1). Total estimated number of species was also larger for the Miage (16.8 ± 2.0 SE, confidence limits: 14.8 – 24.0) than for the Belvedere Glacier (11.7 ± 2.7 SE, confidence limits: 9.5 – 23.0). However, confidence limits of these estimates overlap.

SPECIES / GENUS	TOTAL NUMBER OF INDIVIDUALS		c-p CLASS	FEEDING TYPE	MASS (µg)
	MIAGE	BELVEDERE			
Coslenchus sp.	1	0	0	*H*	0.11
Malenchus bryophilus (Steiner, 1914)	5	0	0	*H*	0.06
Tylenchus davainei (Bastian, 1865)	2	57	0	*H*	0.64
Tylenchus elegans (de Man, 1876)	0	9	0	*H*	0.45
Xenocriconemella macrodora (Taylor, 1936)	1	0	0	*H*	0.15
Aphelenchoides pusillus (Thorne, 1929)	2	5	2	*F*	0.16
Tylencholaimus sp.	2	0	4	*F*	0.51
Acrobeloides tricornis? (Thorne, 1925)	0	4	2	*B*	0.17
Cephalobus sp.	0	1	2	*B*	0.27
Eumonhystera longicaudatula (Gerlach & Riemann, 1973)	0	6	2	*B*	0.12
Chiloplectus andrassyi (Timm, 1971)	2	0	2	*B*	0.97
Plectus geophilus (de Man, 1880)	10	0	2	*B*	0.07
Plectus magadani (Kuzmin 1979)	0	4	2	*B*	0.45
Plectus parietinus (Bastian, 1865)	1	0	2	*B*	2.41
Plectus parvus (Bastian, 1865)	7	1	2	*B*	0.14
Plectus pusteri (Fuchs, 1930)	18	50	2	*B*	1.17
Plectus rhizophilus (de Man, 1880)	20	0	2	*B*	0.63
Prismatolaimus intermedius (Bütschli, 1873)	2	0	3	*B*	0.11
Eudorylaimus brevis/discolaimoideus	10	0	4	*O*	3.40
TOTAL NUMBER OF INDIVIDUALS	**83**	**137**			
NUMBER OF SPECIES	**14**	**9**			
Shannon Diversity Index (base *e*)	**2.17**	**1.45**			
Simpson Diversity Index	**0.85**	**0.68**			

Tab. 1: Nematodes identified in the debris collected on Miage and Belvedere Glacier. Species whose identification was uncertain are indicate with "?". Number of individuals per taxon observed on each glacier is reported. The colonizer-persistent (c-p) gradient consists of five classes: the lower values identified opportunists organisms, the higher values indicated persistent nematodes. In the feeding type column "H" indicates herbivores, "F" fungivores, "B" Bacterivores and "O" Omnivores. Nematode weight was calculated according to Andrássy (1956).

Relative abundance of nematodes was larger on the Miage than on the Belvedere Glacier ($z = 2.11$, $P = 0.03$), thus suggesting that the structure of nematode assemblages differed between the two glaciers. We then pulled together all specimens collected on each glacier to investigate nematode feeding types. This analysis confirmed that nematode assemblages differed between the two glaciers (Fig. 2). In the supraglacial debris of Miage Glacier bacterivores were the dominant feeding type, while omnivores, fungivores and herbivores were limited. On the contrary, in the debris of Belvedere Glacier, the two dominant feeding types were bacterivores and herbivores. Predators were absent on both glaciers.

Rotifers were found in 6 samples collected on the Miage and in 7 samples collected on the Belvedere Glacier. Overall, 38 individuals were found, all belonging to the bdelloid species *Adineta vaga* (Davis, 1873). Average number of individuals collected at each sample was 1.0 ± 0.3 SE (range 0 – 8, $n = 38$ samples). No analysis of the rotifer communities was therefore possible.

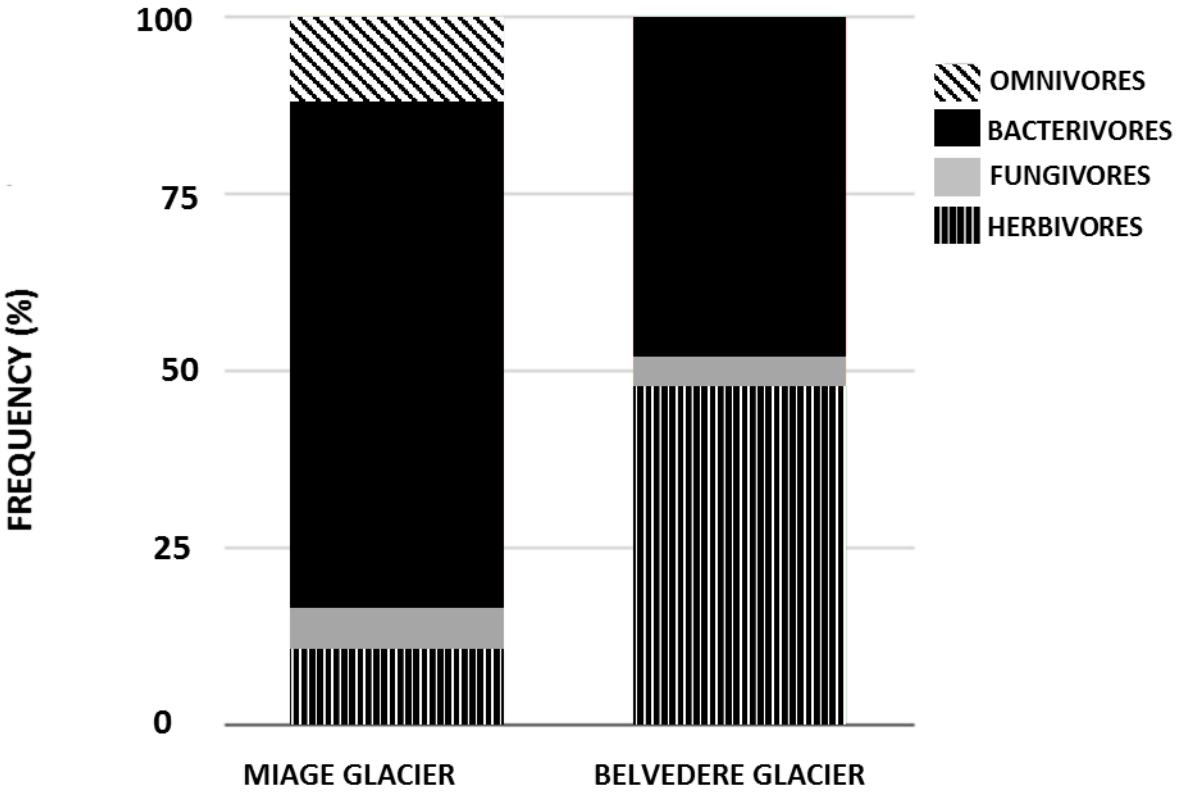

Fig.2: Feeding type composition of nematode assemblages found on the Miage and the Belvedere glaciers.

4.4. Discussion

This work reports a first assessment of nematodes and rotifers living in the debris cover of two Alpine DCGs. The food webs of nematode assemblages, dominated by *Plectus pusteri* and *Plectus rhizophilus* on the Miage and by *Plectus pusteri* and *Tylenchus davainei* on the Belvedere Glacier were classified by the Ninja software as "basal" (Fig. 3), i.e. "food webs that have been diminished due to stress, including limitation of resources, adverse environmental conditions, or recent contamination" (Sieriebriennikov et al. 2014; Ferris et al. 2001). This result suggests that, despite DCGs can be considered among the continental glacier environments richest in life, the ecological conditions in their debris may pose adverse and stressful conditions to soil organisms. In fact, these habitats are characterized by substrate instability due to the glacier motion (up to 76 m per year; on the Miage

Glacier; Pelfini et al. 2007) and rather short exposure of sediments to weathering (less than one century; Pelfini et al. 2007) that prevent the evolution of a supraglacial soil and an enrichment in organic matter. Moreover the debris coverage is characterized by large daily and annual temperature variations (Mihalcea et al. (2008) reported temperature excursions of up to 50 °C on the Miage Glacier), which probably negatively affect soil meiofauna because only very eurythermic species can survive in this environment. In addition, low trophic resource availability, as indicated by the very basal nematode food webs we found, may pose further limits to meiofauna abundance and richness.

Despite the few nematode taxa identified, some ecological patterns are evident. There is a clear dominance of *Plectus*, both in individuals (51%) and in species (37%) for all assemblages. *Plectus* is usually dominant at high latitudes and altitudes all over the world (Artois et al. 2011), and dominance by this genus confirms that the adverse environmental conditions at the surface of DCGs are the most probable forcing factor affecting ecological assemblages living in these environments. Overall, the Miage seems to host more diverse nematodes than the Belvedere Glacier. This may be due to the thicker and more stable debris layer that covers this glacier (Diolaiuti et al. 2003; Mihalcea et al. 2008). The majority of the nematodes we found were bacterivores, whereas predators were absent. This is consistent with the results of other studies suggesting that the principal organic carbon source of the trophic web might be the deposition of allochthonous organic matter (Franzetti et al. 2013; Stibal et al. 2008). Although it has been reported that photosynthetic bacteria and unicellular algae may constitute the main food source of soil nematodes in High-Arctic cryo-ecosystems, the composition of the microbial community on DCGs did not show significant abundance of phototrophs (Franzetti et al., 2013). Moreover, Gobbi et al. (2011) investigated the arthropod communities on the Miage Glacier, and found that they are sustained by inputs of organic matters (i.e. plant debris, insects, animal excrements) from the surrounding areas. External inputs support the supraglacial vegetation as well (Caccianiga et al. 2011), providing resources necessary to sustain the occurrence of plants (e.g.

leaves or plant debris). All these evidences suggest that trophic webs on debris-covered glaciers are sustained from allochthonous inputs of organic matter from surrounding environments.

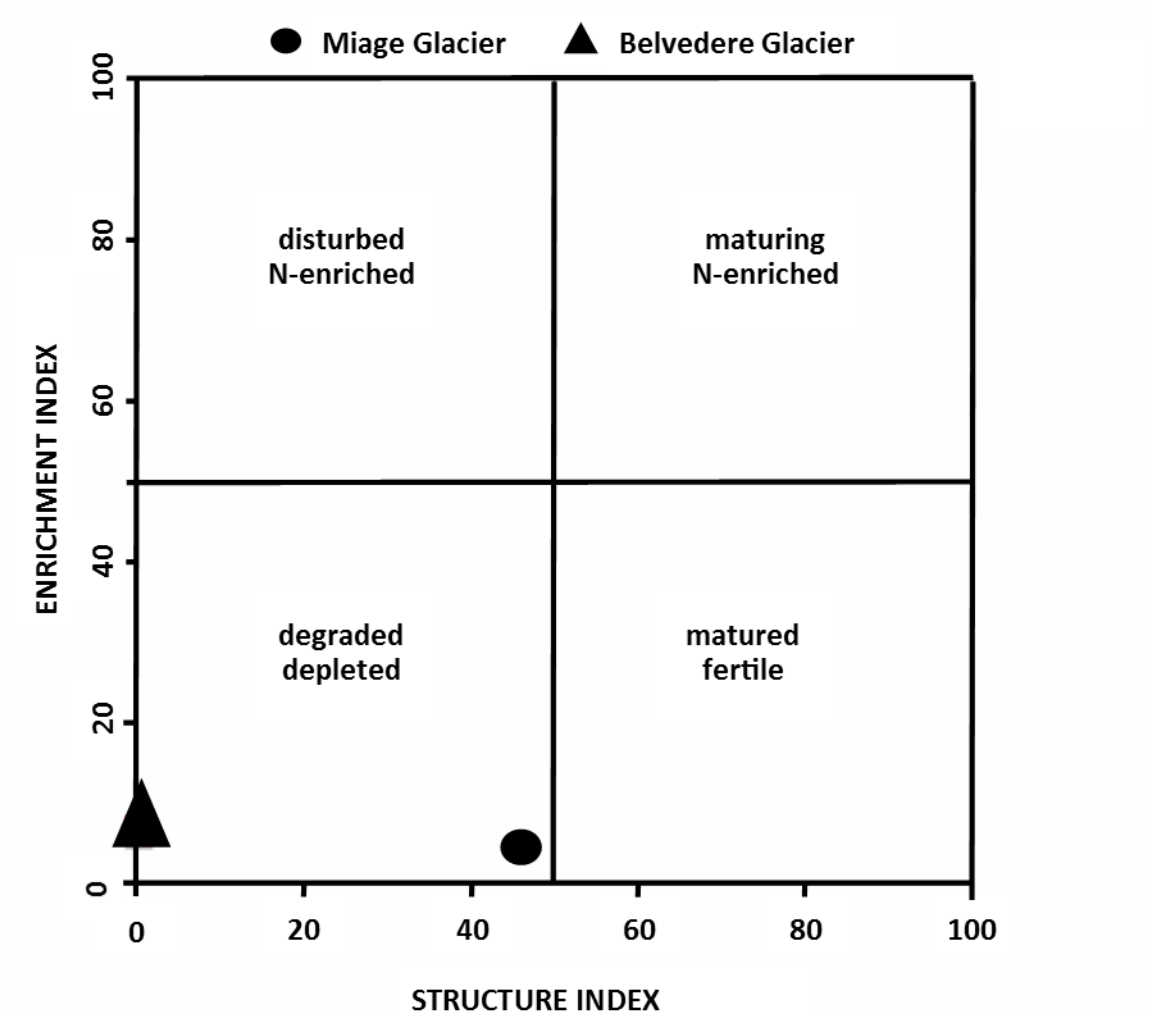

Fig.3: Analysis of the nematode assemblages performed with the NINJA software (Sieriebriennikov et al. 2014).

Despite that our initial aim was to investigate variation in rotifer and nematode assemblages along the glacier surface, the paucity of the specimens we found prevented any analysis at site level. Future studies aiming at investigating rotifer and nematode communities in these environments should therefore collect and extract nematodes from a much larger amount of debris (at least 2000 ml), in order to obtain about 200 individuals on average from each sample, corresponding to a minimum amount for performing nematode analyses (Lison, 1965).

Surprisingly, rotifer diversity was very low, with only one species, *A. vaga,* and few individuals. *A. vaga* is a cosmopolitan species living in any habitat and under very different conditions; moreover, it is

known to be a complex of several taxa each of them potentially with different ecological needs (Fontaneto et al. 2011). Thus, no ecological inference can be performed based only on the morphological identification of this taxon. Rotifers, and especially bdelloid rotifers, are known to be common and sometimes extremely abundant in Arctic (Kaya et al. 2010) and Antarctic environments (Fontaneto et al. 2015) as well as at elevations higher than 3000 m a.s.l. in the Alps (Fontaneto and Ricci 2006). Yet, even from well-studied areas in Antarctica, most records of rotifers do not come from bare periglacial soils, but almost invariably from more structured soils, usually with moss carpets (Fontaneto et al. 2015). Records of rotifers from glaciated habitats as cryoconite holes include also one or few species (Zawierucha et al. 2015), suggesting that DCG's surface could actually be a truly rotifer-poor habitat. The limiting factor for the low abundance and diversity of rotifers in DCG's surface is not the freezing temperature, but we can speculate that the low rotifer diversity could be related to the texture or to the dynamics of organic matter of the debris. However, we stress that very little is known on soil rotifers and on the drivers of their diversity, so that our hypotheses are merely tentative.

In summary, our results indicate that ecological assemblages on DCGs depend on inputs of organic matter from surrounding environments. Pioneer communities in extreme environments may not necessarily be dominated by primary producers, but can be composed by consumers degrading organic matter mainly coming from other ecosystems.

4.5. References

Andrássy G. (1956): Die Rauminhalts- und Gewichtsbestimmung der Fadenwűrmer (Nematoden). *Acta Zoologica,* 2, 1-15.

Anesio A.M. and Laybourn-Parry J. (2012): Glaciers and ice sheets as a biome. *Trends in Ecology and Evolution*, 27, 219–225.

Artois T., Fontaneto D., Hummon W.D., McInnes S.J., Todaro M.A., Sørensen M.V. and Zullini A. (2011): Ubiquity of microscopic animals? Evidence from the morphological approach in species identification. In:

Fontaneto D. (ed.), Biogeography of microscopic organisms, is everything small everywhere? Cambridge University Press, Cambridge, pp. 244-283.

Baermann G. (1917): Eine einfache Methode zur Auffindung von Ankylostomum- (Nematoden) -Larven in Erdproben. Weltevreden Batavia, Geneesk. Lab. Feestbundel. 41-47.

Brock B.W., Mihalcea C., Kirkbride M.P., Diolaiuti G., Cutler M.E.J. and Smiraglia C. (2010) Meteorology and surface energy fluxes in the 2005–2007 ablation seasons at the Miage debris-covered glacier, Mont Blanc Massif, Italian Alps. *Journal of Geophysical Resources*, 115, D09106.

Bongers T. (1990): The maturity index: an ecological measure of environmental disturbance based on nematode species composition. *Oecologia*, 83, 14-19.

Caccianiga M., Andreis C., Diolaiuti G., D'Agata C., Mihalcea C. and Smiraglia C. (2011): Alpine debris-covered glaciers as a habitat for plant life. *The Holocene*, 21, 1011-1020.

Chesworth W. (2008): Encyclopedia of Soil Science. Springer, Dordrecht.

Coleman D.C., Crossley D.A. and Hendrix P.F. (2004): Fundamentals of Soil Ecology. Elsevier Academic Press, San Diego.

Convey P. and McInnes S.J. (2005): Exceptional tardigrade-dominated ecosystems in Ellsworth Land, Antarctica. *Ecology*, 86, 519–527.

Coulson S.J. and Midgley N.G. (2012): The role of glacier mice in the invertebrate colonisation of glacial surfaces: the moss balls of the Falljo kull, Iceland. *Polar Biology*, 35, 1651–1658.

Devetter M. (2010): A method for efficient extraction of rotifers (Rotifera) from soils. *Pedobiologia*, 53, 115–118.

Diolaiuti G., D'Agata C. and Smiraglia C. (2003): Belvedere Glacier, Monte Rosa, Italian Alps: tongue thickness and volume variations in the second half of the 20th century. *Arctic, Antarctic and Alpine Research*, 35, 255–263.

Donner J. (1965): Ordnung Bdelloidea (Rotatoria, Rädertiere). Bestimmungsbücher zur Bodenfauna Europas 6. Akademie Verlag, Berlin.

Dunne J.A., Williams R.J. and Martinez N.D. (2002): Food-web structure and network theory: The role of connectance and size. *Proceedings of the National Academy of Sciences*, 99, 12917-12922.

Ferris H., Bongers T. and De Goede R.G.M. (2001): A framework for soil food web diagnostics: extension of the nematode faunal analysis concept. *Applied Soil Ecology*, 18, 13-29.

Fjellberg A. (2010): Cryophilic Isotomidae (Collembola) of the Northwestern Rocky Mountains, U.S.A. *Zootaxa*, 2513, 27-49.

Fontaneto D., Iakovenko N. and De Smet W.H. (2015): Diversity gradients of rotifer species richness in Antarctica. *Hydrobiologia*, 761, 235-248.

Fontaneto D., Iakovenko N., Eyres I., Kaya M., Wyman M. and Barraclough T.G. (2011): Cryptic diversity in the genus *Adineta* Hudson & Gosse, 1886 (Rotifera: Bdelloidea: Adinetidae): a DNA taxonomy approach. *Hydrobiologia*, 662, 27-33.

Fontaneto D. and Ricci C. (2006): Spatial gradients in species diversity of microscopic animals: the case of bdelloid rotifers at high altitude. *Journal of Biogeography*, 33, 1305-1313.

Franzetti A., Tatangelo V., Gandolfi I., Bertolini V., Bestetti G., Diolaiuti G.A., D'Agata C., Mihalcea C., Smiraglia C. and Ambrosini R. (2013): Bacterial community structure on two alpine debris-covered glaciers and biogeography of *Polaromonas* phylotypes. *The ISME Journal*, 7, 1483-1492.

Gobbi M., Isaia M. and De Bernardi F. (2011): Arthropod colonisation of a debris-covered glacier. *The Holocene*, 21, 343-349.

Gradinger R.R. (2001): Adaptation of Arctic and Antarctic ice metazoa to their habitat. *Zoology*, 104, 339-345.

Hambrey M.J., Quincey D.J., Glasser N.F., Reynolds J.M., Richardson S.J. and Clemmens S. (2008): Sedimentological, geomorphological and dynamic context of debris-mantled glaciers, Mount Everest (Sagarmatha) region, Nepal. *Quaternary Science Reviews*, 27, 2361-2389.

Hill T.C.J., Walsh K.A., Harris J.A. and Moffett B.F. (2003): Using ecological diversity measures with bacterial communities. *FEMS Microbiology Ecology*, 43, 1–11.

Hodson A., Anesio A.M., Tranter M., Fountain A., Osborn M., Priscu J., Laybourn-Parry J. and Sattler B. (2008): Glacial ecosystem. *Ecological Monographs*, 78, 41–67.

Hong S.H., Bunge J., Jeon S.O. and Epstein S.S. (2006): Predicting microbial species richness. *Proceedings of the National Academy of Sciences*, 103, 117–122.

Kaya M., De Smet W.H. and Fontaneto D. (2010): Survey of moss-dwelling bdelloid rotifers from middle Arctic Spitsbergen (Svalbard). *Polar Biology*, 33, 833-842.

Kilpatrick C.W. (2002): Non-cryogenic preservation of mammalian tissues for DNA extraction: An assessment of storage methods. *Biochemical Genetics*, 40, 53–62.

Kohshima S. (1984): A novel cold tolerant insect found in a Himalayan glacier. *Nature*, 310, 225–227.

Kohshima S. (1985): Patagonian glaciers as insect habitats. In Glaciological studies in Patagonia Northern Icefield: 94–99. Nokajima, C. (Ed.), Kyoto: Data Center for Glacier Research Japanese Society of Snow and Ice

Laybourn-Parry J., Tranter M. and Hodson A.J. (2012): The Ecology of Snow and Ice Environments. Oxford University Press: Oxford, UK.

Lison L. (1960): Statistique appliquée à la biologie expérimentale. La planification de l'expérience et l'analyse des résultats. *Population*, 3, 567-578

Mihalcea C., Brock B.W., Diolaiuti G., D'Agata C., Citterio M., Kirkbride M.P. Cutler M.E.J. amd Smiraglia C. (2008): Using ASTER satellite and ground-based surface temperature measurements to derive supraglacial debris cover and thickness patterns on Miage Glacier (Mont Blanc Massif, Italy). *Cold Regions Science and Technology*, 52, 341–354.

Nakawo M. and Rana B. (1999): Estimate of ablation rate of glacier ice under a supraglacial debris layer. *Geografiska Annaler, Series A Physical Geography*, 81, 695–701.

Nakawo M., Raymond C.F. and Fountain A. (2000): Debris-covered glaciers. International Association of Hydrological Sciences, Publication No. 264, IAHS Press, Wallingford.

Nkem J.N., Wall D.H., Virginia R.A., Barrett J.E., Broos E.J., Porazinska D.L. and Adams B.J. (2006): Wind dispersal of soil invertebrates in the McMurdo Dry Valleys, Antarctica. *Polar Biology*, 29, 346-352.

Pelfini M., Diolaiuti G.A., Leonelli G., Bozzoni M., Bressan N. and Brioschi D. (2012): The influence of glacier surface processes on the short-term evolution of supraglacial tree vegetation: a case study of the Miage Glacier, Italian Alps. *The Holocene*, 22, 847–856.

Pelfini M., Santilli M., Leonelli G. and Bozzoni M. (2007): Investigating surface movements of debris-covered Miage Glacier (Western Italian Alps) using dendroglaciological analysis. *Journal of Glaciology*, 53, 141–152.

Peneva V., Bongers AMT. (2013): Nematoda. Fauna Europaea version 2.6.2. Web service available online at: http://www.faunaeur.org

Schütte U.M.E., Abdo Z., Foster J., Ravel J., Bunge J., Solheim B. and Forney L.J. (2010): Bacterial diversity in a High Arctic glacial foreland. *Molecular Ecology*, 19, 54–66.

Seinhorst J.W. (1959): A rapid method for the transfer of nematodes from fixative to anhydrous glycerin. *Nematologica*, 4, 67-69.

Segers H., De Smet W.H., Fischer C., Fontaneto D., Michaloudi E., Wallace R.L. and Jersabek C.D. (2012): Towards a list of available names in zoology, partim Phylum Rotifera. *Zootaxa*, 3179, 61–68.

Shain D.H., Mason T.A., Farrell A.H. and Michalewicz L.A. (2001): Distribution and behavior of ice worms (*Mesenchytraeus solifugus*) in south-central Alaska. *Canadian Journal of Zoology*, 79,1813–1821.

Sieriebriennikov B., Ferris H. and De Goede R.G.M. (2014): NINJA: An automated calculation system for nematode-based biological monitoring. *European Journal of Soil Biology*, 61, 90-93.

Smiraglia C., Azzoni R.S., D'Agata C., Maragno D., Fugazza D. and Diolaiuti G.A. (2015): The evolution of the Italian glaciers from the previous data base to the New Italian Inventory. Preliminary considerations and results. *Geografia Fisica e Dinamica Quaternaria*, 38(1), 79-87.

Sohlenius B., Bostrom S. and Hirschfelder A. (1996): Distribution patterns of microfauna (nematodes, rotifers and tardigrades) on nunataks in Dronning Maud Land, East Antarctica. *Polar Biology*, 16, 191–200.

Stibal M., Tranter M., Benning L.G. and Řehák J. (2008): Microbial primary production on an Arctic glacier is insignificant in comparison with allochthonous organic carbon input. *Environmental Microbiology*, 10, 2172-2178.

Takeuchi N., Kohshima S. and Seko K. (2001): Structure, formation, and darkening process of albedo–reducing material (cryoconite) on a Himalayan glacier: a granular algal mat growing on the glacier. *Arctic, Antarctic and Alpine Resources*, 33, 115–122.

Zawierucha K., Kolicka M., Takeuchi N. and Kaczmarek L. (2015): What animals can live in cryoconite holes? A faunal review. *Journal of Zoology*, 295, 159-169.

Zuur A.F., Ieno E.N., Walker N.G., Saveliev A.A. and Smith G.M. (2009): Mixed effects models and extensions in ecology with R, Springer, New York.

Chapter 5
Bacterial diversity in snow communities from mid-latitude high-altitude areas: Alps, Ararat, Karakoram and Himalaya

Abstract

Snow is considered as an independent ecosystem that hosts active microbial communities. Snow microbial assemblages have been extensively investigated in the Arctic and the Antarctica, but rarely in mid-latitude areas. In this study, we investigated the bacterial communities of snow collected in four glacierized areas (Alps, Eastern Anatolia, Karakoram and Himalaya) by high-throughput DNA sequencing and we reconstructed the origin of the air masses that produced the snowfalls through the analyses of back trajectories. The bacterial communities hosted a limited number of OTUs, moreover, communities from different geographical areas differed significantly to one another. Our results suggest that snow bacterial communities receive a non-negligible input of local air bacteria, maybe by strong deposition of local particulate that occur during snowfall. This notwithstanding, a contribution of bacteria from the area where the air mass originate from cannot be excluded, as well as a selective action of harsh conditions during the long distance atmospheric transport.

5.1. Introduction

Snow covers up to 35% of Earth surface (Miteva, 2007) and, consequently, has a strong impact on the hydrological cycle, the mass balance of glaciers and the climate (Singh et al., 2011). In addition, the feedback mechanisms between snow, ice and the atmosphere influence the whole biosphere (Jones, 1999). Thus, snow and ice play a key role in the dynamics of a large number of ecosystems worldwide (Groisman and Davis, 2001).

Snow-cover can be described as an independent ecosystem, which has drawn attention in recent years (Jones, 1999). Active bacterial communities inhabit the snow cover and have been investigated in different areas of the world. For instance, Cameron et al. (2015) described the microbial communities of the Greenland's ice sheets using High Throughput (Illumina) 16S rRNA sequencing, and found that, independently from the sampling area, snow communities were dominated by Proteobacteria, Acidobacteria and Bacteroidetes. Similar results were obtained by Hell et al. (2013) on the Larsbreen Glacier, Svalbard using the 454 pyrosequencing. Møller et al. (2013) analyzed the bacterial communities of the Greenland snowpack through pyrosequencing of 16S rRNA and found that different snow layers within the snow pack hosted different microbial communities. In particular, the highest diversity was observed in the middle and top snow layers where Proteobacteria, Bacteroidetes and Cyanobacteria dominated, while in the deepest layer, large percentages of Firmicutes and Fusobacteria were found. Michaud et al. (2014) used pyrosequencing to describe the microbial communities in snow samples near Concordia base in Antarctica (75°6'S, 123°20'E), which, again, were dominated by Proteobacteria and Bacteroidetes, with rather large abundance of Cyanobacteria. Thus, the same taxa seem to dominate snow pack bacterial communities in both hemispheres. Antarctic snow communities sampled near four stations (Druzhnaja 69°44′S, 72°42′E; Leninsgradskaja 69°30'S, 159°23'E; Nirnii 66°33'S, 93°01'E and Progress 69°23'S, 76°23'E) were further analyzed with Illumina sequencing by Lopatina et al. (2016). Not surprisingly, the most abundant classes in all

samples were Alphaproteobacteria, Betaproteobacteria, Gammaproteobacteria, Sphingobacteria, Flavobacteria, Cytophagia, Actinobacteria, Chloroplast/Cyanobacteria. Interestingly, these communities were compared to one another and the Progress samples were found to be different from the other ones: indeed, the most abundant class in Progress was Flavobacteria, while in all the other samples the communities were dominated by Beta- and Gammaproteobacteria.

Other studies conducted with different methods confirmed the dominance of few taxa in snow packs. For instance, Amato et al. (2006) isolated several bacterial strains from snow sampled near the station of Ny-Ålesund and on the Kongsvegen Glacier (Svalbard) identifying Proteobacteria, Firmicutes and Actinobacteria as the dominant taxa.

A few studies have been conducted on mountain areas outside the Polar areas. Wundelin et al. (2016) described the microbial communities hosted in the snow on Swiss and Australian Alps by Illumina sequencing: in all the samples, independently from the sampling site, the communities were dominated by Proteobactetria and Bacteroidetes, thus confirming the dominance of these groups in non-Polar areas. Similar results were found by Liu et al. (2006; 2009) in snow sampled from the Tibetan plateau using clone libraries. They found that Proteobacteria, Bacteroidetes and Actinobacteria were the dominant taxa. Segawa et al. (2005) investigated snow from the Tateyama Mountains (Japan) analyzing clone libraries of the 16S rRNA gene. A large part of the retrieved sequences belonged to Alpha-, Beta- and Gamma-Proteobacteria, Flexibacter, Cytophaga, Bacteroides, Bacillus/Clostridium and Actinobacteria. Moreover, they isolated various organisms such as *Aquaspirillum*, *Burkholderia*, *Methylobacterium*, *Haemophilus*, *Serratia* (Proteobacteria), *Corynebacterium*, *Propionibacterium* (Actinobacteria), *Staphylococcus*, *Streptococcus* (Firmicutes). Finally, Meola et al. (2016) analyzed the bacterial composition of a snowfall enriched of Saharan dust on the Suisse Alps and identified Proteobacteria as the most abundant phylum, in particular Betaproteobacteria, (*Variovorax*, *Polaromonas* and *Delftia*), followed by Actinobacteria, Bacteroidetes, Firmicutes, Chloroflexi, Cyanobacteria and Gemmatimonadetes.

From the short review of the snow microbial literature described above it appears that all the papers investigating snow-cover bacterial communities were site-specific and were conducted with approaches that differed from site to site. These differences in the methodologies have hampered the comparison of results among studies, and, consequently, our understanding of the bacterial communities and the ecological processes occurring in the snow-cover in different areas of the world. In addition, to the best of our knowledge, no snow sample from temperate high-altitude regions has been analyzed with High Throughput Sequencing so far.

This variability in the bacterial communities of snow is probably due also to the different physical and chemical features of the air mass that originated the snowfall, which, in turn, depend on the geographical area the air mass originated from and its trajectory (Fierer et al., 2008, Chuvochina et al., 2011).A useful tool for the analysis of the origin and trajectory of an air mass is the NOAA's HYSPLIT model that reconstructed the trajectories of air masses up to 72 hours before the event analyzed ("back trajectory analysis") (Stein et al., 2015), which is widely applied in climatological analysis with a particular attention on snowfall characterization and dust provenance (see e.g. Shahgedanova et al., 2013) or pollutants dispersion (see e.g. Oh, 2015). In addition, the back trajectory analysis has been also applied in air microbiology to determine origin and sources of microbial communities (e.g. Griffin et al., 2006; 2007; Smith et a., 2013).

In this work, we described and compared bacterial communities of snow samples collected in four different high-altitude areas of the world outside the Polar Regions (Alps, Ararat, Karakoram and Himalaya). To ease comparison, all samples were collected and processed according to the same protocol and analyzed with High Throughput (Illumina) Sequencing. In addition, we analyzed the back trajectories of the air masses that originated the snowfalls, in order to assess the possible sources of bacteria. To the best of our knowledge, this is the first analysis of snow bacterial communities ever performed in Eastern Anatolia and Karakoram.

5.2. Material and methods

5.2.1. Study area, field methods and environmental data

We collected snow samples during filed campaigns conducted on four high-elevation areas: Alps (Forni Glacier, Central Alps, Italy), Eastern Anatolia (ice cap on the summit of Ararat/Ağri Dağı, Turkey), Karakoram (Baltoro Glacier, Central Karakoram, Pakistan) and Himalaya (Khumbu Valley, Nepal) (Fig. 1). In the first three sites, the samples were collected on the glacier surface only, whereas in Khumbu Valley snow were sampled both on a glacier (Changri Nup Glacier) and on ice-free areas (near the Pyramid International Laboratory/Observatory jointly managed by the Italian Ev-K2-CNR Committee and the Nepal Academy of Science and Technology). Overall, we collected 23 samples of snow during expeditions in 2013 and 2014. In details, we collected six samples from four different snow events on Forni Glacier, five samples on Ararat, five samples from two separate snowfalls on Baltoro Glacier and seven samples from two different snowfalls in Khumbu (see Table 1 for more details on sampling dates and locations). The snow, both fresh and wet dependently from availability during each expedition, was aseptically collected on the field in sterilized aluminum boxes or in sterilized plastic bags by a snow shovel sterilized with alcohol immediately before collecting each sample. Samples were then transported to the base camp, hut or laboratory where they were melted and filtered on nitrocellulose filters with nominal porosity of 0.42 μm.

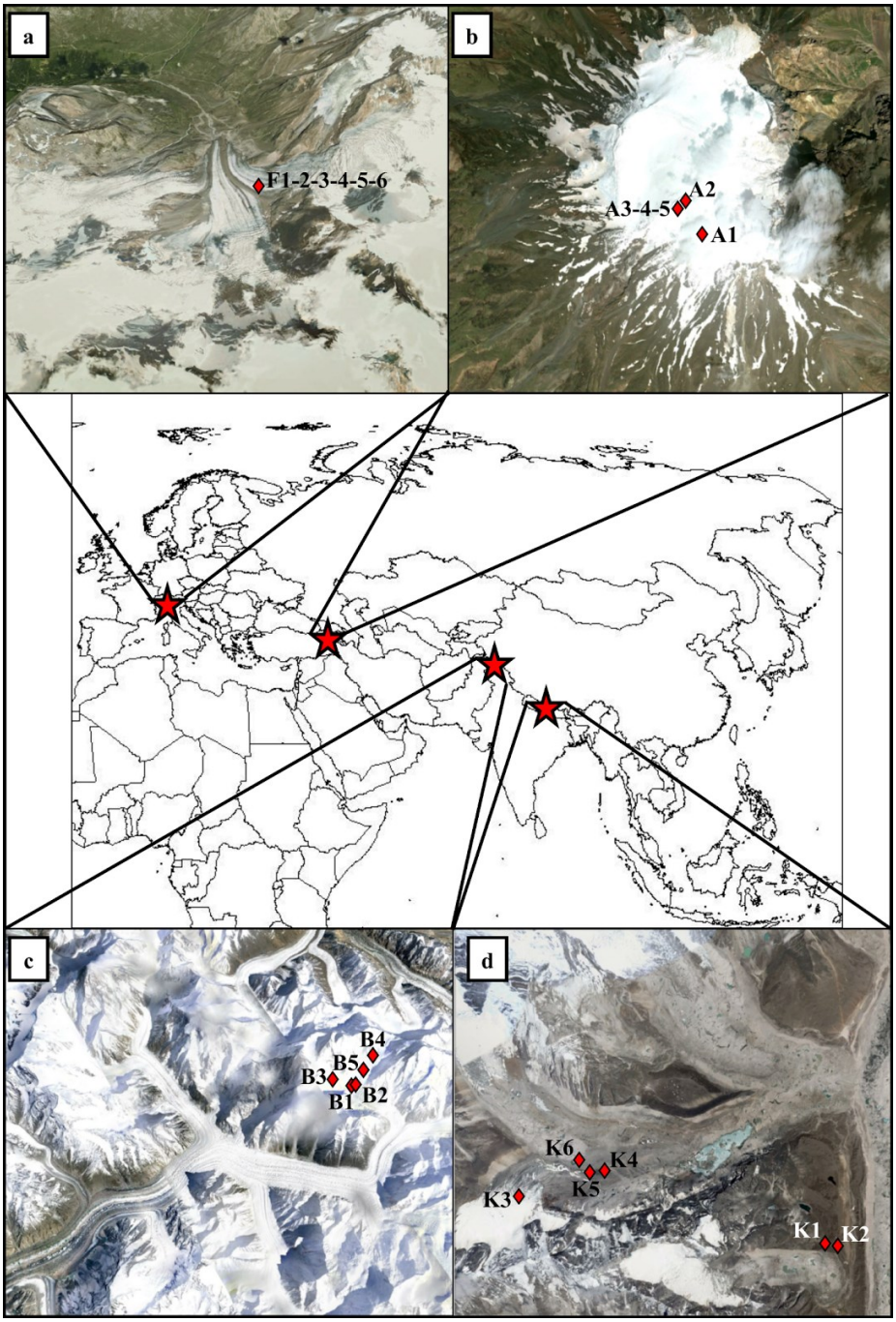

Fig. 1: Geographical position of four sampled areas. Detailed maps from Google EarthTM report the position of each sampling site (red diamonds) on Forni Glacier, Italy (a). Ararat summit ice cap glacier, Turkey (b), Baltoro Glacier, Pakistan (c) and Khumbu Valley, Nepal (d). Multiple numbers indicate multiple samples collected in the same site.

SITE	ID	DATE	SNOWFALL DATA	COORDINATES	ELEVATION (m)	DEPTH (cm)	ORIGIN OF THE AIR MASS	N° OF OTU	GINI INDEX
ARARAT GLACIER	A1	23/7/2014	Unknown	39.10195° N 44.29838° E	5132	10	Unknown	88	0.95
	A2	23/7/2014	Unknown	39.70422° N 44.29507° E	5030	10	Unknown	83	0.94
	A3	23/7/2014	Unknown	39.70367° N 44.29427° E	5020	85	Unknown	98	0.93
	A4	23/7/2014	Unknown	39.70367° N 44.29427° E	5020	55	Unknown	52	0.97
	A5	23/7/2014	Unknown	39.70367° N 44.29427° E	5020	20	Unknown	108	0.92
BALTORO GLACIER	B1	5/7/2013	1-2/7/2013	35.72910° N 76.64286° E	5591	0	Middle East (III)	52	0.97
	B2	5/7/2013	1-2/7/2013	35.72936° N 76.64233° E	5600	0	Middle East (III)	26	0.98
	B3	6/7/2013	1-2/7/2013	35.73907° N 76.63026° E	5735	0	Middle East (III)	44	0.98
	B4	7/7/2013	6/7/2013	35.73365° N 76.67352° E	5861	0	Middle East (IV)	21	0.99
	B5	7/7/2013	6/7/2013	35.73122° N 76.66149° E	5626	0	Middle East (IV)	45	0.98
FORNI GLACIER	F1	31/5/2014	29/1-2/2/2014	46.39737° N 10.59444° E	2702	15	Atlantic (V)	45	0.97
	F2	31/5/2014	4-7/2/2014 Sediment-rich snowfall	46.39737° N 10.59444° E	2702	10	Sahara (VI)	40	0.97
	F3	31/5/2014	10-15/2/2014	46.39737° N 10.59444° E	2702	5	Atlantic (VII)	55	0.96
	F4	31/5/2014	10-15/2/2014	46.39737° N 10.59444° E	2702	5	Atlantic (VII)	37	0.98

	F5	31/5/2014	18-20/2/2014 Sediment-rich snowfall	46.39737° N 10.59444° E	2702	0	Sahara (VIII)	44	0.97
	F6	31/5/2014	18-20/2/2014 Sediment-rich snowfall	46.39737° N 10.59444° E	2702	0	Sahara (VIII)	52	0.96
KHUMBU VALLEY	K1	21/10/2014	13-16/10/2014	27.95776° N 86.81213° E	5000	0	India – cyclone (IX)	140	0.91
	K2	21/10/2014	13-16/10/2014	27.95729° N 86.81326° E	5010	0	India – cyclone (IX)	143	0.88
	K3	26/10/2014	25/10/2014	27.98024° N 86.77572° E	5507	0	Middle East – Westerlies (X)	196	0.86
	K4	26/10/2014	25/10/2014	27.97919° N 86.78802° E	5323	0	Middle East – Westerlies (X)	149	0.86
	K5	26/10/2014	25/10/2014	27.97963° N 86.78680° E	5339	0	Middle East – Westerlies (X)	212	0.83
	K6	26/10/2014	25/10/2014	27.98048° N 86.78642° E	5362	0	Middle East – Westerlies (X)	171	0.85
	K7	26/10/2014	25/10/2014	27.98219° N 86.78270° E	5372	0	Middle East – Westerlies (X)	180	0.85

Tab. 1: Details of snow samples collected in the four areas. The Roman numbers between brackets in the origin of the air mass refers to the back trajectories reported in Figure 5.

5.2.2. 16S rRNA gene fragment sequencing, sequence processing and data analysis

For each sample, total DNA was extracted using the fastDNA Spin for soil kit (MB biomedicals, Solo, OH USA) according to the manufacturer's instructions. To characterize the bacterial diversity in the communities, the V5-V6 hypervariable regions of 16S rRNA gene were sequenced by MiSeqIllumina (Illumina inc., San Diego, CA, USA) with a 250bp × 2 paired-end protocol. This region was PCR-amplified using 783F and 1046R primers (Huber et al. 2007; Wang and Qian, 2009). Cyclic conditions for the amplification were: initial denaturation at 94 °C for 4 min; 28 cycles at 94 °C for 50 s, 47 °C for 30 s and 72 °C for 45 s and a final extension at 72 °C for 5 min. The amplicons were purified with

the Wizard® SV Gel and PCR Clean-up System (Promega Corporation, Madison, WI, USA) and purified DNA was quantified using Qubit® (Life Technologies, Carlsbad, CA, USA). Groups of 9/12 amplicons bearing different barcodes pairs were pooled together to build a single library. Further preparation with the addition of standard Nextera indexes (Illumina, Inc., San Diego, CA, USA) and sequencing were carried out at Parco Tecnologico Padano (Lodi, Italy).

Operational Taxonomic Units (OTUs) were defined by clustering sequences whose similarity was greater than 97%. For each cluster, a consensus sequence was considered as the representative sequence of the OTU. The abundance of each OTU was defined as the number of sequences belonging to each cluster. Operational Taxonomic Units (OTUs) were defined on the whole data set clustering the sequences at 97% similarity and defining a representative sequence for each cluster. The taxonomic classification of the OTU's representative sequences was obtained by RDP classifier (Wang et al., 2007).

5.2.3. Statistical analyses

To avoid any bias given by the difference in the number of sequences retrieved in each sample, we randomly picked 3000 sequence from each sample and calculated alpha diversity indexes on this dataset. We used the number of OTUs as an index of alpha-diversity at each sample, and the Gini index to evaluate the evenness (Gini 1912). The Gini index is a measure of statistical dispersion that ranges from 0 to 1, with increasing values indicating lower evenness (Wittebolle et al., 2009).

Analyses of community structure (beta diversity) were based on subsets of 10000 sequences randomly extracted from the whole set of sequences at each sample for those samples with more than 10000 sequences, and on the number of sequences of each OTU normalised to 10000 for the three samples with less than 10000 sequences (samples B1, B2 and K7 that had 3092, 3595 and 7633 sequences respectively).

The comparison between alpha diversity indices of the samples from different areas was performed with an ANOVA test followed by multiple t-tests, whose P-values were corrected with the Benjamini & Yekutieli (2001) false discovery rate (FDR) procedure in order to account for multiple statistical tests. To assess if the values of each index were normally distributed, we performed the Shapiro-Willks test, while we used the Fligner-Killeen test to verify the assumption of homoschedasticity in ANOVA models.

We explored similarity among community structures by a cluster analysis on Hellinger distances (Legendre & Legendre, 1998; Borchard et al., 2011). In addition, we used redundancy analysis (RDA) to test if structure of the bacterial communities differed among sampling areas. We could not enter in the analyses variation in other conditions like e.g. snow pH, sampling altitude, or snow age because of i) the large variation in these parameters among sampling regions and ii) the rather small number of samples collected at each region. Consequently, sampling region summarizes variation in all the other parameters, while small sample size prevented any within-region analysis. RDA was followed by post-hoc pairwise comparison between locations, whose significance was adjusted according to the FDR procedure (Benjamini & Yekutieli, 2001).

Finally, we identified indicator orders for each sampling region using the Indicator Value method described by De Cáceres et al. (2010). All statistical analyses were performed in R 3.1.3 (R core team, 2015) with the vegan (Oksasen et al., 2016), indicspecies (De Cáceres & Legendre, 2009) and multtest (Pollard et al. 2005) libraries.

5.2.4. Back trajectory definition

The back trajectories of the air masses that generated the sampled snowfalls were estimated using the HYSPLIT model (i.e. Hybrid Single Particle Lagrangian Integrated Trajectory Model) developed by the Air Resources Laboratory of the NOAA (National Oceanic and Atmospheric Administration (Stein et al. (2015); http://ready.arl.noaa.gov/HYSPLIT.php). The model was run analyzing the trajectories of

air masses starting from 72 hours before each event at specific elevations for each area (i.e. 3000 m above sea level for the Forni Glacier, 5000 m a.s.l. for Ararat, Baltoro and Khumbu). For each event the output of the model consisted in 27 different possible trajectories ("ensemble technique", Gneiting & Raftery, 2005) performed using slightly different initial meteorological conditions. A low spread between these trajectories is consistent with a good definition of the origin of the air mass (Stein et al. 2015).

Snow samples of Baltoro and Khumbu were collected fresh, so the exact day when each snowfall event occurred was known. On Forni, we were able to identify the snowfall day of each snow sample because each sample was collected from a single layer of snow, clearly identifiable in the snowpack. Indeed, careful snowpack analysis conducted *in situ* by means of snow pits, allowed identifying and sampling the layers generated by each single snowfall due to the different features of each layer (i.e. snow density, hardness, grain size and shape, liquid water and dust content; see e.g. Citterio et al., 2007 for further information). In particular, the snowpack we sampled on Forni included two different layers of sediment-rich snow, clearly identifiable because of their distinctive orange-brown colour (mostly due to the presence of silt and clay, see Azzoni et al., 2016). These layers originated from the sediment-rich snowfalls of 4-7 February and 18-20 February 2014 observed in the whole Southern Alps (Meola et al., 2015). Thus, we could identify in the field and sample the two sediment-rich snow layers (samples F2-F5 and F6), the sediment-free snow layer between them (samples F3 and F4), which originated from the snowfall of 10-15 February 2014, and the sediment-free snow layer immediately below the deepest sediment-rich layer (F1), originating from the snowfall of 29 January-2 February 2014. Data from an automatic weather station located near the sampling site (46.40°N,10.60°E; 2631 m a.s.l., see Senese et al., 2012 for further details) and equipped with a webcam that focuses on the glacier, further confirmed the accuracy of the dates of snowfalls we sampled. For Alps, Ararat and Baltoro we thus knew the exact date of each snowfall we sampled and therefore we could reconstruct back trajectories of the air masses that generated those snowfalls.

In contrast, we could not date the snowfalls that originated the snow samples we collected on Ararat. In this case, we ran the HYSPLIT model for the dates of all the winter precipitation events in the surroundings of the Ararat, as recorded by the Doğubeyazıt weather station, located 15 km South-West of the Ararat summit (39.55°N, 44.08°E; 1500 m a.s.l.).

5.3. Results

5.3.1. OTU abundance

We identified 341 OTUs from all snow samples. Burkholderiales (phylum Proteobacteria) was the most abundant order representing, on average, 45.7% of sequences in each sample (Fig. 2 and Tab. 2). Other abundant orders were Xanthomonadales (Proteobacteria), Cytophagales (Bacteroidetes) and Bacillales (Firmicutes) representing, respectively 17.7%, 17.0% and 8.0% of each sample. On Forni, Burkholderiales (50.1%) and Cytophagales (47.7%) were the most abundant orders. On Ararat, Burkholderiales were dominant (70.2%), followed by Bacillales (16.8%). On Baltoro, Xanthomonadales (35.2%) and Burkholderiales (23.6%) were the most abundant orders. In the Khumbu Valley, Burkholderiales (41.6%) and Xanthomonadales (21.2%) were dominant.

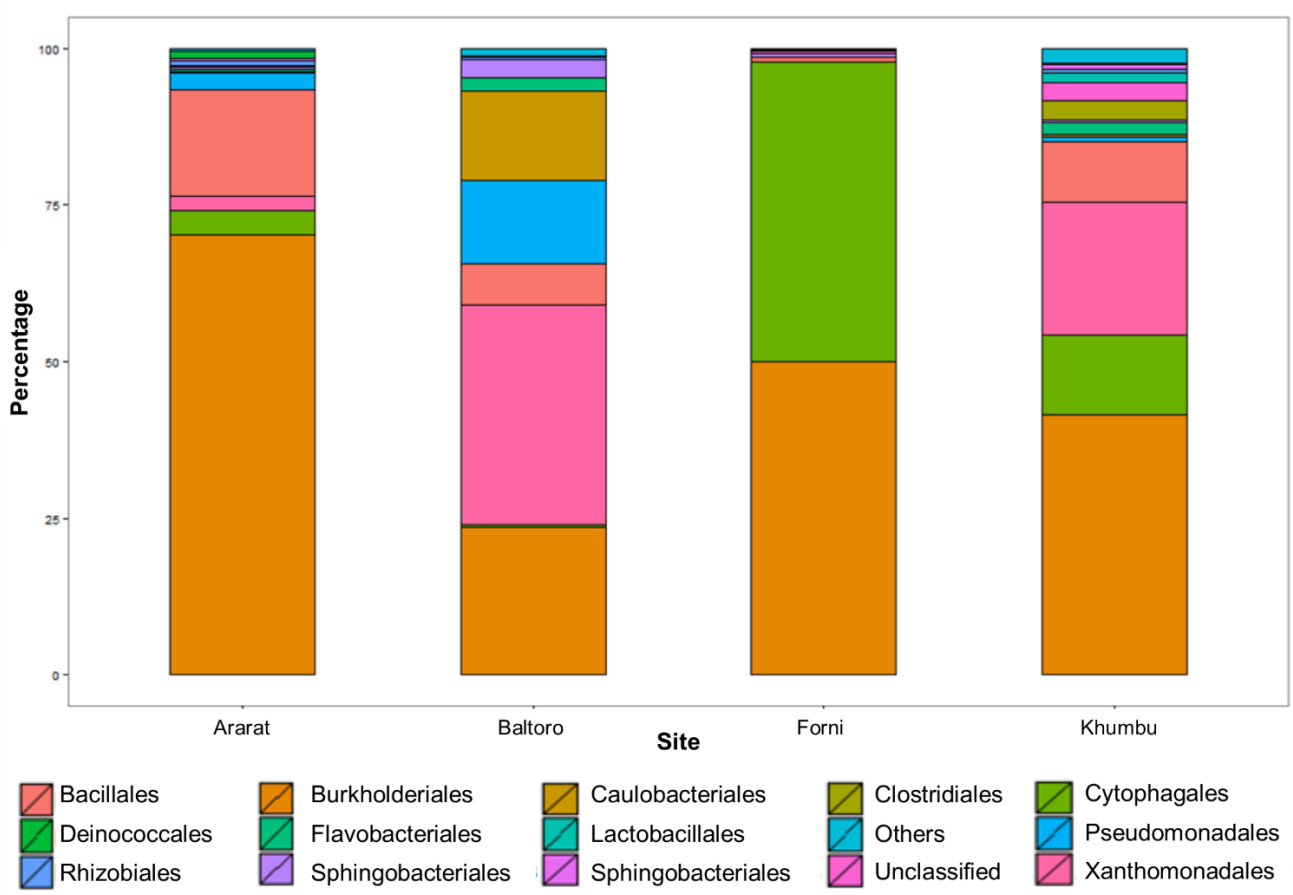

Fig.2: Relative abundance of bacterial orders found in each area. Orders whose abundance was lower than 1.5% were clustered in the "other" group.

Order	Site	Indval Index	P_{FDR}
Bacillales	Ararat	0.894	0.037
Burkholderiales	Ararat	0.622	0.049
Caulobacterales	Baltoro	0.967	0.001
Xanthomonadales	Baltoro	0.817	0.025
Cytophagales	Khumbu	0.893	0.001

Tab. 2: Typical bacterial orders for each area. The Indval Idex is a Statistic calculated as described in De Caceres (2010). PFDR indicates p-value corrected for multiple statistical tests according to the false discovery rate (Benjamini & Yekutieli 2001).

5.3.2. α diversity

Number of OTUs at each sample varied between 21 (sample B4 from Baltoro Glacier) and 212 (sample K5 from Khumbu Valley). Significant differences in OTU number were observed between sampling areas ($F = 60.6$; $df = 3,19$; $P < 0.001$, Figure 3A). Post-hoc tests showed that samples from Khumbu valley hosted a significantly larger number of OTUs than those from all the other areas ($|t| \geq 5.635$; $df = 10$; $P \leq 0.001$). Similarly, OTU number in the samples from Ararat was significantly larger than that from both Forni and Baltoro ($|t| \geq 4.223$; $df = 8$; $P \leq 0.006$); which, in turn, did not differ significantly ($t = 1.139$; $df = 9$; $P = 0.696$, Figure 4).

Gini index varied significantly among sampling areas ($F = 50.46$; $df= 3,19$; $P<0.001$; Figure 3B). Post hoc tests revealed that samples from Khumbu showed significantly lower values than those from the other areas ($|t| \geq 5.429$; $df = 10$; $P < 0.001$). Samples from Ararat showed lower values than those from Baltoro ($t = 5.429$; $df = 10$; $P = 0.021$), while samples from Forni showed intermediate values among those from Ararat and Baltoro ($|t| \geq 2.637$; $df = 9$; $P \leq 0.062$). Both the number of OTUs and the Gini index were normally distributed ($W > 0.86$, $P \geq 0.154$) and homoscedastic ($\chi^2 \leq 5.912$, $df = 3$, $P \geq 0.116$).

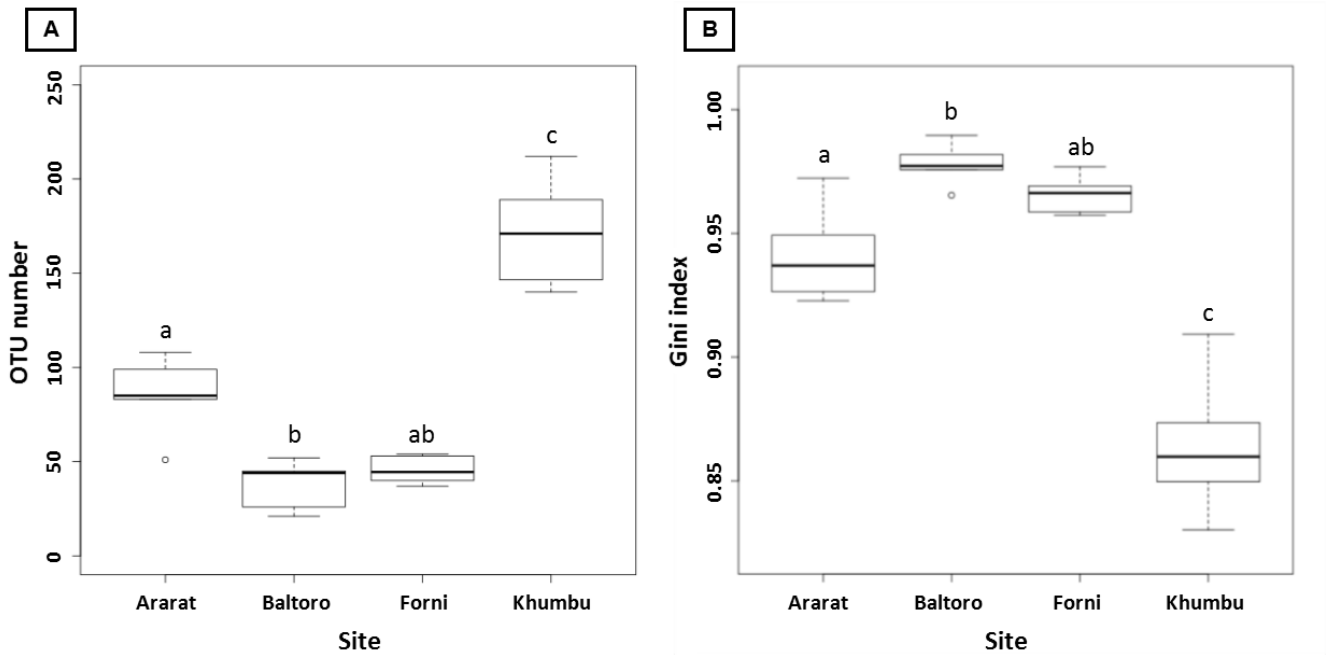

Fig.3: Boxplot of number of OTU a) and Gini index (b)in each area. The tight horizontal lines represent the median, boxes enclose values between 1st and 3rd quartile. Whiskers indicate maximum and minimum values. Dots represent outlier. Different letters denote samples that differed significantly at post-hoc tests ($P < 0.05$).

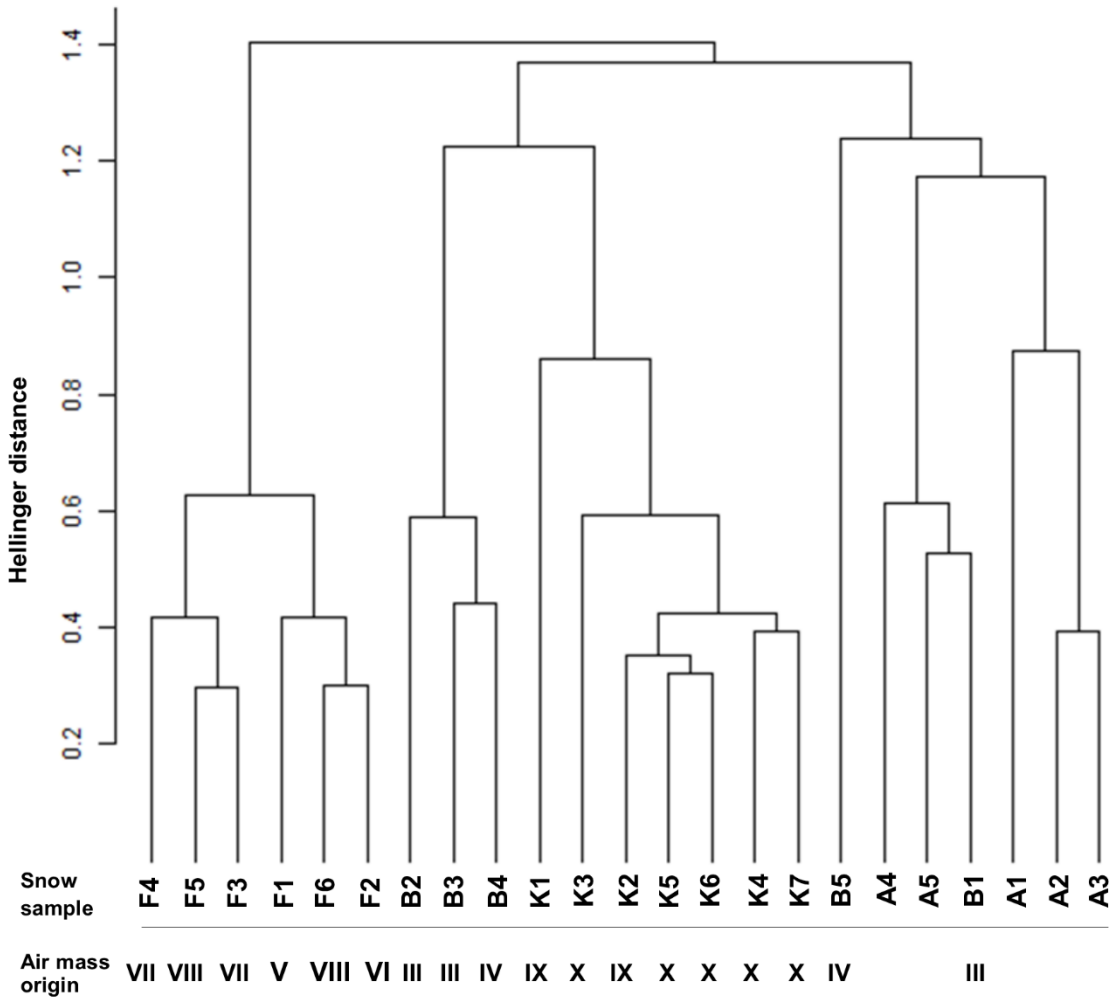

Fig. 4: Dendrogram from the cluster analysis of the structure of bacterial communities in snow samples. A = Ararat, B = Baltoro, F = Forni, K = Khumbu. The Arabic numbers denote different samples collected in the same area. The Roman numbers denote the origin of the air masses according to the back trajectory of the Figure 5.

5.3.3. β Diversity

Snow samples collected in the same area clustered together (Fig. 4). The only exceptions to this general pattern were samples B1 and B5, collected on Baltoro that clustered with samples from Ararat. RDA analysis indicated that structure of bacterial communities significantly differed among areas (Pseudo-F = 11.492; df = 3,19; P = 0.001) confirming the result of the cluster analysis.

A few indicator orders for each area were found, all belonging to phyla Proteobacteria, Bacteroidetes and Firmicutes (Table 2).

5.3.4. Back trajectories and origin of air masses

The back trajectories allowed reconstructing the origin and motion of the air masses involved in the precipitations. The analyses of the snowfall events of the 2013/2014 winter season for the Ararat highlighted two sources of the air masses: seven snowfalls (30 November and 9 December 2013, 14, 23, 31 January, 26 February and 11 March 2014) were brought from a western circulation, with air masses originating from the central-south Europe. The air mass source of the remaining five events (13 and 26 December 2013, 27 and 29 January, 29 March 2014) was the north Sahara, mainly Libya and Egypt (Figure 5). The snow samples collected on Baltoro were deposed in two different snowfalls (1-2 July and 6 July 2013), both originated from a prevailing westerlies circulation, with a probable western Mediterranean source (Figure 5). Snowfalls of 29 January-2 February and 10-15 February 2014 on Forni were driven by a western (Atlantic) circulation pattern whereas those of 4-7 and 18-20 February 2014 originated from the Algerian desert (Figure 5). The Khumbu samples were deposed in two different snowfall events. The one that occurred in 13-16 October 2014 was related to a typical monsoon circulation pattern, with an origin of the air mass in the Indian sub-continent. This event, in particular, was generated from a 4-category Hudhud cyclone that brought huge snowfalls in Nepal area (Wang et al., 2015). The snowfall of 25 October 2014 originated from a westerly's circulation pattern (Figure 5).

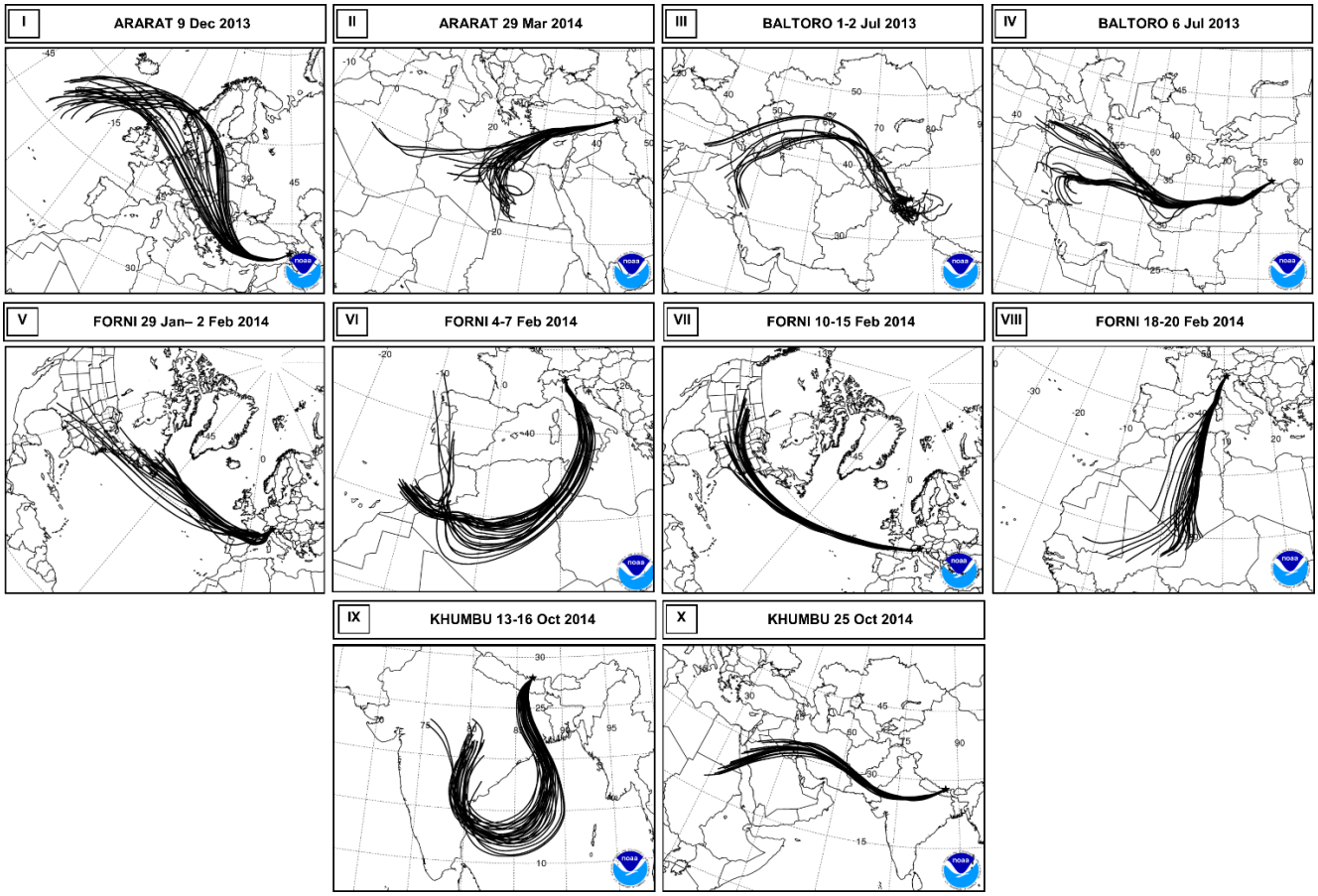

Fig.5: Back trajectories of the principal circulation pattern observed in the four sites during the snowfall sampled. For the Ararat we consider only two typical patterns. In particular, a Western (I) and a Saharan origin (II) of Ararat snowfalls; a Middle-East origin of Baltoro snowfalls (III, IV); Atlantic (VI, VII) and a Saharan origin of Forni snowfalls (V, VII); cyclonic (IX) and westerly circulation (X) of Khumbu snowfalls.

5.4. Discussion

In this study, we investigated the bacterial communities of snow samples collected in four mid-latitude mountain areas (Alps, Anatolia, Karakoram and Himalaya). We identified 341 OTUs, which were mostly affiliated to Burkholderiales (Proteobacteria), Xanthomonadales (Proteobacteria), Cytophagales (Bacteroidetes) and Bacillales (Firmicutes). Bacterial communities were similar to those reported by previous works on snow bacteria: Proteobacteria were very abundant in snow samples collected in Antarctic (Michaud et al. 2014, Lopatina et al. 2016) and Arctic (Haupmann 2014, Cameron et al. 2015), as well as in snow samples collected in high altitude areas in both hemispheres (Wunderlin et

al, 2016). Bacterial community composition in the snow covers around the world is therefore very similar, suggesting that snow cover is a very selecting environment for bacteria, probably because only few groups can survive air transport and permanence in the snow (Liu et al., 2006).

We observed rather small numbers of OTUs and high values (0.83-0.99) of Gini index in all samples. These Gini index values indicate that evenness was comparable to that is found in other environments like e.g. soil (Lawlor et al., 2000; Pankhurst et al., 2001), ocean water (Kirchmann et al., 2010), urban air particulate (Franzetti et al., 2011) and also other glacial and near-glacier environments (Edwards et al., 2011; Franzetti et al., 2016). However, we observed differences in the alpha diversity of samples collected from different areas. Indeed, Khumbu samples presented on average a larger number of OTUs than those from other area, and Ararat samples hosted more OTUs than Forni and Baltoro samples. A similar pattern was observed for community evenness. Admittedly, we have few cues for interpreting these difference in OTU number and community evenness. We can speculate, that Khumbu samples may host larger number of OTUs because the Himalayan range is close to highly polluted areas in the Indian subcontinent, which may enrich atmosphere of particulate matter, including bacteria, even at high altitude areas (Ramanathan et al. 2007). However, Forni is similarly close to the Po plain, which is among the areas in Europe where the highest concentrations of PM are recorded (EEA 2015), but snow samples showed much lower bacterial diversity.

The structure of bacterial communities found in samples from different geographical areas differed significantly to one another, as clearly indicated by both the cluster and the RDA analyses. The only exceptions to this pattern were samples B1 and B5 from Baltoro, which clustered with samples from Ararat. Variation in snow bacterial communities seems therefore due mainly to the area where the snowfall occurred, and local conditions at deposition sites seem to strongly affect snow bacterial communities, probably more than air mass origin. Such local effect could be appreciated on samples from Khumbu valley, where snowfalls originated by an air mass coming from in the Indian sub-continent and those from westerly's circulation pattern clustered together (Figure 4). Similarly, Forni

samples related to the Saharan events and those from western sources showed similar microbial communities (Figure 4). However, on Forni, snow was collected old, thus we cannot exclude that meltwater can have percolated into the snowpack transporting bacteria and homogenizing communities in different snow layers. The same process may have occurred on Ararat. The very few indicator taxa we could identity, which also differed between areas, further indicate the overall rather low diversity of snow bacterial communities and their differences among geographical areas.

However, we cannot totally rule out the hypothesis that the origin of the air mass may contribute to shape snow bacterial communities, at least partly. Indeed, some samples we collected on Baltoro clustered with those from Ararat, and the back trajectories indicated that the air masses that generated snowfalls on Baltoro Glacier originated from the geographical area where the Ararat is located. However, other samples from the same snowfalls clustered apart. We can therefore speculate that the air masses that brought the snowfalls on Baltoro may have retained part of the bacterial community harvested from the area of origin during air mass formation because these air masses moved through areas with persistent anticyclonic patterns that did not favor air mass uplift (Kulshrestha and Kumar, 2014). Indeed, in high-pressure systems, a subsidence (i.e. a movement toward the ground) of the air mass occurs, which, in turn, limits the possibility for the air mass to harvest bacteria and transport them far away. Thus, the air masses that originated the snowfalls on Baltoro were rather isolated from the ground during their movement over rather long geographical distances. This process may also have determined the low bacterial diversity observed in these samples. Moreover, a closer inspection of the bacterial communities obswrved of Forni may also suggest that snow bacterial communities are influenced by the origin of the air masses. In particular, the snow fallen on the Alps on 18-20 February 2014 was investigated also by Meola et al. (2015) from samples collected on Jungfraujoch (Swiss Alps). They also identified the Saharan origin of the air mass that determined the snowfall by mineralogical characterization of dust particles by means of scanning electron microscope and X-ray spectroscopy analyses. They found that the Saharan dust-rich snow presented a dominance of

Proteobacteria and Bacteroidetes (Meola et al., 2015), consistently with what we observed on Forni. This result suggests that air masses can harvest dust and the associated bacteria from the area where they originated, and depose them with precipitation in faraway areas. Indeed, air masses can harvest dust and bacteria from the ground where i) the air is forced to uplift by orography or by warm surface which determine deep dry convection (Parker et al., 2005), and ii) there is a wide availability of mineral aerosols due to the scarcity of vegetation and/or a very low soil humidity (Tourè et al., 2012). After this uplift phase, the particulate and the bacteria are transported over long distances with few changes in their composition (Marsham et al., 2008). Indeed, particulate eventually harvested during air mass movement is usually confined in the lowest layers of the air mass (boundary layer), which can transport it over short distances only (Marsham et al., 2008). Thus, particulate and bacteria harvested during air mass uplift are transported long distance and are deposed mainly by rainfalls or snowfalls (Marsham et al., 2008). It should be noted, however, that snowfall determines also strong deposition of particulate (Davenport & Peters, 1978; Chate & Pranesha, 2004) and therefore bacteria present in the lower boundaries of the atmosphere over the area where it occurs. Thus, bacteria transported over long range can mix with those in the local atmosphere during snowfall.

5.5. Results

Our analyses of the bacterial communities of snow from different high-elevation areas at the mid-latitudes showed that communities were dominated by similar taxa, particularly Proteobacteria, which were reported as dominant also in previous studies on snow from Arctic and Antarctica. However, each area hosted different bacterial communities. This finding upports the hypothesis that structure of snow bacterial communities are mainly driven by bacteria present in the atmosphere over the area where snowfall occurred, with a possible contribution of the bacteria collected during air mass uplift, or, at least, of those taxa that can survive long atmospheric transport. Although the snow samples were collected opportunistically in four different expeditions with different snow conditions, this is the first

comparison between different bacterial communities in different areas with the same method of analyses. We also observed low diversity of snow bacterial communities, probably due to the challenging environment represented by snow.

5.6. Acknowledgements

Authors thank all the components of the three scientific expeditions on Ararat, Baltoro and Khumbu Glaciers. In particular, the Ararat expedition was conducted within the framework of the Central Scientific Committee of the Italian Alpine Club with the participation of Riccardo Avanzinelli, Raffaello Cioni, Daniele Bocchiola, Simone Tommasini, Giulia Enrione, Luigi Vanoni. The Baltoro expedition was funded by the PAPRIKA project (supported by Ev-K2-CNR Association), by the SEED project (funded by the Italian and the Pakistani governments), by the Italian Ministry of Research (PRIN grant 2010AYKTAB to CS), with the participation of Daniele Bernasconi, Luigi Bonetti and Astrid Lambrecht. We also thank Ev-K2-CNR Association for the organization and logistics of the Khumbu and Baltoro expeditions. This study was also funded by DARAS (Department of Regional Affairs, Autonomies and Sport) of the Presidency of the Council of Ministers of the Italian government through the GlacioVAR project. The authors also gratefully acknowledge the NOAA Air Resources Laboratory (ARL) for the provision of the HYSPLIT transport and dispersion model and/or READY website (http://www.ready.noaa.gov) used in this publication.

5.7. References

Amato P., Hennebelle R., Magand O., Sancelme M., Delort A.M., Barbante C., Boutron C. and Ferrari C. (2006): Bacterial characterization of the snowcover at Spitzberg, Svalbard. *FEMS*, 59, 255-264.

Azzoni R.S., Senese A., Zerboni A., Maugeri M., Smiraglia C. and Diolaiuti G.A. (2016): Estimating ice albedo from fine debris cover quantified by a semi-automatic method: the case study of Forni Glacier, Italian Alps. *The Cryosphere,* 10, 665–679.

Borchard D., Gillet F. and Legendre F. (2011): Numerical Ecology with R. Springer, New York.

Benjamini Y. and Yekutieli D. (2001): The control of the false discovery rate in multiple testing under dependency. *Annals of Statistics*, 29, 1165–1188.

Cameron K.A., Hagedorn B., Dieser M., Christner B.C., Choquette K., Sletten R., Crump B. and Kellogg C. (2015): Diversity and potential sources of microbiota associated with snow on western portions of the Greenland Ice Sheet. *Environmental Microbiology*, 17(3), 594-609.

Chate D.M. and Pranesha T.S. (2004): Field studies of scavenging of aerosols by rain events. *Journal of Aerosol Sciences*, 35(6), 695-706.

Chuvochina M.S., Marie D., Chevaillier S., Petit JR., Normand P., Alekhina I.A. and Bulat S.A. (2011): Community variability of bacteria in alpine snow (Mont Blanc) containing saharan dust deposition and their snow colonisation potential. *Microbes Environmental*, 26(3), 234-247.

Citterio M., Diolaiuti G., Smiraglia C., Verza G. and Meraldi E. (2007): Initial results from the automatic weather station (AWS) on the ablation tongue of Forni Glacier (Upper Valtellina, Italy). *Geografia Fisica e Dinamica* Quaternaria, 30, 141-151.

Davenport H.M. and Peters L.K. (1978): Field studies of atmospheric particulate concentration changes during precipitation. *Atmospheric Environment,* 12(5), 997-1008.

De Cáceres M. and Legendre P. (2009): Associations between species and groups of sites: indices and statistical inference. *Ecology*, 90(12), 3566-3574.

De Cáceres M., Legendre P. and Moretti M. (2010): Improving indicator species analysis by combini groups and sites. *Oikos*, 119(10), 1674-1684.

European Environment Agency (EEA) (2015): Air quality in Europe - 2015 report. European Environment Agency, Copenhagen, Denmark, doi: 10.2800/62459.

Edwards A., Anesio A.M., Rassner S.M., Sattler B., Hubbard B., Perkins W.T. Young M. and Griffith G.W. (2011): Possible interactions between bacterial diversity, microbial activity and supraglacial hydrology of cryoconite holes in Svalbard. *The ISME Journal*, 5(1), 150–160.

Fierer N., Liu Z., Rodríguez-Hernández M., Knight R., Henn M. and Hernandez M.T. (2008): Short-term temporal variability in airborne bacterial and fungal populations. *Applied and Environmental Microbiology*, 74, 200-207.

Franzetti A., Gandolfi I., Gaspari E., Ambrosini R. and Bestetti G. (2011): Seasonal variability of bacteria in fine and coarse urban air particulate matter. *Applied Microbiology Biotechnology*, 90, 745-753.

Franzetti A., Navarra F., Tagliaferri I., Bestetti G., Minora U., Azzoni R.S., Diolaiuti G., Smiraglia C. and Ambrosini R. (2016): Temporal variability of bacterial communities in cryoconite on an Alpine glacier. *Environmental Microbiology Reports*.

Gneiting T. and Raftery A.E. (2005): Weather Forecasting with Ensemble Methods. *Science*, 310(5746), 248-249.

Gou H., Lu J., Li S., Tong Y., Xie C. and Zheng X (2016): Assessment of microbial communities in PM 1 and PM 10 of Urumqui during winter. *Environmental Pollution*, 214, 202-210.

Griffin D.W., Westphal D.L. and Gray M.A. (2006): Airborne microorganisms in the African desert dust corridor over the mid-Atlantic ridge, Ocean Drilling Program, Leg 209. *Aerobiologia*, 22, 211-226.

Griffin D.W., Gray M.A., Borden T.C. and Shinn E.A. (2007a): Airborne desert dust and aeromicrobiology over the Turkish Mediterranean coastline. *Atmospheric Environmental*, 41(19), 4050–4062.

Groisman P.Y. and Davies T. (2001): Snow cover and the Climate system. In Snow Ecology, Jones HG, Pomeroy JW, Walker DA, Hoham R. (eds); Cambridge University Press: Cambridge, UK.

Harding T., Jungblut A.D., Lovejoy C. and Vincent W.F. (2011): Microbes in High Arctic snow and implications for the cold biosphere. *Applied Environmental Microbiology*, 77, 3234–3243.

Hell K., Edwards A., Zarsky J., Podmirseg S.M., Girdwood S., Pachebat J.A., Insam H. and Sattler B. (2013): The dynamic bacterial communities of a melting High Arctic glacier snowpack. *The ISME Journal*, 7, 1814-1826.

Hauptman A.L., Stibal J., Bælum,J., Sicheritz-Pontén, T., Søren, B., Bowman, J.S., Hansen, L.H., Jacobsen C.S. and Blom N. (2014): Bacterial diversity in snow on North Pole ice floes. *Extremophiles*, 18, 945-951.

Jones H.G. (1999): The ecology of snow-covered systems: a brief overview of nutrient cycling and life in the cold. *Hydrological Processes*, 13, 2135-2147.

Kirchmann D.L., Cottrell M.T. and Lovejoy C., (2010): The structure of bacterial communities in the western Arctic Ocean as revealed by pyrosequencing of 16S rRNA genes. *Environmental Microbiology*, 12(5), 1132-1143.

Kulshrestha U. and Kumar B. (2014): Air mass trajectories and long range transport of pollutants: Review of wet deposition scenario in South Asia. Advances in Meteorology, ID596041, 14p.

Lawlor K., Knight B.P., Barbosa-Jefferson V.L., Lane P.W., Lilley A.K., Paton G.I., McGrath S.P., O'Flaherty S.M. and Hirsch P.R. (2000): Comparison of methods to investigate microbial populations in soils under different agricultural management. *FEMS,* 33,129-137.

Lazzaro A., Wismer A., Scheenbeli M., Erny I. and Zeyer J. (2014): Microbial abundance and community structure in a melting alpine snowpack. *Extremophiles,* 19, 613-642.

Legendre P. and Legendre L. (1998): Numerical ecology. Elsevier, Amsterdam.

Liu Y., Yao T., Kang S., Jiao N. and Zeng Y.H. (2006): Seasonal variation of snow microbial community structure in the East Rogbuk Glacier, Mt. Everest. *Chinese Science Bulletin*, 51, 1476–1486.

Liu Y., Yao T., Jiao N., Kang S. and Xu B. (2009): Bacterial diversity in the snow over Tibetan Plateau Glaciers. *Extremophiles*, 13,411–423.

Lopatina A., Medvedeva S., Shmakov S., Logacheva M.D., Krylenkov V. and Severinov K. (2016): Metagenomic Analysis of Bacterial Communities of Antarctic Surface Snow. *Frontiers in Microbiology*, 7, 398.

Marsham J.H., Parker D.J., Grams C.M., Johnson B.T., Grey W.M.F. and Rossi A.N. (2008): Observations of mesoscale and boundary-layer scale circulations affecting dust transport and uplift over the Sahara. *Atmospheric Chemistry and. Physics*, 8, 6979-6993.

Michaud L., Lo Giudice A., Mysara M., Monsieurs P., Raffa C., Leys N., Amalfitano S. and Van Houdt R. (2014): Snow Surface Microbiome on the High Antarctic Plateau (DOME C). *PLOS One*, 9(8), 1-12.

Miteva V. (2007): Bacteria in snow and glacier ice. In Margesin, R., Schinner, F., and Marx, J.-C. (eds.), Psychrophiles: from Biodiversity to Biotechnology. Berlin: Springer, pp. 31–50.

Meola M., Lazzaro A. and Zeyer J. (2015): Bacterial composition and survival on Sahara dust particles transported to the European Alps. *Frontiers in Microbiology*, 6 (1454), 1-17.

Møller A.K., Søborg D.A., Al-Soud W.A., Sørensen S.J. and Kroer N. (2013): Bacterial community structure in High-Arctic snow and freshwater as revealed by pyrosequencing of 16S rRNA genes and cultivation. *Polar Research*, 32, 17390.

Oh H., Ho C., Kim J., Chen D., Lee S., Choi Y., Chang L. and Song C. (2015): Long-range transport of air pollutants originating in China : A possible major cause of multi-day high-PM 10 episodes during cold season in Seoul, Korea. A*tmospheric Environment*, 109, 23–30.

Oksanen J.F., Blanchet G., Kindt R., Legendre P., Minchin P.R., O'Hara R.B., Simpson G.L., Solymos P., Stevens M.H.H. and Wagner H. (2016): Vegan: Community Ecology Package. R package version 2.3-5. https://CRAN.R-project.org/package=vegan

Pankhurst C.E., Yu S., Hawke B.G. and Harch B.D. (2001): Capacity of fatty acid profiles and substrate utilization patterns to describe differences in soil microbial communities associated with increased salinity or alkalinity at three locations in South Australia. *Biology and Fertility of Soils*, 33, 204–217.

Parker D.J., Thorncroft C.D., Buron R.R. and Diongue-Niang A. (2005): Analysis of the African easterly jet, using aircraft observations from the JET2000 experiment. Q*uarterly Journal of the Royal Meteorological Society*, 131, 1461–1482.

Pollard K.S., Dudoit S. and Van Der Laan M.J. (2005): multiple testing procedures: R multtest Package and applications to Genomics, in Bioinformatics and Computational Biology solutions using R and Bioconductor in "Gentleman, R., Carey, V., Huber, W., Irizarry, R. and Dudoit (Editors). Springer (Statistics for Biology and Health Series), pp. 251-272.

Ramanathan V., Ramana M.V, Roberts G., Kim D., Corrigan C., Chung C. and Winker D. (2007): Warming trends in Asia amplified by brown cloud solar absorption. *Nature*, 448, 575–8

R Core Team (2015): R: A language and environment for statistical computing. R Foundation for Statistical Computing, Vienna, Austria. URL http://www.R-project.org/.

Segawa T., Miyamoto K., Ushida K., Agata K., Okada N. and Kohshima S. (2005): Seasonal change in bacterial flora and biomass in mountain snow from the Tateyama Mountains, Japan, analyzed by 16S rRNA gene sequencing and real-time PCR. *Applued Environmental Microbiology*, 71(1), 123-130

Senese A, Diolaiuti G, Mihalcea C. and Smiraglia C. (2012): Energy and mass balance of Forni Glacier (Stelvio National Park, Italian Alps) from a four-year meteorological data record. *Arctic, Antarctic, and Alpine Research*, 44(1), 122–134.

Shahgedanova M., Kutuzov S., White K.H. and Nosenko G. (2013): Using the significant dust deposition event on the glaciers of Mt. Elbrus, Caucasus Mountains, Russia on 5 May 2009 to develop a method for dating and "provenancing" of desert dust events recorded in snowpack. *Atmospheric Chemistry and Physics*, 13, 1797-1808.

Singh V.P., Singh P. and Harutashya UK eds. (2011): Encyclopedia of Snow, Ice and Glaciers. Springer (Netherlands) publication, 1253 pp.

Smith D.J., Timonen H.J., Jaffe D.A., Griffin D.W., Birmele M.N., Perry K.D., Ward P.D. amd Roberts M.S. (2013): Intercontinental Dispersal of Bacteria and Archaea by Transpacific Winds. *Applied Environmental Microbial*, 79(4), 1134–1139.

Stein A.F., Draxler R.R, Rolph G.D., Stunder B.J.B., Cohen M.D., and Ngan F., (2015): NOAA's HYSPLIT atmospheric transport and dispersion modeling system. *Bulletin of American Meteorological Society*, 96, 2059-2077.

Tourè N.E, Konaré A. and Silué S. (2012): Intercontinental Transport and Climatic Impact of Saharan and Sahelian Dust. Adv. Meteorol. 157020, 14pp.

Wang Q., Garrity G.M., Tiedje J.M. and Cole J.R. (2007): Naive Bayesian classifier for rapid assignment of rRNA sequences into the new bacterial taxonomy. *Applied and Environmental Microbiology,* 73(16), 5261-5267.

Wang S.Y., Gillies R., Fosu B. and Singh P.M. (2015): The deadly Himalayan snowstorm of October 2014: synoptic conditions and associated trends. *Bullettin of the American Meteorological Society*, 96(12), S89-S94.

Wittebolle L., Marzorati M., Clement L., Balloi A., Daffonchio D. and Heylen K. (2009): Initial community evenness favours functionality under selective stress. *Nature,* 458, 623–626.

Wunderlin T., Ferrari B. and Power M. (2016): Global and local-scale variation in bacterial community structure of snow from the Swiss and Australian Alps. *FEMS microbiology*, 92.

Chapter 6

Potential sources of bacteria colonizing the cryoconite of an Alpine glacier

Chapter submitted to Plos One

Franzetti A., Navarra F., Tagliaferri I., Gandolfi I., Bestetti G., Minora U., Azzoni R.S., Diolaiuti G., Smiraglia C. and Ambrosini R. - Potential sources of bacteria colonizing the cryoconite of an Alpine glacier. Submitted to PlosOne.

Abstract

We investigated the potential contribution of ice-marginal environments to the microbial communities of cryoconite holes, small depressions filled with meltwater that form on the surface of Forni Glacier (Italian Alps).

Cryoconite holes are considered the most biologically active environments on glaciers. Bacteria can colonize these environments by short-range transport from ice-marginal environments or by long-range transport from distant areas. We used high throughput DNA sequencing to identify Operational Taxonomic Units (OTUs) present in cryoconite holes and three ice-marginal environments, the moraines, the proglacial plain, and a large (> 3 m high) ice cored dirt cone. Bacterial communities of cryoconite holes were different from those of ice-marginal environments and hosted fewer OTUs. However, a network analysis revealed that the cryoconite holes shared more OTUs with the moraines and the dirt cone than with the proglacial plain. Ice-marginal environments may therefore act as sources o f bacteria for cryoconite holes, but differences in environmental conditions limit the number of bacterial strains that may survive in them. At the same time, cryoconite holes host a few OTUs that were not found in any ice- marginal environment we sampled, thus suggesting that some bacteria may reach cryoconite from distant sources.

6.1. Introduction

Glaciers and ice sheets represent the largest part of the cryosphere on the continents (Anesio and Laybourn-Parry, 2012; Laybourn-Parry et al., 2012) and include most of the Earth's freshwater. Cryoconite holes are small depressions on glacier surfaces filled with water, whose formation is due to tiny supraglacial debris (cryoconite). The dark cryoconite melts the underlying ice when heated by solar radiation (Wharton et al., 1985) and forms a depression the can be filled by meltwater. Cryoconite holes can cover up to 10% of the ablation zone of glaciers (Anesio and Laybourn-Parry, 2012) and are considered the most biologically active environments on the glaciers due to their high metabolic versatility (Franzetti et al., 2016). In addition, recent studies demonstrated that microbial growth in cryoconite significantly reduces the albedo, thus increasing glacier melting rate (Bagshaw et al., 2016). Finally, cryoconite holes of mountain glaciers are connected by superficial and sub-superficial water flows (MacDonell and Fitzsimons, 2008). This affects the spatial pattern of community diversity among the holes (Franzetti and others, submitted) and may have impacts on the functionality and chemistry of down-valley ecosystems (Segawa et al., 2014).

Diversity, functions and assembly processes of microbial communities in cryoconite have been investigated both on Arctic and Antarctic glaciers (Christner et al., 2003; Edwards, Douglas, et al., 2013; Foreman et al., 2007; Zarsky et al., 2013) and on temperate mountain glaciers (Edwards et al., 2014; Edwards, Pachebat, et al., 2013; Hamilton et al., 2013; Margesin, 2003; Margesin et al., 2002, 2012; Segawa et al., 2014; Takeuchi et al., 2010; Telling et al., 2010). These studies highlighted that, on three High-Arctic glaciers, cryoconite and ice-marginal environments host distinct communities, and only a minority of bacterial phylotypes occurred in both environments (Edwards, Rassner, et al., 2013). However, cryoconite holes on Arctic glaciers show large difference from those on mountain glaciers. Indeed, on Arctic glaciers, they are remarkably stable features of glacier surface, and can persist up to decades (Irvine-Fynn et al., 2011). In

contrast, on mountain glaciers, they are ephemeral features of ice surface (Franzetti and others, submitted). Ecological processes shaping microbial assemblies in cryoconite holes of mountain glaciers may therefore largely differ from those observed on Arctic glaciers.

In this study, we aimed at assessing the potential sources of bacteria found in the cryoconite by investigating the similarities and the differences in bacterial community composition between cryoconite holes and ice-marginal environments, a topic that has been poorly addressed in temperate glaciers (Segawa et al., 2014). To this end, we collected debris samples from lateral and supraglacial moraines, from a large (about 30 m wide and > 3 m high) ice cored 'dirt cone', which occurred close to the cryoconite hole area, and from the proglacial plain, which was at about 1 km from the area where we sampled the cryoconite holes.

6.2. Materials and Methods

6.2.1. Study area, field methods, and environmental data

Forni Glacier (46°12'30'' N, 10°13'50'' E; Figure 1) is one of the largest Italian valley glaciers. It covers an area of 11.34 km^2 and ranges in elevation between 2501 and 3673 m a.s.l. (Smiraglia et al., 2015). The ablation season spans from early July to late September on this glacier (Senese et al., 2012), and mean monthly temperatures are above 0 °C during all three months. Katabatic winds blowing from SE dominate air circulation on the glacier, but winds flowing up-valley also occur (Senese et al., 2012). During July-October 2013, we collected 60 samples of cryoconite from cryoconite holes and 23 samples from surrounding and supraglacial moraines, the proglacial plain and the dirt cone. Twenty cryoconite samples werecollected during each of three visits to the glaciers conducted on 10 July, 28 August, and 25 September 2013. In addition, on 10 July, 28 August, 25 September and 4 October, 23 samples were aseptically collected from lateral and supraglacial moraines (7 samples), the proglacial plain (10 samples) and the dirt cone (6 samples). One

sample of 2-5 g of cryoconite and of 30-50 g of sediment was aseptically collected from each hole or sampling location in 50 ml Falcon™ tubes by laboratory spoons and kept at 4 °C during transport to the laboratory, which occurred within 8 hours. For each sampling site, the UTM coordinates were assessed through a GPS receiver (Garmin eTrex Vista HCz, Schaffhausen, Switzerland).

Data from cryoconite holes have been used in a previous paper (Franzetti and others, submitted). However, the present paper uses different pieces of information than the previous one. Indeed, a) it considers only presence or absence of OTUs and not their relative abundance; b) it does not consider environmental features of holes; c) it does not investigate temporal or spatial variability of bacterial communities in the holes. In addition, data on bacterial communities in ice-marginal environments are very new. This paper therefore presents new and original results on the assembly processes shaping bacterial communities in cryoconite holes on Forni Glacier.

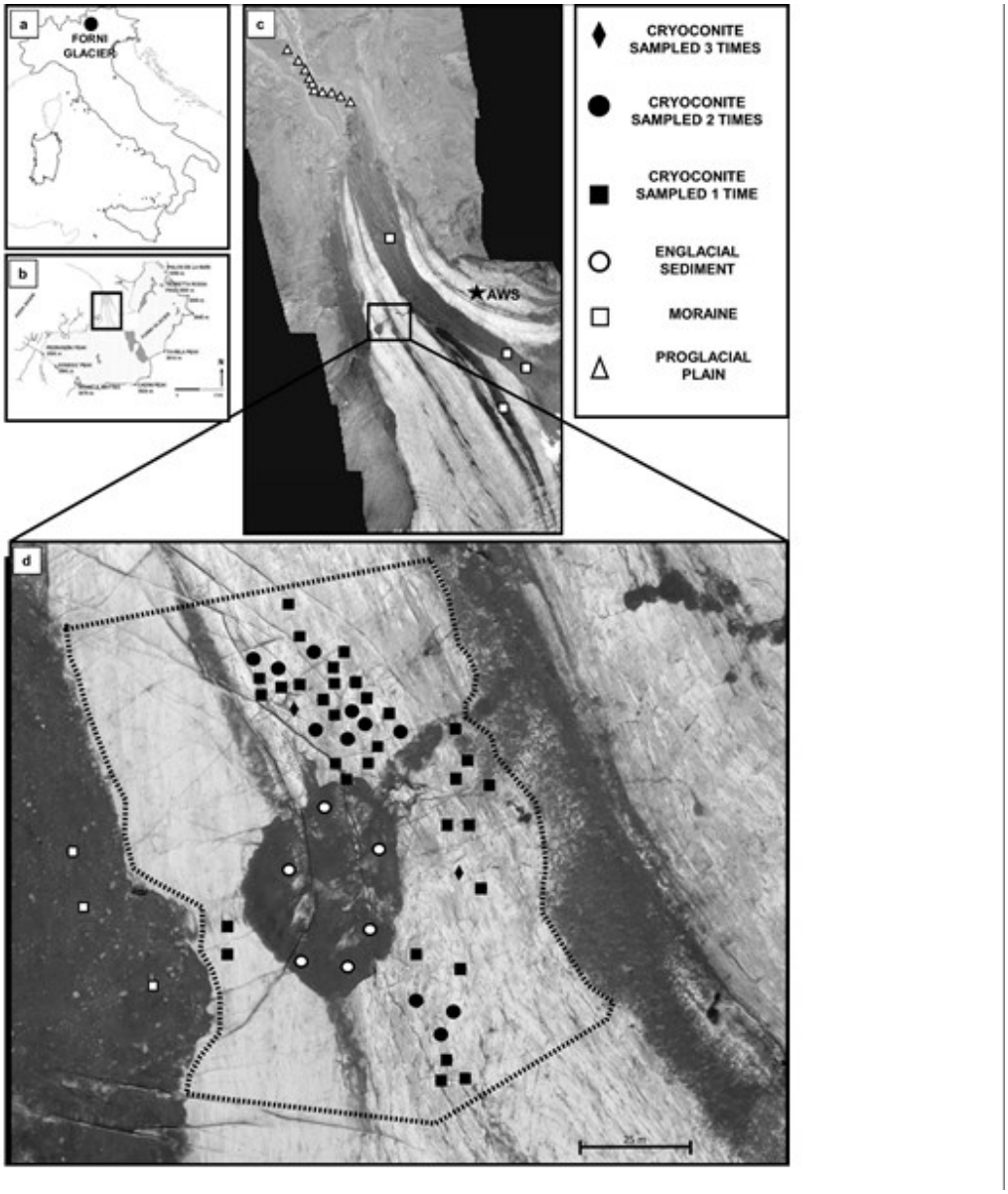

Fig. 6: a) Position of the Forni Glacier in Italy; b) map of the Forni Glacier. The box highlights the glacier tongue; c) composite aerial photograph of the tongue of the Forni glacier with the proglacial plain. White symbols indicate the position where we collected samples on the supraglacial moraine and on the proglacial plain; d) aerial photograph of the study area. Position of each cryoconite hole is shown. Different symbols denote holes with overlapping positions sampled at different months. The dashed line delimits the study area. White symbols indicate the position of samples collected on the lateral moraine and on the dirt cone.

6.2.2. 16S rRNA gene fragment sequencing, sequence processing and data analysis

Total bacterial DNA was extracted from 0.7 g of cryoconite using the FastDNA Spin for Soil kit (MP Biomedicals, Solon, OH) according to the manufacturer's instructions, and quality of extracted

DNA was evaluated electrophorectically. The V5-V6 hypervariable regions of the 16S rRNA gene were PCR-amplified using 783F and 1046R primers (Huber et al., 2007; Wang and Qian, 2009) and sequenced by MiSeq Illumina (Illumina, Inc., San Diego, CA) with a 250 bp × 2 paired-end protocol. The multiplexed libraries were prepared using a dual PCR amplification protocol. The first PCR was performed in 3 × 75 μL volume reactions with GoTaq® Green Master Mix (Promega Corporation, Madison, WI) and 1 μM of each primer and the cycling conditions were: initial denaturation at 98 °C for 30 s; 20 cycles at 98 °C for 10 s, 47 °C for 30 s, and 72 °C for 5 s and a final extension at 72 °C for 2 min. The second PCR was performed in 3 × 50 μL volume reactions by using 23 μL of the purified amplicons (Wizard® SV Gel and PCR Clean-up System, Promega Corporation, Madison, WI) from the first step as template and 0.2 μM of each primer. Primers contained regions complementary to the Illumina adapters and standard Nextera indexes (Illumina, Inc., San Diego, CA). The cycling conditions were: initial denaturation at 98 °C for 30 s; 15 cycles at 98 °C for 10 s, 62 °C for 30 s, and 72 °C for 6 s and a final extension at 72 °C for 2 min. After the amplification, DNA quality was evaluated spectrophotometrically and DNA was quantified using Qubit® (Life Technologies, Carlsbad, CA). The DNA extraction and amplification protocol was run also on negative controls and they did not result in any PCR amplification. The sequencing was carried out at Parco Tecnologico Padano (Lodi, Italy).

Forward and reverse reads were merged with perfect overlapping and quality filtered with default parameters using Uparse pipeline (Edgar, 2013). Suspected chimeras and singletons sequences (i.e. sequences appearing only once in the whole data set) were removed. OTUs were defined on the whole data set by clustering the sequences at > 97% of similarity and defining a representative sequence for each cluster. The taxonomic classification of the OTU representative sequences was inferred with RDP classifier (Wang et al., 2007).

6.2.3. Statistical methods

6.2.3.1. ***Alpha-diversity***

The number of sequences at each sample varied from 2,203 to 126,734. To compare number of OTUs among samples that largely differed in the number of sequences, 2000 reads were randomly selected from all libraries and used to calculate number of OTUs at each sample. A Generalized Linear Model (GLM) assuming a Poisson error distribution, corrected for overdispersion, was used to compare the number of OTUs, which was considered an index of alpha diversity, in cryoconite and in the ice-marginal environments.

6.2.3.2. ***Beta-diversity***

In order to give similar coverage to each sample while not discarding a large number of sequences from most samples, we randomly extracted 10,000 samples from the 74 samples with a number of sequences larger than 10,000, and assessed presence or absence of each OTU on this sample of 10,000 sequences. For the remaining nine samples, presence or absence of each OTU was assessed on the original sample.

OTUs found in one sample only (singletons) were removed because they may inflate variance explained by models (Legendre and Legendre, 1998).

We aimed at comparing the presence or absence of OTUs among cryoconite and ice-marginal environments (beta diversity). Indeed, we reasoned that the ice-marginal environments that are sources of bacteria found in cryoconite holes should share the same OTUs with cryoconite, but OTU relative abundance may differ between the two environments due to different ecological conditions. Hereafter we will refer to presence or absence of OTUs as the "composition" of a bacterial community.

This analysis was performed by Constrained Canonical Analysis (CCA) on presence or absence of OTUs (Borcard et al., 2011; Legendre and Legendre, 1998). The environment (i.e. cryoconite, moraine, dirt cone, or proglacial plain) was entered as a four-level factor. CCA was followed by post-hoc pairwise comparisons between bacterial communities at cryoconite holes on the one side, and those at each of the ice-marginal environments on the other. The rationale behind this procedure was that we were interested only in comparing bacterial community composition of cryoconite holes with those of each of the ice-marginal environments that may act as source of bacteria for them, and not in comparing composition of bacterial communities found in the different ice-marginal environments. Significance of these tests was adjusted according to the False Discovery Rate (FDR) procedure of Benjamini and Yekutiely (Benjamini & Yekutieli, 2001). We also checked whether significant differences detected by CCA arose because of within-habitat variation in the composition of bacterial communities (Hartmann et al., 2012) by performing an analysis of homogeneity of OTU composition among environments (Legendre and Andersson, 1999) with the function *betadisper* implemented in the VEGAN package (Oksanen et al., 2015) of R. This test is a multivariate analogue of Levene's test for homogeneity of variance. Large dispersion within a habitat indicates that that habitat hosts heterogeneous bacterial communities.

6.2.3.3. ***Dispersal of bacteria between ice-marginal environments and cryoconite***

We aimed at investigating potential dispersal of bacteria between ice-marginal environments and cryoconite. As the library sizes and the number of samples differed among environments, we first investigated rarefaction curves generated with the rarecurve function in VEGAN by pooling all sequences for each environment. Rarefaction curves showed that a subsample of 50000 sequences from each environment should give equal and good OTU coverage. We therefore randomly extracted 50000 sequences from those obtained after pooling all sequence obtained from all samples collected at

each environment, and assessed presence or absence of OTUs at each environment based on these samples of sequences.

We then performed two different analyses. First, we estimated the likelihood of dispersal of OTUs between each of the near-glacier environments and cryoconite holes by calculating the coefficient of dispersal direction (DD), (Legendre and Legendre, 2012) by the *bgdispersal* function implemented in VEGAN.

Second, we conducted an indicator species analysis to identify taxon-habitat association patterns. This analysis was used to identify not only OTUs associated to one habitat, but also OTUs associated with two or three habitats ("indicator OTUs" hereafter). This analysis was done with the *multipatt* function (with 99,999 permutations) implemented in the INDICSPECIES package of R (De Cáceres et al., 2010). This procedure returns an IndVal statistics that is a measure of the strength of the association between an OTU and a habitat (or a combination of habitats) with larger numbers indicating stronger association. Also in this case, we accounted for multiple testing by correcting P-value according to the FDR procedure. Indicator OTUs with a $P_{FDR} < 0.05$ were considered significantly associated to a habitat or a combination of habitats. Indicator taxa were then represented in a network by using the IGRAPH package of R, where habitats were connected by their indicator OTUs (see Rime, Hartmann and Frey 2016 for a similar approach). Our investigation focused on cryoconite. In order to simplify network representation, we considered only OTUs associated either with single environments or OTUs associated to cryoconite and one or two ice- marginal environments (i.e. we represented e.g. bacteria associated to the moraine or those associated to both the moraine and the cryoconite, but not those associated to both the moraine and the englacial sediment, but not to the cryoconite).

We stress that all our analyses were based on presence or absence of bacteria because we were looking for potential sources of bacteria for the cryoconite, not for (obvious) difference in the

structure of bacterial communities between cryoconite holes and near-glacier environments, which may be due to very different ecological conditions.

All analyses were performed with R 3.1.2 (R Core Team, 2013).

6.3. Results

6.3.1. Alpha-diversity

Number of OTUs obtained from the 2000 sequences randomly extracted per sample differed significantly among environments ($F_{3,79} = 9.691$, $P < 0.001$), being significantly lower in cryoconite holes than in ice-marginal environments, as assessed by post-hoc tests (Figure 2a).

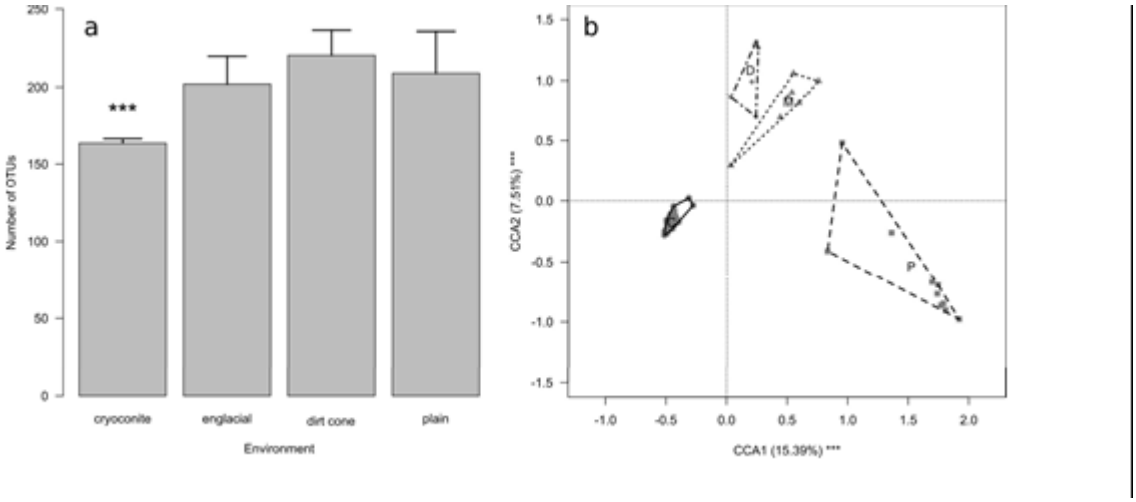

Fig. 2: a) Barplot of the number of OTUs at cryoconite holes and ice-marginal environments. Asterisks denote significant differences at post-hoc tests (* = P < 0.001). b) Biplot of first and second components from CCA of bacterial communities in cryoconite holes, moraines, englacial debris and proglacial plain. Each symbol represents the bacterial community in one sample. Different symbols represent different environments and polygons include samples at each environment (cryoconite holes = dots and solid line, moraines = triangles and dotted line, dirt cone = diamonds and dashed-dotted line, proglacial plain = squares and dashed line,). Letters denote the centroid of bacterial communities at each environment (C = cryoconite holes, D = dirt cone, M = moraines, P = proglacial plain). The amount of variance explained by each axis is shown as well as significance of each axis as assessed by a randomization test (*** = P < 0.001).**

6.3.2. Beta-diversity

We found significant differences in the composition of bacterial communities between cryoconite holes and ice-marginal environments (CCA: $F_{3,79} = 9.301$, $P = 0.001$; Figure 2b). Post-hoc tests also confirmed that composition of bacterial communities of cryoconite holes was different from that of all the other ice-marginal environments ($F_{1,15} \geq 12.638$, $P_{FDR} \leq 0.001$ in all cases). Indeed, among the 695 OTUs that occurred in the cryoconite, only 67 (14.8%) were not found in the other environments, while 674 of the 1302 (51.8%) OTUs found in any of the three ice-marginal environments we sampled were not found in the cryoconite holes (Figure 3).

OTU heterogeneity within environments differed among environments ($F_{3,79} = 98.181$, $P < 0.001$). In particular, dispersion was lower in the cryoconite holes than in the other ice-marginal environments (Figure 2b).

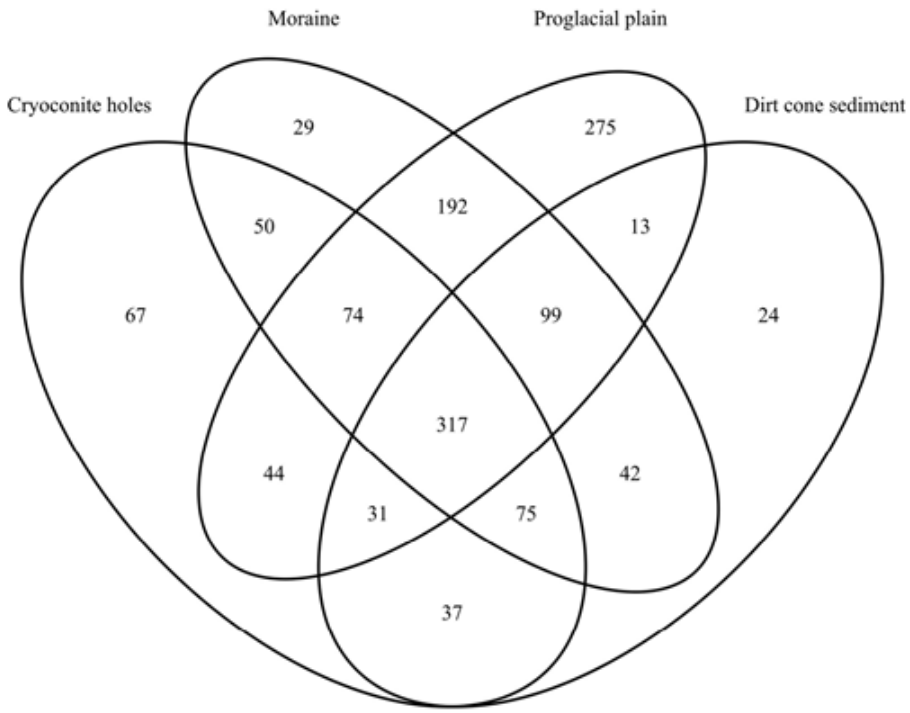

Fig. 3: Venn diagram showing the number of OTUs shared by cryoconite holes and ice- marginal environments.

6.3.3. Dispersal

DD coefficients indicated that dispersal should have occurred from all the near glacier environments towards the cryoconite holes (McNemar $\chi^2 \geq 60.06$, $P < 0.001$ in all cases, Figure 4).

The indicator taxa analysis identified 219 OTUs significantly associated to one environment or to a combination of environments that included the cryoconite. The network analysis revealed some patterns of association among OTUs and environments. Particularly, the cryoconite holes were the environment with the lowest number of indicator OTUs. Indeed, only six OTUs were significantly associated to the cryoconite holes, while a much larger number of OTUs (63) was associated to a combination of environments including the cryoconite holes (Figure 5). Importantly, the number of OTUs significantly associated to both the cryoconite holes, the dirt cone and the moraine (43) was larger than the number of OTUs significantly associated to each of these environments alone. In contrast, no OTU was significantly associated to both the cryoconite and the proglacial plain. In addition, OTUs belonging to cyanobacteria were associated to the cryoconite only, or to a combination of the cryoconite, the dirt cone, and the moraine, but not to the proglacial plain.

Finally, 74 OTUs were significantly associated to both the dirt cone and the moraine, 51 to both the moraine and the englacial plain, and 51 to all these three habitats, but not to the cryoconite (these OTUs were not reported in Figure 5). No OTU was significantly associated to both the dirt cone and the proglacial plain.

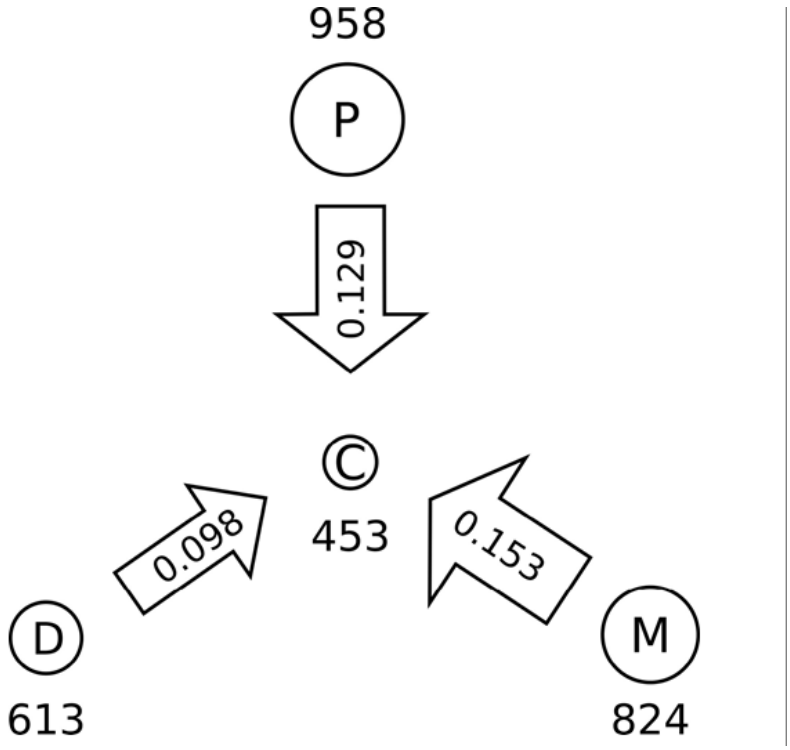

Fig. 4: Schematic representation of dispersal processes between the ice-marginal environments and the cryoconite holes. Circles represent each environment (C = cryoconite holes, D = dirt cone, M = moraines, P = proglacial plain). Circle size is proportional to the number of OTUs at each environments (numbers near circles). Arrows represents dispersal directions as indicated by the sign of the dispersal direction (DD) coefficient and their size is proportion to the DD coefficient (numbers within arrows).

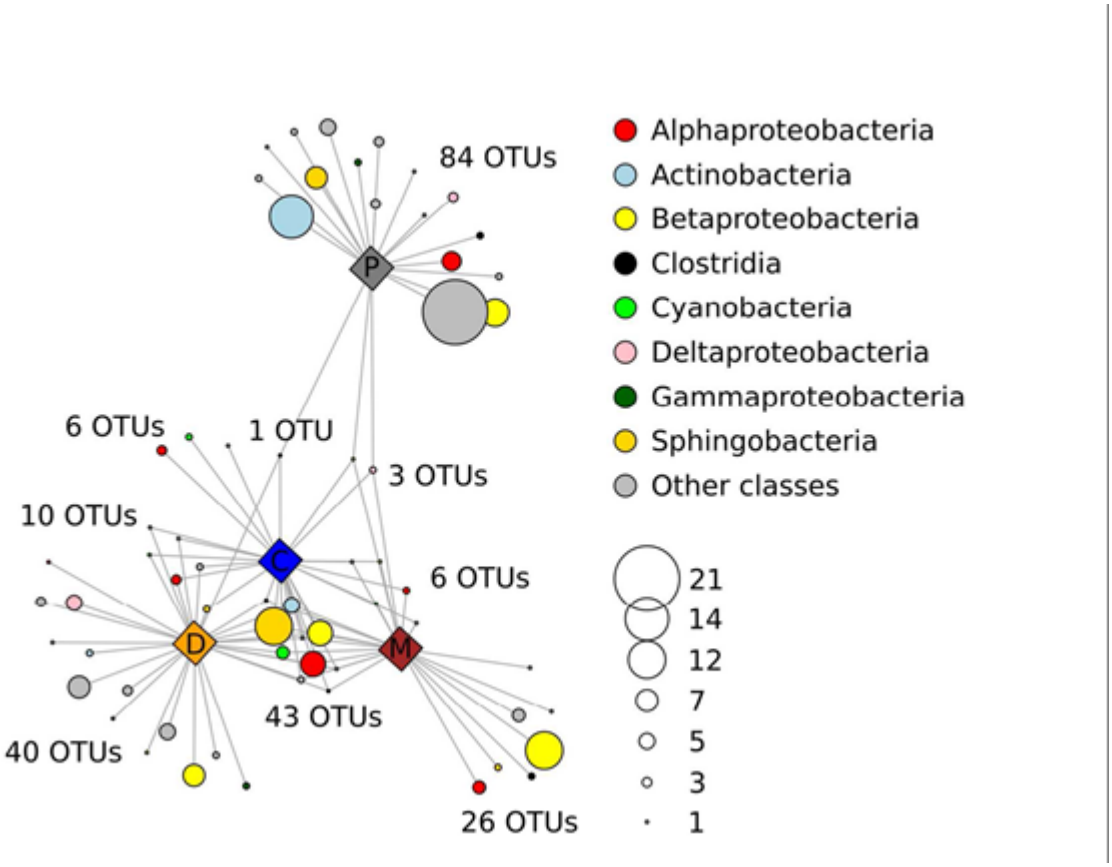

Fig. 5: Association networks showing significant (PFDR < 0.05) associations between indicator OTUs and specific habitats (diamonds; C = cryoconite holes, D = dirt cone, M = moraines, P = proglacial plain), or groups of habitats. OTUs (circles) were grouped according to classes. The most abundant classes are shown with different colours and circle size indicates the number of OTUs of each class (see legend in the graph). OTUs were connected to the environments to which they were significantly associated according to the Indicator Species analysis. In order to simplify the network, only OTUs associated to single habitats or to groups of habitats including the cryoconite were represented.

6.4. Discussion

In this study, we compared OTU composition of bacterial communities found in the cryoconite holes on the Forni Glacier in different months within the same ablation season and in three ice-marginal environments that may act as sources of bacteria found in the cryoconite. We observed large differences in the composition of microbial communities between cryoconite holes and all the ice-marginal environments we sampled (Figures 3b). In addition, the cryoconite holes hosted a lower number of OTUs than these ice-marginal environments (Figure 3a).

The Hellinger distances among communities in cryoconite holes were also on average lower than those among communities in the other ice-marginal environments, as indicated by the significantly lower dispersion (Figure 3b). This indicated that communities in cryoconite holes were significantly more homogeneous than those at the other environments. Hence, not only alpha-diversity, but also beta-diversity was lower in cryoconite than in the other ice- marginal environments we investigated. These findings are in agreement with the results of previous studies on both mountain (Segawa et al., 2014) and arctic glaciers (Edwards, Rassner, et al., 2013), which showed that microbial communities in ice-marginal habitats significantly differed from those in cryoconite holes. In details, bacterial communities of ice- marginal environments showed higher biodiversity than those in cryoconite holes, suggesting that glacier surface is a more selective environment. Indeed, more than 60% of OTUs in ice- marginal samples were not present in cryoconite (Figure 3).

Importantly, cryoconite holes showed a lower alpha- and beta-diversity, despite they were studied in larger details than the other environments. Indeed, the number of samples taken from cryoconite holes (60) was larger than the number of samples collected at all the other environments (23). Hence, the difference in sampling effort should have determined, at least, an underestimate of the total alpha- and beta-diversity of ice-marginal environments with respect to that of cryoconite holes. In addition, cryoconite samples were collected in three different months, while samples from ice-marginal environments were collected in only one time point each. However, communities in cryoconite holes were significantly more homogeneous than those of the ice-marginal environments. Hence, also this difference in sampling effort should not have determined, at least, an underestimate of community dispersion in cryoconite holes. Finally, to reduce the possible biases arising from different coverage of environments due to differences in sampling efforts and differences in the number of sequences at each sample, we ran the analyses on a subset of 50,000 sequences randomly chosen from all the sequences from each environment. We were therefore very conservative when running our analyses. Differences in sampling effort among environments should therefore have not affected our conclusions.

We found that dispersal should have occurred from all the ice-marginal environments and the cryoconite. This pattern is consistent with an assembly of bacterial communities in cryoconite due to species sorting (Lindström and Langenheder, 2012). Indeed, without dispersal limitation between ice-marginal environments and glacier surface, the community composition of cryoconite holes is determined by the different environmental conditions between them and ice-marginal environments, which allow recruiting into the community only those taxa that in the cryoconite holes find the conditions to outcompete the other populations. For example, Cyanobacteria are the most abundant taxon in cryoconite holes and among the less abundant ones in ice-marginal environments (Figure S1).

The indicator species analysis and the network analysis indicated that 59 OTUs were significantly associated to a combination of environments including the cryoconite holes, the dirt cone, and the moraines. In contrast, we found that four OTUs only were significantly associated to both the

cryoconite holes and the proglacial plain, while a larger number of OTUs was also associated to either the moraine or the dirt cone sediments (Figure 5). These results suggest that the dirt cone and the moraine sediments were important sources of bacteria for the cryoconite. These ice-marginal environments are very close to the cryoconite holes we sampled (20-150 m), while the proglacial plain is farer (800-1,000 m) and 200 m lower. Despite katabatic winds dominate air circulation on the Forni glacier, periodic winds flowing up-valley are not rare, and may therefore transport sediment and bacteria from the proglacial plane (Azzoni et al., 2016; Senese et al., 2012). However, our results suggest that aeolian transport of sediment that forms the cryoconite, and of the associated bacteria, may occur more easily from surrounding environments than from those down-valley.

Dispersal direction coefficients gave partially different results. Indeed, this analysis suggested that the proglacial plain was the most important source of bacteria for cryoconite holes, and that the dirt cone was the least important one. However, the magnitude of the dispersal coefficient obtained from the dispersal analysis depends on the balance between the number of OTUs present in either environment (Legendre and Legendre, 2012). Hence, the large value of the dispersal coefficient from the proglacial plain may be simply because this environment hosted the largest number of OTUs, and may not indicate that this environment was the source from which bacteria colonize the cryoconite.

In this study, we did not collect snow or dust samples deposed on the glacier surface by long- range air transport. This may have limited our ability to assess the importance of long-range transports in seeding bacterial communities of cryoconite. However, bacteria deposited with air particulate should deposit over all the environments we sampled. This means that OTUs deriving from these sources should be found in both the cryoconite and in the ice-marginal environments we sampled. Consequently, the fact that we neglected these potential sources of bacteria, at least, may have inflated the number of OTUs shared by the cryoconite holes and the ice-marginal environments. Finally, we consider unlikely that snow may provide inocula for the bacterial communities in the cryoconite holes. Indeed, snow samples collected on

Forni Glacier in spring 2014 (i.e. some months after we sampled cryoconite) were dominated by Burkholderiales and Cytophagales and strongly differed from those observed in the cryoconite. Despite bacterial communities in different snowfalls may differ, the same taxa dominated snow samples collected in different areas of the world (Alps, Anatolia, Karakoram and Himalaya) in different years (Tagliaferri and others, in prep.), thus suggesting that bacterial communities in the snow are not an important source of bacteria for cryoconite holes.

In summary, the results reported in the present study indicate that cryoconite holes host different and less diverse bacterial communities than ice-marginal environments. However, taxa are probably recruited from the surrounding environments and the bacterial populations not adapted to this supraglacial habitat are filtered out. Our results therefore supports the hypothesis that the composition of bacterial communities of the cryoconite holes is mainly driven by species sorting processes.

6.5. References

Anesio A.M. and Laybourn-Parry J. (2012): Glaciers and ice sheets as a biome. *Trends in Ecology and Evolution*, 27(4), 219–225.

Azzoni R.S., Senese A., Zerboni A., Maugeri M., Smiraglia C. and Diolaiuti G.A. (2016): Estimating ice albedo from fine debris cover quantified by a semi-automatic method: the case study of Forni Glacier, Italian Alps. *The Cryosphere,* 10(2), 665–679.

Bagshaw E.A., Jemma L.W. and Tranter M. (2016): Experimental evidence that microbial activity lowers the albedo of glaciers. *Geochemical Perspectives Letters,* 106, 116.

Benjamini Y. and Yekutieli D. (2001): The control of the false discovery rate in multiple testing under dependency. *Annals of Statistics,* 29, 1165–1188.

Borcard D., Gillet F. and Legendre F. (2011): Numerical Ecology with R. New York: Springer. Christner BC

Kvitko B.H. and Reeve J.N. (2003): Molecular identification of bacteria and Eukarya inhabiting an Antarctic cryoconite hole. *Extremophiles: life under extreme conditions,* 7(3), 177–183.

De Cáceres M., Legendre P. and Moretti M. (2010): Improving indicator species analysis by combining groups of sites. *Oikos,* 119(10), 1674–1684.

Edgar R.C. (2013): UPARSE: highly accurate OTU sequences from microbial amplicon reads. *Nature Methods,* 10(10), 996–998.

Edwards A., Douglas B., Anesio A.M., Rassner S.M., Irvine-Fynn T.D., Sattler B. and Griffith G.W. (2013): A distinctive fungal community inhabiting cryoconite holes on glaciers in Svalbard. *Fungal Ecology,* 6(2), 168–176.

Edwards A., Pachebat J., Swain M., Hegarty M., Hodson A.J., Irvine-Fynn T.D.L., Rassner S.M, and Sattler B. (2013): A metagenomic snapshot of taxonomic and functional diversity in an alpine glacier cryoconite ecosystem. *Environmental Research Letters,* 8(3), 035003.

Edwards A., Rassner S.M., Anesio A.M., Worgan H.J., Irvine-Fynn T.D., Williams H.W. and Griffith G.W. (2013): Contrasts between the cryoconite and ice-marginal bacterial communities of Svalbard glaciers. *Polar Research*, 32, 19468.

Edwards A., Mur L.A., Girdwood S.E., Anesio A.M., Stibal M., Rassner S.M. and Cameron S.J. (2014): Coupled cryoconite ecosystem structure–function relationships are revealed by comparing bacterial communities in alpine and Arctic glaciers. *FEMS microbiology ecology*, 89(2), 222-237.

Foreman C.M., Sattler B., Mikucki J.A., Porazinska D.L. and Priscu J.C. (2007): Metabolic activity and diversity of cryoconites in the Taylor Valley, Antarctica. *Journal of Geophysical Research: Biogeosciences*, 112(G4), 1-11.

Franzetti A., Tagliaferri I., Gandolfi I., Bestetti G., Minora U., Mayer C., Azzoni R.S., Smiraglia C., Diolaiuti G. and Ambrosini, R. (2016): Light-dependent microbial metabolisms drive carbon fluxes on glacier surfaces. *The ISME journal*, 10, 2984-2988.

Hamilton T.L., Peters J.W., Skidmore M.L. and Boyd E.S. (2013): Molecular evidence for an active endogenous microbiome beneath glacial ice. *The ISME Journal,* 7(7), 1402–1412.

Hartmann M., Howes C.G., VanInsberghe D., Yu H., Bachar D., Christen R. and Mohn W.W. (2012): Significant and persistent impact of timber harvesting on soil microbial communities in Northern coniferous forests. *The ISME Journal*, 6(12), 2199–2218.

Huber J.A., Welch D.B.M., Morrison H.G., Huse S.M., Neal P.R., Butterfield D.A. amd Sogin, M. L (2007) Microbial Population Structures in the Deep Marine Biosphere. *Science,* 318(5847), 97–100.

Irvine-Fynn T.D.L, Bridge J.W. and Hodson A.J. (2011): In situ quantification of supraglacial cryoconite morphodynamics using time-lapse imaging: An example from Svalbard. *Journal of Glaciology,* 57(204), 651–657.

Laybourn-Parry J., Tranter M. and Hodson A. (2012): The ecology of snow and ice environments. Oxford: Oxford University Press.

Legendre P. and Andersson M.J. (1999): Distance-based redundancy analysis: Testing multispecies responses in multifactorial ecological experiments. *Ecological Monographs,* 69(1), 1–24.

Legendre P. and Legendre L. (1998): Numerical ecology. 2nd Englis. Amstrerdam: Elsevier.

Legendre P. and Legendre L. (2012): *Numerical Ecology*. 3rd English. Amsterdam: Elsevier Science B.V.

Lindström E.S. and Langenheder S. (2012): Local and regional factors influencing bacterial community assembly. *Environmental Microbiology Reports,* 4(1), 1–9.

Macdonnel S. and Fitzsimons S. (2008): The formations and hydrological significance of cryoconite holes. *Progress in Physical Geography*, 32, 595-610.

Margesin R. (2003): Pedobacter cryoconitis sp. nov., a facultative psychrophile from alpine glacier cryoconite. *International Journal of Systematic and Evolutionary Microbiology,* 53(5), 1291–1296.

Margesin R., Zacke G. and Schinner F. (2002): Characterization of heterotrophic microorganisms in alpine glacier cryoconite. *Arctic, Antarctic, and Alpine Research,* 34(1), 88–93.

Margesin R., Spröer C., Zhang D.C. and Busse H.J. (2012): Polaromonas glacialis sp. nov. and Polaromonas cryoconiti sp. nov., isolated from alpine glacier cryoconite. *International Journal of Systematic and Evolutionary Microbiology,* 62(11), 2662–2668.

Oksanen J., Blanchet F.G. and Kindt R. (2015): vegan: Community Ecology Package. Available from: http://cran.r-project.org/package=vegan.

R Core Team (2013): R: A Language and Environment for Statistical Computing. Vienna, Austria.

Rime T., Hartmann M. and Frey B. (2016): Potential sources of microbial colonizers in an initial soil ecosystem after retreat of an alpine glacier. *The ISME Journal*, 1–17.

Segawa T., Ishii S., Ohte N., Akiyoshi A., Yamada A., Maruyama F. and Takeuchi N. (2014): The nitrogen cycle in cryoconites: Naturally occurring nitrification-denitrification granules on a glacier. *Environmental Microbiology*, 16(10), 3250–3262.

Senese A., Diolaiuti G., Verza G.P., Meraldi E. and Smiraglia C. (2012): Surface energy budget and melt amount for the years 2009 and 2010 at the Forni Glacier (Italian Alps, Lombardy). *Geografia Fisica e Dinamica Quaternaria,* 35(1), 69–77.

Smiraglia C., Azzoni R.S., D'Agata C., Maragno D., Fugazza D. and Diolaiuti G.A. (2015): The evolution of the Italian glaciers from the previous data base to the New Italian Inventory. Preliminary considerations and results. *Geografia Fisica e Dinamica Quaternaria*, 38(1), 81–94.

Takeuchi N., Nishiyama H. and Li Z. (2010): Structure and formation process of cryoconite granules on Ürümqi glacier No. 1, Tien Shan, China. *Annals of Glaciology,* 51(56), 9–14.

Telling J., Anesio A. M., Hawkings J., Tranter M., Wadham J.L., Hodson A.J. and Yallop M. L. (2010): Measuring rates of gross photosynthesis and net community production in cryoconite holes: A comparison of field methods. *Annals of Glaciology,* 51, 153–162.

Wang Q., Garrity G.M., Tiedje J.M. and Cole J.R. (2007): Naive Bayesian classifier for rapid assignment of rRNA sequences into the new bacterial taxonomy. *Applied and Environmental Microbiology*, 73(16), 5261–5267.

Wang Y. and Qian P.Y. (2009): Conservative fragments in bacterial 16S rRNA genes and primer design for 16S ribosomal DNA amplicons in metagenomic studies. *Plos One,* 4(10), e7401.

Wharton Jr R.A., McKay C.P., Simmons Jr G.M. and Parker B.C. (1985): Cryoconite holes on glaciers. *BioScience*, 499-503.

Zarsky J.D., Stibal M., Hodson A., Sattler B., Schostag M., Hansen L.H. and Psenner R. (2013): Large cryoconite aggregates on a Svalbard glacier support a diverse microbial community including ammonia-oxidizing archaea. *Environmental Research Letters*, 8(3), 035044.

Chapter 7
Temporal variability of bacterial communities in cryoconite on an Alpine glacier

Chapter published on Environmental Microbiology Reports

Franzetti A., Navarra F., Tagliaferri I., Gandolfi I., Bestetti G., Minora U., Azzoni R.S., Diolaiuti G.A., Smiraglia C. and Ambrosini R. (2016) – Temporal variability of bacterial communities in cryoconite on an Alpine glacier. *Environmental Microbiology Reports*, DOI: 10.1111/1758-2229.12499.

Abstract

Cryoconite holes, i.e. small ponds that form on glacier surface, are considered the most biologically active environments on glaciers. Bacterial communities in these environments have been extensively studied, but often through snapshot studies based on the assumption of a general stability of community structure. In this study, we investigated the temporal variation of bacterial communities in cryoconite holes on the Forni Glacier (Italian Alps) by high throughput DNA sequencing. We found a temporal change of bacterial communities, with autotrophic Cyanobacteria populations dominating communities after snowmelt, and heterotrophic Sphingobacteriales populations increasing in abundance later in the season. Bacterial communities also varied according to hole depth and area, amount of organic matter in the cryoconite and oxygen concentration. However, variation in environmental features explained a lower fraction of the variation in bacterial communities than temporal variation. Temporal change along ablation season seems therefore more important than local environmental conditions in shaping bacterial communities of cryoconite of the Forni Glacier. These findings challenge the assumption that bacterial communities of cryoconite holes are stable.

7.1. Introduction

The cryosphere is the portion of Earth where water is frozen either seasonally or permanently, thus including snow, ice and permafrost (van der Veen, 1999; Laybourn-Parry et al., 2012). Although general ecological conditions are extreme in these environments, they host viable and metabolically active microorganisms, and the study of the ecological processes occurring in them intensified in recent years (Boetius et al., 2015).

Cryoconite holes are small depressions on glacier surfaces that are filled with water and whose formation is due to wind-borne fine debris (cryoconite) deposited on glacier surface and comprising both mineral and biological material. The dark cryoconite promotes stronger melt rates of the underlying ice when heated by solar radiation (Wharton et al., 1985), thus driving the genesis of a depression that can be filled by meltwater. Cryoconite holes range in diameter from a few centimetres to more than a meter and are very common features of ablating ice surfaces (Anesio & Laybourn-Parry, 2012).

The study of cryoconite holes has gained interest among ecologists and microbiologists because they are considered the most biologically active environments on the glaciers (Säwström et al., 2002; Stibal et al., 2006; Edwards et al., 2014; Cook et al., 2016). The microbial ecology of cryoconite holes has been investigated both on Arctic and Antarctic glaciers (e.g. Christner et al. 2003; Foreman et al. 2007; Edwards et al. 2013a; Zarsky et al. 2013) and on temperate mountain glaciers (e.g. Margesin et al. 2002, 2012; Margesin 2003; Telling et al. 2010; Takeuchi et al. 2010; Edwards et al. 2013b, 2014; Hamilton et al. 2013; Segawa et al. 2014; see also Cook et al., 2015). However, there is a geographical bias in the literature that favours polar over mountain glaciers (Cook et al., 2016).

Studies of cryoconite holes identified several environmental factors that can affect bacterial communities, including sediment thickness (Telling et al., 2012), hole area (Cook et al., 2010) and hydrology (Edwards et al., 2011). However, microbiological studies on these supraglacial

environments have been mostly limited to snapshots, and studies on temporal variability of bacterial communities of cryoconite holes are lacking (Cook et al., 2016). Indeed, temporal variation in the bacterial communities of cryoconite holes has been investigated only in two studies conducted on Arctic glaciers (Musilova et al., 2015; Stibal et al., 2015) and, to the best of our knowledge, it has never been investigated on a mountain glacier. In particular, the question whether microbial succession occurs in cryoconite holes, and to what extent it shapes bacterial communities is still open (Cook et al., 2016), particularly for cryoconite of Alpine glaciers.

In this study, we aimed at contributing to filling this gap by investigating the concomitant effects of temporal variation during the melt season and variation in environmental conditions of the holes in shaping t the bacterial communities of cryoconite holes on the Forni Glacier (Italian Alps).

7.2. Experimental procedures

Forni Glacier (46°12'30'' N, 10°13'50'' E; Fig. 1) is one of the largest Italian valley glaciers covering 11.34 km^2 in 2007 (Smiraglia et al., 2015). Glacier elevation ranges between 2600 and 3670 m a.s.l. The ablation season spans from early July to late September, as assessed by the data from an automatic weather station operating on the glacier (Supplementarly Information; see also Senese et al., 2014).

Twenty samples of cryoconite (2-5 g, one sample per hole) were aseptically collected on 10 July, 28 August, and 25 September from a flat area of the glacier. Samples were stored in 50 ml Falcon™ tubes kept at 4 °C during transport to the laboratory, which occurred within 8 hours. After sample collection, oxygen concentration in the pool, pH and temperature were measured in each hole with a portable oximeter/pH meter (HACH LANGE HQ40D, Loveland, CO), and maximum depth recorded by a ruler (precision 1 mm). Hole area was estimate from a picture of the hole with a reference ruler by an automatic method of cryoconite holes delimitation through ImageJ software (Hodson et al., 2010). Organic matter content of cryoconite was measured with the loss-on-ignition method by heating the

samples at 400 °C overnight (ASTM, 2000). Attempts were made to measure sediment depth with a ruler, but sediment was very tiny (always < 3 mm), and its thickness varied within each hole due to irregularities of hole bottom (A. Franzetti and R.S. Azzoni, personal observations).

Total DNA was extracted from 0.5 g of cryoconite using the FastDNA Spin for Soil kit (MP Biomedicals, Solon, OH) according to the manufacturer's instructions. DNA processing, PCR amplifications and Operational Taxonomic Unit definitions were conducted according to Daghio et al. (2016) (see also Supplementary Information). The sequencing was carried out at Parco Tecnologico Padano (Lodi, Italy). Fig. S1 shows the relative abundance of OTUs classified at order level.

The number of sequences of each sample varied from 2203 to 85070. To compare diversity among samples that largely differ in the number of sequences, 2000 reads were randomly selected from all libraries and used to calculate the number of OTUs, which was considered an index of alpha diversity, and the Gini inequality index (Gini, 1912), a measure of statistical dispersion that is used in ecology to measure community evenness (Wittebolle et al., 2009). Gini index ranges from 0 to 1, with increasing values indicating lower evenness. In contrast, analyses of community compositions were based on relative abundance of OTUs calculated on 10000 randomly chosen sequences for the 54 out of 60 samples where the number of sequences was larger than 1000, and as the number of sequences of each OTU normalised to 10000 for the other six samples.

We relied on generalized linear models or generalized linear mixed models to assess variation of number of OTUs and Gini index, or variation in the abundance of bacterial orders among months and according to environmental conditions at each hole, while we used redundancy analysis and variation partitioning (Borcard et al., 1992) to determine the amount of variation in bacterial community structure that can be explained separately and jointly by time during the breeding season and ecological conditions at each hole. Since multivariate statistical analyses necessitate of datasets with no missing values, we imputed missing data present in our dataset by Markov Chain Monte Carlo

(MCMC) multiple imputation by Gibbs sampling. Data imputation is strongly recommended as it can avoid biased estimates from statistical analyses (Nakagawa and Freckleton, 2008).

Analyses were performed with the LMERTEST, MASS, MICE, MULTCOMP, MULTTEST, PACKFOR and VEGAN packages in R 3.2.2 (R Core Team, 2013).

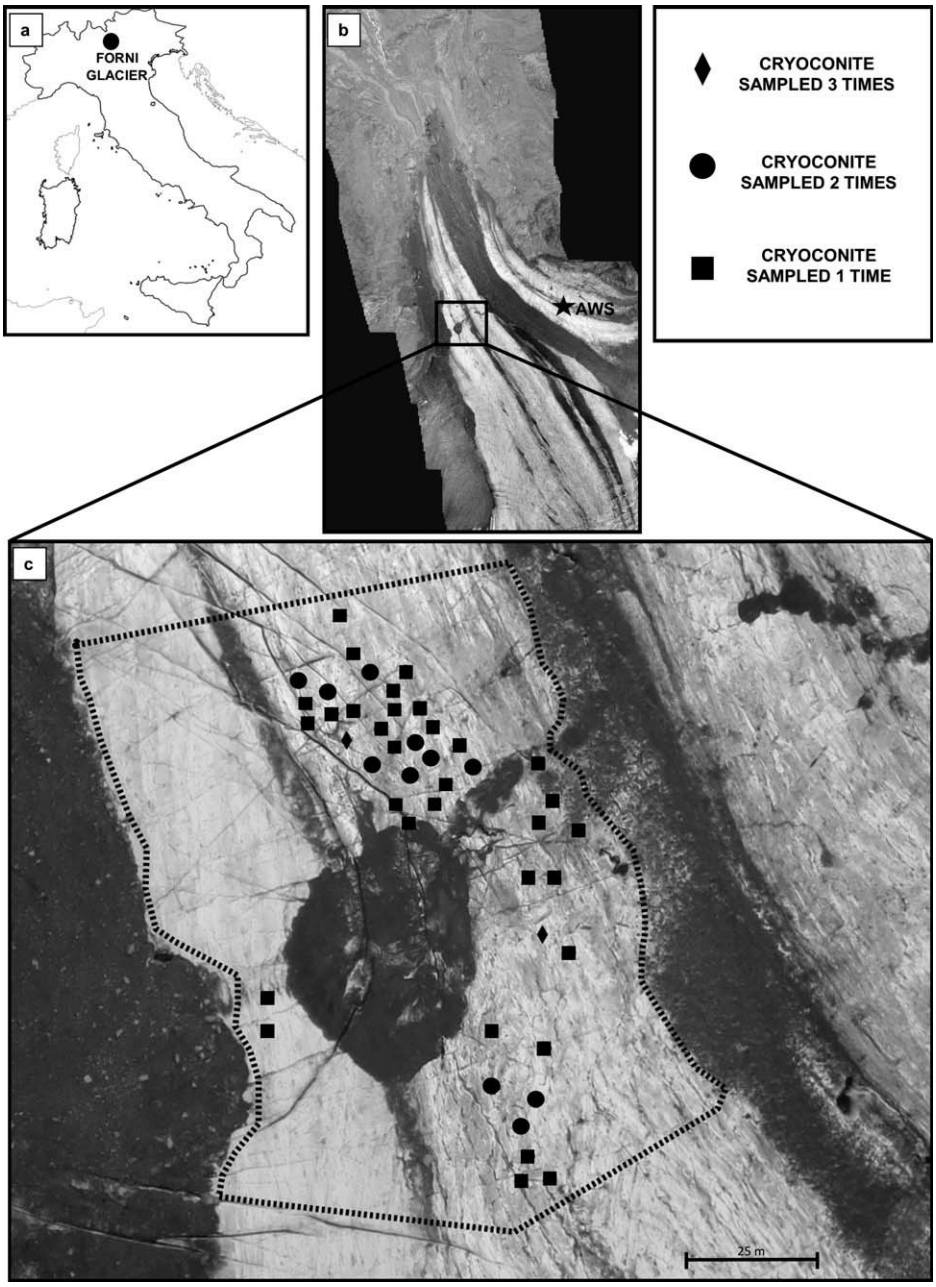

Fig. 1: a) Position of the Forni Glacier in Italy; b) composite aerial photograph of the tongue of the Forni Glacier with the position of the automatic weather station; c) aerial photograph of the study area. Position of each cryoconite hole is shown. Different symbols denote holes with overlapping positions sampled in different months. The dashed line delimits the study area.

7.3. Results

We collected 60 samples of cryoconites during tree visits to the glacier conducted in July, August and September 2013 (Fig. 1). Twenty samples were collected at each visit. Overall, 596 Operational Taxonomic Units (OTUs) were retrieved, excluding singletons. Sphingobacteriales, Pseudomonadales, Rhodospirillales, Burkholderiales and Clostridiales were the five most abundant bacterial orders and, together with Cyanobacteria and one unclassified order belonging to Actinobacteria (class), represented more than 80% of bacteria in cryoconite holes.

Redundancy analysis (RDA) showed that the structure of bacterial communities in cryoconite holes changed among months (Pseudo-$F_{2,57}$ = 11.565, P = 0.005) and that such variation accounted for 26.4% of total variance in bacterial communities (Fig. 2a). Post-hoc tests disclosed significant differences between all pairs of months (Pseudo-$F_{1,38} \geq 2.425$, $P_{FDR} \leq 0.010$ in all cases). Structure of bacterial communities also changed according to environmental conditions, namely hole depth and area, amount of organic matter in the cryoconite and oxygen concentration (Pseudo-$F_{4,55}$ = 3.431, P = 0.001), which overall explained 14.2% of variance (Fig. 2b).

Variation partitioning analysis indicated that month was the variable accounting for the largest unique fraction of variation (17.2%), while the unique contribution of environmental conditions, albeit significant, was much lower (5.0%). Importantly, this fraction was lower than that explained by the shared contribution of month and environmental conditions (9.2%), thus suggesting that variation in environmental conditions among months contributed to the observed variation in bacterial communities.

Generalized linear mixed models showed that the abundance of Cyanobacteria, Clostridiales, Sphingobacteriales and Burkholderiales changed among months ($\chi^2_2 \geq 15.235$; $P_{FDR} \leq 0.002$). Post-hoc tests also indicated that the abundance of Cyanobacteria and Clostridiales was higher in July than in August and September. In contrast, Sphingobacteriales and Burkholderiales where more abundant in

August and September than in July. The abundance of Clostridiales also differed between August and September. Abundance of Clostridiales decreased with hole depth ($F_{1,58} = 25.305$, $P_{FDR} < 0.001$), while that of the other taxa did not vary significantly with any environmental variable ($F_{1,58} \leq 9.102$, $P_{FDR} \geq 0.115$ in all cases).

Number of OTUs and Gini inequality indices differed significantly among months ($F_{2,57} \geq 89.39$, $P < 0.001$ in both cases, but not according to other environmental variables ($F_{1,44} \leq 1.265$ $P \geq 0.267$ in all cases). In particular, post-hoc tests showed that values observed in July differed significantly from those at the other months ($|t|_{57} \geq 10.023$, $P < 0.001$; Fig. 2a,b).

Sediment thickness was always < 3 mm and difficult to measure precisely because hole bottom was often irregular, probably because they formed by coalescence of smaller nearby holes. Similarly, no flux of water was observed in in the holes, probably because the cryoconite area was almost flat (A. Franzetti e R.S. Azzoni, personal observations). We therefore did not consider these variables. In contrast, depth of cryoconite holes and oxygen concentration changed significantly between months ($F_{2,52} \geq 8.794$, $P_{FDR} \leq 0.002$) while organic matter and hole area did not ($F_{2,52} \leq 3.235$, $P_{FDR} \geq 0.132$). Holes were deeper in September than in the other months (Fig. 3c), and oxygen concentration was higher in August than in the other months (Fig. 3d).

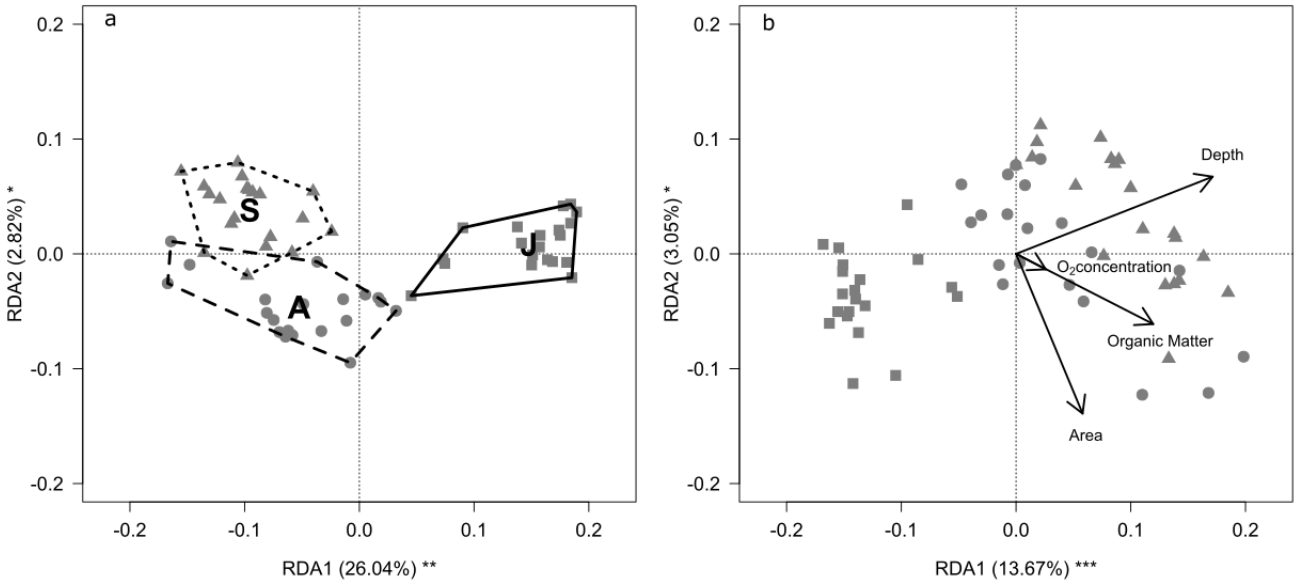

Fig. 2: Biplot of first and second components from RDAs of variation of bacterial communities in cryoconite holes with a) month, b) environmental conditions at each hole. Each symbol represents the bacterial community in a cryoconite hole. Different symbols represent different months and polygons include cryoconite holes sampled in each month (July = squares, August = dots, September = triangles). The amount of variance explained by each axis is shown as well as significance of each axis as assessed by a randomization test (* = P < 0.05, ** = P < 0.01, *** = P < 0.001). In a) letters denote the centroid of bacterial communities sampled in each month (J = July, A = August, S = September).and lines include samples collected in each month (July = solid line, August = dashed line, September = dotted line). In b) arrows represent constraining variables.

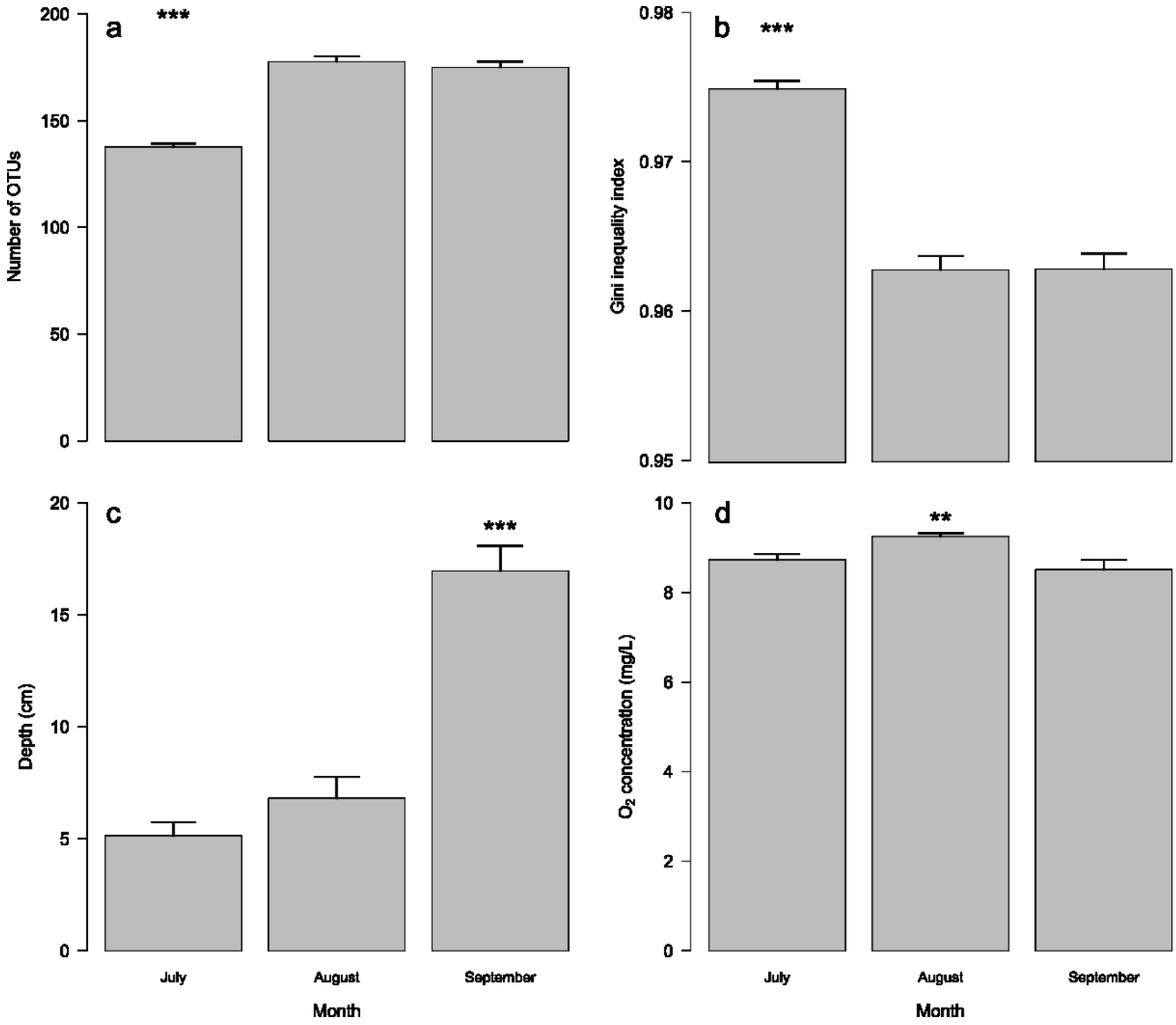

Fig. 3: Barplots of a) number of OTUs, b) Gini inequality index, c) hole depth and d) oxygen concentration in cryoconite holes in different months. Bars represent standard errors. Stars denote the month that significantly differed from the other ones at post-hoc tests (= P < 0.01, *** = P < 0.001).**

7.4. Discussion

In this study, we collected cryoconite samples from holes on the Forni Glacier in different months within the same ablation season and found that the structure of bacterial communities in cryoconite holes changed among months, with a decrease in the relative abundance of photosynthetic bacteria, particularly Cyanobacteria, and a concurrent increase in heterotrophic populations late in the ablation

season. This temporal pattern of variation is consistent with the results of previous studies on glacial environments, which reported colonization by autotrophic populations followed by an ecological succession both in forelands of retreating glaciers (Sigler et al., 2002) and at the surface of debris-covered glaciers (Franzetti et al., 2013). We also found significant effects of environmental conditions at each hole on the structure of bacterial communities. These results are consistent with those from previous investigations of bacterial communities of cryoconite on Arctic glaciers (Edwards et al., 2011; Gokul et al., 2016). However, environmental conditions explained a lower fraction of variance than month. In addition, we found that hole features changes along the melting season, particularly hole depth and oxygen concentration, so that temporal changes in bacterial communities may be mediated, at least partly, by changes in hole features. The variation partitioning analyses, however, indicated that variation among months per se was the most relevant effect, explaining 17.2% of the observed variation in bacterial communities. Similarly, temporal trends of alpha-diversity, indicated by the number of OTUs, and evenness, indicated by the Gini index, in cryoconite are consistent with ecological succession of recently colonized substrates. Indeed, we found communities with low biodiversity and dominated by few colonizing taxa at early stages of colonization, followed by communities with higher diversity and evenness at later stages (Jackson et al., 2001; Sigler and Zeyer, 2002).

We also observed that cryoconite holes seldom persist for a whole ablation season on the surface of the Forni Glacier. Indeed, melting rate was high on the tongue of the Forni Glacier during the ablation season 2013, and led to the loss of 6 m of ice in the sampled area (Senese et al., 2014). Consequently, a large number of cryoconite holes disappeared between consecutive visits to the glacier. (A. Franzetti and R.S. Azzoni, personal observations). Since cryoconite holes seem ephemeral environments on the surface of the Forni Glacier, as observed also on other mountain glacier (Takeuchi et al., 2000), we hypothesized that variation in the structure of bacterial communities could be driven mainly by

temporal changes of ecological conditions on the glacier surface rather than to ecological succession within the holes.

One of the main limits of the present study is that we collected samples only once per month during the ablation season. Therefore, we cannot exclude that changes in bacterial community structure may occur even at shorter time scales. Similarly, we cannot exclude that an ecological succession actually occurs in each hole at short temporal scale (i.e. from hole formation to its disappearance), particularly at the beginning of the ablation season when we observed larger variation in bacterial communities. Other variables, not included in the present study, may have affected bacterial communities. For instance melt season duration (Gokul et al., 2016), and sediment thickness (Telling et al., 2012) have been shown to significantly affect bacterial communities of cryoconite. However, all the holes we measured were within a rather small area and were at very similar altitude (Table S2) and, importantly, sediment thickness was always lower than the 3 mm threshold that seem to separate cryoconite holes dominated by autotrophic and heterotrophic communities (Telling et al., 2012). Therefore, our results should not have been biased by the fact that we did not consider these variables.

The results reported in the present study combined with previous knowledge on the microbial ecology of cryoconite holes therefore suggest that variation in bacterial communities occurred in cryoconite holes during one ablation season, and that temporal variation along the ablation season seems more important than local environmental conditions in shaping bacterial community structure.

7.5. Acknowledgments

Authors thank Parco Tecnologico Padano, (Lodi, Italy) and Science for Life Laboratories (Stockholm, Sweden) for sequencing and Parco Nazionale dello Stelvio (Sondrio Italy) for hosting instruments, sensors and researchers. This work was partially funded by Italian Ministry of Research (PRIN grant

2010AYKTAB to CS), by University of Milano-Bicocca (grant 7-19-2001100-2 to RA) and by Sanpellegrino S.p.A. – brand Levissima through an agreement with University of Milano. Some bioinformatics analyses were run on PLX server (CINECA, Bologna, Italy). The authors gratefully thank two anonymous reviewers and the Editor for useful suggestions and comments on earlier versions of the paper.

7.6. References

Anesio A.M. and Laybourn-Parry J. (2012): Glaciers and ice sheets as a biome. *Trends in Ecology and Evolution,* 27, 219–225.

ASTM (2000): Standard Test Methods for Moisture, Ash, and Organic Matter of Peat and Other Organic Soils - Method D 2974-00 American Society for Testing and Materials, West Conshohocken, PA.

Boetius A., Anesio A.M., Deming J.W., Mikucki J. and Rapp J.Z. (2015): Microbial ecology of the cryosphere : sea ice and glacial habitats. *Nature Reviews Microbiology,* 13, 677–690.

Borcard D., Legendre P. and Drapeau P. (1992); Partialling out the spatial component of ecological variation. *Ecology,* 73, 1045–1055.

Christner B.C., Kvitko B.H. and Reeve J.N. (2003): Molecular identification of bacteria and Eukarya inhabiting an Antarctic cryoconite hole. *Extremophiles,* 7, 177–183.

Cook J., Edwards A., Takeuchi N., and Irvine-Fynn T. (2016): Cryoconite: The dark biological secret of the cryosphere. *Progress in Physical Geography,* 40, 66–111.

Cook J.M., Hodson A.J., Telling J., Anesio A.M., Irvine-Fynn T.D.L. and Bellas C. (2010): The mass-area relationship within cryoconite holes and is implications for primary production. *Annals of Glaciology,* 51, 106–110.

Daghio M., Vaiopoulou E., Patil S.A., Suárez-Suárez A., Head I.M., Franzetti A. and Rabaey K. (2016): Anodes stimulate anaerobic toluene degradation via sulfur cycling in marine sediments. *Applied Environmental Microbiology,* 82, 297–307.

Edwards A., Anesio A.M., Rassner S.M., Sattler B., Hubbard B., Perkins W.T. (2011): Possible interactions between bacterial diversity, microbial activity and supraglacial hydrology of cryoconite holes in Svalbard. The *ISME Journal,* 5, 150–160.

Edwards A., Douglas B., Anesio A.M., Rassner S.M., Irvine-Fynn T.D.L., Sattler B. and Griffith G.W. (2013): A distinctive fungal community inhabiting cryoconite holes on glaciers in Svalbard. *Fungal Ecology,* 6, 168–176.

Edwards A., Mur L. a J., Girdwood S.E., Anesio A.M., Stibal M. and Rassner S.M.E. (2014): Coupled cryoconite ecosystem structure-function relationships are revealed by comparing bacterial communities in

alpine and Arctic glaciers. *FEMS Microbiology Ecology,* 89, 222–237.

Edwards A., Pachebat J., Swain M., Hegarty M., Hodson A.J. and Irvine-Fynn T.D.L. (2013): A metagenomic snapshot of taxonomic and functional diversity in an alpine glacier cryoconite ecosystem. *Environmental Research Letters,* 8, 35003.

Foreman C.M., Sattler B., Mikucki J.A., Porazinska D.L. and Priscu J.C. (2007): Metabolic activity and diversity of cryoconites in the Taylor Valley, Antarctica. *Journal of Geophysical Resources,* 112: G04S32.

Franzetti A. Tatangelo V., Gandolfi I., Bertolini V., Bestetti G., Diolaiuti G. D'Agata C., Smiraglia C. and Ambrosini R. (2013): Bacterial community structure on two alpine debris-covered glaciers and biogeography of Polaromonas phylotypes. *The ISME Journal,* 7, 1483–1492.

Gini C. (1912): Variabilità e mutuabilità. Contributo allo studio delle distribuzioni e delle relazioni statistiche C. Cuppini, Bologna.

Gokul J.K., Hodson A.J., Saetnan E.R., Irvine-Fynn T.D.L., Westall P.J. and Detheridge A.P. (2016): Taxon interactions control the distributions of cryoconite bacteria colonizing a High Arctic ice cap. *Molecular Ecolology,* 25, 3752–3767.

Hamilton T.L., Peters J.W., Skidmore M.L. and Boyd E.S. (2013): Molecular evidence for an active endogenous microbiome beneath glacial ice. *The ISME Journal,* 7, 1402–1412.

Hodson A., Cameron K., Bøggild C., Irvine-Fynn T., Langford H., Pearce D. and Banwart S. (2010): The structure, biological activity and biogeochemistry of cryoconite aggregates upon an Arctic valley glacier: Longyearbreen, Svalbard. *Journal of Glaciology,* 56, 349–362.

Jackson C.R., Churchill P.F. and Roden E.E. (2001): Successional changes in bacterial assemblage structure during epilithic biofilm development. *Ecology,* 82, 555–566.

Laybourn-Parry J., Tranter M. and Hodson A. (2012): The ecology of snow and ice environments Oxford University Press, Oxford.

Margesin R. (2003) *Pedobacter cryoconitis* sp. nov., a facultative psychrophile from alpine glacier cryoconite. *International Journal of Systematic and Evolutionary Microbiology,* 53, 1291–1296.

Margesin R., Spröer C., Zhang D.C. and Busse H.J. (2012): *Polaromonas glacialis* sp. nov. and *Polaromonas cryoconiti* sp. nov., isolated from alpine glacier cryoconite. *International Journal of Systematic and Evolutionary Microbiology,* 62, 2662–2668.

Margesin R., Zacke G. and Schinner F. (2002): Characterization of heterotrophic microorganisms in alpine glacier cryoconite. *Arctic, Antarctic and Alpine Resources,* 34, 88–93.

Musilova M., Tranter M., Bennett S.A., Wadham J. and Anesio A.M. (2015): Stable microbial community composition on the Greenland Ice Sheet. *Frontiers in Microbiology,* 6, 1–10.

Nakagawa S. and Freckleton R.P. (2008): Missing inaction: the dangers of ignoring missing data. *Trends in Ecology and Evolution,* 23, 592–596.

R Core Team (2013): R: A Language and Environment for Statistical Computing.

Säwström C., Mumford P., Marshall W., Hodson A. and Laybourn-Parry J. (2002): The microbial communities and primary productivity of cryoconite holes in an Arctic glacier (Svalbard 79°N). *Polar Biology,* 25, 591–596.

Segawa T., Ishii S., Ohte N., Akiyoshi A., Yamada A. and Maruyama F. (2014): The nitrogen cycle in

cryoconites: Naturally occurring nitrification-denitrification granules on a glacier. *Environmental Microbiology,* 16, 3250–3262.

Senese A., Maugeri M., Vuillermoz E., Smiraglia C. and Diolaiuti G. (2014): Using daily air temperature thresholds to evaluate snow melting occurrence and amount on Alpine glaciers by T-index models: the case study of the Forni Glacier (Italy). *The Cryosphere,* 8, 1921–1933.

Sigler W.V, Crivii S. and Zeyer J. (2002): Bacterial succession in glacial forefield soils characterized by community structure, activity and opportunistic growth dynamics. *Microbial Ecology,* 44, 306–316.

Sigler W.V and Zeyer J. (2002): Microbial diversity and activity along the forefields of two receding glaciers. *Microbial Ecology,* 43, 397–407.

Smiraglia C., Azzoni R.S., D'Agata C., Maragno D., Fugazza D. and Diolaiuti G.A. (2015): The evolution of the Italian glaciers from the previous data base to the New Italian Inventory. Preliminary considerations and results. *Geografia Fisica e Dinamica Quaternaria,* 38, 79–87.

Stibal M., Šabacká M. and Kaštovská K. (2006): Microbial communities on glacier surfaces in Svalbard: Impact of physical and chemical properties on abundance and structure of cyanobacteria and algae. *Microbial Ecology,* 52, 644–654.

Stibal M., Schostag M., Cameron K.A., Hansen L.H., Chandler D.M., Wadham J.L. and Jacobsen C.S. (2015): Different bulk and active bacterial communities in cryoconite from the margin and interior of the Greenland ice sheet. *Environmental Microbiology Reports,* 7, 293–300.

Takeuchi N., Kohshima S., Yoshimura Y., Seko K. and Fujita K. (2000): Characteristics of cryoconite holes on a Himalayan glacier, Yala Glacier Central Nepal. *Bulletin of Glaciological Resources,* 17, 51–59.

Takeuchi N., Nishiyama H. and Li Z. (2010): Structure and formation process of cryoconite granules on Ürümqi glacier No. 1, Tien Shan, China. *Annals of Glaciology,* 51, 9–14.

Telling J., Anesio A.M., Hawkings J., Tranter M., Wadham J.L. and Hodson A.J. (2010): Measuring rates of gross photosynthesis and net community production in cryoconite holes: A comparison of field methods. *Annals of Glaciology,* 51, 153–162.

Telling J., Anesio A.M., Tranter M., Stibal M., Hawkings J. and Irvine-Fynn T. (2012): Controls on the autochthonous production and respiration of organic matter in cryoconite holes on high Arctic glaciers. *Journal of Geophysical Resources,* 117: G01017.

Van der Veen C.J. (1999): Fundamentals of Glacier Dynamics Balkema, Rotterdam.

Wharton R., McKay C.P., Simmons G.M. and Parker B.C. (1985): Cryoconite holes on glaciers. *Bioscience,* 35: 499–503.

Wittebolle L., Marzorati M., Clement L., Balloi A., Daffonchio D. and Heylen K. (2009): Initial community evenness favours functionality under selective stress. *Nature,* 458, 623–626.

Zarsky J.D., Stibal M., Hodson A., Sattler B., Schostag M. and Hansen L.H. (2013): Large cryoconite aggregates on a Svalbard glacier support a diverse microbial community including ammonia-oxidizing archaea. *Environmental Research Letters,* 8: 35044.

Chapter 8
Light-dependent microbial metabolisms drive carbon fluxes on glacier surfaces

Chapter published on the ISME Journal

Franzetti A., Tagliaferri I., Gandolfi I., Bestetti G., Minora U., Mayer C., Azzoni R.S., Diolaiuti G.A., Smiraglia C. and Ambrosini R. (2016) - Light-dependent microbial metabolisms drive carbon fluxes on glacier surfaces. *The ISME Journal*, 10(12), 2984-2988.

Abstract

Biological processes on glacier surfaces affect glacier reflectance, influence surface energy budget and glacier response to climate warming, and determine glacier carbon exchange with the atmosphere. Currently, carbon balance of supraglacial environment is assessed as the balance between the activity of oxygenic phototrophs and the respiration rate of heterotrophic organisms. Here we present a metagenomic analysis of tiny wind-blown supraglacial sediment (cryoconite) from Baltoro (Pakistani Karakoram) and Forni (Italian Alps) glaciers providing evidence for the occurrence in these environments of different and previously neglected metabolic pathways. Indeed, we observed high abundance of heterotrophic anoxygenic phototrophs, suggesting that light might directly supplement the energy demand of some bacterial strains allowing them to use as carbon source organic molecules which otherwise would be respired. Furthermore, data suggest that CO_2 could be produced also by microbiologically mediated oxidation of CO, which may be produced by photodegradation of organic matter.

8.1. Main text

Climate change is determining a global cryosphere shrinkage and mountain glacier environments are declining (IPPC, 2014). The consequent loss of biodiversity is still to be fully assessed, particularly the loss of functional biodiversity in extreme environments (Stibal et al., 2012; Boetius et al., 2015). Cryoconite holes, i.e. small depressions on glacier surfaces whose formation is due to wind-borne debris (cryoconite), are the most biologically active environments on glaciers (Boetius et al., 2015).

We used whole metagenomic sequencing to investigate the main functions of six cryoconite holes from Forni (Italian Alps) and six from Baltoro (Pakistani Karakoram) glaciers. We focused on carbon and energy metabolisms by comparing the total coverage of marker genes for photosynthesis, use of inorganic and organic compounds as energy source, and autotrophy/heterotrophy. We also used metagenomic sequences for the taxonomic attribution of microorganisms carrying specific metabolic (Fig.1). The main hypothesis tested was whether oxygenic phototrophy and organotrophic respiration represent the only significant metabolisms affecting carbon balance on glacier surface, as currently conceived, or other microbial processes could contribute to it.

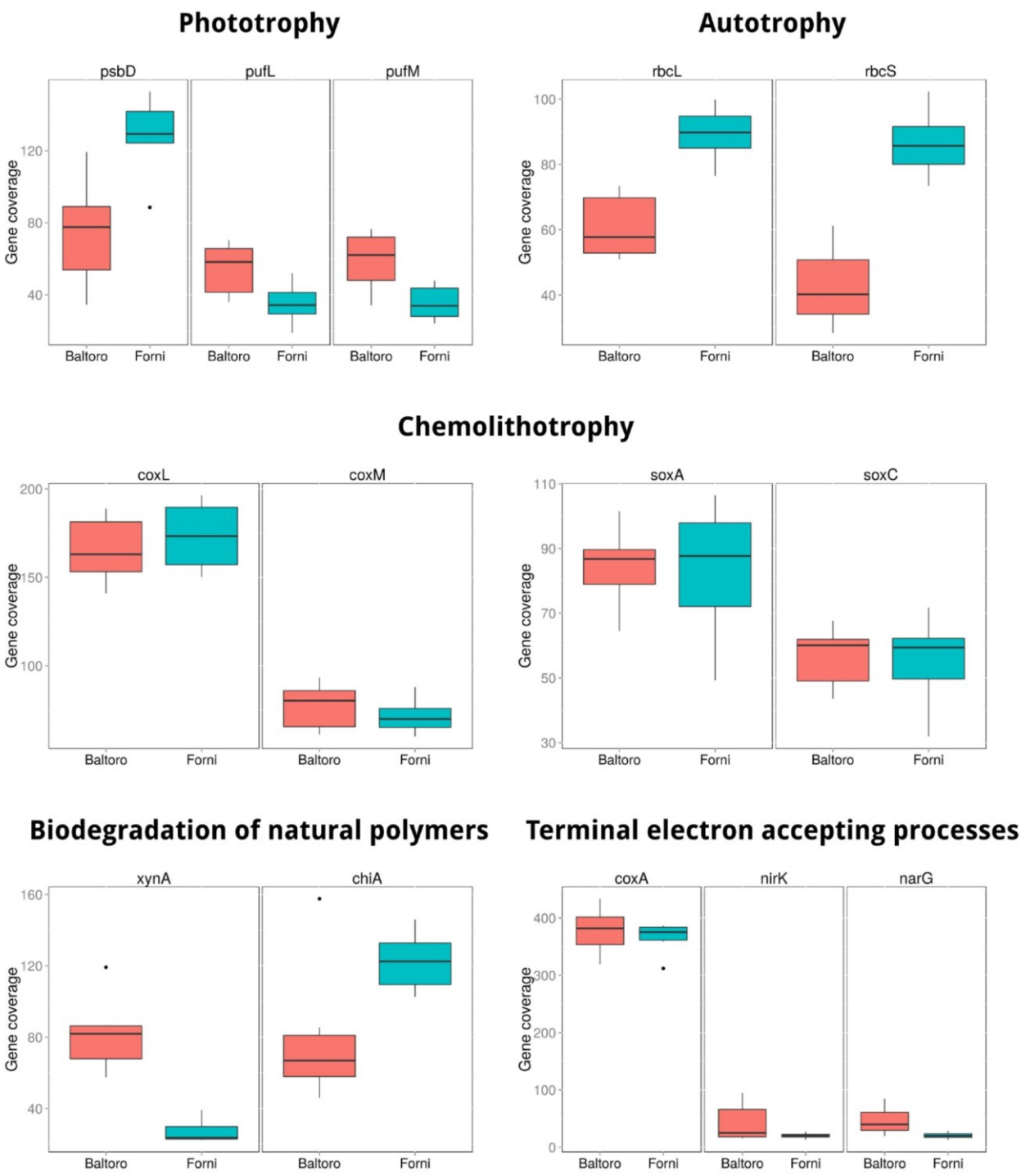

Fig. 1: Box plots of marker gene coverages in Forni and Baltoro cryoconite metagenomes. psbD, photosystem II P680 reaction center D2 protein; pufLM, photosynthetic reaction center L and M subunits; rbcLS, ribulose bisphosphate carboxylase small and large chain (RubisCO); soxAC, sulfur-oxidizing proteins SoxAC; coxML, carbon-monoxide dehydrogenase medium and large subunits; chiA, chitinase; xynA, endo-1,4-beta-xylanase; coxA, cytochrome c oxidase subunit I; narG, nitrate reductase alpha subunit; nirK, nitrite reductase.

Based on 16S rRNA gene sequencing (Franzetti et al, submitted for Forni), Cyanobacteria represented 22% and 3% of the microbial community on Forni and Baltoro, respectively (Figure S3). High

abundance of cyanobacteria has been already observed in polar and alpine cryoconite (Segawa et al., 2014; Stibal et al., 2014), while low abundance was reported on Rotmoosferner Glacier (Tirol, Austria) (Edwards et al., 2013). Consistently, coverage of psbD (photosystem II P680 reaction center D2 protein gene) was (mean ± SE) 128.0 ± 9.5 on Forni and 74.5 ± 12.5 on Baltoro, similar to that reported for Arctic and Antarctic supraglacial microbial mats (Varin et al., 2013). This suggests that oxygenic photosynthesis is among the dominant metabolisms in cryoconite holes. The significantly higher coverage of psbD gene on Forni than on Baltoro (Mann-Whitney U-test: $U = 34$, $P = 0.009$) is consistent with the higher oxygen concentrations in cryoconite hole water observed on this glacier ($U = 36$, $P = 0.005$). However, on the days of sampling, we observed strong oxygenic phototrophic activities in only two out of six holes on Forni. The high pufLM (photosynthetic reaction center L and M subunits) gene coverage, mostly affiliated to Proteobacteria suggests that aerobic anoxygenic phototrophs (AAPs) may contribute to energy input of the ecosystem (Yurkov and Hughes, 2013). AAPs are obligate heterotrophic phototrophs whose presence has been recently documented in cold environments. AAPs use light to supplement their metabolic demands and organic molecules as carbon source: under light conditions, they replace oxidative respiration with photophosphorylation, thus saving carbon, which is used in anabolic reactions for building cell biomass (Čuperová et al., 2013; Caliz and Casamayor, 2014). Interestingly, puf gene coverages were significantly higher on Baltoro than Forni ($U \geq 31$, $P \leq 0.041$), where oxygen consumption rates were also higher in dark conditions ($U = 21$, $P = 0.041$), when AAPs switch to a more respiratory metabolism. In contrast, oxygen consumption rates in light conditions were similar on the two glaciers ($U = 23$, $P = 0.485$).

CO_2 fixation was also widespread and almost completely achieved through Calvin-Benson cycle, as revealed by the high coverages of rbcLS genes (ribulose bisphosphate carboxylase - RubisCO), mostly affiliated to Proteobacteria, and by the negligible presence of reductive acetyl-CoA pathway and reductive citric acid cycle (details not shown). Although the taxonomic attribution of rbcLS genes showed that autotrophs mainly belonged to Cyanobacteria, it also revealed that Proteobacteria

substantially contribute to CO_2 fixation. Indeed, Proteobacteria represented 16-22% of bacteria harbouring rbcL genes respectively on Forni and Baltoro. This suggests that autotrophic chemolithotrophs, might also occur in cryoconite. Indeed, high coverages of sulfur oxidation genes (soxAC) and carbon-monoxide oxidation genes (coxLM) were detected on both glaciers. Conversely, no presence of amoAB was detected, suggesting the low relevance of ammonia oxidation and nitrification processes. sox gene clusters have been described in both anoxygenic sulfur oxidising phototrophs and chemolitotrophs (Friedrich et al., 2005). CO-oxidizers are a phylogenetically diverse group of bacteria inhabiting different environments (King and Weber, 2007). Interestingly, CO can form rapidly from organic carbon (OC) in melting snow exposed to light (Haan et al., 2001; Xie and Zafiriou, 2009). We speculate that CO-oxidizers occur in the melting snow cover of glaciers, and then persist on glacier surfaces, where photochemical CO production may occur, thanks to high light intensity and abundant OM in cryoconite. Direct measurements of CO in the holes are not available, however, CO photochemical formation rates were found to be correlated with the concentrations of dissolved organic carbon (DOC) in the snow (Haan et al., 2001). DOC, in turn, seems more abundant in mountain glacier cryconite (0.71 mg/L; Hood et al., 2015) than in the snow (0.07-0.30 mg/L; Legrand et al., 2013). Therefore, despite we have no direct evidence that CO actually forms in cryoconite holes and to which amount, it might represent a bioavailable substrate on glacier surface, which supplements the energy demand of microbial populations through its oxidation to CO_2 (King and Weber, 2007). Importantly, cyanobacteria produce extracellular polymeric substances (EPS) that represent an important DOC component (Bhatia et al., 2010). Hence, oxygenic phototrophs may contribute to the amount of DOC in the cryoconite, which in turn might be photodegraded to CO and sustain CO-oxidizers. Surprisingly, CO-oxidizers have not been reported in glacier environments previously, probably because of lack of functional studies on these environments. However, phylogenetic assignment of coxM gene revealed that CO-oxidizers mostly belonged to Actinobacteria (up to 26%), α- (up to 25%) and β-Proteobacteria (up to 69%), particularly Comamonadaceae (34% on

Baltoro) (Figures S3), which are known to occur on glacier surfaces (Edwards et al., 2014; Boetius et al., 2015). To gain more insight into the role of Comamonadaceae, we reconstructed from metagenomic data ten partial genomes of Polaromonas, a genus of Comamonadaceae, which is ubiquitous in glacial environments (Darcy et al., 2011; Franzetti et al., 2013; Michaud et al., 2012). Genomes annotation revealed widespread presence of CO dehydrogenase and absence of a complete CO_2 fixation pathway, consistently with the complete genome of Polaromonas JS666. This suggests that Polaromonas in cryoconite might use CO as energy source in presence of OC (mixotrophy) (Mattes et al., 2008).

We observed high coverages of genes coding for enzymes involved in the use of several OC sources, such as cellulose, extracellular polymeric substances (EPS) produced by cyanobacteria (xylA) and chitin (chiA). Furthermore, measures revealed that cryoconite holes were fully oxygenated environments. This condition explains the very high coverages of cytochrome-c oxidase subunit I gene (coxA). However, we observed also presence of nirK/narG genes, which suggest occurrence of anaerobic conditions. Conversely, the abundance of marker genes for dissimilatory sulfate reduction (dsrAB) was negligible.

In summary, supraglacial bacterial communities exhibit a high functional biodiversity as they can exploit OC both as energy and carbon source. The high solar radiation at glacier surface may favour both oxygenic and anoxygenic photosynthesis, likely by organisms with both pure autotrophic and mixotrophic lifestyles. Light might also support photochemical CO production and its microbiologically mediated consumption (Figure 2). Despite the presence of the genetic potential for the above-described metabolisms does not necessarily imply that they are actually active, we propose that models of carbon fluxes on glacier surfaces should integrate also alternative metabolisms that has been overlooked so far, such as anoxygenic photosynthesis and CO-oxidation.

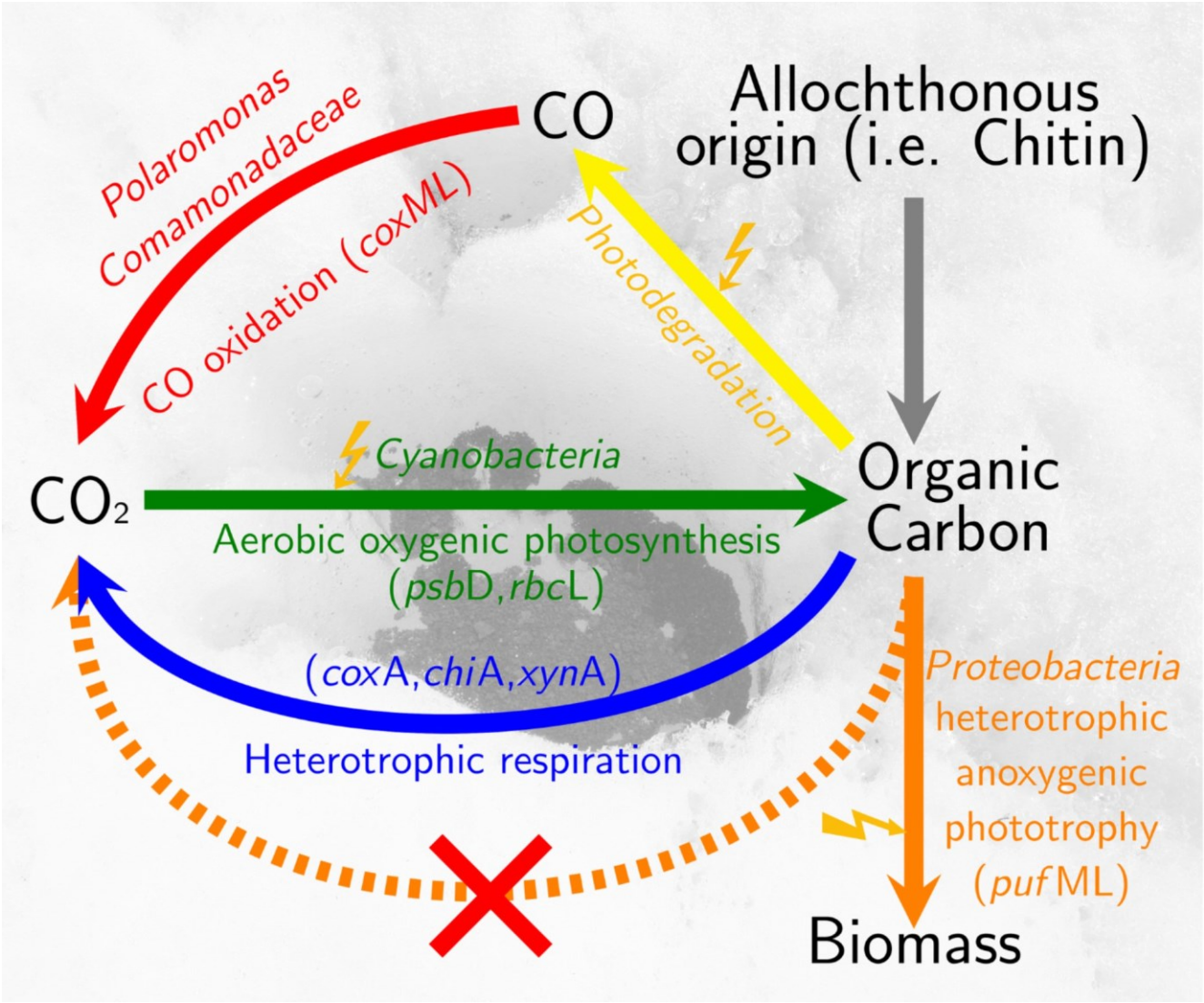

Fig. 2: Proposed cryoconite carbon "interactome".

8.2. Acknowledgements

Authors thank Parco Tecnologico Padano (Lodi, Italy) for technical assistance and sequencing. Authors also thank Ev-K2-CNR association for support and logistics during expedition on Baltoro Glacier. This work was partially funded by Italian Ministry of Research (PRIN grant 2010AYKTAB to CS) and by University of Milano-Bicocca (grant 7-19-2001100-2 to RA). Bioinformatics analyses have been run on PICO server (CINECA, Bologna, Italy) (project MEGABIT – grant ID: HP10CLG7F to AF).

8.3. References

Bhatia M.P., Das S.B., Longnecker K., Charette M.A., Kujawinski E.B. (2010): Molecular characterization of dissolved organic matter associated with the Greenland ice sheet. *Geochimica et Cosmochima Acta,* 74, 3768–3784.

Boetius A., Anesio A.M., Deming J.W., Mikucki J.A. and Rapp J.Z. (2015): Microbial ecology of the cryosphere: sea ice and glacial habitats. *Nature Reviews Microbioogy*, 13, 677-690.

Caliz J. and Casamayor E.O. (2014): Environmental controls and composition of anoxygenic photoheterotrophs in ultraoligotrophic high-altitude lakes (Central Pyrenees). *Environmental Microbiology Reports,* 6, 145–51.

Čuperová Z., Holzer E., Salka I., Sommaruga R. amd Koblízek M. (2013): Temporal changes and altitudinal distribution of aerobic anoxygenic phototrophs in mountain lakes. *Applied Environmental Microbiology,* 79, 6439–6446.

Darcy J.L., Lynch R.C., King A.J., Robeson M.S., Schmidt S.K. (2011): Global Distribution of Polaromonas Phylotypes - Evidence for a Highly Successful Dispersal Capacity. *PLoS One,* 6(8), e23742.

Edwards A., Mur L.A.J., Girdwood S.E., Anesio A.M., Stibal M. and Rassner S.M.E. (2014): Coupled cryoconite ecosystem structure-function relationships are revealed by comparing bacterial communities in alpine and Arctic glaciers. *FEMS Microbiology Ecology,* 89,222–37.

Edwards A., Pachebat J.A., Swain M., Hegarty M., Hodson A.J. and Irvine-Fynn T.D.L. (2013): A metagenomic snapshot of taxonomic and functional diversity in an alpine glacier cryoconite ecosystem. *Environmental Research Letters,* 8, 035003.

Franzetti A., Tatangelo V., Gandolfi I., Bertolini V., Bestetti G., Diolaiuti G. and Ambrosini R. (2013): Bacterial community structure on two alpine debris-covered glaciers and biogeography of Polaromonas phylotypes. *ISME Journal,* 7,1483–1492.

Friedrich C.G., Bardischewsky F., Rother D., Quentmeier A. and Fischer J. (2005): Prokaryotic sulfur oxidation. *Current Opinions in Microbiology,* 8, 253–259.

Haan D., Zuo Y., Gros V. and Brenninkmeijer C.A.M. (2001): Photochemical production of carbon monoxide in snow. *Journal of Atmospheric Chemistry,* 40, 217–230.

Hood E., Battin T.J., Fellman J., O'Neel S., Spencer R.G.M. (2015): Storage and release of organic carbon from glaciers and ice sheets. *Nature Geosciences,* 8,91–96.

IPPC. (2014): Climate Change 2013 – The Physical Science Basis: Working Group I Contribution to the Fifth Assessment Report of the Intergovernmental Panel on Climate Change. Cambridge University Press.

King G.M. and Weber C.F. (2007): Distribution, diversity and ecology of aerobic CO-oxidizing bacteria. *Nature*

Reviews Microbiology, 5,107–118.

Legrand M., Preunkert S., Jourdain B., Guilhermet J., Alekhina I. and Petit J.R. (2013): Water-soluble organic carbon in snow and ice deposited at Alpine, Greenland, and Antarctic sites: a critical review of available data and their atmospheric relevance. *Climate of the Past*, 9(5), 2195-2211.

Mattes T.E., Alexander A.K., Richardson P.M., Munk A.C., Han C.S. and Stothard P. (2008): The genome of Polaromonas sp strain JS666: Insights into the evolution of a hydrocarbon- and xenobiotic-degrading bacterium, and features of relevance to biotechnology. *Applied Environmental Microbiology,* 74,6405–6416.

Michaud L., Caruso C., Mangano S., Interdonato F., Bruni V. and Lo Giudice A. (2012): Predominance of Flavobacterium, Pseudomonas, and Polaromonas within the prokaryotic community of freshwater shallow lakes in the northern Victoria Land, East Antarctica. *FEMS Microbiology Ecology,* 82, 391–404.

Segawa T., Ishii S., Ohte N., Akiyoshi A., Yamada A. and Maruyama F. (2014): The nitrogen cycle in cryoconites: naturally occurring nitrification-denitrification granules on a glacier. *Environmental Microbiology,* 16, 3250–3262.

Stibal M., Šabacká M. and Žárský J. (2012): Biological processes on glacier and ice sheet surfaces. *Nature Geosciemces,* 5, 771–774.

Stibal M., Schostag M., Cameron K.A., Hansen L.H., Chandler D.M. and Wadham J.L. (2014): Different bulk and active bacterial communities in cryoconite from the margin and interior of the Greenland ice sheet. *Environmental Microbiology Reports,* 7(2), 293-300.

Varin T., Lovejoy C., Jungblut A.D., Vincent W.F., Corbeil J. and Edwards A. (2013): Metagenomic analysis of stress genes in microbial mat communities from Antarctica and the High Arctic. *Applied Environmental Microbiology,* 78,035003.

Xie H. and Zafiriou O.C. (2009): Evidence for significant photochemical production of carbon monoxide by particles in coastal and oligotrophic marine waters. *Geophysical Research Letters,* 36, L23606.

Yurkov V. and Hughes E. (2013): Genes associated with the peculiar phenotypes of the aerobic anoxygenic phototrophs. *Advance in Botanical Researches,* 66, 327–358.

Chapter 9
Microbial degradation on glacier surface is the missing piece of environmental fate of pesticide in cold areas

Abstract

Organic contaminants deposited on cold areas undergo different partition and degradation processes which determine their environmental fate and accumulation into the trophic chain. Among these processes, biodegradation by supraglacial bacteria has been neglected so far. To assess the relevance of these biodegradative processes, in situ microcosm experiments were conducted simulating cryoconite hole system on an Alpine glacier exposed to the organophosphorus insecticide chlorpyrifos (CPF). Results showed that biodegradation is the most efficient process contributing to the removal of CPF on glacier surface. The high concentrations of CPF in cryoconite and its half-life in the range of 35 – 69 days indicated that biodegradation process can significantly contrast the accumulation of CPF transported on glaciers. Moreover, the metabolic versatility of cryoconite bacteria suggest that these habitats might contribute to the degradation of a wide class of pollutants with different physical–chemical properties. Therefore, cryoconite might act as a "biofilter" for organic pollutants on glaciers by accumulating them and promoting their biodegradation.

9.1. Fate of pollutants in cold areas

It is widely documented that organic contaminants are present in polar and mountain regions far from their emission sources (Carrera et al., 2001; Wang et al., 2006; Daly and Wania, 2004; Kallenborn et al., 2007; Bidleman et al., 2010). High mountains, acting as cold condensers (Calamari et al., 1991), interfere with the atmospheric transport and global cycle of semi volatile organic compounds (SVOC) (Carrera et al., 2001; Wang et al., 2006; Villa et al., 2003). These organic pollutants can be efficiently scavenged from atmosphere by snow (Grannas et al., 2013), along with aerosol, microorganisms and nutriments (Price et al., 2009). When delivered on glaciers, pollutants undergo partitioning among different environmental matrices (i.e. snow, ice, atmosphere and supraglacial sediments) and post-depositional alteration processes. Currently, physical-chemical post-depositional alterations, such as photodegradation, hydrolysis and revolatilization, of contaminant burden in snowpack and ice have been considered (Wania et al., 1997; Klàn et al., 2001; Herbert et al., 2006; Matykiewiczová et al., 2007; Grannas et al., 2007). Conversely, until now, the microbial degradation of pollutants on glaciers have received less attention. Indeed, only one lab-study has been conducted to determine the potential of the cryoconite microbial community to degrade xenobiotics (Stibal et al., 2012), but it has never been estimated through field experiments. Furthermore, metagenomics studies revealed that glacial ice microorganisms have the potential to degrade a wide range of substrates (Simon et al., 2009). These findings might suggest that bacteria activity on glacier surface can be a relevant process in biogeochemical cycles of contaminant in cold areas. Particularly, cryoconite holes, which are holes are small depressions on glacier surfaces filled with water and whose formation is due to wind-borne fine debris (cryoconite) deposited on glacier surface, are considered the most biologically active habitat on glaciers (Cook et al., 2015). Moreover, owing to their high concentration of organic carbon, cryconite can accumulate organic pollutants (Li et al., 2017).

In this work we wanted to test the hypothesis that cryoconite might act as a "biofilter" for organic pollutants on glaciers by accumulating them and promoting their biodegradation, thus significantly contributing to the removal of these contaminants.

To this end, *in situ* microcosm experiments have been conducted simulating cryoconite hole system on an Alpine glacier exposed to the organophosphorus insecticide chlorpyrifos (CPF). CPF is one of the most widely used pesticides (George et al., 2014) and represent an ideal model compound for this study. Indeed, although it is not officially classified as Persistent Organic Pollutant (POP) or Persistent, Bioaccumulative and Toxic Substance (PBT), it shows a great potential to undergo long-range atmospheric transport and to reach cold areas (Mackay et al., 2014). In fact, CPF is frequently detected both in several Arctic matrices (air, water, sediment and biota) (Hageman et al., 2010; Hoferkamp et al., 2010; Landers et al., 2008) and in Alpine ones, like glacial meltwater (Ferrarui et al., 2017), ice core (Infante, 2016). The experiments were carried out on the Forni Glacier (glacier code IT4L01137024 in the World Glacier Inventory), one of the largest Italian valley glaciers. It is about 3 km long, stretches over an elevation range of 2,600 to 3,670 m a.s.l. (Senese et al., 2012a) and its surface area was 11.34 km^2 in 2007 (Smiraglia et al., 2015). The criteria for selection of Forni Glacier for the microcosms experiment were based on previous study that showed the presence of CPF in alpine meltwater in the order of ng/L (Ferrario et al., 2017). The analyses of CPF in cryoconite in this study revealed that the concentration ranged from 0.2 mg/Kg to 3 mg/Kg.

9.1.1. Study area

The microcosms were placed on the Eastern ablation tongue of the glacier at about 2700 m a.s.l. near an Automatic Weather Station (named AWS1 Forni; 46°23′51.96″N, 10°35′29.16″E), equipped with sensors for measuring air temperature and humidity, wind speed and direction, atmospheric pressure, liquid precipitation, snow depth, and longwave and shortwave radiation (Citterio et al., 2007; Senese et al., 2012b; Azzoni et al., 2016). The site was chosen because the glacier surface is flat and without crevasses. Ice melting occurred during the experiment was measured with some ablation stakes

installed near the weather station. Moreover, two thermistors were placed in two pyrex bottles located on glacial surface for measuring temperature variation in microcosms during the experiment.

Microcosms were prepared by using cryoconite and water collected on the Forni Glacier. Four experimental conditions have been tested: *i)* Light biotic (Lb) accounting for hydrolysis, photolysis and biodegradation under light conditions, *ii)* Dark biotic (Db) accounting for hydrolysis and biodegradation under dark conditions, *iii)* Light sterile (Ls) accounting for hydrolysis and photolysis, *iv)* Dark sterile (Ds) accounting for hydrolysis.

9.2. Methods

9.2.1. Microcosms set up

Microcosms were prepared by using cryoconite and water collected on the Forni Glacier on 17 July 2015. Sediment was taken from cryoconite hole with a spoon sterilized with alcohol and flame and transferred into sterile Falcon tubes (50 mL). The meltwater was gathered from the proglacial stream in a sterilized bottle. After collection, 42 transparent pyrex bottles (50 mL) were filled with 2 g of sediment and 36 mL of meltwater. In each bottle, 8 μg of CPF, dissolved in DMSO, were spiked. Six bottles were immediately brought to the lab for the analyses, which occurred within 4 hours from CPF injection, and served as a control at time 0 (t0). Eighteen of the remaining bottles were covered with tinfoil ("dark" condition, hereafter) in order to exclude the contribution of photolysis processes, while eighteen were kept transparent ("light" condition, hereafter). In addition, nine dark and nine light bottles were sterilized by a pressure-cooker in order to determine the degradation solely due by photolysis. So we ended up with four experimental groups of nine microcosms (dark biotic, dark sterilized, light biotic, light sterilized).

Bottles (except for t0 samples) were then placed in three plexiglas racks. They were covered with a plastic net to avoid bottle overturning and dispersal, and placed on the glacier surface bound to a

wooden stake drilled in the ice. Three bottles from each experimental group were then collected on July 27, August 10, August 26 and kept to the lab within 4 hours for analyses.

9.2.2. Chemical analysis

Chlorpyrifos (IUPAC name: O,O-diethyl O-3,5,6-trichloropyridin-2-yl phosphorothioate) was purchased from Sigma-Aldrich (product number: 45395-100 MG, Saint Louis, USA, purity >99.7%). All solvents were checked by gas chromatography (GC) before use.

Water samples were filtered on a glass fiber filter (0.45 μm, Whatman, Maidstone, England), before SPE procedure. Prior to the extraction of suspended solid samples, glass fiber filters were cleaned with n-hexane (Carlo Erba, Milan, Italy, purity N99.8%). A 10 ml aliquote of filtered water of each samples was extracted using OASIS HLB cartridges (Oasis HLB, 6 cc/500 mg, LP Extraction cartridge, 60 μm; Waters Corporation Milford, Massachussetts, USA). Cartridges were conditioned with 5 mL of methanol (J.T. Baker, purity N99.8%) and 5 mL of deionized water (Milli-Q). Samples were drawn under vacuum through the cartridges at a regulated flow rate of 10 mL/min. After the extraction, the cartridges were dried using a vacuum pump and subsequently eluted (under gravity) with 3+3 mL of ethyl acetate (Carlo Erba, Milan, Italy, purity N99.8%) and 4 mL of acetone (Carlo Erba, Milan, Italy, purity N99.8%). The extracts were then concentrated to 0.5 mL by a gentle stream of nitrogen.

The extracted suspended solids were dried adding Sodium Sulfate Anhydrous (Granular 12-60 Mesh J.T. Baker, Ultra Resi-Analyzed), transferred into extraction thimbles cellulose (19x90 mm, Albet Labscience) and exctracted with n-hexane for 24 h. The extracts were then concentrated to 0.5 mL by a gentle stream of nitrogen.

Both water and suspended solid extracts were transferred into GC micro-vials. An internal standard (PCB 40, lot: 40714, Dr. Ehrenstorfer GmbH, Augsburg, Germany, purity 99.0%) was added for subsequent analysis in GC–MS (Agilent Technologies, Santa Clara, CA, USA), in SIM (Single Ion Monitoring). Identification and quantification ions were 314 and 316 for CPF and 290 and 292 for PCB 40. The GC analysis was performed with an Agilent Technologies 6890N Series gas

chromatograph equipped with a 30-m long, 0.25-mm internal diameter capillary column (Zebron Capillary GC Column, ZB-Semivolatiles Guardian). Samples were injected by an Agilent Technologies 7683 Series autoinjector, with the injection port at 250 °C in splitless mode. Samples were run in splitless mode using helium as a carrier gas (flow= 1 mL/min).

The oven program started with a temperature of 70 °C and increased of 15 °C per min to 280 °C, hold for 2 min.

A series of procedural blanks was analyzed contextually to the extraction tests. Field blanks were generated and handled in a manner identical to that of water samples and CPF was not found. Two different fortification levels were used to validate the analytical procedure. Average recoveries were of 107% for 0.4 µg/ml and 96% for 0.004 µg/ml respectively. The method detection limit was determined as the instrument detection limit of the lowest concentration standard of CPF, which was 3 ng/mL. Analyses were repeated on fifty randomly chosen samples to estimate repeatability of the measurement. The operator was unaware of measurements collected on the previous measure. Repeatability of the measures was high (ANOVA-based repeatability = 0.919; 55 Nakagawa and Schielzeth 2010), so we used one measure for each microcosm for all the following analyses.

9.2.3. Microbiological analysis

For each sample, total DNA was extracted using the fastDNA Spin for soil kit (MB biomedicals, Solo, OH USA) according to the manufacturer's instructions.

To characterize the bacterial community, the V5-V6 hypervariable regions of 16S rRNA gene were sequenced by MiSeq (Illumina inc., San Diego, CA,USA) with a 250bp x 2 paired-end protocol. This region were PCR-amplified using 783F and 56,57(Huber et al. 2007; Wang and Qian, 2009). Cyclic conditions for the amplification were: initial denaturation at 94 °C for 4 min; 28 cycles at 94 °C for 50 s, 47 °C for 30 s and 72 °C for 45 s and a final extension at 72 °C for 5 min. The amplicons were purified with the Wizard® SV Gel and PCR Clean-up System (Promega Corporation, Madison, WI, USA) and purified DNA was quantified using Qubit® (Life Technologies, Carlsbad, CA, USA).

Groups of 9 amplicons bearing different barcodes pairs were pooled together to build a single library. Further preparation with the addition of standard Nextera indexes (Illumina, Inc., San Diego, CA, USA) and sequencing were carried out at Parco Tecnologico Padano (Lodi, Italy).

16S rRNA genes and mpd gene, coding for Methyl Parathion Hydrolases, were quantified with quantitative PCR (qPCR) to estimate the total number of bacteria and the putative populations with degradative abilities towards CPF, respectively. 16S rRNA gene amplicon for qPCR standard was amplified from environmental samples whereas mpd gene was obtained through synthetic gene sequencing by Eurofins Genomics. 16S rRNA and mpd fragments were cloned in pGEM vector (Promega Corporation, Madison WI, USA) according to the manufacturer's instructions. All qPCR amplifications were carried out with FluoCycle II Master Mix (Euroclone, Italy) containing SYBR Green. Cycle conditions for the amplification of the 16 rRNA gene were initial denaturation at 95°C for 4 min; 40 cycles at 95°C for 15 s, 60°C for 30 s and 72°C for 30 s. Primer sequence are: forward 3'-TCCTACGGGAGGCAGCAGGT-5' and reverse 3'GGACTACCAGGGTATCTAATCCTGTT 5' 58 (Nadkarni et al. 2002). Cycle conditions for the amplification of the mpd gene were initial denaturation at 95°C for 4 min; 40 cycles at 95°C for 15 s, 58°C for 30 s and 72°C for 40 s. No primer pair were reliable for the mpd gene and were, therefore, designed with the primer design tool from NCBI (http://www.ncbi.nlm.nih.gov/tools/primer-blast/). Primer sequence are: forward 5'-AGTTCAAGCCTTTCTCGGGG-3' and reverse 5'-CACTTGGGGTTACGACCGAG-3'. All reactions were conducted with Illumina Eco themocycler (Illumina).

9.2.4. Analysis of metagenomics data

Whole metagenome sequences of 6 cryoconite samples on Forni glacier were retrieved from a previous study 37 and analysed as follows. Paired-end reads were quality-trimmed (minimum length: 80 bp; minimum average quality score: 30) using Sickle (https://github.com/najoshi/sickle). Filtered reads were co-assembled using IDBA-UD 59 (Peng et al. 2012). Contigs were binned in putative

reconstructed genomes using MaxBin 60 (Wu et al. 2014). The presence of genes related to CPF biodegradation 61 into the reconstructed genome was performed as follows. First, sequences of methyl parathion hydrolases (mpd), organophosphorus acid anyhydrolase (opaa) and organophosphorus hydrolases (opd) genes were retrieved from nr database. The reconstructed genomes were annotated using Prokka 62 (Seemann, 2014) using these retrieved sequences as preferential proteins to first annotate from. This resulted in the annotation of 81 predicted genes as mpd. However, due to the high similarity of these protein with β lactamases, we checked the annotation by aligning the nucleotidic sequence of these predicted genes to nt database with Blastn and we conservatively considered as mpd those genes showing at least one mpd gene entry from nt database in the first ten best-matching entries. Genome annotation was visualised with CGView 63 (Grant and Stothard, 2008).

9.2.5. Statistical analyses

Analyses were conducted by linear models on log-transformed contaminant mass. Experimental treatment was included as a four-level factor (dark bacteria, dark sterile, light bacteria, light sterile) and time (in days) as covariate. Since contaminant measures at t0 were the same for all experimental groups, we constrained regression lines to have a common intercepts by including in the mode the factor by covariate interaction while excluding the factor per se. With this parameterization, the model fits to the log-transformed data four regression lines, with different slopes, but a common intercept. Since data were log-transformed before the analyses, slopes indicate first-order decay rate of CPF under each experimental condition. Analyses were followed by post-hoc comparison of regression slopes. All the analyses were performed in R 3.1.2 [64] (R core team, 2015) with the lsmeans package.

9.3. Results

9.3.1. Decay rates of Chlorpyrifos in cryoconite

Residual mass of CPF in microcosms over time are reported in Figure 1. CPF decay rates and half-life, calculated following first-order kinetics (Hui et al., 2010), in the different conditions were reported in

Table 1. Results showed that the rate of decay of CPF mass differed significantly among the four experimental groups ($F_{3,26} = 9.771$, $P < 0.001$). In particular, post-hoc comparisons of slopes indicated that decay rate of CPF was significantly larger under light bacteria condition than under other conditions ($t_{26} \geq 3.055$, $P \leq 0.026$), which, in turn, did not differ significantly to one another ($|t_{26}| \leq 2.044$, $P \geq 0.198$). To estimate decay rates due to individual chemical-physical or biological processes we calculated the differences in decay rates observed under the four experimental conditions (Table 2).

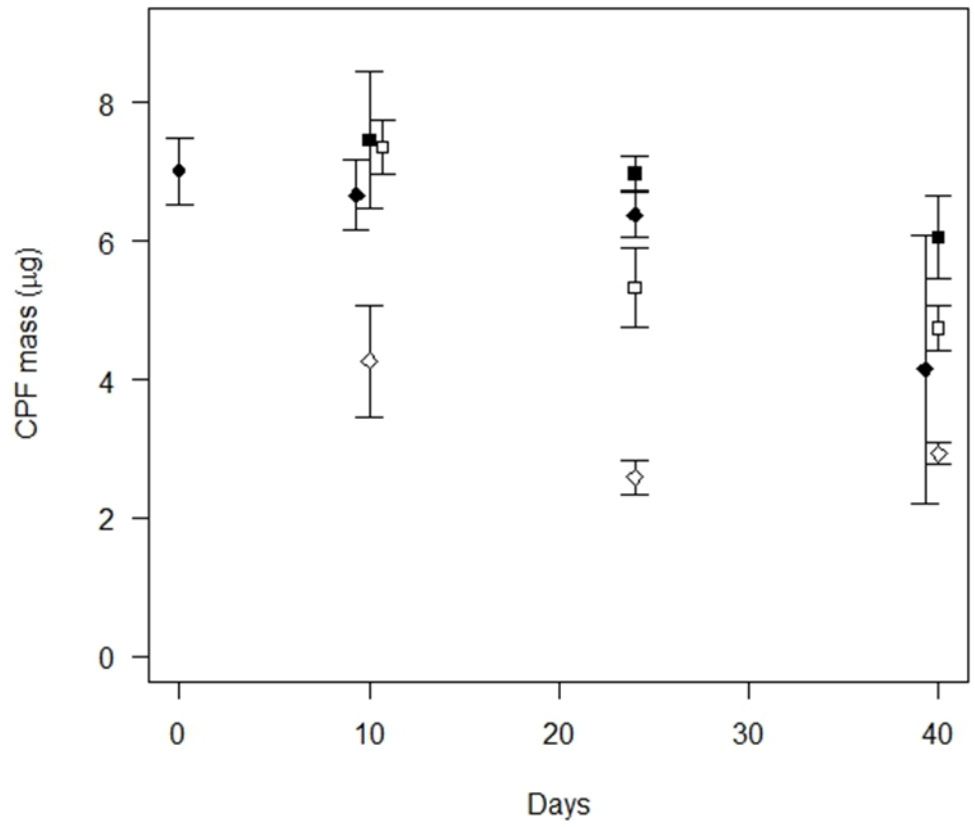

Fig. 1: CPF concentration in microcosm experiments. Different symbols denote different conditions (squares: sterilized samples, diamond: bacteria samples, filled symbols: dark conditions, open symbols: light conditions, dot: time zero). Bars represent standard errors.

Condition	Decay rate (d^{-1})	SE	95% CL		$t_{1/2}$ (d)
			Lower	Upper	
Dark-sterile	-0.003	0.004	-0.011	0.005	230.05
Light -sterile	-0.010	0.004	-0.019	-0.001	69.31
Dark-bacteria	-0.013	0.004	-0.022	-0.004	53.32
Light -bacteria	-0.028	0.004	-0.037	-0.019	24.76

Tab. 1: Decay rate of CPF and half-life of first order kinetics in the four experimental groups.

Degradation process	Difference used for the estimate	Decay rate (d^{-1})	SE	$t_{1/2}$ (d)
Hydrolysis	Ds	-0.003	0.004	231.05
Photodegradation	Ls-Ds	-0.006	0.005	115.52
Biodegradation dark	Db-Ds	-0.010	0.005	69.31
Biodegradation light	Lb-Ls	-0.020	0.005	34.66

Tab. 2: Decay rates due to individual chemical-physical or biological processes estimated as the differences in decay rates observed under different conditions

Decay rate under dark sterile condition estimated the degradation due to hydrolysis. Investigation of model coefficients disclosed that the amount of CPF did not decline significantly in the dark sterile group, while it did in all the other groups, as indicated by the fact that confidence limits of decay rate included zero in the first group only (Table 1). The hydrolysis rate of CPF in aquatic environments is influenced by environmental factors such as pH, temperature and concentration of total suspended solids. Based on previous experimental data31, cryoconite on Forni Glacier have pH values ranging from 6 to 8 and temperature between 0 to 3°C. Due to inevitable greenhouse effect that occurs inside the bottles, temperatures recorded in microcosms are less stable than those in natural cryoconite. In fact, during all the exposure time, microcosms temperature ranged from -4.7 °C to 15.2 °C.

Nevertheless, the result obtained confirmed that the degradation rate of CPF increases as the temperature rises. In literature, the rate of hydrolysis was reported to increase of 3.5-5 folds for each 10°C rise in temperature. The DT50hyd estimated in the present study was higher than the half-life recorded at the same pH conditions at 25°C that ranged from 16-35 days (k=-0.04 – -0.02 d-1) 34 to 72-81 days (k= -0.01 d-1) 35. In addition, concentrations of total suspended solids greater than 10 mg/L result in lesser rates of hydrolysis of CPF 20 (Mackay et al., 2014).

The water photolysis half-life (DT50pho) of CPF reported in the Pesticide Properties Database is about 29.6 days. In our study, photodegradation rate was estimated from the difference between light-sterile and dark-sterile conditions (Table 2). During the exposure time, microcosms collected on July 27, August 10, August 26 have been irradiated by 50, 125 and 184 kW/m2 of shortwave radiation incoming from the Sun, respectively. Kinetic studies of CPF photodegradation in various types of water (river, lake, ground and drinking waters, distilled) allowed to estimate a DT50pho value of about 1.5 days, with a decay rate of -0.46 d-1 36 under mean solar radiation intensity recorded ranging from 603 to 729 W/m2 (285-2800 nm). The lower decay rate estimated in our study was probably caused by the effect of the lower temperature because in Muhamad (2010) 36 work the photodegradation experiments were carried out at room temperature at 30°C.

Biodegradation rate resulted higher than those of photolysis and hydrolysis, indicating that biological processes have the highest contribution to the removal of CPF deposited on glaciers. We also estimated biodegradation rates under dark and light conditions from the difference between dark-sterile and dark-bacteria conditions and between light-sterile and light-bacteria conditions, respectively (Table 2). Although the biodegradation rate under light condition is double compared with that under dark conditions, the difference is not statistically significant ($t_{26} = -1.311$, $P = 0.201$). Therefore, it is not possible, with our data, to claim that the biodegradation of CPF was increased by light.

9.3.2. Microbial populations involved in Chlorpyrifos biodegradation in cryoconite

To gain more insight the biodegradation processes contributing to the removal of CPF, the structure of the bacterial communities in cryoconite used for microcosms set up and in those collected from one replicate of the different experimental groups were described by high-throughput sequencing (HTS) of 16S rRNA gene. Furthermore, 16S rRNA genes and *mpd* gene, coding for Methyl Parathion Hydrolases, were quantified with quantitative PCR (qPCR) to estimate the total number of bacteria and the putative populations with degradative abilities towards CPF, respectively.

HTS data showed 446 Operational Taxonomic Units (OTUs) in 7 samples. Number of OTUs in each hole ranged from 136 to 292. In Figure S1, the structure of the bacterial communities based on abundance of OTUs classified at Order level is reported. In natural cryoconite, *Cyanobacteria* was the dominant taxon representing for more than 50% of the community. *Burkholderiales* and *Sphingobacteriales* were also abundant, accounting for 14.9% and 8.9% of the community. In the experimental groups collected at subsequent times *Cyanobacteria* abundance generally decreased under both light and dark conditions, while *Burkholderiales* and *Sphingobacteriales* increased. Surprisingly, *Cyanobacteria* abundance was lower in light microcosms than in dark. Absolute number of 16S rRNA copies ranged from 0.6×10^8 to 1.1×10^8 without significant difference between dark and light conditions, and over time. Conversely, *mdp* gene copy number was never detected above the detection limit (10^2 copy number per gram). Microbial community structures in cryoconite are similar to those previously reported on Forni Glacier related to cryconite samples collected in previous years. Temporal changes in microbial community also followed the general trend observed in cryoconite during the ablation seasons in absence of spiked CPF (Franzetti et al., 2016a). The comparison of the microbial community structure and the bacterial abundance between dark and light conditions suggest that biodegradation of CPF did not lead either to a selection of CPF-degrading populations or to a significant growth of bacteria. This is consistent with the negligible amount of the spiked CPF compared with the native organic matter present in cryoconite (ranging from 6 to 8%). It is worth

noting that CPF did not have an appreciable toxic effect of microbial communities at the experimental concentrations as the bacterial abundance in natural cryoconite did not significantly differ from those spiked with CPF.

Since taxonomic data did not disclose significant information about the microbial population involved in CPF, metagenomics data of natural cryoconite from Forni glacier were analyzed (Franzetti et al., 2016b). From metagenomics data, 65 partial genomes were reconstructed and annotated, and genes involved in CPF biodegradation were searched. Among them, the reconstructed genome "bin 6" harbored the *mpd* gene. The complete annotation of bin 6 genome is provided as Supplementary Information. This reconstructed genome is one of the most abundant in the metagenome displaying a relative coverage in Forni metagenome of 6% and is phylogenetically related to *Burkholderiales* according to RAST annotation service (Overbeek et al., 2014). Bin 6 also harbored *puf*ML genes, which code for photosynthetic reaction center L and M subunits and were used as marker genes for the detection of Aerobic Anoxygenic Phototrophs (AAPs) (Caliz et al., 2014), thus suggesting that AAPs might be involved in CPF biodegradation. AAPs are obligate aerobic bacteria (Koblížek et al., 2015) which use light to supplement their metabolic demands and organic molecules as carbon source. Under light and aerobic conditions, they replace oxidative respiration with photophosphorylation, thus saving carbon, which is used in anabolic reactions for building cell biomass (Caliz et al., 2014; Čuperová et al., 2013). Our finding suggest that AAPs might be involved in CPF without the energy constrain of using the pesticide as sole energy and carbon source. To the best of our knowledge, studies regarding pollutants degradation by AAPs are not reported in the literature. However, central pathways and peripheral pathways for aromatic compound metabolism have been described in many members of *Burkolderiales* (Parnell et al., 2006; Hristova et al., 2007; Providenti et al., 2006; Mattes et al., 2008). Conversely, pesticide biodegradation by anoxygenic Purple Phototrophic Bacteria (PPB) has been extensively reported (Idi et al., 2014). PPB had a high versatility that allows them to switch among phototrophic, aerobic, and anaerobic modes of metabolism and differ from AAPs because the latter are

obligate aerobes (Koblížek, 2015). PPB showed high biodegradation efficiency of aromatic compounds both dark/anaerobic (Van Der Woude et al., 1994), light/anaerobic (Frigaard, 2015) and aerobic conditions (Harwood and Gibson, 1988). Annotation also revealed that bin 6 also harbored gene coding for carbon monoxide dehydrogenase (*cox*LM), thus suggesting that this population can also use CO as source of energy. CO-oxidizers are a phylogenetically diverse group of bacteria inhabiting different environments (King and Weber, 2007) that can be fed by CO which might form rapidly from organic carbon (OC) in melting snow exposed to light (Franzetti et al., 2016b; Haan et al., 2001; Xie et al., 2009). Bin 6 genome also showed the presence of genes involved in biodegradation of aromatic hydrocarbons such as benzoic acid (Figure 2).

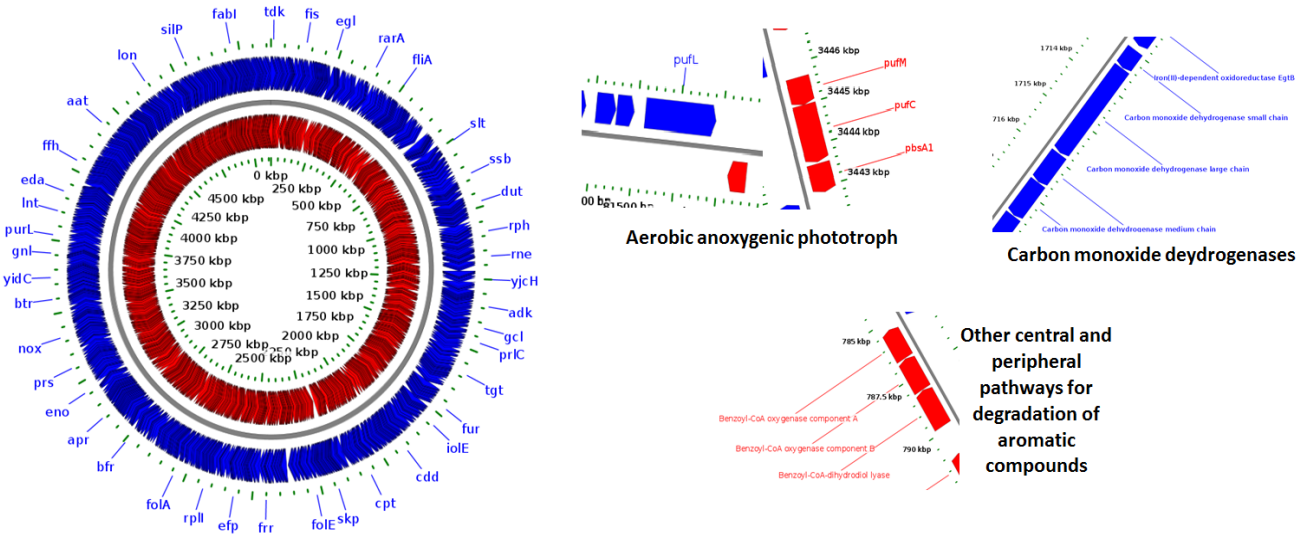

Fig. 2: Main features of genome annotation of the putative CPF degrading bacterial population (bin 6).

9.3.3. Extent of CPF biodegradation in cryoconite

The results of this study suggest that supraglacial microbial communities can degrade contaminants able to reach cold sites. Our data indicated that biodegradation is the most efficient process leading to CPF degradation in cryoconite (Table 2). The other post-depositional alterations investigated (hydrolysis and photodegradation) have proved to be not relevant in the considered environment. To evaluate the relevance of the biodegradation in cryoconite for the fate of CPF in the glacier, we

considered the total water discharge from the ablation area of Forni glacier, which has been estimated as 300,000 m^3, and the mean concentration of CPF (1 ng/L) in meltwater, to obtain an estimation of the total mass of CPF discharged in a melting season equal to 300 mg. It was also estimated that the amount of cryoconite in the ablation area of the glacier was 20 Kg with a mean concentration of CPF of 2 mg/Kg, that leads to an estimation of the CPF mass into the cryoconite of 40 mg. Considering that microbial activity could degrade up to 75% of the loaded CPF mass during melting period (Table 2), the biodegraded CPF could represent 10% of the discharged mass of CPF. The environmental relevance of biodegradation is also supported by the facts that the biologically active area might cover about 5% of the surface area of glaciers, with 1,014 to 1,017 microbial cells km^{-2} (Stibal et al., 2012) and that cryoconite holes are present on glacier surface when climatic conditions and lowland pesticides application period favor the contamination of Alpine mountains (Ferrario et al., 2017). These findings, therefore, allow to confirm that cryoconite might actually accumulate and promote the biodegradation of a relevant fraction of pesticides deposited on glacier ablation area. Bacteria activities on glacier surface cannot be neglected and should be included in the models predicting the fate of pesticides in cold areas since these processes can significantly contrast the accumulation of contaminants transported on glaciers, their possible re-emission back to the atmosphere or to the freshwater systems and their impact on surrounding ecosystems that can bioaccumulate these pollutants due to glacial melting (Bizzotto et al., 2009).

9.4. References

Azzoni R.S., Senese A., Zerboni A., Maugeri M., Smiraglia C. and Diolaiuti G. (2016): Estimating ice albedo from fine debris cover quantified by a semi-automatic method: the case study of Forni Glacier, Italian Alps. *The Cryosphere*, 10, 665–679.

Bidleman T.F., Helm P.A., Braune B.M. and Gabrielsen G.W. (2010): Polychlorinated naphthalenes in polar environments — A review. *Science of the Total Environment*, 408, 2919–2935.

Bizzotto E.C., Villa S. and Vighi M. (2009): POP bioaccumulation in macroinvertebrates of alpine freshwater systems. *Environmental Pollution*, 157, 3192–3198.

Calamari D., Bacci E., Focardi S., Gaggi C., Morosini, M. and Vighi M. (1991): Role of plant biomass in the global environmental partitioning of chlorinated hydrocarbons. *Environmental Science & Technology*, 25(8), 1489-1495.

Caliz J. and Casamayor E.O. (2014): Environmental controls and composition of anoxygenic photoheterotrophs in ultraoligotrophic high-altitude lakes (Central Pyrenees). *Environmental Microbiology Reports*, 6, 145–151.

Carrera G., Fernández P., Vilanova R.M. and Grimalt, J.O. (2001): Persistent organic pollutants in snow from European high mountain areas. *Atmospheric Environment*, 35, 245–254.

Chishti Z., Hussain S., Arshad K.R., Khalid A. and Arshad M. (2013): Microbial degradation of chlorpyrifos in liquid media and soil. *Journal of Environmental Management*, 114, 372–380.

Citterio M., Diolaiuti G., Smiraglia C., Verza G. and Meraldi E (2007): Initial results from the Automatic Weather Station (AWS) on the ablation tongue of Forni Glacier (Upper Valtellina, Italy). *Geografia Fisica e Dinamica Quaternaria*, 30.

Cook J., Edwards A., Takeuchi N. and Irvine-Fynn T. (2015): Cryoconite: The dark biological secret of the cryosphere. *Progress in Physical Geography*, doi:10.1177/0309133315616574

Čuperová Z., Holzer E., Salka I., Sommaruga R. and Koblízek M. (2013): Temporal changes and altitudinal distribution of aerobic anoxygenic phototrophs in mountain lakes. *Applied and Environmental Microbiology*, 79, 6439–6446.

Daly G.L. and Wania F. (2004): Organic Contaminants in Mountains. doi:10.1021/ES048859U

European Commission (2005): Review report for the active substance chlorpyrifos

Ferrario C., Finizio A. and Villa S. (2017) Legacy and emerging contaminants in meltwater of three Alpine glaciers. *Science of the Total Environment*, 574, 350–357.

Franzetti A., Navarra F., Tagliaferri I., Gandolfi I., Bestetti G., Minora U., Azzoni R.S., Diolaiuti G. and Ambrosini R. (2016): Temporal variability of bacterial communities in cryoconite on an Alpine glacier. *Environmental Microbiology Reports*.

Franzetti, A., Tagliaferri, I., Gandolfi, I., Bestetti, G., Minora, U., Mayer, C., Azzoni R.S. and Ambrosini, R. (2016): Light-dependent microbial metabolisms drive carbon fluxes on glacier surfaces. *The ISME Journal*, 10, 2984–2988.

Frigaard N.U. (2016): Biotechnology of anoxygenic phototrophic bacteria. In R. Hatti-Kaul, G. Mamo, & B. Mattiasson (Eds.), Anaerobes in biotechnology. (pp. 139-154). Springer.

George N., Chauhan P.S., Sondhi S., Saini S., Puri N. and Gupta N. (2014): Biodegradation and analytical methods for detection of organophosphorous pesticide: chlorpyrifos. *International Journal of Pure and Applied Sciences and Technology*, 20(2), 79.

Grannas A.M., Bogdal C., Hageman K.J., Halsall C., Harner T., Hung H. and Meyer T. (2013): The role of the global cryosphere in the fate of organic contaminants. *Atmospheric Chemistry and Physics*, 13(6), 3271-3305.

Grannas A.M., Jones A.E., Dibb J., Ammann M., Anastasio C., Beine H.J. and Chen G. (2007): An overview of snow photochemistry: evidence, mechanisms and impacts. *Atmospheric Chemistry and Physics*, 7(16), 4329-4373.

Grant J.R. and Stothard P. (2008): The CGView Server: a comparative genomics tool for circular genomes. *Nucleic Acids Research*, 36, W181–W184.

Haan D., Zuo Y., Gros V. and Brenninkmeijer C.A.M. (2001): Photochemical production of carbon monoxide in snow. *Journal of Atmospheric Chemistry*, 40, 217–230.

Hageman K.J., Hafner W.D., Campbell D.H., Jaffe D.A., Landers D.H. and Simonich S.L.M. (2010): Variability in pesticide deposition and source contributions to snowpack in western US national parks. *Environmental Science and Technology*, 44(12), 4452-4458.

Harwood C.S. and Gibson J. (1988): Anaerobic and aerobic metabolism of diverse aromatic compounds by the photosynthetic bacterium Rhodopseudomonas palustris. *Applied and Environmental Microbiology*, 54, 712–717.

Herbert B.M.J., Villa S. and Halsall C.J. (2006): Chemical interactions with snow: Understanding the behavior and fate of semi-volatile organic compounds in snow. *Ecotoxicology and Environmental Safety*, 63, 3–16.

Hoferkamp L., Hermanson M.H. and Muir D.C.G. (2010): Current use pesticides in Arctic media; 2000–2007. *Science of Total Environment*, 408, 2985–2994.

Hristova K.R., Schmidt R., Chakicherla A.Y., Legler T.C., Wu J., Chain P. S. and Kane S.R. (2007): Comparative transcriptome analysis of Methylibium petroleiphilum PM1 exposed to the fuel oxygenates methyl tert-butyl ether and ethanol. *Applied and Environmental Microbiology*, 73(22), 7347-7357.

Huber J.A., Welch D.B.M., Morrison H.G., Huse S.M., Neal P.R., Butterfield D.A. and Sogin M.L. (2007): Microbial population structures in the deep marine biosphere. *Science*, 318(5847), 97-100.

Hunter N., Nadkarni M.A., Jacques N.A. and Martin F.E. (2002): Determination of bacterial load by real-time PCR using a broad-range (universal) probe and primers set. *Microbiology*, 148, 257–266.

Idi A., Md Nor M.H., Abdul Wahab M.F. and Ibrahim Z. (2014): Photosynthetic bacteria: an eco-friendly and cheap tool for bioremediation. *Reviews in Environmental Sciences and Bio/Technology,* 14, 271–285.

Infante S. (2016): Ricostruzione storica dell'accumulo di contaminanti emergenti nei ghiacciai. (University of Milano Bicocca).

Kallenborn R., Christensen G., Evenset A., Schlabach M. and Stohl A. (2007): Atmospheric transport of persistent organic pollutants (POPs) to Bjørnøya (Bear Island). *Journal of Environmental Monitoring*, 9, 1082.

King G.M. and Weber C.F. (2007): Distribution, diversity and ecology of aerobic CO-oxidizing bacteria. *Nature Reviews in Microbiology*, 5, 107–118.

Klán P., Del Favero D., Ansorgová A., Klánová J. and Holoubek I. (2001): Photodegradation of halobenzenes in water ice. *Environmental Science and Pollution Research International*, 8, 195–200.

Koblížek M. (2015): Ecology of aerobic anoxygenic phototrophs in aquatic environments. *FEMS Microbiology Reviews,* 39, 854–870.

Landers D.H., Simonich S.L., Jaffe D.A., Geiser L.H., Campbell D.H., Schwindt A.R. and Hageman K.J. (2008): The fate, transport, and ecological impacts of airborne contaminants in western national parks (USA). Western Airborne Contaminants Assessment Project Final Report. Corvallis.

Li Q., Kang S., Wang N., Li Y., Li X., Dong Z. and Chen P. (2017): Composition and sources of polycyclic aromatic hydrocarbons in cryoconites of the Tibetan Plateau glaciers. *Science of the Total Environment*, 574, 991-999.

Mackay D., Giesy J.P. and Solomon K.R. (2014): in 35–76 (Springer International Publishing, 2014). doi:10.1007/978-3-319-03865-0_3

Mattes T.E., Alexander A.K., Richardson P. M., Munk A.C., Han C.S., Stothard P. and Coleman N.V. (2008): The genome of Polaromonas sp. strain JS666: insights into the evolution of a hydrocarbon-and xenobiotic-degrading bacterium, and features of relevance to biotechnology. *Applied and Environmental Microbiology*, 74(20), 6405-6416.

Matykiewiczová N., Klánová J. and Klán P. (2007): Photochemical degradation of PCBs in snow. *Environmental Science and Technology*, 41, 8308–8314.

Meikle R.W. and Youngson C.R. (1978): The hydrolysis rate of chlorpyrifos,O-O-diethylO-(3,5,6-trichloro-2-pyridyl) phosphorothioate, and its dimethyl analog, chlorpyrifos-methyl, in dilute aqueous solution. *Archives of Environmental Contamination and Toxicology*, 7, 13–22.

Muhamad S.G. (2010): Kinetic studies of catalytic photodegradation of chlorpyrifos insecticide in various natural waters. *Arabian Journal of Chemistry*, 3, 127–133.

Nakagawa S. and Schielzeth H. (2010) Repeatability for Gaussian and non-Gaussian data: a practical guide for biologists. *Biological Reviews*, 85(4), 935-956.

Noblet J.A. (1997): Hydrolysis, sorption and supercritical fluid extraction of triazine and organophosphate pesticides. (University of California, Los Angeles, 1997).

Overbeek R., Olson R., Pusch G.D., Olsen G.J., Davis J.J., Disz T. and Vonstein V. (2014): The SEED and the Rapid Annotation of microbial genomes using Subsystems Technology (RAST). *Nucleic Acids Resources*, 42, D206-D214.

Parnell J.J., Park J., Denef V., Tsoi T., Hashsham S., Quensen J. and Tiedje J.M. (2006): Coping with polychlorinated biphenyl (PCB) toxicity: physiological and genome-wide responses of Burkholderia xenovorans LB400 to PCB-mediated stress. *Applied and Environmental Microbiology*, 72(10), 6607-6614.

Peng Y., Leung H.C.M., Yiu S.M. and Chin F.Y.L. (2012): IDBA-UD: a de novo assembler for single-cell and metagenomic sequencing data with highly uneven depth. *Bioinformatics*, 28, 1420–1428.

Price P.B., Rohde R.A. and Bay R.C. (2009): Fluxes of microbes, organic aerosols, dust, sea-salt Na ions, non-sea-salt Ca ions, and methanesulfonate onto Greenland and Antarctic ice. *Biogeosciences* 6, 479–486.

Providenti M.A., O'Brien J.M., Ruff J., Cook A.M. and Lambert I.B. (2006): Metabolism of isovanillate, vanillate, and veratrate by Comamonas testosteroni strain BR6020. *Journal of Bacteriology*, 188, 3862–3869.

R Core Team (2013): R: A Language and Environment for Statistical Computing.

Seemann T. (2014): Prokka: rapid prokaryotic genome annotation. *Bioinformatics*, 30, 2068–2069.

Senese A., Diolaiuti G., Mihalcea C. and Smiraglia C. (2012b) Energy and mass balance of forni glacier (Stelvio National Park, Italian Alps) from a four-year meteorological data record. *Arctic, Antarctic and Alpine Resources,* 44.

Senese A., Diolaiuti G., Verza G. P. and Smiraglia C. (2012a): Surface energy budget and melt amount for the years 2009 and 2010 at the Forni Glacier (Italian Alps, Lombardy). *Geografia Fisica e Dinamica Quaternaria*, 35, 69–77.

Simon C., Wiezer A., Strittmatter A.W. and Daniel R. (2009): Phylogenetic diversity and metabolic potential revealed in a glacier ice metagenome. *Applied and Environmental Microbiology*, 75, 7519–7526.

Smiraglia C. Azzoni R.S., D'Agata C., Maragno D., Fugazza D. and Diolaiuti G.A. (2015): The evolution of the Italian glaciers from the previous data base to the new Italian inventory. preliminary considerations and results. Geografia Fisica e Dinamica Quaternaria, 38, 79-87.

Stibal M., Bælum J., Holben W.E., Sørensen S.R., Jensen A. and Jacobsen C.S. (2012): Microbial degradation of 2, 4-dichlorophenoxyacetic acid on the Greenland ice sheet. *Applied and Environmental Microbiology*, 78(15), 5070-5076.

Stibal M., Šabacká M. and Žárský J. (2012): Biological processes on glacier and ice sheet surfaces. *Nature Geosciences*, 5, 771–774.

Van der Woude B.J., De Boer M., Van der Put N.M.J., Van der Geld F.M., Prins R.A. and Gottschal J. C. (1994): Anaerobic degradation of halogenated benzoic acids by photoheterotrophic bacteria. *FEMS Microbiology Letters*, 119(1-2), 199-207.

Villa S., Vighi M., Maggi V., Finizio A. and Bolzacchini E. (2003): Historical Trends of Organochlorine Pesticides in an Alpine Glacier. *Journal of Atmospheric Chemistry*, 46, 295–311.

Wang X.P., Yao T.D., Cong Z.Y., Yan X.L., Kang S.C. and Zhang Y. (2006): Gradient distribution of persistent organic contaminants along northern slope of central-Himalayas, China. *Science of Total Environment*, 372, 193–202.

Wang Y. and Qian P.Y. (2009): Conservative Fragments in Bacterial 16S rRNA Genes and Primer Design for 16S Ribosomal DNA Amplicons in Metagenomic Studies. *PLoS One*, 4.

Wania F. (1997): Modelling the fate of non-polar organic chemicals in an ageing snow pack. *Chemosphere*, 35, 2345–2363.

Williams W.M., Giddings J.M., Purdy J., Solomon K.R. and Giesy J.P. (2014): Exposures of aquatic organisms to the organophosphorus insecticide, chlorpyrifos resulting from use in the United States. *Reviews of Environmental Contamination and Toxicology*, 231, 77–117.

Wu Y.W., Tang Y.H., Tringe S.G., Simmons B.A. and Singer S.W. (2014): MaxBin: an automated binning method to recover individual genomes from metagenomes using an expectation-maximization algorithm. *Microbiome*, 2, 26.

Xie H. and Zafiriou O.C. (2009): Evidence for significant photochemical production of carbon monoxide by particles in coastal and oligotrophic marine waters. *Geophysical Research Letters*, 36, L23606.

Conclusions

A modern approach to face the study of glaciers could not be effective without a deep knowledge of supraglacial debris. Indeed, as demonstrated in the previous chapters, debris significantly influences the evolution of glacier surface, its energy balance, and the carbon fluxes and storage. In this work through a multi-disciplinary approach, we focused on this *dark side of the glaciers* from two different points of view: the glaciological and the biological one.

Deep and accurate sedimentological analyses to describe rock debris features are essential to support many glaciological studies. Moreover, high-resolution remote-sensing data as the one from UAVs can really improve methods and timing of debris mapping; in addition, the investigation of the biological communities and the ecological processes occurring in this environments needs further and more detailed attention.

In the last decades, the large majority of glaciers, including those on the Italian Alps, showed a great increase of supraglacial debris cover. The analyses performed on aerial and UAVs imagery on a wide glacierized sector of Italy, highlighted that the debris-covered area doubled in the period 2003–2012, reaching an increase up to 30.10% of the whole glacier area (Chapter 1). However, these changes in surface features, fed by an increased availability of debris, occurred with different patches, according to the physical properties of the bedrocks hosting the glaciers. This suggests that further studies are needed to quantify the occurrence and distribution of supraglacial debris on all the Italian glaciation.

The ice albedo and, consequently, the energy balance of glaciers not only are affected by the presence or absence of a thick and continuous debris cover on the glacier surface, but also by the amount and distribution of the fine and sparse debris and dust that discontinuously cover glaciers. Sparse debris is thus important for determining the evolution of ice bodies, but its quantification is arduous, as the availability of high-resolution imagery, both from satellite and UAV, is mandatory. In Chapter 2 we showed that the processing of an UAV image of the glacier through a segmentation approach allows

describing ice features at a small-scale, including the distribution of fine debris. Moreover, we found evidence of darkening phenomena due to an increased amount of fine and sparse debris on the surface of glaciers, thus further extending the results presented in the Chapter 1, where this type of debris was not be properly considered due to the lower image resolution. In Chapter 3, we showed that occurrence of fine and sparse debris also strongly affected the ice albedo, but we also highlighted that a proper quantification of its variation over large spatial areas and over longer times is problematic.

The darkening of glaciers is probably favoring organisms living in the supraglacial debris; however, organisms can promote glacier darkening because they produce dark matter (e.g. humic substances) and are themselves part of the dark debris quantified in glaciological analyses. A positive feedback seems therefore to occur on glacier surface, promoting the increase of supraglacial debris. The analyses of the life on supraglacial debris indicates that a glacier cannot be considered as an isolated environment, although it has different characteristics than the surrounding areas. Nematodes and Rotifers (Chapter 4), for instance, can diffusely colonize supraglacial debris only in the presence of allochthonous organic matter, which represents the main source of organic carbon for these organisms in supraglacial environments where primary producers are scarce.

Moreover, the study of bacterial communities in snow highlighted a possible contribution of organisms transported from the area where the air masses originated (Chapter 5), as well as a non-negligible input of local air bacteria, maybe due to the deposition of local particulate during snowfall. This strong relation between glacier and ice-marginal environments is observable also from the bacterial community of the cryoconite holes (Chapter 6). Indeed, we showed that ice-marginal environments may act as sources of bacteria for these micro habitats, but differences in environmental conditions limit the number of bacterial strains that may survive in them. At the same time, cryoconite holes host some organisms that were not found in any ice-marginal environment we sampled, thus suggesting that some bacteria may reach cryoconite from distant sources.

In Chapter 7 we also showed that the bacterial communities of cryoconite holes have a wide temporal evolution throughout an ablation season, with autotrophic Cyanobacteria populations dominating communities after snow melt, and heterotrophic populations increasing in abundance later in the season.

The complex bacterial communities that inhabit glacier surface have large impacts on biogeochemical processes, in particular on the carbon cycle. In Chapter 8, we provided evidence for the occurrence in these environments of metabolic pathways that differ from those of oxygenic phototrophs and the respiration of heterotrophic organisms beforehand described on glacier surface. Indeed, we observed high abundance of heterotrophic anoxygenic phototrophs, suggesting that light might supplement the energy needed by the organisms permitting them to use some organic molecules as carbon sources. Furthermore, these communities could produce CO_2 also by the oxidation of CO, which may be produced by photodegradation of organic matter present in the cryoconite. Finally, in Chapter 9 we investigated the fate of contaminats on the glaciers surface assessing a key role of the bacteria in the chlorpyrifos degradation.

In summary, the results presented in this PhD thesis improved our knowledge of the supraglacial debris, its components and its evolution. The double view on the glacier system, both glaciological and biological, permits a deeper description of the mutual relations between bio and geo components. This multi-disciplinary analysis permit to define the ice-marginal areas as one of the principal sources of debris thanks to the description of possible sources of bacteria that we have found on glacier. Moreover, the presence of phototrophs, absorbing the solar radiation, can significantly influence the reflectivity of the glacier surface. Furthermore, the widening of supraglacial debris can be related to an increase presence of microbes, which in turn have a non-negligible impact on ice albedo. Finally, microbial CO_2 fixation is important for the glacier system thus offering organic carbon availability for further communities.

Moreover, this inter-disciplinary analysis paved the way for further deeper investigation of abiotic and biotic aspects of supraglacial environments. In particular, a more detailed quantification of supraglacial dust is needed for better assessing the darkening phenomena connected to the anthropic emissions and the related impacts on ice albedo. The description of the life forms in supraglacial debris is just beginning. The characterization of other organisms that inhabit the glacier surfaces is warmly required for a deeper analysis of the carbon cycle in these environments. Among the others, collembola were observed on ice bodies since the late 1800s, but a detailed investigation of their communities is still lacking. The bacterial communities need a more detailed description, particularly their role in the ice darkening processes. Finally, a proper quantification of carbon fluxes on glacier surface, which include the contribution of previously neglected metabolic pathways is needed to assess the contribution of this wide biome to the global carbon cycle.

Acknowledgments

I would like to thank my supervisors Prof. Guglielmina Adele Diolaiuti, PhD Andrea Zerboni, PhD Roberto Ambrosini and PhD Andrea Franzetti for numerous helpful advices, comments and support. We also thank Prof. Smiraglia for his precious recommendations.

I would like to thank all the co-authors that have worked in the papers produced in these three years of my PhD. In particular, for the great help on field activities and data processing, I gratefully thank Claudia Ferrario, Ilario Tagliaferri and Francesca Pittino for the biological investigations and Antonella Senese, Davide Fugazza, Eraldo Meraldi and Gian Pietro Verza for the glaciological side of this work. I thank all the thesis students (bachelor and master degree) for their kind help on the field.

This thesis, and the works here presented, has been performed under the framework of different projects. In particular, the field activities and the analyses were supported by DARAS (Department of Regional Affairs, Autonomies and Sport) of the Presidency of the Council of Ministers of the Italian government through the GlacioVAR project, by the Central Scientific Committee of the Italian Alpine Club, by Sanpellegrino Levissima Spa, by Regione Lombardia (SHARE-Stelvio Project), by the Italian Ministry of Research (PRIN grant 2010AYKTAB to Claudio Smiraglia and PRIN grant 7-19-2001100-2 to Roberto Ambrosini).

We are also kindly grateful to the Stelvio Park management staff, the municipality of Valfurva and the Italian Alpine Club for the collaboration in the field activities.

List of publication

Accepted

Ambrosini R, Musitelli F, Navarra F, Tagliaferri I, Gandolfi I, Bestetti G, Mayer C, Minora U, **Azzoni RS**, Diolaiuti GA, Smiraglia C and Franzetti A (2016) - Diversity and Assembling Processes of Bacterial Communities in Cryoconite Holes of a Karakoram Glacier. *Microbial Ecology*, DOI: 10.1007/s00248-016-0914-6.

Franzetti A, Navarra F, Tagliaferri I, Gandolfi I, Bestetti G, Minora U, **Azzoni RS**, Diolaiuti GA, Smiraglia C and Ambrosini R (2016) – Temporal variability of bacterial communities in cryoconite on an Alpine glacier. *Environmental Microbiology Reports*, DOI: 10.1111/1758-2229.12499.

Franzetti A, Tagliaferri I, Gandolfi I, Bestetti G, Minora U, Mayer C, **Azzoni RS**, Diolaiuti GA, Smiraglia C and Ambrosini R (2016) - Light-dependent microbial metabolisms drive carbon fluxes on glacier surfaces. *The ISME Journal*, 10(12), 2984-2988.

Azzoni RS, Senese A, Zerboni A, Maugeri M, Smiraglia C and Diolaiuti GA (2016) - Estimating ice albedo from fine debris cover quantified by a semi-automatic method: The case study of Forni Glacier, Italian Alps. *The Cryosphere*, 10(10), 665-679.

Fugazza D, Senese A, **Azzoni RS**, Maugeri M and Diolaiuti GA (2016) - Spatial distribution of surface albedo at the Forni Glacier (Stelvio National Park, Central Italian Alps). *Cold Regions Science and Technology*, 125, 128-137.

Azzoni RS, Franzetti A, Fontaneto D, Zullini A and Ambrosini R (2015) - Nematodes and rotifers on two Alpine debris-covered glaciers. *Italian Journal of Zoology*, 82(4), 1-8.

Fugazza D, Senese A, **Azzoni RS**, Smiraglia C, Cernuschi M, Severi D and Diolaiuti GA (2015) - High resolution mapping of glacier surface features. The UAV survey of the Forni Glacier (Stelvio National Park, Italy). *Geografia Fisica e Dinamica Quaternaria*, 38(1), 25-33.

Smiraglia C, **Azzoni RS**, D'Agata C, Maragno D, Fugazza D and Diolaiuti GA (2015) - The evolution of the Italian glaciers from the previous data base to the New Italian Inventory. Preliminary considerations and results. *Geografia Fisica e Dinamica Quaternaria,* 38(1), 79-87.

Smiraglia C, **Azzoni RS**, D'Agata C, Maragno D, Fugazza D and Diolaiuti GA (2015) - The New Italian Glacier Inventory: a didactic tool for a better knowledge of the natural Alpine environment. *Journal of Research and Didactics in Geography,* 1, 81-94.

Senese A, Vuillermoz E, **Azzoni RS**, Verza GP, Smiraglia C and Diolaiuti GA (2015) - Air temperature thresholds to assess snow melt at the Forni Glacier surface (Italian Alps) in the April–June period: a contribution to the application of temperature index models, *Engineering Geology for Society and Territory*, 1, 61-68.

Azzoni RS, Senese A, Zerboni A, Maugeri M, Smiraglia C and Diolaiuti GA (2014) - A novel integrated method to describe dust and fine supraglacial debris and their effects on ice albedo: the case study of Forni Glacier (Italian Alps). *The Cryosphere Discussion*, 8, 3171-3206.

Submitted

Azzoni RS, Fugazza D, Zerboni A, Senese A, D'Agata C, Maragno D, Carzaniga A, Cernuschi M and Diolaiuti GA – The evolution of debris mantling glaciers in the Stelvio Park (Italian Alps) over the time window 2003-2012 from high-resolution remote-sensing data. Submitted to Progress in Physical Geography.

Azzoni RS, Zerboni A, Pelfini M, Garzonio CA, Cioni F, Meraldi E, Smiraglia C and Diolaiuti GA - Geomorphological map of Mount Ararat/Ağri Dağı (Ağri Dağı Milli Parki, Eastern Anatolia, Turkey). In revision for Journal of Maps.

Diolaiuti G, **Azzoni RS**, D'Agata C, Maragno D, Fugazza D, Vagliasindi M, Mortara G, Perotti L, Bondesan A, Carton A, Pecci M, Dinale R, Trenti A, Casarotto C, Colucci RR, Cagnati A, Crepaz A and Smiraglia C – Present extent and features of the Italian glaciers, a non negligible water resources for the Alps. Submitted to Houille Blanche.

Franzetti A, Navarra F, Tagliaferri I, Gandolfi I, Bestetti G, Minora U, **Azzoni RS**, Diolaiuti G, Smiraglia C and Ambrosini R - Potential sources of bacteria colonizing the cryoconite of an Alpine glacier. Submitted to PlosOne.